University of Sussex

Dynamics of Neural Systems with Time Delays

By

Bootan Mohammed Rahman

Submitted for the degree of Doctor of Philosophy

University of Sussex

October 2016

Declaration

I hereby declare that this thesis has not been submitted, either in the same or different form to this or any other University for a degree.

Signature:.....

Bootan Rahman

Dedication

To my parents and Kharman.

Acknowledgements

There are many people who deserve to be mentioned and thanked for their support throughout the period of this research. I will begin by thanking my supervisors Dr. Yuliya Kyrychko and Dr. Konstantin Blyuss, for their guidance, support, encouragement and friendship kindness. They are the two people that made this tiresome endeavour really interesting.

I am deeply indebted to my wonderful wife, Kharman, who gave me everything a man could ever dream of including my two little sons Daryan and Dyako. I thank this wonderful family of mine for their patience and for being there as a solace and a source of great joy. Kharman, my love for you is by far the most precious thing that ever happened to me. Thank you dear. Thank you for your kindness but most importantly for your tender heart.

Additionally, I would like to express my gratitude to Professor John Hogan at University of Bristol, and Mahmoud Bukar Maina, a Ph.D. Neuroscience student at the University of Sussex for sharing their expertise and for giving me some helpful feedback that in many ways helped advance this thesis.

Also, I am indebted to my postgraduate colleagues, including Abubakar Kagu, Aminu Murtala, Neofytou Giannis, Muhammad Yau, Barzan Ali, Najmadeen Rashid, Laura Murphy, Benard Kipchumba, Eduard Campillo Funollet, Muflih Alhazmi, Fuad Wahid, Pakhshan Hamand, Mehdi Mahmud for their friendship and the memorable years of smiles, travels and ever memorable fun.

I would also like to record my great appreciation for ministry of higher education in Kurdistan/Iraq for give me a chance to study abroad under HCDP scholarship.

Finally, I would like to thank my family back home in Kurdistan, who has been extremely patient with me while I was in a far away land pursuing a worthy objective. Your support and confidence in me is beyond measure. Hence, no words can express my gratitude. You have been a great pillar for me and my family throughout my studies. This I will always remember. and I am grateful.

Abstract

Complex networks are ubiquitous in nature. Numerous neurological diseases, such as Alzheimer′s, Parkinson′s, epilepsy are caused by the abnormal collective behaviour of neurons in the brain. In particular, there is a strong evidence that Parkinson′s disease is caused by the synchronisation of neurons, and understanding how and why such synchronisation occurs will bring scientists closer to the design and implementation of appropriate control to support desynchronisation required for the normal functioning of the brain. In order to study the emergence of (de)synchronisation, it is necessary first to understand how the dynamical behaviour of the system under consideration depends on the changes in system′s parameters. This can be done using a powerful mathematical method, called bifurcation analysis, which allows one to identify and classify different dynamical regimes, such as, for example, stable/unstable steady states, Hopf and fold bifurcations, and find periodic solutions by varying parameters of the nonlinear system.

In real-world systems, interactions between elements do not happen instantaneously due to a finite time of signal propagation, reaction times of individual elements, etc. Moreover, time delays are normally non-constant and may vary with time. This means that it is vital to introduce time delays in any realistic model of neural networks. In this thesis, I consider four different models. First, in order to analyse the fundamental properties of neural networks with time-delayed connections, I consider a system of four coupled nonlinear delay differential equations. This model represents a neural network, where one subsystem receives a delayed input from another subsystem. The exciting feature of this model is the combination of both discrete and distributed time delays, where distributed time delays represent the neural feedback between the two sub-systems, and the discrete delays describe neural interactions within each of the two subsystems. Stability properties are investigated for different commonly used distribution kernels, and the results are compared to the corresponding stability results for networks with no distributed delays. It is shown how approximations to the boundary of stability region of an equilibrium point can be obtained analytically for the cases of delta, uniform, and gamma delay distributions.

Numerical techniques are used to investigate stability properties of the fully nonlinear system and confirm our analytical findings.

In the second part of this thesis, I consider a globally coupled network composed of active (oscillatory) and inactive (non-oscillatory) oscillators with distributed time delayed coupling. Analytical conditions for the amplitude death, where the oscillations are quenched, are obtained in terms of the coupling strength, the ratio of inactive oscillators, the width of the uniformly distributed delay and the mean time delay for gamma distribution. The results show that for uniform distribution, by increasing both the width of the delay distribution and the ratio of inactive oscillators, the amplitude death region increases in the mean time delay and the coupling strength parameter space. In the case of the gamma distribution kernel, we find the amplitude death region in the space of the ratio of inactive oscillators, the mean time delay for gamma distribution, and the coupling strength for both weak and strong gamma distribution kernels.

Furthermore, I analyse a model of the subthalamic nucleus (STN)-globus palidus (GP) network with three different transmission delays. A time-shift transformation reduces the model to a system with two time delays, for which the existence of a unique steady state is established. Conditions for stability of the steady state are derived in terms of system parameters and the time delays. Numerical stability analysis is performed using traceDDE and DDE-BIFTOOL in Matlab to investigate different dynamical regimes in the STN-GP model, and to obtain critical stability boundaries separating stable (healthy) and oscillatory (Parkinsonian-like) neural firing. Direct numerical simulations of the fully nonlinear system are performed to confirm analytical findings, and to illustrate different dynamical behaviours of the system.

Finally, I consider a ring of n neurons coupled through the discrete and distributed time delays. I show that the amplitude death occurs in the symmetric (asymmetric) region depending on the even (odd) number of neurons in the ring neural system. Analytical conditions for linear stability of the trivial steady state are represented in a parameter space of the synaptic weight of the self-feedback and the coupling strength between the connected neurons, as well as in the space of the delayed self-feedback and the coupling strength between the neurons. It is shown that both Hopf and steady-state bifurcations may occur when the steady state loses its stability. Stability properties are also investigated for different commonly used distribution kernels, such as delta function and weak gamma distributions. Moreover, the obtained analytical results are confirmed by the numerical simulations of the fully nonlinear system.

Contents

List of Figures

Chapter 1

Introduction

Contemporary developments in the field of neuroscience reveal an area of research, where scholars have become increasingly keen to use quantitative methods in order to explore new topics of interest. This development has led to the emergence of computational neuroscience, an interdisciplinary field that has brought together the domain of nonlinear dynamics and a variety of other areas, including biology, cognitive science and artificial intelligence. Since it was first introduced in 1980′s, the study of neural networks has greatly benefited from the steady growth of computing and, from a mathematical perspective, cultivated the development of appropriate mathematical tools with which neural dynamics can be investigated. As such, computational neuroscience has not only expanded itself but also offered significant contributions in numerical analysis, biological modelling and other emerging fields of neural networks [159].

Modern scholars of neural networks have continued to develop some of the earlier research, such as the work done by Hopfield in 1984, where he proposed a simple method of constructing a neural network model. The model was capable of simulating the development of human memory in which the linear circuit of each individual neuron consisted of a capacitor and a resistor. He went further to show that through these electrical components, the connection between these neurons can be described by a nonlinear sigmoidal activation function. This profound realisation subsequently aspired the development of a field in which electric circuits can be utilized to perform different tasks such as linear programming, signal processing, optimisation, associative memory and pattern recognition [1, 4, 40, 118, 168]. In the past few decades, one of the fascinating topics of research in neural models is that of coupled networks [147]. The appeal comes from the fact that, although by themselves, uncoupled elements may exhibit very simple and well-understood behaviour, when coupled together, they produce a wealth of new dynamical regimes, such

as full and/or partial synchronisation, amplitude death, and chimera states. One such example is the case of coupled nonlinear oscillators which demonstrate exceptionally rich dynamical behaviour in a system, where the nodes are connected through the distributed-delay coupling [80]. A common theme of coupled oscillators is that every unit is active, however, it is important to consider the potential consequences arising from the external perturbations, which may turn some of the units into inactive [30]. Coupled networks and coupled oscillators are common in various scientific disciplines ranging from power grids [123] to cardiac pacemaker cells [49, 97], circadian clocks [10, 16, 42], and arrays of Josephson junctions [156].

Another important aspect of neural networks is that the transmission of information among neurons is not generally assumed to occur instantaneously due to inherit biological limitations. Hence, time delays become an important feature in modelling of the neural networks, and their inclusion has shown to cause instabilities in the model, not present in a non delayed analogue [34, 53, 94, 145]. Researchers have obtained many results for the dynamics of neural network with discrete time delays, as these can be used to represent the typical time lag that occurs in the communication between neurons [14, 22, 26, 66, 96, 109]. However, in reality the time delays are not constant; they may vary over time and/or depend on system parameters, and may, therefore, be better represented by distributed delays [37, 47, 52].

Though the analysis of neural networks with or without time delays, is a very challenging work, they process a vast number of features and an immense variety of dynamical behaviour that makes their study even more desirable.

The main objective in this thesis is to study the influence of time delay in Hopfield-type neural (coupled sub-networks and ring network) model with combination of both discrete and distributed delay, STN-GP model with three discrete delays, and Stuart-Landau oscillators with distributed delay coupling. A crucial issue to be explained is how discrete and/or distributed time delays change the stability of the steady states. In order to study the emergence of synchronised oscillations, it is first necessary to understand how the dynamical behaviour of the system under consideration depends on the changes of system parameters. This can be done using a powerful mathematical method, called bifurcation analysis, which allows one to identify and classify different dynamical regimes, for instance, stable/unstable steady states, steady-state and Hopf bifurcations, and find periodic solutions by varying the parameters of the fully nonlinear system.

In this introductory chapter, we review the basic structure of a single biological neuron,

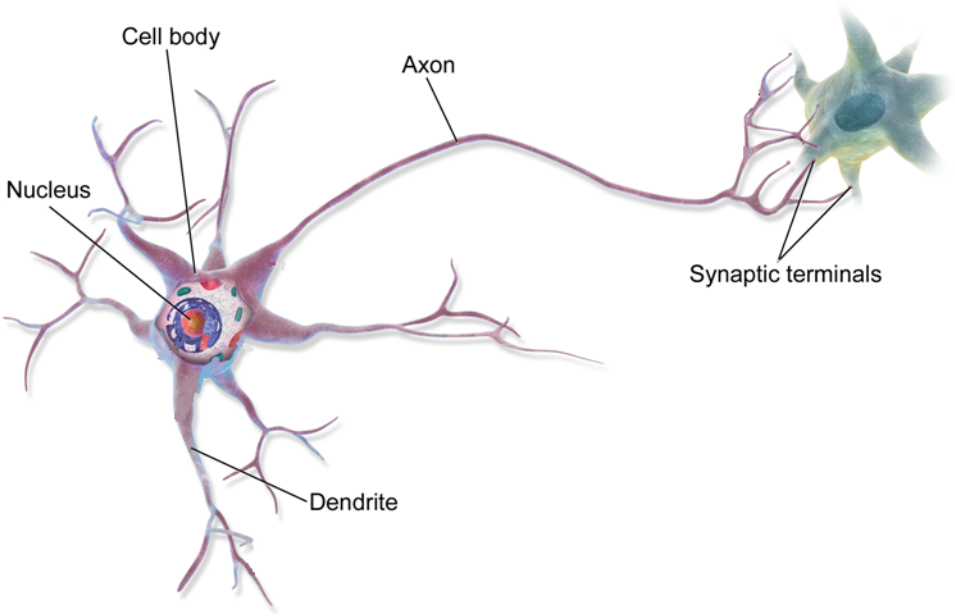

Figure 1.1: Prototypical nerve cell or neuron [www.sciencebeta.com/neuron].

as well as the artificial neural networks. In the following section, we give a literature review on time delays (discrete and/or distributed) in neural networks in general, and their effects on the dynamics of the Hopfield-type model, Stuart-Landau oscillators, and STN-GP model. The section is concluded by the outline of the thesis.

1.1 Basic neuroanatomy

The human central nervous system is responsible for controlling all movements and biological processes that occur in the human body, and consists of highly specialized cells called nerves or neurons, which have the cell body at the centre and its nucleus. From the cell body emanates a dendrite which conducts the impulses received from other neural cells to the cell body. Another cell, called axon also emanates from the cell body that conducts nerve impulses away from the cell body to other neurons and muscles. The axons' ends form a synaptic terminal which connects the neuron with other neurons or a muscle, over which nerve impulses pass [159]. There are approximately 100 billion neurons and an estimated 100 trillion synapses among them [5]. They come in a variety of shapes, sizes and properties, but their typical anatomical features are as shown in Figure 1.1.

1.2 Artificial neural system

Artificial neural networks, usually called neural networks are designed following the principles of a biological nervous system, and are used to perform tasks similar to those the

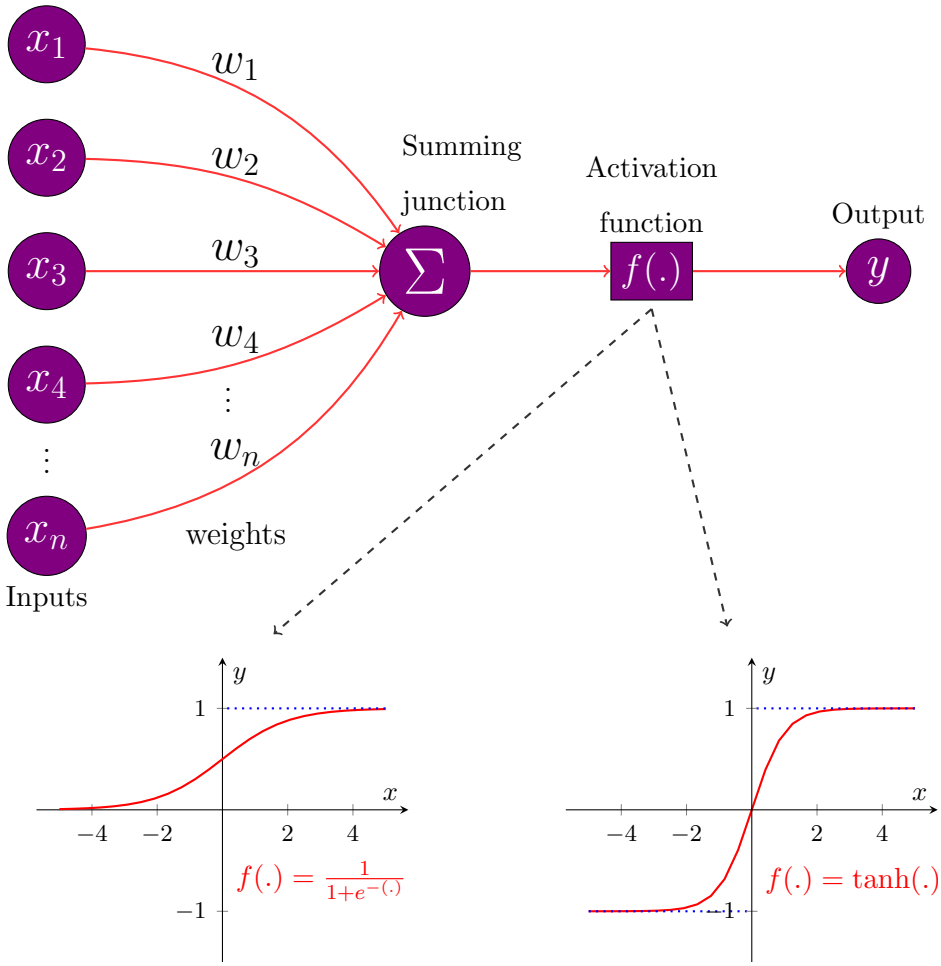

Figure 1.2: A sketch of the artificial neural network with a sigmoid transfer/activation function.

human brain can perform. Such networks are made up of a large number of nodes (neurons) highly interconnected together using unidirectional signal channels called connections (synapses). They are built to work jointly to perform specific tasks. The architecture of these networks is such that each single neuron is connected to a large number of other neurons, they have the ability to arrange into ensembles to perform specific tasks, and they involve plasticity, i.e. the adjustment of synaptic connection required for the adaptation to the environment and the ability to learn [135, 148, 159].

In order to describe the neural network consisting of n neurons mathematically, we consider a set of n nodes, where each node, denoted as x_i, $i = 1, \cdots, n$, can transmit signals to an output neuron y through a transfer/activation function $f(\cdot)$. Usually, the input neurons have synaptic weights, denoted as w_i, which can be negative or positive. A negative sign for the synaptic weight indicates an inhibitory connection, while a positive sign shows an excitatory connection. A neuron receives one or more inputs, and then sums

them up to create a corresponding output. This sum is then put through an activation or transfer function $f : \mathbb{R} \to \mathbb{R}$. The transmitted information or output can be evaluated as follows

$$y = f\left(\sum_{i=1}^{n} w_i x_i\right). \tag{1.1}$$

There are three main activation functions used in the literature, namely, threshold, piecewise-linear, and sigmoid functions. Among them, the sigmoid-shaped function is the most commonly used in the neural network literature, and is usually taken to be strictly increasing and differentiable [13, 94]. The logistic function $f(v) = \dfrac{1}{1+e^{-av}}$ and hyperbolic tangent function $f(v) = \tanh(av)$ are the two examples of a sigmoid function, plotted in in Figure 1.2, where a is the slope of the function.

A Hopfield neural network [60] is an extension of (1.1), which can be written in the form

$$C_k \frac{du_k(t)}{dt} = -\frac{1}{R_k} u_k(t) + \sum_{i=1}^{n} w_{ki} f_i(u_i(t)) + I_k, \qquad k = 1, \cdots, m, \tag{1.2}$$

where C_k is the capacitance of neuron k, R_k is the resistance of neuron k, w_{ki} is the connection synaptic weight between the k^{th} neuron and the i^{th} neuron, $u_k(t)$ describes the voltage of the k^{th} neuron at time t, I_k is the constant external input to the k^{th} neuron, and f_k is the transfer function.

1.3 Time delays in neural networks

The inclusion of time delays into the mathematical models of various biological, physical and engineering problems has long been proved vital in order to correctly represent the processes under consideration. For example, in population biology, they account for age structure or maturation time period, while in epidemiological setting they represent, for example, latency or immunity. In neural network modelling, time delays are used to take into account the fact that in the majority of both biological and artificial neural networks, some processes do not happen instantaneously due to a finite propagation velocity of neural signals, times required for information processing, and so forth. Undoubtedly, their inclusion is a non-negligible component of the process and leads to qualitatively new behaviour in the dynamical system not observed in the same system without time delays [8, 38, 39, 67, 81, 131, 144, 167].

A simple delayed self-excitation neuron with discrete time delay can be modelled as follows:

$$\dot{u}(t) = -\kappa u(t) + \alpha f(u(t-\tau)), \tag{1.3}$$

where $\kappa > 0$, $u(t)$ is the voltage input of the neuron, the constant delay τ refers to the transmission time between the input and the output, α is a synaptic weight, and $f : \mathbb{R} \to \mathbb{R}$ is nonlinear transfer function. Since in the majority of systems the precise value of the time delay is rarely known, it is more reasonable to use distributed time delays. The corresponding distributed delay version of model (1.3) can be made by replacing the last term of model (1.3) as follows

$$\dot{u}(t) = -\kappa u(t) + \alpha \int_0^\infty g(s) f(u(t-s)) ds, \tag{1.4}$$

where the term

$$\int_0^\infty g(s) f(u(t-s)) ds, \tag{1.5}$$

represents the *distributed delay* with the kernel $g(s)$, which generally has the following properties:

$$g(s) \geq 0 \text{ and } \int_0^\infty g(s) ds = 1.$$

In the next subsection, we will review the most commonly used distribution kernels, and discuss several results from the literature on the comparison between the systems with discrete and distributed time delays.

1.3.1 Distribution kernels

In most applications, including neural networks, the time delays are non-constant, and this naturally leads to the idea of representing the delays in the connections using the distribution [9, 47, 48, 52, 64, 111, 171]. The majority of models in the literature use specific kernels for delay distribution, such as

(i) *Dirac delta function*, i.e. the distribution kernel is taken in a form $g(s) = \delta(s)$, which is characterised by the following two properties

$$\delta(s) = \begin{cases} 0 & \text{for} \quad s \neq 0, \\ \infty & \text{for} \quad s = 0, \end{cases} \qquad \text{and} \qquad \int_{-\infty}^{\infty} f(s)\delta(s) ds = f(0).$$

Substituting this kernel into the equation (1.4) gives its non-delayed equation equivalent

$$\dot{u}(t) = -\kappa u(t) + \alpha \int_0^\infty \delta(s) f(u(t-s)) ds = -\kappa u(t) + \alpha f(u(t)).$$

If $g(s) = \delta(s-\tau)$, the Dirac distribution is shifted by τ to the right, and has the following properties

$$\delta(s-\tau) = \begin{cases} 0 & \text{for} \quad s \neq \tau, \\ \infty & \text{for} \quad s = \tau, \end{cases} \qquad \text{and} \qquad \int_{-\infty}^{\infty} f(s)\delta(s-\tau) ds = f(\tau).$$

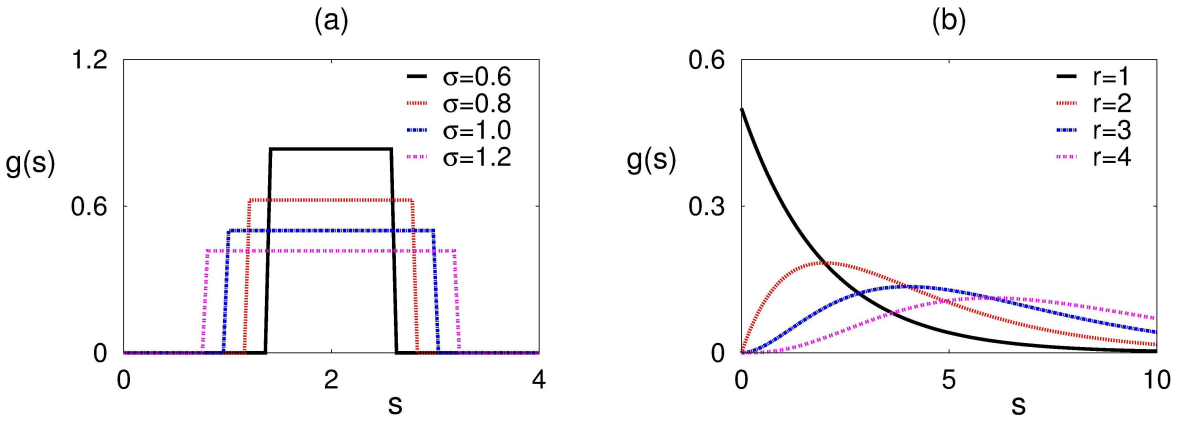

Figure 1.3: (a) The uniform distribution for the mean delay $\tau = 2$. (b) The gamma distribution for the mean delay $\tau_m = 2$.

Inserting this kernel into the equation (1.4) reduces it to a model with a single discrete time delay as follows

$$\dot{u}(t) = -\kappa u(t) + \alpha \int_0^\infty \delta(s-\tau) f(u(t-s))ds = -\kappa u(t) + \alpha f(u(t-\tau)).$$

(ii) The second most-commonly used distribution kernel is the *uniform distribution*, which can be written in the form

$$g(s) = \begin{cases} \dfrac{1}{2\sigma} & \text{for} \quad \tau - \sigma \leq u \leq \tau + \sigma, \\ \\ 0 & \text{otherwise}, \end{cases} \tag{1.6}$$

which has the mean time delay τ, and the parameter σ controls the width and height of the distribution. Figure 1.3 (a) shows examples of the uniformly-distributed kernel for mean time delay $\tau = 2$ and different values of σ. As σ gets smaller, the width of the distribution become narrower and the height become higher. Hence, as σ approaches zero, the uniform distribution becomes the Dirac distribution, $\delta(s-\tau)$:

$$\lim_{\sigma \to 0} \int_0^\infty g(s) f(u(t-s))ds = \int_0^\infty \delta(s-\tau) f(u(t-s))ds = f(u(t-\tau)).$$

This type of distribution has been extensively used to study the dynamics of ecological models [107], traffic dynamics with delayed driver response [136], and genetic regulation [12].

(iii) *Gamma distribution* is the third most commonly used distribution kernel, which can be written as follows

$$g(s) = g_\gamma^r(s) = \frac{s^{r-1}\gamma^r e^{-\gamma s}}{(r-1)!}. \tag{1.7}$$

It is a distribution with an integer shape (order) parameter $r \in \mathbb{N}_0$, $(r \geq 0)$ and scale parameter $\gamma \in \mathbb{R}$, $(\gamma > 0)$. *Weak* kernel refers to the case of gamma distribution of order $r = 1$. One can see in Figure 1.3 (b) for $r = 1$, $g(s)$ decreases with increasing s, and in terms of neural network modelling can be interpreted as the maximum weighted response depends on the current voltage while the past voltage has a decreasing influence [125]. The weak delay kernel $g^1_\gamma(s)$ in this case becomes exponential distribution $g^1_\gamma(s) = \gamma e^{-\gamma s}$.

When $r = 2$, it is known as the *strong* delay kernel and shown in Figure 1.3 (b). In this case, in the context of neural networks, the contribution from the past voltages is more present compared to the weak kernel [56]. The weak distribution (1.7) has the mean delay

$$\tau_m = \int_0^\infty s g^r_\gamma(s) ds = \frac{r}{\gamma}, \tag{1.8}$$

and the variance

$$\sigma^2 = \int_0^\infty (s - \tau_m)^2 g^r_\gamma(s) ds = \frac{r}{\gamma^2}. \tag{1.9}$$

The gamma distribution for a fixed value of the mean delay $\tau_m = 2$, and order $r = 1$, 2, 3, and 4 is illustrated in Figure 1.3 (b). As r increases, the peak becomes smaller, and for a very large integer number r, the gamma distribution (1.7) approaches the Dirac distribution, $\delta(s - \tau)$. Gamma delay distribution has been extensively used in models of population dynamics [17, 26], intracellular dynamics of HIV infection [100], and machine tool vibrations [146].

It is possible to convert a scalar delay differential equation with a distributed delay into a non-delayed system of equations by using the so-called *linear chain trick* described in [91, 137]. The linear chain trick allows one to replace the system with distributed delays by a system of ordinary differential equations of order $r + 1$. Suppose that $g(s)$ in (1.4) is a general gamma distribution $g^r_\gamma(s)$, and let

$$v_k(t) = \int_0^\infty g^k_\gamma(s) f(u(t - s)) ds, \quad k = 1, \cdots, r.$$

Differentiate $v_k(t)$ with respect to t

$$\begin{aligned} \dot{v}_1(t) = &\quad \gamma u(t) - \gamma v_1(t), \\ \dot{v}_k(t) = &\quad \gamma v_{k-1}(t) - \gamma v_k(t), \quad k = 2, \cdots, r. \end{aligned}$$

The model (1.4) with gamma distributed kernel now becomes

$$\begin{aligned} \dot{u}(t) = &\quad -\kappa u(t) + \alpha v_k(t), \\ \dot{v}_1(t) = &\quad \gamma u(t) - \gamma v_1(t), \\ \dot{v}_k(t) = &\quad \gamma v_{k-1}(t) - \gamma v_k(t), \quad k = 2, \cdots, r. \end{aligned}$$

Such an approach may seem attractive as the model can then be analysed using the theoretical and numerical methods for ordinary differential equations.

There is a number of studies of mathematical models with distributed delay, using one of the above-mentioned distributions (Dirac, uniform, and gamma), which are analysed and then compared to their versions with discrete time delays.

Cooke and Grossman [26] have compared the behaviour of a differential equation with single constant time delay and the corresponding equation with a gamma-distributed kernel. They showed that for a differential equation with constant time delay, there exists a value of the delay such that a zero steady state loses its stability, and never re-stabilises again. For the distributed delay, increasing the mean time delay can also destabilise the zero equilibrium, however, it will always be re-stabilised for a large enough mean time delay. Bernard et al. [14] analysed the linear stability of a scalar system with one and two delays characterised by the distribution kernel properties, such as mean, variance and skewness. For uniform and continuous distributions, they postulated that distributed delay increases the stability region of an equilibrium compared to the discrete delay. Thiel et al. [154] used uniformly-distributed delay for three different models with distributed delay and observed that as the width of the distribution gets wider, the region of oscillations gets smaller.

Atay [7] has investigated a system consisting of two simple oscillators with a gap junctional coupling. He has shown that it is easier to quench oscillations in a system with distributed delays than in a system with a discrete time delay in a sense that there is a larger region of coupling strengths for which the steady state can be stabilised. In particular, it was deduced that as the variance of the distribution increases, the size of the stability region increases. Jirsa *et al.* [66] have analysed an $n \times n$ linear system with linear decay and arbitrary connections with a common delay. They have shown that under some mild assumptions, the stability region of the trivial solution for any distribution of time delays is larger and contains the stability region for a discrete delay. Meyer *et al.* [96] have found that distributed delays enhance the stability of the system, so that with the increased width of the distribution of delays, the system converges faster to a fixed point and converges slower toward a limit cycle. Moreover, the introduction of distributed delays leads to an increased range of the average values of time delays for which the equilibrium is stable. The dynamics of the system is then determined almost exclusively by the mean and the variance of the delay distribution and shows very little dependence on the particular type of the distribution. Bernard and Crauste [15] have shown that given

the mean time delay, the linear equation with distributed delay is stable if the associated differential equation with a discrete delay is stable.

Campbell and Jessop [22] developed a method for approximating the stability region of an equilibrium for nonlinear distributed delay equations, knowing only the first few moments of the delay distributions, using the analysis of the characteristic equation. They also demonstrated a way of approximating the delay-independent stability region using Rouche′s Theorem. Yuan and Belair [165] developed a method of assessing the stability region for a number of differential equations with distributed delay using local stability analysis. They compared the results for the three most commonly used delay distributions: Dirac delta, uniform, and general gamma distribution. They observed that for the equations considered, the stability region with the distributed delay is larger than that corresponding to the discrete delay. They also discussed Hopf bifurcation that takes place on the boundary of the stability and determined the stability and the direction of bifurcating periodic solutions. The authors established that while for their system with discrete delay stability of the steady state once lost cannot be regained, in the system with the gamma distribution, as the mean delay grows, the stability of the steady state can be regained.

1.3.2 Hopfield-type neural models

A time-delayed version of the Hopfield-type neural network was first considered by Marcus and Westervelt [94]. By assuming that the neurons are identical, and no exterior input is applied, they found sufficient conditions, which ensure the local stability of the zero steady state, and have analysed the dependence of the stability region on the time delay. Under these assumptions, after scaling their parameters, the system (1.2) can be modified into a system of delay differential equation as

$$\frac{du_k(t)}{dt} = -u_k(t) + \sum_{i=1}^{n} w_{ki} f_i(u_i(t-\tau)), \qquad k = 1, \cdots, m, \tag{1.10}$$

where $\tau \geq 0$ represents the time needed for the electric signal to propagate among the neurons.

Gopalsamy and He [50] generalised the system (1.10) by assuming that the neurons are non-identical and applying external input. Their investigation gives sufficient conditions for global asymptotic stability of the steady state, and investigates the delay-independent stability region for the Hopfield network with discrete delay. Furthermore, they have briefly discussed the distributed case of the system (1.10).

Liao *et al.* [88] considered a two neuron network with distributed delay. They have shown that a Hopf bifurcation occurs when the average delay passes through a critical value. Furthermore, they have investigated the direction of the Hopf bifurcation and the stability of the bifurcating periodic orbits by applying the normal form approach and the centre manifold reduction theory. Gupta *et al.* [55] investigated the dynamics of a three neuron network with distributed delay and self-connection. Using the weak delay kernel, they have obtained the conditions for which a Hopf bifurcation occurs. The direction and stability of the bifurcating periodic solutions are discussed by applying the normal form theory and centre manifold theorem. Han and Song [58] have analysed the effect of distributed delay in a unidirectional ring with three neurons. Taking the average delay as a bifurcation parameter, they have shown that the system undergoes Hopf bifurcation via two critical values. They have determined the stability region in a product of coupling strength and the average time delay parameter space; they have observed that the absolute stable region occupied larger space compared to the case of the system with a discrete time delay. Song *et al.* [140] generalised their result in [58] to n unidirectional neurons on a ring connected with a distributed delay. They have illustrated how the stability region of the steady state depends on the size of the network, coupling strength, and the time delay. In particular, they have noticed that as the network size gets larger, the stability region of the trivial solution shrinks.

According to Cowan [28], the firing of a neuron depends on both external input and internal interaction within the model, while Sokolove [139] considered neural adaptation in his modified model. The modification made by Ogûztöreli [108] on the other hand included the neural interaction history and the adaptation to the model in order to describe a discrete system containing a finitely many neurons. This formulation indicates that the neuron′s reaction is influenced by the input signal, the individual neuron′s history, and its coupling to other neurons. These findings suggest that the neural model is naturally better represented by inclusion of both discrete and distributed delays together [126].

Ruan and Filfil [126] have investigated the stability of steady state in a two neuron model with both discrete and distributed delays simultaneously in a model with single feedback for each neuron. Zhu and Huang [172] went further to study Ruan′s model in [126] for tri-neuron with single feedback for each neuron. Their result shows that a Hopf bifurcation can occur when the steady state loses its stability. Feng [37] has analysed a mathematical network for gene transcription model with both discrete and distributed delay simultaneously. His result shown that the distributed delay is dominated by the

discrete delay. Feng [36] has discussed the oscillatory behaviour of the solutions for a three node model with discrete and distributed delays, by using strong delay as a kernel distribution. He has formulated and proved two theorems, which ensure the existence of oscillating solutions for the model.

Despite a large number of previous research that investigated the dynamics of the individual neural networks with time delays, much less attention has been paid to the analysis of the situations when they are coupled among themselves. A decade ago, Campbell *et al.* [21] have started the investigation of two coupled sub-networks, each with three unidirectional neurons. Further, Hsu and Yang [61] considered a similar structure but with n unidirectional neurons within each sub-networks. In both studies, the authors considered only the presence of a unidirectional delayed-coupling between a single neuron of each sub-system. Peng and Song [117] have extended the research from [21] by assuming unidirectional delayed-coupling of every neuron between sub-networks. Song *et al.* [143] has considered two unidirectional sub-systems of two neurons, for which two-way coupling was included using discrete time delay. The majority of the research has concentrated on the cases, where there are no internal delays in the interactions within each of the sub-networks. Song *et al.* [141] have studied a neural network model with a discrete time delay appearing not only in the coupling between the sub-networks but also in the connection within each individual sub-network. Ge and Xu [44] have analysed the system of two coupled sub-networks, each with two neurons and four time delays. A neural model that has been studied by Mao and Wang [92, 93] consists of two and four bidirectional sub-networks, each has three neurons and bidirectional couplings between all neurons of the individual sub-network. In their models, different time delays are considered in the connection within the individual sub-network, as well as in the couplings between the sub-networks.

As noticed above, in the analysis which has been done on Hopfield-type neural network whether coupled or not, the size of the networks are always simplified to a low dimensional network. However, the actual biological network is made up of an extremely large number of interconnected neurons. The more in the dimension of the networks increases, the more complex theoretical analysis becomes. Another possibility to simplify the complexity of the network is to consider a Hopfield-type neural model with a simple architecture such as *ring network*. Even though the biological relevance of ring neural network is restricted, they may be regarded as building blocks for more realistic structures [11].

Baldi and Atiya [11] have investigated the dynamics of the unidirectional ring neural

model with time-delayed coupling, and derived conditions for the onset of oscillations, as well as bifurcation boundaries, and the periods of the bifurcating limit cycles. Campbell et al. [23] modified the model in [11] by adding self-connected delay to the system. Yuan and Campbell [166] developed the ring model further by considering bidirectional delayed coupling between neurons. In the two latter papers, the stability regions have been shown in the space of the sum of time delay coupling and the product of coupling strength parameter, and they illustrate the presence of both steady-state and Hopf bifurcation when steady state loses its stability. Xu [161] has explored the dynamics of a ring neural model with two-way delayed coupling and a delayed self-connection. By using the Lyapunov functional, the global asymptotic stability of the steady state has been shown under delay-independent and delay-dependent criteria. The steady state can also lose its stability through Hopf bifurcation, which is leading to periodic oscillation. Mitra *et al.* [99] have analysed the model based on the system with delayed unidirectional ring topology with self-feedback in the specific case of Mackey-Glass model. The authors have shown the occurrence of the phenomena such as amplitude death and synchronisation in their model. Lai *et al.* [82] have investigated multistability and bifurcation in a ring-like neural network with four units, including the cases of one-way delayed coupling and delayed self-coupling. Using Lyapunov theory, the authors have showed that the system supports a co-existence of 16 stable states with their own domains of attraction.

1.3.3 Aging transition

In large complex networks, an important practical consideration is the robustness of the network structure and function to the external perturbations and disturbances. Of a particular interest is the ability of large systems of coupled units to continue maintaining their dynamical activity when some part of the system becomes inactive due to deterioration or inactivation. In this context, an interesting phenomenon, called *aging transition* can occur in systems of coupled active (oscillatory) and inactive (non-oscillatory) elements, whereby as the fraction of inactive oscillators increases, at some point the system may completely lose its oscillatory dynamics, effectively exhibiting an amplitude death. Aging transition was originally discovered in globally coupled Stuart-Landau oscillators [30], and has been subsequently analysed in a variety of networks with different types of coupling, including examples from physical and biological systems. For instance, a macroscopic synchronisation is found among the pacemaker cells. When a disease or aging damages a ratio of cells, the lack of synchronised region indicated the need for the implantation of an electronic

pacemaker. A new alternative electronic technique aiming to create genetically engineered pacemakers has been developed in [97]. Another important example of coupled oscillators having this kind of architecture are mixed active and inactive clock cells in mammalian circadian clocks [10]. Phase transitions in a mixed population composed of active and inactive oscillators on complex network have also been theoretically analysed to derive the critical ratio using system reduction for both random and scale-free networks [150]. Apart from mixed populations of active and inactive oscillators, there are other forms of mixed populations such as excitable and oscillatory units of globally coupled oscillators [116]. A mixture of oscillatory, passive, and excitable cells have been analysed in [76]. Phase transitions in mixed populations of interacting limit cycle units and period-doubled ones with different periods have been investigated in [152]. The robustness and mismatches with respect to the effectiveness and the connection of interlayer couplings and their influence on the multilayer networks with mixed populations of oscillators have also been studied in [102]. Dynamical analysis of both weighted and unweighted, as well as homogeneous and heterogeneous networks have been analysed in [59]. The dynamical robustness procedure has been explored to argue an efficient recovery of oscillation in damaged oscillator networks [103]. The effect of the time delay on the dynamical behaviour of oscillator networks that have a mix of active and inactive oscillators has been investigated in [153]. Furthermore, the area of target inactivation and recovery in two-layer networks have been studied in [160].

Amplitude death (AD), which refers to coupling-induced suppression of oscillations, has been extensively studied in systems of coupled oscillators with both instantaneous [6, 98], and time-delayed coupling [7, 20, 120, 121, 122, 130]. While in the case of instantaneous coupling AD can only occur provided the frequencies of oscillators are sufficiently different, when there is a delay in the coupling, AD can happen even for identical oscillators. Furthermore, we mentioned earlier in the previous section that when the constant time delay is replaced by some delay distribution, it can also have a profound effect on the amplitude death and the emergence of different kinds of phase-locked solutions [78, 79, 80]. Whilst AD represents quenching of oscillations through stabilisation of a previously unstable fixed point, another possibility to suppress oscillations is through *oscillation death*, which means the emergence of a stable coupling-induced inhomogeneous steady state that did not exist in the original system [74, 75, 167]. In the specific context of aging transition, Thakur *et al.* [153] have investigated the dynamics of N globally coupled active and inactive oscillators with discrete time delay in the coupling, and they found that the time delay can be

used to decrease the coupling and the proportion of inactive oscillators above which the system exhibits aging transition.

1.3.4 Subthalamic nucleus (STN)-globus palidus (GP) model

All activities, such as movement, perception and conscious experience manifest themselves in rhythmic brain oscillations, and disruption or increased activity of neural networks can lead to various brain pathologies. Neurodegenerative diseases, including Alzheimer's disease, epilepsy, Parkinson's disease, selectively disrupt these networks, affecting various neuronal functions [51]. For instance, in Alzheimer's disease, the most prevalent form of dementia, a number of studies have shown a significantly reduced clustering coefficient associated with a lower local network connectivity [128, 149].

Parkinson's disease (PD), first identified as shaking palsy nearly 200 years ago by James Parkinson [112], is the second most common form of dementia. Symptoms include resting tremor, rigidity, slowness/absence of voluntary movement, and postural instability [31]. This is linked to the principal loss of dopaminergic neurons of the substantia nigra and leads to the reduction in the level of dopamine, which plays an important role in motor control. This affects motor functions that are regulated through the network formed by the substantia nigra and other brain structures, such as striatum, globus palidus (GP) and Subthalamic nucleus (STN), which collectively form the basal ganglia (BG). The basal ganglia regulates movement, such that, without its help, the cortex is unable to coordinate a well-executed voluntary movement. Animal and human recordings have revealed the presence of neuronal beta oscillations (10-35 Hz) in the BG network that could relate to its role in motor regulation [43]. In PD, this network becomes aberrant [138, 163, 170], and shows a persistent pattern of beta oscillations, especially in the STN and GP [89].

The pioneering work of Wilson and Cowan [158], which described the time evolution of the mean level of activity of a population of neurons, has been successfully used to understand several problems in computational neuroscience, such as visual hallucinations, and the existence of beta oscillations in the basal ganglia [33, 68]. This model and its various extensions, including modifications incorporating time delays, have played a very important role in the analysis of neural populations. In the absence of time delays, Ermentrout and Cowan used bifurcation analysis and group theory to show the existence of doubly-periodic patterns in a visual hallucinations model [33]. The olfactory bulb, which helps mammals to distinguish odours, was modelled by Li and Hopfield [87]. They showed that the odour input determines the appearance of output oscillations of the bulb. Gillies

et al. [45] have used a computational model describing STN-GP interactions, and observed that, depending on the external input, there exist three types of behaviour, such as high and low activity states, as well as repeated oscillatory bursts of high-frequency activity. Monteiro *et al.* [101] considered the Wilson-Cowan model with a non-traditional (traditionally, either hyperbolic tangent or logistic curves are chosen as transfer functions) sigmoidal function and analytically proved the existence of an stable limit cycle. Ledoux and Brunel [85] investigated the dynamics of a two-population excitatory and inhibitory neural network in the presence of time-dependent inputs with instantaneous connections, as well as in the presence of the time delays corresponding to the latencies, grow and decay times of synaptic currents between the sub-populations. In particular, they systematically analysed the dynamic behaviour of the transfer function as a function of connectivity, and showed that, depending on the connection strength and synaptic time constants, it can be low pass, or with double or single resonance. Merrison-Hort *et al.* [95] studied oscillations in a number of channels mean-field model, where each channel consists of a connected pair of STN and GP sub-populations. Using two-dimensional bifurcation analysis for each individual channel, they calculated the critical boundaries separating different dynamical regimes, such as steady state, bi-stable, and oscillatory behaviour.

The classical Wilson-Cowan model can be modified in order to account for inevitable time delays in the connections between neural populations. Whilst the stability properties and oscillations appearing in the classical model are well understood, in the presence of time delays, the stability analysis become more complicated, with stability oscillatory regions strongly dependent on the time delay [27, 83, 105, 106, 113, 114, 126, 127]. The oscillatory regime in dynamical systems is often the result of Hopf bifurcation, when a stable steady state loses its stability, resulting in the appearance of a stable limit cycle. In time-delayed dynamical systems, the existence of Hopf bifurcation is closely connected to time delays, which can destabilise a stable motion or stabilise unstable behaviour [34]. Nevado-Helgado *et al.* [106] have introduced a mathematical model that explains the generation of beta oscillations in the STN-GP circuit under the assumption of the strong connection between STN and GP. Their model also takes into account a short synaptic delay between these structures in the case when the excitatory input from the cortex to STN is stronger than the inhibitory input from striatum to GP, and the synaptic time delay between the STN and GP is negligibly small. Experimental data from an animal study suggest that the delay between STN and GP is about 6 ms [41, 73]. Pavlides *et al.* [114] modified the model first introduced in [106] in order to incorporate physiologically

relevant time delay in the STN-GP interactions, and obtained more analytical conditions on stability for realistic values of the time delay between STN and GP neural populations. Pasillas-Lépine [113] has used a modified Wilson-Cowan model with four time delays, and derived a necessary and sufficient condition for the existence and local stability of multiple steady states, as well as found a sufficient condition for the global stability of these equilibria.

1.4 Thesis outline

The thesis focusses on the mathematical analysis of the coupled systems with time-delayed connections, and each chapter is based on the following research papers:

• B. Rahman, K.B. Blyuss & Y.N. Kyrychko. Dynamics of neural systems with discrete and distributed time delays, SIAM J. Applied Dynamical Systems, Vol. 14, No. 4, pp. 2069-2095, 2015.

• B. Rahman, K.B. Blyuss, Y.N Kyrychko. Aging transition in system of oscillators with global distributed-delay coupling, submitted, 2016.

• B. Rahman, Y.N Kyrychko, K.B. Blyuss, & S.J. Hogan. Dynamics of a subthalamic nucleus-globus palidus network with three delays, in preparation, 2016.

• B. Rahman, K.B. Blyuss, Y.N Kyrychko. Dynamics of a ring neural network system with discrete and distributed delays, in preparation, 2016.

In **Chapter** 2, we study the dynamical behaviour of coupled two sub-networks with a combination of discrete and distributed time delay. In Section 2.1 we start by modifying the model for the coupled sub-networks from a single sub-network model. In Section 2.2 we derive general conditions for stability of the trivial steady state of coupled network for any distribution kernel. Section 2.3 is devoted to the analysis of the model with Dirac delta distributed kernel, and we show how one can obtain explicit conditions on the system parameters that ensure the stability of the trivial steady state. In Sections 2.4 and 2.5 we consider the cases of uniform distribution kernel, weak and strong gamma distribution kernels, find conditions on the stability of the trivial steady state, and numerically identify stability regions in the parameter space. Numerical simulations of the full nonlinear system are presented in Section 2.6, and the discussion of results is in Section 2.7.

Chapter 3 is concerned with aging transition in a system of oscillators with global distributed-delay coupling. First in Section 3.1 we derive and describe the method to reduce N-dimensional oscillators network to a two-dimensional system. In Section 3.2 aging transition in system of N globally coupled Stuart-Landau oscillators is analysed for

the case of the uniform distribution kernel. This includes finding analytical expressions for stability regions of the zero steady state, as well as numerical analysis of the eigenvalues of the corresponding characteristic equations. Section 3.3 is devoted to the analysis of aging transition for the case of gamma distribution kernel for both weak and strong cases. We illustrate how regions of amplitude death are affected by the properties of the delay distribution and the coupling parameters. In Section 3.4, direct numerical methods of the fully nonlinear system are presented, and results are summarised in Section 3.5.

In **Chapter** 4, we consider a model of the subthalamic nucleus (STN)-globus palidus (GP) network with three independent transmission delays. In Section 4.1, we introduce the model describing STN and GP neural populations. In Section 4.2, a time-shift transformation is used to reduce the number of time delays, prove positivity of solutions for all times, and implicitly calculate a steady state of the model. In Sections 4.3, we derive analytical conditions for local stability of the steady state in the case of a non-zero delay in the self-interaction of the GP population, and an instant cross-interaction between GP and STN neural populations. We also give main analytical conditions for local stability of the steady state in the case when there is a delay in the cross-interaction between GP and STN populations, and an instant self-interaction in the GP population. In Section 4.4, with the presence of delayed self-interaction in the GP population and delayed cross-interaction between STN and GP populations simultaneously. Numerical simulations of the fully nonlinear system are performed to confirm analytical conditions, and illustrate different dynamical behaviours of the system. The chapter concludes with a discussion in Section 4.5.

Chapter 5 is devoted to the analysis of the amplitude death regions for a ring neural network with both discrete and distributed delays. In Section 5.1 we perform the stability analysis of the trivial steady state of the system by looking at the characteristic equation without choosing a particular distribution, and we show how one can derive explicit conditions on the system parameters that shows a part of stability region when the actual distribution is not known. Sections 5.2 and 5.3 are complementary of Section 5.1 by considering two familiar distributions such as Dirac and weak gamma distribution kernels, where we find conditions on the stability of the trivial steady state, and identify full stability regions analytically. In Section 5.4 we give two particular examples, which confirm our analytical findings. Finally, we give the discussion of the results in Section 5.5.

Overall summary and conclusions are presented in **Chapter** 6, which also contains future potential extensions of this research.

Chapter 2

Dynamics of neural systems with discrete and distributed time delays

In this chapter, we study the stability and bifurcation of distributed delay-coupled of two sub-networks, each has two neurons with unidirectional discrete delay. First, without choosing any particular distribution kernel, we show some analytical results and determine the characteristic equation of the trivial steady state analytically for a general distribution kernel. Next, in order to make further analytical progress, we specify the most commonly used distribution kernels in the literature, namely, delta distribution, uniform distribution, and gamma distribution for both weak and strong kernels. Finally, we use numerical techniques to investigate stability properties of the fully nonlinear system. The results in this chapter have been already published [119].

2.1 Model derivation

The simplest time-delayed model, which describes neural interaction, can be written in the form

$$\begin{aligned} \dot{u}_1(t) &= -u_1(t) + a_{12} f(u_2(t-\tau)), \\ \dot{u}_2(t) &= -u_2(t) + a_{21} f(u_1(t-\tau)), \end{aligned} \tag{2.1}$$

where u_i, $i = 1, 2$, describe the voltage input of the neuron i, a_{12} and a_{21} are synaptic weights or connection strengths, τ is the synaptic time delay and $f : \mathbb{R} \to \mathbb{R}$ is a nonlinear activation/transfer function. This model can be used to describe a Hopfield network,

where individual neurons are connected to each other through an activation (or transfer) function with certain weights [60]. The time delay τ is assumed to be positive, and the connection strengths a_{12} and a_{21} can be positive or negative, describing excitatory or inhibitory connections, respectively. The dynamical properties of the system (2.1), such as stability of the steady states and existence of the Hopf bifurcation have been extensively studied by several authors (for example, [35, 94, 155], and references therein).

Despite a large number of results related to neural network models of the type shown in (2.1), systems of coupled sub-networks have received less attention. In particular, in the majority of the models considered in the literature, the connection time delay is assumed to be constant, see, for example, [21, 143]. In this analysis, we focus on the role of the distribution of delay times between the two sub-networks, rather than the influence of discrete time delays inside a single sub-network. Furthermore, we analyse the dynamics of a system where both discrete and distributed time delays are simultaneously present.

We expand the Hopfield-type model (2.1) and its modification considered in [143] by introducing a distribution of time delays in the feedback connection *between* the two sub-networks, and within each sub-network, the neurons are coupled with a constant time delay. Explicitly incorporating the above assumptions leads to the following model

$$\begin{aligned}
\dot{u}_1(t) &= -u_1(t) + a_{12} f(u_2(t-\tau)) + \alpha \int_0^\infty g(s) f(u_4(t-s)) ds, \\
\dot{u}_2(t) &= -u_2(t) + a_{21} f(u_1(t-\tau)), \\
\dot{u}_3(t) &= -u_3(t) + a_{12} f(u_4(t-\tau)) + \alpha \int_0^\infty g(s) f(u_2(t-s)) ds, \\
\dot{u}_4(t) &= -u_4(t) + a_{21} f(u_3(t-\tau)),
\end{aligned} \tag{2.2}$$

where u_i, are voltages of neurons i, $i = 1, ..., 4$, a_{12} and a_{21} denote the strength of connections between neurons within each sub-network, they can be positive or negative, and α measures the strength of the long-range coupling between the two sub-networks. We assume that locally, a time delay τ arising due to a finite speed of signal propagation between individual neurons inside each sub-network is a non-negative constant, while the long-range transmission delays between the sub-networks are characterised by a distribution with the kernel $g(\cdot)$. In the most general formulation, all neural interactions (both within and between the sub-networks) could be represented by distributed time delays. However, due to a close proximity of neurons inside each sub-network, it is reasonable to assume that the variation of the time delays in the connection between them is neg-

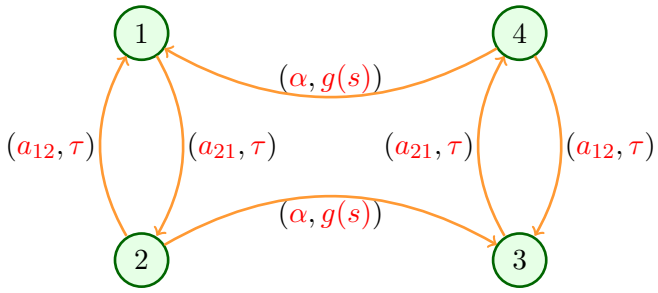

Figure 2.1: Diagrammatic sketch of the Hopfield-type neural network described by the system (2.2). The delays τ inside each of the sub-networks are assumed to be constant and discrete, and long-range interactions between the two sub-networks are represented by the distributed delay kernel $g(s)$.

ligibly small compared to the variation of the time delays in the long-range connections between sub-networks [141]. This justifies the choice of a discrete time delay within the sub-networks and distributed time delays in the interactions between them, and makes analytical investigations more tractable.

The synaptic transfer function $f : \mathbb{R} \to \mathbb{R}$ is assumed to be $\mathcal{C}^1$ and sigmoidal with a maximum slope at zero [13, 94]. For the linear stability analysis, we only require $f(0) = 0$, $f'(0) \neq 0$, and use a particular choice of $f(\cdot) = \tanh(\cdot)$ in the numerical simulations.

Without loss of generality, the distribution kernel $g(\cdot)$ is assumed to be positive-definite and normalised to unity, i.e.

$$g(s) \geq 0, \quad \int_0^\infty g(s)ds = 1.$$

The schematic sketch of the system (2.2) is shown in Figure 2.1. If the distribution kernel is taken in the form of the Dirac delta function, that is $g(s) = \delta(s)$, one recovers the instantaneous coupling between the two sub-networks, where the two sub-networks interact without time delays. If $g(s) = \delta(s - \tau)$, the coupling takes the form of a discrete time delay $\alpha f(u_i(t-\tau))$, $i = 2, 4$. Song *et al.* [143] have considered the case of discrete time delays in system (2.2) and derived conditions for stability, Hopf bifurcation and emergence of spatio-temporal patterns from bifurcating periodic solutions.

2.2 Stability Analysis

Equilibria of the system (2.2) satisfy $\dot{u}_i = 0$, $i = 1, 2, 3, 4$. Since $f(0) = 0$, the system has is a trivial steady state $(u_1, u_2, u_3, u_4) = (0, 0, 0, 0)$ and all other steady states $(u_1, u_2, u_3, u_4) = (u_1^*, u_2^*, u_3^*, u_4^*)$ satisfy

$$\begin{aligned} u_1^* &= a_{12} f(u_2^*) + \alpha \int_0^\infty g(s) f(u_4^*) ds, \\ u_2^* &= a_{21} f(u_1^*), \\ u_3^* &= a_{12} f(u_4^*) + \alpha \int_0^\infty g(s) f(u_2^*) ds, \\ u_4^* &= a_{21} f(u_3^*). \end{aligned} \tag{2.3}$$

Depending on the signs of the coupling weights a_{ij}, $i, j = 1, 2$, coupling strength α and the specific form of the transfer function f, there may exist a number of non-trivial steady states $(u_1, u_2, u_3, u_4) = (u_1^*, u_2^*, u_3^*, u_4^*)$, but their existence is not guaranteed in general [13, 141]. As mentioned above, by the assumption $f(0) = 0$, the system (2.2) always has a trivial, or rest steady state $(u_1, u_2, u_3, u_4) = (0, 0, 0, 0)$. The importance of this trivial steady state lies in the fact that it represents a state of background activity, which is fundamental for many neural processes [158, 169]. Therefore, we concentrate our analysis on the stability of the trivial steady state, and similar considerations can be made for all other steady states when they are permitted by the model. A linearisation of the system (2.2) near the trivial steady state has the form

$$\dot{\mathbf{u}}(t) = L_0 \mathbf{u}(t) + L_1 \mathbf{u}(t - \tau) + M \int_0^\infty g(s) \mathbf{u}(t - s) ds, \tag{2.4}$$

with $\mathbf{u} = (u_1, u_2, u_3, u_4)$, $L_0 = -I$, where I is the 4×4 identity matrix, and L_1 and M are given by

$$L_1 = \begin{pmatrix} 0 & a_{12}\beta & 0 & 0 \\ a_{21}\beta & 0 & 0 & 0 \\ 0 & 0 & 0 & a_{12}\beta \\ 0 & 0 & a_{21}\beta & 0 \end{pmatrix}, \quad M = \begin{pmatrix} 0 & 0 & 0 & \alpha\beta \\ 0 & 0 & 0 & 0 \\ 0 & \alpha\beta & 0 & 0 \\ 0 & 0 & 0 & 0 \end{pmatrix},$$

where $\beta = f'(0) \neq 0$. To analyse the stability of the linearised system, we assume that there are solutions of (2.4) of the form $u(t) = \mathbf{C} e^{\lambda t}$ where λ is a complex number and $\mathbf{C} = (c_1, c_2, c_3, c_4)^T \neq 0$. Substituting this into (2.4) we obtain

$$[(\lambda + 1)I - L_1 e^{-\lambda\tau} - M\widehat{G}(\lambda)]\mathbf{C} = 0,$$

and since $\mathbf{C} \neq 0$ we obtain

$$\det[\Delta(\tau, \lambda)] = \det[(\lambda + 1)I - L_1 e^{-\lambda\tau} - M\widehat{G}(\lambda)] = 0,$$

where

$$\widehat{G}(\lambda) = \int_0^\infty e^{-\lambda s} g(s) ds,$$

is the Laplace transform of the function $g(\cdot)$. The corresponding characteristic equation factorises as follows,

$$\det[\Delta(\tau, \lambda)] = \Delta_-(\tau, \lambda) \cdot \Delta_+(\tau, \lambda) = 0, \tag{2.5}$$

where $\Delta_-(\tau, \lambda)$ and $\Delta_+(\tau, \lambda)$ are given by

$$\Delta_-(\tau, \lambda) = (\lambda + 1)^2 - a_{12}a_{21}\beta^2 e^{-2\lambda\tau} - \widehat{G}(\lambda)a_{21}\alpha\beta^2 e^{-\lambda\tau}, \tag{2.6}$$

$$\Delta_+(\tau, \lambda) = (\lambda + 1)^2 - a_{12}a_{21}\beta^2 e^{-2\lambda\tau} + \widehat{G}(\lambda)a_{21}\alpha\beta^2 e^{-\lambda\tau}. \tag{2.7}$$

It is easy to see that λ is a root of the characteristic equation (2.5) if and only if it is a root of either Δ_+ or Δ_-.

Lemma 2.2.1. *$\lambda = 0$ is a solution of (2.5) if and only if $|a_{21}\alpha\beta^2| = |1 - a_{12}a_{21}\beta^2|$.*

Proof. From the factorisation of the characteristic equation $\det[\Delta(\tau, \lambda)] = \Delta_+(\tau, \lambda) \cdot \Delta_-(\tau, \lambda) = 0$ it follows that either $\Delta_+(\tau, \lambda) = 0$ or $\Delta_-(\tau, \lambda) = 0$. Computing $\widehat{G}(\lambda)$ at $\lambda = 0$, yields

$$\widehat{G}(0) = \int_0^\infty g(s) ds = 1.$$

Substituting this into $\Delta_+(\tau, 0) = 0$ and $\Delta_-(\tau, 0) = 0$ given in (2.6) and (2.7), one finds that either

$$\Delta_+(\tau, 0) = 1 - a_{12}a_{21}\beta^2 + a_{21}\alpha\beta^2 = 0,$$

or

$$\Delta_-(\tau, 0) = 1 - a_{12}a_{21}\beta^2 - a_{21}\alpha\beta^2 = 0.$$

The last two expressions imply

$$|a_{21}\alpha\beta^2| = |1 - a_{12}a_{21}\beta^2|,$$

which completes the proof. □

Next, we can determine a condition in the parameter space where the trivial steady state is unstable for any distribution $g(s)$.

Theorem 2.2.1. *If either $|a_{21}\alpha\beta^2| > |1 - a_{12}a_{21}\beta^2|$ or $|a_{21}\alpha\beta^2| < a_{12}a_{21}\beta^2 - 1$, then the characteristic equation (2.5) has a root with positive real part for any $\tau \geq 0$.*

Proof. Substituting $\lambda = 0$ into equations (2.6) and (2.7) gives

$$\det[\Delta(\tau, 0)] = \Delta_+(\tau, 0) \cdot \Delta_-(\tau, 0) = (1 - a_{12}a_{21}\beta^2 + a_{21}\alpha\beta^2) \cdot (1 - a_{12}a_{21}\beta^2 - a_{21}\alpha\beta^2).$$

Under the assumption $|a_{21}\alpha\beta^2| > |1 - a_{12}a_{21}\beta^2|$, we have either

$$\Delta_+(\tau, 0) > 0 \text{ and } \Delta_-(\tau, 0) < 0,$$

or

$$\Delta_+(\tau, 0) < 0 \text{ and } \Delta_-(\tau, 0) > 0,$$

which both imply that $\det[\Delta(\tau, 0)] < 0$. On the other hand,

$$\lim_{\lambda\to\infty} \det[\Delta(\tau, \lambda) = \lim_{\lambda\to\infty} [\Delta_+(\tau, \lambda) \cdot \Delta_-(\tau, \lambda)] = \infty.$$

Since $\det[\Delta(\tau, \lambda)]$ is a continuous function of λ, there exists $\lambda^* > 0$ such that $\det[\Delta(\tau, \lambda^*)] = 0$ for any $\tau \geq 0$ and $|a_{21}\alpha\beta^2| > |1 - a_{12}a_{21}\beta^2|$. Thus, the characteristic equation (2.5) has a real positive root.

In the case when $|a_{21}\alpha\beta^2| < a_{12}a_{21}\beta^2 - 1$, we have

$$\Delta_+(\tau, 0) < 0 \text{ and } \Delta_-(\tau, 0) < 0.$$

Since

$$\lim_{\lambda\to\infty} \Delta_+(\tau, \lambda) = \lim_{\lambda\to\infty} \Delta_-(\tau, \lambda) = \infty,$$

this implies that both $\Delta_+(\tau, \lambda)$ and $\Delta_-(\tau, \lambda)$ will cross zero at some positive λ^*, which completes the proof. □

The analytical results illustrate that for some parameters, the characteristic equation has a zero root if $|a_{21}\alpha\beta^2| = |1 - a_{12}a_{21}\beta^2|$, for any general distribution kernels. Moreover, Theorem 2.2.1 shows that the trivial steady state is unstable for any distribution kernel if either $|a_{21}\alpha\beta^2| > |1 - a_{12}a_{21}\beta^2|$ or $|a_{21}\alpha\beta^2| < a_{12}a_{21}\beta^2 - 1$.

2.3 Dirac delta function

In the case of the delay distribution being given by the Dirac delta function, we have to consider two different cases. In the case $g(s) = \delta(s - \tau)$, the system (2.2) reduces to the case of a system with discrete time delay. Song *et al.* [143] have shown that if $|a_{21}\alpha\beta^2| > 1 - a_{12}a_{21}\beta^2$, the trivial steady state of the system (2.2) with $g(s) = \delta(s - \tau)$ is unstable for all $\tau \geq 0$; if $a_{12}a_{21}\beta^2 - 1 < |a_{21}\alpha\beta^2| \leq a_{12}a_{21}\beta^2 + 1$, the trivial steady state

is stable for all $\tau \geq 0$, and if $1 + a_{12}a_{21}\beta^2 < |a_{21}\alpha\beta^2| < 1 - a_{12}a_{21}\beta^2$, there exists $\tau_0 > 0$ such that the trivial steady state is stable for all $\tau \in [0, \tau_0)$ and unstable for $\tau > \tau_0$.

Considering the distribution kernel of the form $g(s) = \delta(s)$, i.e.

$$\int_0^\infty \delta(s) f(\mathbf{u}(t-s))ds = f(\mathbf{u}(t)), \tag{2.8}$$

the system (2.4) reduces to a system with discrete time delay of the form

$$\dot{\mathbf{u}}(t) = L_0\mathbf{u}(t) + L_1\mathbf{u}(t-\tau), \tag{2.9}$$

where $\mathbf{u} = (u_1, u_2, u_3, u_4)$, L_0 and L_1 are given by

$$L_0 = \begin{pmatrix} -1 & 0 & 0 & \alpha\beta \\ 0 & -1 & 0 & 0 \\ 0 & \alpha\beta & -1 & 0 \\ 0 & 0 & 0 & -1 \end{pmatrix}, \quad L_1 = \begin{pmatrix} 0 & a_{12}\beta & 0 & 0 \\ a_{21}\beta & 0 & 0 & 0 \\ 0 & 0 & 0 & a_{12}\beta \\ 0 & 0 & a_{21}\beta & 0 \end{pmatrix}.$$

The characteristic equation of the system (2.9) can be factorized in a manner similar to (2.5):

$$\det[\Delta(\tau, \lambda)] = \Delta_-(\tau, \lambda) \cdot \Delta_+(\tau, \lambda) = 0, \tag{2.10}$$

where

$$\Delta_-(\tau, \lambda) = (\lambda + 1)^2 - a_{12}a_{21}\beta^2 e^{-2\lambda\tau} - a_{21}\alpha\beta^2 e^{-\lambda\tau}, \tag{2.11}$$

and

$$\Delta_+(\tau, \lambda) = (\lambda + 1)^2 - a_{12}a_{21}\beta^2 e^{-2\lambda\tau} + a_{21}\alpha\beta^2 e^{-\lambda\tau}. \tag{2.12}$$

In the following, we study the distribution of roots of the characteristic equation (2.10).

Lemma 2.3.1. *Let* $|1 - a_{12}a_{21}\beta^2| = |a_{21}\alpha\beta^2|$. *If*

$$1 + a_{12}a_{21}\beta^2 > 0 \quad \textit{and} \quad a_{12}a_{21}\beta^2 \neq 1, \tag{2.13}$$

or

$$1 + a_{12}a_{21}\beta^2 < 0 \quad \textit{and} \quad \tau \neq \tau_d = -\frac{2}{1 + a_{12}a_{21}\beta^2}, \tag{2.14}$$

then $\lambda = 0$ *is a simple root of the characteristic equation (2.10). If*

$$a_{12}a_{21}\beta^2 = 1, \tag{2.15}$$

or

$$1 + a_{12}a_{21}\beta^2 < 0 \quad \textit{and} \quad \tau = \tau_d, \tag{2.16}$$

then $\lambda = 0$ *is a double root of the characteristic equation (2.10).*

Proof. It follows from Lemma 2.2.1 that whenever the condition $|1-a_{12}a_{21}\beta^2| = |a_{21}\alpha\beta^2|$ holds, $\lambda = 0$ is a root of the characteristic equation (2.10). In order to determine the multiplicity of this root, we compute

$$\frac{d\Delta}{d\lambda}\Big|_{\lambda=0} = 2(1-a_{12}a_{21}\beta^2)[2+\tau(1+a_{12}a_{21}\beta^2)]. \tag{2.17}$$

If the condition (2.13) holds, then $d\Delta(\tau,0)/d\lambda \neq 0$ for any τ, implying that $\lambda = 0$ is a simple root of the characteristic equation (2.10). Likewise, if the condition (2.14) holds, it follows from (2.17) that

$$\frac{d\Delta}{d\lambda}\Big|_{\lambda=0} > 0 \quad \text{for} \quad \tau < \tau_d,$$

$$\frac{d\Delta}{d\lambda}\Big|_{\lambda=0} < 0 \quad \text{for} \quad \tau > \tau_d.$$

Hence, $\lambda = 0$ is a simple root. When the condition (2.15) is satisfied, we have

$$\frac{d\Delta}{d\lambda}\Big|_{\lambda=0} = 0, \qquad \frac{d^2\Delta}{d\lambda^2}\Big|_{\lambda=0} = 8(\tau+1)^2 > 0,$$

and, therefore, $\lambda = 0$ is a double root. Finally, if the condition (2.16) holds, one has

$$\frac{d\Delta}{d\lambda}\Big|_{\lambda=0,\tau=\tau_d} = 0, \quad \frac{d^2\Delta}{d\lambda^2}\Big|_{\lambda=0,\tau=\tau_d} = \frac{4(1-a_{12}a_{21})(a_{12}^2a_{21}^2-4a_{12}a_{21}-1)}{(1+a_{12}a_{21})^2} > 0,$$

which means that $\lambda = 0$ is a double root of the equation (2.10). This completes the proof. □

Below we concentrate on the analysis of the equation

$$\Delta_-(\tau,\lambda) = (\lambda+1)^2 - a_{12}a_{21}\beta^2 e^{-2\lambda\tau} - a_{21}\alpha\beta^2 e^{-\lambda\tau} = 0, \tag{2.18}$$

and the same analysis applies to the case of $\Delta_+(\tau,\lambda) = 0$. In order to identify further stability changes, we look for solutions in the form $\lambda = i\omega$, $\omega \neq 0$. When $\tau = 0$, $\Delta_-(\tau,\lambda) = 0$ turns into

$$\Delta_-(0,\lambda) = (\lambda+1)^2 - a_{21}\alpha\beta^2 - a_{12}a_{21}\beta^2 = 0. \tag{2.19}$$

The following lemma can be easily obtained using the Routh-Hurwitz criterion.

Lemma 2.3.2. *Assume $a_{21}\alpha\beta^2 < 1-a_{12}a_{21}\beta^2$. Then all roots of the equation (2.19) with $\tau = 0$ always have negative real parts.*

When $\tau \neq 0$, an iterative procedure can be employed to find a new function $F(\omega)$, whose roots ω give the Hopf frequency associated with purely imaginary roots of the

characteristic equation (2.18). The procedure to find the function $F(\omega)$ works as follows. Consider a general transcendental characteristic equation [53, 77, 86]

$$\Delta(\tau,\lambda)=\sum_{k=0}^{n}p_k(\lambda)e^{-k\lambda\tau}, \tag{2.20}$$

where $\tau\geq 0$, $p_k(\lambda)$, $k=0,1,2,...$ are polynomials in λ, and $|p_k(\lambda)/p_0(\lambda)|<1$, $k=1,2,...,n$, for $|\lambda|\to\infty$ and $\mathrm{Re}(\lambda)\geq 0$. Substituting $\lambda=i\omega$ into the equation (2.20) and conjugating $\Delta(\tau,i\omega)$ gives

$$\Delta(\tau,i\omega)=\sum_{k=0}^{n}p_k(i\omega)e^{-ki\omega\tau},\qquad \overline{\Delta(\tau,i\omega)}=\sum_{k=0}^{n}\overline{p_k(i\omega)}e^{ki\omega\tau}.$$

Clearly, $\Delta(\tau,i\omega)=0$ if and only if $\overline{\Delta(\tau,i\omega)}=0$. Define $\Delta^{(j)}(\tau,i\omega)$ recursively as

$$\begin{aligned}
\Delta^{(1)}(\tau,i\omega) &= \overline{p_0(i\omega)}\Delta(\tau,i\omega)-p_n(i\omega)e^{-ni\omega\tau}\overline{\Delta(\tau,i\omega)}=\sum_{k=0}^{n-1}p_k^{(1)}(i\omega)e^{-ki\omega\tau},\\
&\vdots\\
\Delta^{(j)}(\tau,i\omega) &= \overline{p_0^{(j-1)}(i\omega)}\Delta^{(j-1)}(\tau,i\omega)-p_{n-j+1}^{(j-1)}(i\omega)e^{-(n-j+1)i\omega\tau}\overline{\Delta^{(j-1)}(\tau,i\omega)}\\
&= \sum_{k=0}^{n-j}p_k^{(j)}(i\omega)e^{-ki\omega\tau},\\
&\vdots\\
\Delta^{(n-1)}(\tau,i\omega) &= p_0^{(n-1)}(i\omega)+p_1^{(n-1)}(i\omega)e^{-i\omega\tau}.
\end{aligned}$$

From $p_0^{(j+1)}(i\omega)$ we obtain

$$p_0^{(j+1)}(i\omega)=|p_0^{(j)}(i\omega)|^2-|p_{n-j}^{(j)}(i\omega)|^2,\quad j=0,1,2,\cdots,n-2.$$

Moreover, from $\Delta^{n-1}(\tau,i\omega)$, let

$$F(\omega)=|p_0^{(n-1)}(i\omega)|^2-|p_1^{(n-1)}(i\omega)|^2.$$

If $\Delta(\tau,i\omega)=0$, then ω is a root of $F(\omega)=0$.

Returning to the equation (2.18), we can use the same argument as above with $n=2$ to find the function $F(\omega)$:

$$F(\omega)=|p_0^{(1)}(i\omega)|^2-|p_1^{(1)}(i\omega)|^2. \tag{2.21}$$

where

$$\begin{aligned}
p_0^{(1)}(i\omega) &= (\omega^2+1)^2-a_{12}^2a_{21}^2\beta^4,\\
p_1^{(1)}(i\omega) &= a_{21}\alpha\beta^2[(\omega^2-1)-a_{12}a_{21}\beta^2+2i\omega].
\end{aligned} \tag{2.22}$$

The function $F(\omega)$ is explicitly given by

$$F(\omega)=\omega^8+4\omega^6+a_1\omega^4+a_2\omega^2+a_3, \tag{2.23}$$

where the coefficients a_i, $i = 1, 2, 3$, are expressed through the parameters of the system (2.2) in the following way

$$a_1 = 6 - 2a_{12}^2 a_{21}^2 \beta^4 - a_{21}^2 \alpha^2 \beta^4, \quad a_2 = 2(2 - 2a_{12}^2 a_{21}^2 \beta^4 - a_{21}^2 \alpha^2 \beta^4 + a_{21}^3 \alpha^2 a_{12} \beta^6),$$

$$a_3 = 1 - 2a_{12}^2 a_{21}^2 \beta^4 + a_{12}^4 a_{21}^4 \beta^8 - a_{21}^2 \alpha^2 \beta^4 - 2a_{21}^3 \alpha^2 a_{12} \beta^6 - a_{21}^4 \alpha^2 a_{12}^2 \beta^8.$$

Lemma 2.3.3. *If $a_3 < 0$ in (2.23), then the function $F(\omega)$ given by (2.23) has at least one positive root ω, i.e. $F(\omega) = 0$.*

Proof. Assumption $a_3 < 0$ implies that $F(0) = a_3 < 0$. Since $F(\omega)$ as defined by (2.23) is a continuous function of ω, and also $\lim_{\omega \to \infty} F(\omega) = \infty$, this means that there exists a positive root $\omega > 0$ of the equation $F(\omega) = 0$. □

Let us now consider the case when the assumption $a_3 < 0$ does not hold. Introducing the notation $s = \omega^2$, the equation $F(\omega) = 0$ can be rewritten as

$$h(s) = s^4 + 4s^3 + a_1 s^2 + a_2 s + a_3 = 0. \tag{2.24}$$

From (2.24), we have

$$h'(s) = 4s^3 + 12s^2 + 2a_1 s + a_2. \tag{2.25}$$

Existence and the number of positive roots of the equation (2.24) depend on the coefficients a_1, a_2, a_3, which themselves depend on system parameters.

Without loss of generality, suppose that the equation (2.24) has four positive roots denoted by s_1, s_2, s_3, s_4. Then the equation $F(\omega) = 0$ will have four positive real roots

$$\omega_1 = \sqrt{s_1}, \ \omega_2 = \sqrt{s_2}, \ \omega_3 = \sqrt{s_3}, \ \omega_4 = \sqrt{s_4}.$$

On the other hand, substituting $\lambda = i\omega$ into (2.18) gives

$$(i\omega + 1)^2 - a_{21}\alpha\beta^2 e^{-i\omega\tau} - a_{12}a_{21}\beta^2 e^{-2i\omega\tau} = 0. \tag{2.26}$$

Separating this equation into real and imaginary parts yields

$$\begin{aligned} -\omega_k^2 + 1 &= a_{21}\alpha\beta^2 \cos(\omega_k \tau_k) + a_{12}a_{21}\beta^2 \cos(2\omega_k \tau_k), \\ -2\omega_k &= a_{21}\alpha\beta^2 \sin(\omega_k \tau_k) + a_{12}a_{21}\beta^2 \sin(2\omega_k \tau_k), \end{aligned} \tag{2.27}$$

where $k = 1, 2, 3, 4$. Using trigonometric formulas, the system (2.27) can be rewritten in the form

$$\begin{aligned} \cos(\omega_k \tau_k) &= \frac{-a_{21}\alpha\beta^2 \pm \sqrt{a_{21}^2\alpha^2\beta^4 + 8a_{12}^2a_{21}^2\beta^4 + 8a_{12}a_{21} - 8a_{12}a_{21}\omega_k^2}}{a_{12}a_{21}\beta}, \\ \sin(\omega_k \tau_k) &= \frac{4\omega_k}{\beta(-a_{21}\alpha\beta^2 \pm \sqrt{a_{21}^2\alpha^2\beta^4 + 8a_{12}^2a_{21}^2\beta^4 + 8a_{12}a_{21} - 8a_{12}a_{21}\omega_k^2})}. \end{aligned} \tag{2.28}$$

Dividing the equations (2.28), we obtain

$$\tau_k^j = \frac{1}{\omega_k}\left[\arctan\left(\frac{-2\omega_k}{1-\omega_k^2+a_{12}a_{21}\beta^2}\right)+j\pi\right], \tag{2.29}$$

where $k=1,2,3,4$, $j=0,1,2,....$ Therefore, the solutions of the equation (2.26) are pairs (τ_k^j,ω_k), where $\lambda=\pm i\omega_k$ are pairs of purely imaginary roots of (2.18) with $\tau=\tau_k^j$. Define

$$\tau_0=\tau_{k_0}^0=\min_{1\le k\le 4}\{\tau_k^0\},\ \omega_0=\omega_{k_0},\quad k_0\in\{1,2,3,4\}.$$

Then τ_0 is the first value of the time delay τ for which the roots of the characteristic equation (2.18) cross the imaginary axis. Let $\lambda(\tau)=\alpha(\tau)\pm i\omega(\tau)$ be the root of equation (2.11) near $\tau=\tau_k^0$ satisfying $\alpha(\tau_k^0)=0$, $\omega(\tau_k^0)=\omega_0$. It can be easily shown that the following transversality condition holds.

Lemma 2.3.4. *Suppose $h'(s_0)\neq 0$ and $p_0^{(1)}(\omega_0)\neq 0$, where $h(s)$ and $p_0^{(1)}(\omega_0)$ are defined in (2.22) and (2.24), respectively, and $s_0=\omega_0^2$. Then the following transversality condition holds*

$$\operatorname{sgn}\left\{\frac{d\mathrm{Re}[\lambda(\tau)]}{d\tau}\bigg|_{\tau=\tau_k^0}\right\}=\operatorname{sgn}\left[p_0^{(1)}(\omega_0)h'(s_0)\right].$$

Proof. Substituting $\lambda(\tau)$ into the characteristic equation (2.18) and taking derivative with respect to τ gives

$$\left\{\frac{d\lambda(\tau)}{d\tau}\right\}^{-1}=-\frac{2\lambda+2}{2a_{12}a_{21}\beta^2\lambda e^{-2\lambda\tau}+a_{21}\alpha\beta^2\lambda e^{-\lambda\tau}}-\frac{\tau}{\lambda}.$$

From this equation, one can find

$$\left\{\frac{d\mathrm{Re}\{\lambda(\tau)\}}{d\tau}\right\}^{-1}_{\tau=\tau_k^0}=\mathrm{Re}\left\{-\frac{2\lambda+2}{2a_{12}a_{21}\beta^2\lambda e^{-2\lambda\tau}+a_{21}\alpha\beta^2\lambda e^{-\lambda\tau}}\right\}_{\tau=\tau_k^0}-\mathrm{Re}\left\{\frac{\tau}{\lambda}\right\}_{\tau=\tau_k^0}$$

$$=\frac{2\omega_0\left[2\omega_0a_{12}a_{21}\beta^2\cos(2\omega_0\tau_k^0)+2a_{12}a_{21}\beta^2\sin(2\omega_0\tau_k^0)+\omega_0a_{21}\alpha\beta^2\cos(\omega_0\tau_k^0)+a_{21}\alpha\beta^2\sin(\omega_0\tau_k^0)\right]}{\left[2\omega_0a_{12}a_{21}\beta^2\sin(2\omega_0\tau_k^0)+\omega_0a_{21}\alpha\beta^2\sin(\omega_0\tau_k^0)\right]^2+\left[2\omega_0a_{12}a_{21}\beta^2\cos(2\omega_0\tau_k^0)+\omega_0a_{21}\alpha\beta^2\cos(\omega_0\tau_k^0)\right]^2}.$$

Using (2.27) and (2.28), this expression can simplified into

$$\left\{\frac{d\mathrm{Re}\{\lambda(\tau)\}}{d\tau}\right\}^{-1}_{\tau=\tau_k^0}=\frac{\omega_0^2\left[4\omega_0^6+12\omega_0^4+2(6-2a_{12}^2a_{21}^2\beta^4-a_{21}^2\alpha^2\beta^4)\omega_0^2\right]}{\Lambda(\omega_0^4+2\omega_0^2+1-a_{12}^2a_{21}^2\beta^4)}$$

$$+\frac{\omega_0^2\left[2(2-2a_{12}^2a_{21}^2\beta^4-a_{21}^2\alpha^2\beta^4-a_{21}^3\alpha^2a_{12}\beta^6)\right]}{\Lambda(\omega_0^4+2\omega_0^2+1-a_{12}^2a_{21}^2\beta^4)}=\frac{s_0\left[4s_0^3+12s_0^2+2a_1s_0+a_2\right]}{\Lambda p_0^{(1)}(\omega_0)},$$

where

$$\Lambda=\left[2\omega_0a_{12}a_{21}\beta^2\sin(2\omega_0\tau_k^0)+\omega_0a_{21}\alpha\beta^2\sin(\omega_0\tau_k^0)\right]^2$$
$$+\left[2\omega_0a_{12}a_{21}\beta^2\cos(2\omega_0\tau_k^0)+\omega_0a_{21}\alpha\beta^2\cos(\omega_0\tau_k^0)\right]^2,$$

and $p_0^{(1)}(\omega_0)=(\omega_0^2+1)^2-a_{12}^2a_{21}^2\beta^4$. Since $s_0=\omega_0^2>0$ and $\Lambda>0$, this implies

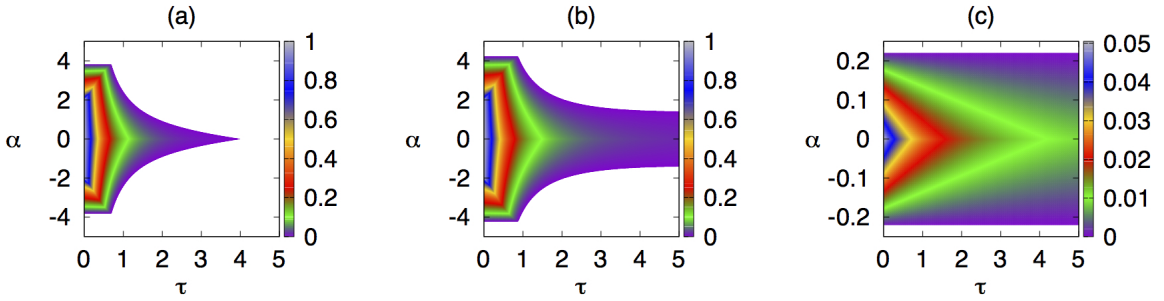

Figure 2.2: Stability regions of the trivial steady state of the system (2.2) with delta distribution $g(s) = \delta(s)$ and $a_{12} = 2$, $\beta = 1$. (a) $a_{21} = -0.55$. (b) $a_{21} = -0.45$. (c) $a_{21} = 0.45$. Colour code denotes $[-\max\{\mathrm{Re}(\lambda)\}]$ for $\max\{\mathrm{Re}(\lambda)\} \leq 0$.

$$\mathrm{sgn}\left\{\frac{d\mathrm{Re}[\lambda(\tau)]}{d\tau}\bigg|_{\tau=\tau_k^0}\right\} = \mathrm{sgn}\left\{\frac{d\mathrm{Re}[\lambda(\tau)]}{d\tau}\bigg|_{\tau=\tau_k^0}\right\}^{-1} = \mathrm{sgn}\left\{\frac{1}{\Lambda p_0^{(1)}(\omega_0)}h'(s_0)\right\} = \mathrm{sgn}[p_0^{(1)}(\omega_0)h'(s_0)],$$

which completes the proof. □

By Lemmas 2.3.2 and 2.3.4, we have the following result regarding the stability of the trivial steady state of the system (2.2) and the existence of the Hopf bifurcation.

Theorem 2.3.1. *Suppose* $|a_{21}\alpha\beta^2| < |1 - a_{12}a_{21}\beta^2|$. *If the equation (2.24) has at least one positive root,* $p_0^{(1)}(\omega_0) \neq 0$ *and* $h'(s_0) \neq 0$, *then the trivial steady state of the system (2.2) is stable for* $0 \leq \tau < \tau_0$, *and undergoes a Hopf bifurcation at a critical value of the time delay* $\tau = \tau_0$.

In order to illustrate the effects of varying the coupling strength α and the time delay τ on the stability of the trivial steady state, we numerically compute stability boundaries of this steady state in the $\alpha - \tau$ plane using a pseudospectral algorithm developed by Breda *et al.* in [19].

Figure 2.2 (a) shows a closed stability region in the $\alpha - \tau$ plane for the case when $a_{12} = 2$, $a_{21} = -0.55$ and $\beta = 1$. We can observe that the steady state is stable inside the coloured region, where colour corresponds to $[-\max\{\mathrm{Re}(\lambda)\}]$ for $\max\{\mathrm{Re}(\lambda)\} \leq 0$. For small values of the time delay τ, there is a large interval of the coupling strength values, where the steady state is stable. As τ gets larger, the stability region become narrower, and eventually, for large enough values of the time delay τ, the trivial steady state becomes unstable independently of the value of the coupling strength α. The situation for any values of the parameters a_{12}, a_{21} and β satisfying $a_{12}a_{21}\beta^2 < -1$ is qualitatively the same as the one shown in Figure 2.2 (a).

In the case when the parameters of the system (2.2) satisfy the condition $-1 \leq a_{12}a_{21}\beta^2 < 0$, the stability region is illustrated in Figure 2.2 (b). One can see that compared to the case $a_{12}a_{21}\beta^2 < -1$, the stability region is larger, and for all values of the time delay τ, there is always a range of values of the coupling strength α, for which the trivial steady state of the system (2.2) is stable. It is noteworthy that whenever a_{12} and a_{21} have opposite signs, the boundary of the stability region consists of two parts. The trivial steady state can lose its stability via a Hopf bifurcation in accordance with Theorem 2.3.1 or undergo a steady-state bifurcation, as described in Lemma 2.3.1. In Figures 2.2 (a) and (b), the horizontal part of the stability boundary corresponds to $|1-a_{12}a_{21}\beta^2| = |a_{21}\alpha\beta^2|$.

If $0 \leq a_{12}a_{21}\beta^2 \leq 1$, the trivial steady state can only lose its stability via a steady-state bifurcation as shown in Figure 2.2 (c). Once again, the horizontal boundaries are defined by $|1 - a_{12}a_{21}\beta^2| = |a_{21}\alpha\beta^2|$. Finally, for $a_{12}a_{21}\beta^2 > 1$, the trivial steady state is always unstable independently of the time delay τ, following the results of Theorem 2.2.1.

2.4 Uniform distribution kernel

In this section we consider the system (2.2) in the case of the uniformly distributed kernel (1.6). Taking the Laplace transform of the uniform distribution $g(s)$ given in (1.6), we obtain

$$\widehat{G}(\lambda) = \frac{1}{2\sigma\lambda}e^{-\lambda\tau}(e^{\lambda\sigma} - e^{-\lambda\sigma}) = e^{-\lambda\tau}\frac{\sinh(\lambda\sigma)}{\lambda\sigma}. \tag{2.30}$$

Lemma 2.4.1. *Let $|1-a_{12}a_{21}\beta^2| = |a_{21}\alpha\beta^2|$. If $a_{12}a_{21}\beta^2 \neq 1$, then $\lambda = 0$ is a simple root of the characteristic equation (2.5) with the delay kernel (1.6), otherwise, it is a double root.*

The proof of Lemma 2.4.1 is analogous to the proof of Lemma 2.3.1.

Substituting the Laplace transform (2.30) into the characteristic equation (2.6) and looking for solutions in the form $\lambda = i\omega$ yields

$$(i\omega + 1)^2 - [a_{12}a_{21}\beta^2 + a_{21}\alpha\beta^2\gamma(\omega,\sigma)]e^{-2i\omega\tau} = 0, \tag{2.31}$$

where

$$\gamma(\omega,\sigma) = \frac{\sin(\omega\sigma)}{\omega\sigma}.$$

Separating equation (2.31) into real and imaginary parts gives

$$\begin{aligned} -\omega^2 + 1 &= [a_{12}a_{21}\beta^2 + a_{21}\alpha\beta^2\gamma(\omega,\sigma)]\cos(2\omega\tau), \\ -2\omega &= [a_{12}a_{21}\beta^2 + a_{21}\alpha\beta^2\gamma(\omega,\sigma)]\sin(2\omega\tau). \end{aligned} \tag{2.32}$$

Squaring and adding the last two equations gives a transcendental equation for the Hopf frequency ω

$$\omega^2 + 1 = \pm[a_{12}a_{21}\beta^2 + a_{21}\alpha\beta^2\gamma(\omega, \sigma)]. \tag{2.33}$$

In a similar way, dividing the two equations in (2.32), we obtain

$$\tan(2\omega\tau) = \frac{2\omega}{\omega^2 - 1}. \tag{2.34}$$

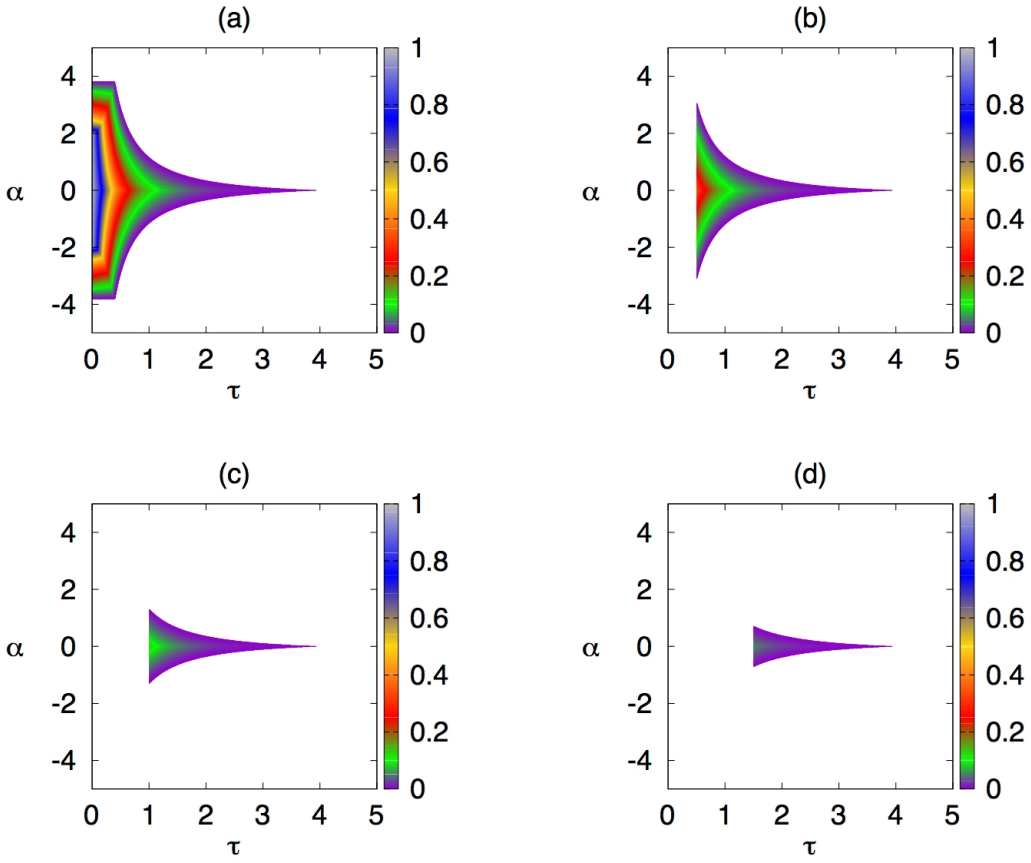

Figure 2.3: Stability region of the trivial steady state of the system (2.2) with the uniform distribution (1.6) for $a_{12} = 2$, $a_{21} = -0.55$, and $\beta = 1$. Colour code denotes $[-\max\{\mathrm{Re}(\lambda)\}]$ for $\max\{\mathrm{Re}(\lambda)\} \leq 0$. (a) $\sigma = 0$, (b) $\sigma = 0.5$, (c) $\sigma = 1$ and (d) $\sigma = 1.5$.

To illustrate the effects of changing the coupling between the two sub-networks α and the time delay τ on stability of the trivial steady state, we numerically find the stability boundary in the $\alpha - \tau$ plane parametrised by the Hopf frequency ω. We rewrite the linearised system with the uniformly distributed kernel as follows

$$\dot{\mathbf{u}}(t) = L_0\mathbf{u}(t) + L_1\mathbf{u}(t-\tau) + \frac{\alpha}{2\sigma}\int_{-(\tau+\sigma)}^{-(\tau-\sigma)} M\mathbf{u}(t+s)ds, \tag{2.35}$$

where $\mathbf{u} = (u_1, u_2, u_3, u_4)$, $L_0 = -I$, I is the 4×4 identity matrix, and L_1 and M are

given by

$$L_1 = \begin{pmatrix} 0 & a_{12}\beta & 0 & 0 \\ a_{21}\beta & 0 & 0 & 0 \\ 0 & 0 & 0 & a_{12}\beta \\ 0 & 0 & a_{21}\beta & 0 \end{pmatrix}, \qquad M = \begin{pmatrix} 0 & 0 & 0 & \beta \\ 0 & 0 & 0 & 0 \\ 0 & \beta & 0 & 0 \\ 0 & 0 & 0 & 0 \end{pmatrix}.$$

The system (2.35) is now in the form suitable for computing the maximum real part of the characteristic eigenvalues using the algorithm described in [19] and implemented in traceDDE suite in MATLAB.

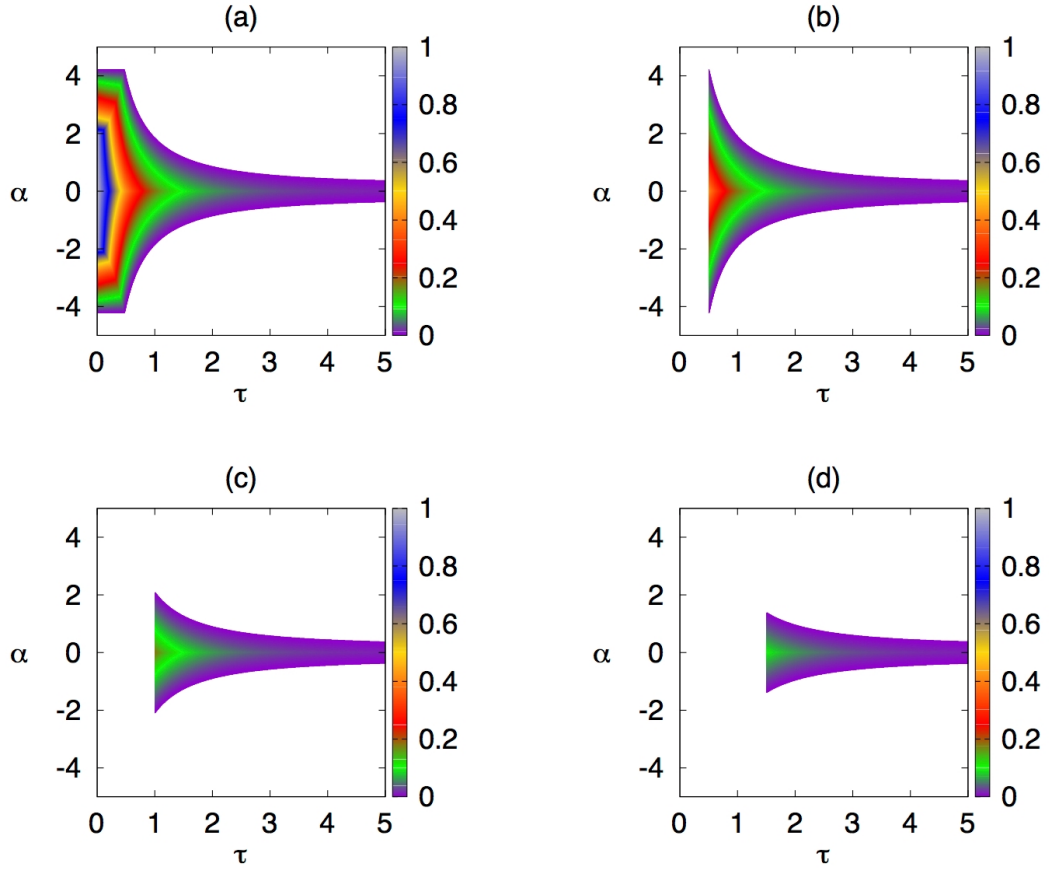

Figure 2.4: Stability region of the trivial steady state of the system (2.2) with the uniform distribution (1.6) for $a_{12} = 2$, $a_{21} = -0.45$ and $\beta = 1$. Colour code denotes $[-\max\{\mathrm{Re}(\lambda)\}]$ for $\max\{\mathrm{Re}(\lambda)\} \leq 0$. (a) $\sigma = 0$, (b) $\sigma = 0.5$, (c) $\sigma = 1$ and (d) $\sigma = 1.5$.

If $\sigma = 0$, the last term in the equation (2.35) becomes $\alpha M\mathbf{u}(t-\tau)$, and the system (2.2) reduces to the system with a single discrete time delay τ, which was analysed in [143]. When $\sigma \neq 0$, we have to consider separately different values of $a_{12}a_{21}\beta^2$, and compute the stability of the trivial steady state of the system (2.2) as the distribution width σ is varied. Figure 2.3 shows the stability boundary when the condition $a_{12}a_{21}\beta^2 < -1$ is satisfied. In this case, when $\sigma = 0$, the stability region is the same as in the case of a single discrete

time delay and coincides with the Figure 2.2 (a), where for $\tau = 0$, there is an interval of α values, for which the trivial steady state of the system (2.2) is stable. As σ is increased, the stability region detaches from the α-axis, and for $\tau = 0$ it is not possible to stabilise the trivial steady state, as shown in Figure 2.3 (b). In Figures 2.3 (c) and (d), increasing σ further still leads to shrinking of the stability region in the $\alpha - \tau$ plane, thus reducing the range of α values for which the trivial steady state of the system (2.2) is stable.

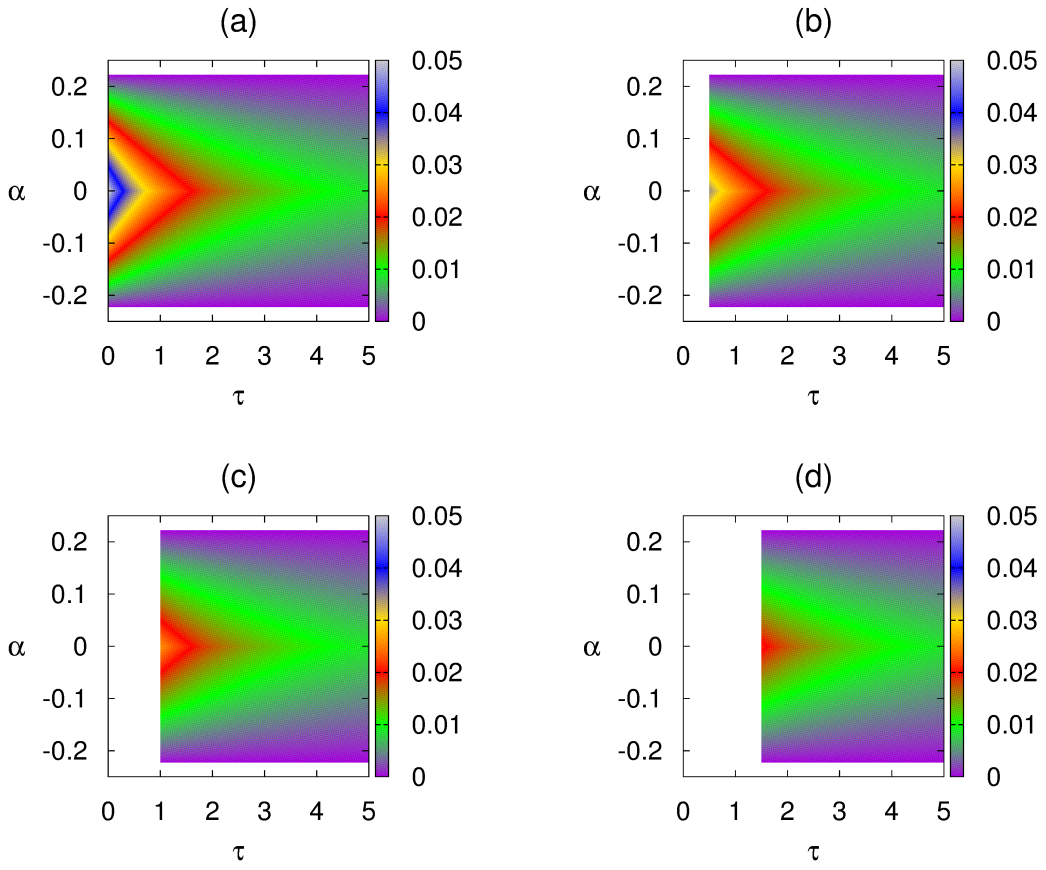

Figure 2.5: Stability region of the trivial steady state of the system (2.2) with the uniform distribution (1.6) for $a_{12} = 2$, $a_{21} = 0.45$ and $\beta = 1$. Colour code denotes $[-\max\{\mathrm{Re}(\lambda)\}]$ for $\max\{\mathrm{Re}(\lambda)\} \leq 0$. (a) $\sigma = 0$, (b) $\sigma = 0.5$, (c) $\sigma = 1$ and (d) $\sigma = 1.5$.

In the case when parameter values of the system (2.2) satisfy the condition $-1 \leq a_{12}a_{21}\beta^2 < 0$ with $\sigma = 0$, we again recover the case of a single discrete time delay, and the stability region shown in Figure 2.4 (a) is the same as in Figure 2.2 (b). As the distribution width is increased, as shown in Figures 2.4 (b)-(d), it is no longer possible to stabilise the trivial steady state with $\tau = 0$ for any values of the coupling strength α. Moreover, the larger the distribution width, the smaller is the interval of α values where the stability is observed. However, unlike the situation when $a_{12}a_{21}\beta^2 < -1$, in this case, the stability

region does not become an isolated island but rather becomes a narrow stretch in the $\alpha-\tau$ plane.

For the case when the parameter values $a_{12}a_{21}\beta^2 \in [0,1]$, the stability region does not depend on the time delay τ and the trivial steady state loses its stability only through steady-state bifurcation in horizontal lines $|1-a_{12}a21\beta^2| = |a_{21}\alpha\beta|$ as shown in Figure 2.5. Figure 2.5 (a) once again coincides with Figure 2.2 (c) for single discrete delay case when $\sigma = 0$. Further, when σ increases, similar to the previous cases $-1 \leq a_{12}a_{21}\beta^2 < 0$ and $a_{12}a_{21}\beta^2 < -1$, the stability region detaches from α-axis, and for $\tau = 0$ it is no longer possible to stabilise the trivial steady state with $\tau = 0$ as shown in Figure 2.5 (b)-(d). For $a_{12}a_{21}\beta^2 > 1$, the trivial steady state is unstable for any $\tau \geq 0$ and any σ.

2.5 Gamma distribution kernel

In this section we consider the gamma distribution kernel (1.7) to analyse the stability of the trivial steady state of the system (2.2). One can use the same strategy as in the previous Section by taking the Laplace transform of the distribution kernel, which gives

$$\widehat{G}(\lambda) = \left(\frac{\gamma}{\lambda+\gamma}\right)^r. \tag{2.36}$$

Recalling the characteristic equation (2.5) and substituting the Laplace transform (2.36) into (2.6) and (2.7), we get

$$\Delta_-(\tau,\lambda) = (\lambda+\gamma)^r(\lambda+1)^2 - (\lambda+\gamma)^r a_{12}a_{21}\beta^2 e^{-2\lambda\tau} - \lambda^r a_{21}\alpha\beta^2 e^{-\lambda\tau} = 0, \tag{2.37}$$

$$\Delta_+(\tau,\lambda) = (\lambda+\gamma)^r(\lambda+1)^2 - (\lambda+\gamma)^r a_{12}a_{21}\beta^2 e^{-2\lambda\tau} + \lambda^r a_{21}\alpha\beta^2 e^{-\lambda\tau} = 0. \tag{2.38}$$

For $r = 1$, the gamma distribution becomes an exponential distribution, also called a *weak delay kernel*. For $r = 2$, the gamma distribution (1.7) is called a *strong delay kernel*. We analyse both cases in the following two subsections.

2.5.1 Weak gamma distributed delayed kernel

In this subsection we consider the system (2.2) with a weak distribution kernel (1.7), i.e. $r = 1$. The analysis of the characteristic equation can be performed either by using the Laplace transform (2.36), or employing the *linear chain trick* described in [91]. The linear chain trick allows one to replace the original system with discrete and distributed delays by the system of delay differential equations with discrete time delay only. Introducing

the new variables

$$u_5(t) = \int_0^\infty \gamma e^{-\gamma s} u_2(t-s)ds,$$

$$u_6(t) = \int_0^\infty \gamma e^{-\gamma s} u_4(t-s)ds,$$

allows one to rewrite the system (2.2) as follows

$$\begin{cases} \dot{u}_1(t) = -u_1(t) + a_{12}\beta u_2(t-\tau) + \alpha\beta u_6(t), \\ \dot{u}_2(t) = -u_2(t) + a_{21}\beta u_1(t-\tau), \\ \dot{u}_3(t) = -u_3(t) + a_{12}\beta u_4(t-\tau) + \alpha\beta u_5(t), \\ \dot{u}_4(t) = -u_4(t) + a_{21}\beta u_3(t-\tau), \\ \dot{u}_5(t) = \gamma u_2(t) - \gamma u_5(t), \\ \dot{u}_6(t) = \gamma u_4(t) - \gamma u_6(t). \end{cases} \tag{2.39}$$

The characteristic equation (2.5) for the system (2.39) with weak distribution kernel has the form

$$\det[\Delta(\tau,\lambda)] = \Delta_-(\tau,\lambda)\cdot\Delta_+(\tau,\lambda) = 0, \tag{2.40}$$

where

$$\Delta_-(\tau,\lambda) = (\lambda+\gamma)(\lambda+1)^2 - (\lambda+\gamma)a_{12}a_{21}\beta^2 e^{-2\lambda\tau} - \gamma a_{21}\alpha\beta^2 e^{-\lambda\tau}, \tag{2.41}$$

and

$$\Delta_+(\tau,\lambda) = (\lambda+\gamma)(\lambda+1)^2 - (\lambda+\gamma)a_{12}a_{21}\beta^2 e^{-2\lambda\tau} + \gamma a_{21}\alpha\beta^2 e^{-\lambda\tau}. \tag{2.42}$$

Lemma 2.5.1. *Let* $|1 - a_{12}a_{21}\beta^2| = |a_{21}\alpha\beta^2|$. *If*

$$-1 \le a_{12}a_{21}\beta^2 \le 1 + 2\gamma \quad \textit{and} \quad a_{12}a_{21}\beta^2 \ne 1,$$

or

$$a_{12}a_{21}\beta^2 > 1 + 2\gamma \quad \textit{or} \quad a_{12}a_{21}\beta^2 < -1 \quad \textit{and} \quad \tau \ne \tau_\gamma = \frac{a_{12}a_{21}\beta^2 - 2\gamma - 1}{\gamma(1 + a_{12}a_{21}\beta^2)},$$

then $\lambda = 0$ *is a simple root of the characteristic equation (2.40). If*

$$a_{12}a_{21}\beta^2 = 1,$$

or

$$a_{12}a_{21}\beta^2 > 1+2\gamma \quad or \quad a_{12}a_{21}\beta^2 < -1 \quad and \quad \tau = \tau_\gamma,$$

then $\lambda = 0$ is a double root of the characteristic equation (2.40).

The proof of Lemma 2.5.1 is similar to the proof of Lemma 2.3.1.

We will analyse the case of $\Delta_-(\tau,\lambda)$ given by (2.41), and the analysis is the same for $\Delta_+(\tau,\lambda)$ in (2.42). The transcendental equation for eigenvalues λ for $\Delta_-(\tau,\lambda)$ has the form:

$$\Delta_-(\tau,\lambda) = (\lambda+\gamma)(\lambda+1)^2 - (\lambda+\gamma)a_{12}a_{21}\beta^2 e^{-2\lambda\tau} - \gamma a_{21}\alpha\beta^2 e^{-\lambda\tau} = 0. \tag{2.43}$$

Note that when $\tau = 0$, this equation reduces to

$$\lambda^3 + (\gamma+2)\,\lambda^2 + \left(2\,\gamma + 1 - a_{12}a_{21}\beta^2\right)\lambda + \gamma(1 - a_{12}a_{21}\beta^2 - \, a_{21}\alpha\,\beta^2) = 0. \tag{2.44}$$

In view of the Routh-Hurwitz criterion, we have the following result.

Lemma 2.5.2. *Assume that condition*

$$a_{21}a_{12}\beta^2 < \min\{2\gamma+1, 1-a_{21}\alpha\beta^2\} \tag{2.45}$$

holds. Then all roots of the equation (2.44) have negative real part.

When $\tau > 0$, we can use the same technique as in the case of the delta distributed kernel in order to calculate $F(\omega)$ as follows:

$$\begin{aligned} p_0^{(1)}(i\omega) &= \left[\gamma - (\gamma+2)\,\omega^2\right]^2 + \left[\omega^3 - (2\,\gamma+1)\,\omega\right]^2 - \left(\gamma^2+\omega^2\right) {a_{21}}^2\beta^4 {a_{12}}^2, \\ p_1^{(1)}((i\omega) &= -a_{21}\alpha\,\beta^2\gamma^2 + a_{21}\alpha\,\beta^2\gamma^2\omega^2 + 2\,a_{21}\alpha\,\beta^2\gamma\,\omega^2 - {a_{21}}^2\alpha\,\beta^4 a_{12}\gamma^2 \\ &\quad + \left(-a_{21}\alpha\,\beta^2\gamma\,\omega^3 + 2\,a_{21}\alpha\,\beta^2\gamma^2\omega + a_{21}\alpha\,\beta^2\gamma\,\omega - {a_{21}}^2\alpha\,\beta^4 a_{12}\gamma\,\omega\right) i, \end{aligned} \tag{2.46}$$

and, hence,

$$F(\omega) = \omega^{12} + b_1\omega^{10} + b_2\omega^8 + b_3\omega^6 + b_4\omega^4 + b_5\omega^2 + b_6, \tag{2.47}$$

where

$$b_1 = 2\gamma^2 + 4, \quad b_2 = -2\,{a_{12}}^2{a_{21}}^2\beta^4 + 8\,\gamma^2 + \gamma^4 + 6,$$

$$b_3 = -4\,{a_{12}}^2{a_{21}}^2\beta^4 + 4 + 12\,\gamma^2 + 4\,\gamma^4 - {a_{21}}^2\alpha^2\beta^4\gamma^2 - 4\,{a_{12}}^2{a_{21}}^2\beta^4\gamma^2,$$

$$b_4 = 1 + 6\,\gamma^4 - 8\,{a_{12}}^2{a_{21}}^2\beta^4\gamma^2 - 2\,\gamma^4{a_{12}}^2{a_{21}}^2\beta^4 - 2\,{a_{12}}^2{a_{21}}^2\beta^4 + {a_{12}}^4{a_{21}}^4\beta^8$$

$$-2\,{a_{21}}^2\alpha^2\beta^4\gamma^2 + 8\,\gamma^2 - {a_{21}}^2\alpha^2\beta^4\gamma^4 - 2\,{a_{21}}^3\alpha^2\beta^6\gamma^2 a_{12},$$

$$b_5 = 4\,\gamma^4 + 2\,\gamma^2 - 4\,\gamma^4{a_{12}}^2{a_{21}}^2\beta^4 + 8\,{a_{21}}^3\alpha^2\beta^6\gamma^3 a_{12} + 2\,{a_{12}}^4{a_{21}}^4\beta^8\gamma^2 - {a_{21}}^2\alpha^2\beta^4\gamma^2$$

$$+2\,{a_{21}}^3\alpha^2\beta^6\gamma^4 a_{12} - {a_{21}}^4\alpha^2\beta^8{a_{12}}^2\gamma^2 2\,{a_{21}}^2\alpha^2\beta^4\gamma^4 - 4\,{a_{12}}^2{a_{21}}^2\beta^4\gamma^2 + 2\,{a_{21}}^3\alpha^2\beta^6\gamma^2 a_{12},$$

$$b_6 = -{a_{21}}^2\alpha^2\beta^4\gamma^4 - 2\,{a_{21}}^3\alpha^2\beta^6\gamma^4 a_{12} - 2\,\gamma^4{a_{12}}^2{a_{21}}^2\beta^4 - {a_{21}}^4\alpha^2\beta^8{a_{12}}^2\gamma^4 + {a_{12}}^4{a_{21}}^4\beta^8\gamma^4 + \gamma^4.$$

Lemma 2.5.3. *Assume that $b_6 < 0$. Then the equation $F(\omega) = 0$ has at least one positive root.*

Proof. Assumption $b_6 < 0$ implies that $F(0) = b_6 < 0$. Since $F(\omega)$ as defined by (2.47) is a continuous function of ω, and also $\lim_{\omega\to\infty} F(\omega) = \infty$, this means that there exists a positive root $\omega > 0$ of the equation $F(\omega) = 0$. □

Let $s = \omega^2$, then the equation $F(\omega) = 0$ becomes

$$h(s) = s^6 + b_1 s^5 + b_2 s^4 + b_3 s^3 + b_4 s^2 + b_5 s + b_6 = 0. \tag{2.48}$$

Without loss of generality, suppose that the equation (2.48) has six positive roots, denoted by $s_1, s_2, s_3, s_4, s_5, s_6$, respectively. This implies that the equation $F(\omega) = 0$ also has six positive real roots given by

$$\omega_1 = \sqrt{s_1},\ \omega_2 = \sqrt{s_2},\ \omega_3 = \sqrt{s_3},\ \omega_4 = \sqrt{s_4},\ \omega_5 = \sqrt{s_5},\ \omega_6 = \sqrt{s_6}.$$

At the same time, substituting $\lambda = i\omega$, $\omega > 0$ into the equation (2.43) we obtain

$$(i\omega + \gamma)(i\omega + 1)^2 e^{i\omega\tau} - \gamma a_{21}\alpha\beta^2 - (i\omega + \gamma)a_{12}a_{21}\beta^2 e^{-i\omega\tau} = 0. \tag{2.49}$$

Separating this equation into the real and imaginary parts gives

$$\gamma(-\omega^2 + 1) - 2\omega^2 - \gamma a_{21}\alpha\beta^2\cos(\omega\tau) = \gamma a_{12}a_{21}\beta^2\cos(2\omega\tau) + \omega a_{12}a_{21}\beta^2\sin(2\omega\tau),$$

$$\omega(-\omega^2 + 1) + 2\gamma\omega + \gamma a_{21}\alpha\beta^2\sin(\omega\tau) = \omega a_{12}a_{21}\beta^2\cos(2\omega\tau) - \gamma a_{12}a_{21}\beta^2\sin(2\omega\tau). \tag{2.50}$$

Using trigonometric formulas, the system (2.50) can be simplified as follows

$$(1-\omega^2+a_{12}a_{21}\beta^2)\gamma-2\omega^2$$

$$=\left[\gamma a_{21}\alpha\beta^2+2\gamma a_{12}a_{21}\beta^2\cos(\omega\tau)+2\omega a_{12}a_{21}\beta^2\sin(\omega\tau)\right]\cos(\omega\tau),$$

$$\omega(1-\omega^2+2\gamma-a_{12}a_{21}\beta^2)$$

$$=-\left[\gamma a_{21}\alpha\beta^2+2\gamma a_{12}a_{21}\beta^2\cos(\omega\tau)+2\omega a_{12}a_{21}\beta^2\sin(\omega\tau)\right]\sin(\omega\tau).$$

Dividing the above two equations gives

$$\tan(\omega\tau)=-\frac{\omega(1-\omega^2+2\gamma-a_{12}a_{21}\beta^2)}{(1-\omega^2+a_{12}a_{21}\beta^2)\gamma-2\omega^2}. \tag{2.51}$$

We can now define

$$\tau_k^j=\frac{1}{\omega_k}\left[\arctan\left(-\frac{\omega_k(1-\omega_k^2-a_{12}a_{21}\beta^2+2\gamma)}{(1-\omega_k^2+a_{12}a_{21}\beta^2)\gamma-2\omega_k^2}\right)+j\pi\right], \tag{2.52}$$

where $k=1,\ldots,6$, $j=0,1,2,....$ The pairs (τ_k^j,ω_k) are the solutions of the characteristic equation (2.49), and $\lambda=\pm i\omega_k$ are pairs of purely imaginary roots of the characteristic equation (2.43) for $\tau=\tau_k^j$. Let

$$\tau_0=\tau_{k_0}^0=\min_{1\le k\le 6}\{\tau_k^0\},\ \omega_0=\omega_{k_0}, \tag{2.53}$$

where $k_0\in\{1,\ldots,6\}$. Then $\tau=\tau_0$ is the first value of the time delay such that (2.43) has purely imaginary roots. Using the time delay τ as the bifurcation parameter, let $\lambda(\tau)=\alpha(\tau)\pm i\omega(\tau)$ be the root of the equation (2.43) near $\tau=\tau_0$ such that $\alpha(\tau_0)=0$, $\omega(\tau_0)=\omega_0$. In order to show that we have a Hopf bifurcation at $\tau=\tau_0$, we have to show that $d\mathrm{Re}[\lambda(\tau_0)]/d\tau>0$.

Theorem 2.5.1. *Suppose the conditions of Lemma 2.5.2 hold, and $h'(s_0)p_0^{(1)}(i\omega_0)>0$, where $p_0^{(1)}(i\omega)$ and $h(s)$ are defined in (2.46) and (2.48), respectively, and $s_0=\omega_0^2$. Then the trivial steady state of the system (2.39) is stable for $\tau\in[0,\tau_0)$ and undergoes a Hopf bifurcation at $\tau=\tau_0$.*

Proof. Lemma 2.5.2 ensures that at $\tau=0$, all eigenvalues of the characteristic equation have negative real part. From the definition of τ_0 in (2.53) it follows that τ_0 is the first positive value of τ, for which the characteristic equation (2.43) has a pair of complex conjugate eigenvalues $\lambda=\pm i\omega_0$. In this case, however, it does not prove possible to use the direct computation as in the proof of Lemma 3.4 to show that $\lambda=i\omega_0$ is a simple root

of the characteristic equation (2.43). Following the methodology of Li *et al.* [86] instead, we introduce a function

$$S_1(\omega) = \text{sgn}[\omega F'(\omega) p_0^{(1)}(i\omega)],$$

which determines possible changes in the number of roots with positive real part of the equation (2.43). From the definition of the function $h(s)$, we have

$$F(\omega) = h(\omega^2) \quad \Longrightarrow \quad F'(\omega) = 2\omega h'(\omega^2) = 2\omega h'(s),$$

which under the assumptions of the theorem implies

$$S_1(\omega_0) = \text{sgn}[\omega_0 F'(\omega_0) p_0^{(1)}(i\omega_0)] = \text{sgn}[2\omega_0^2 h'(s_0) p_0^{(1)}(\omega_0)] = \text{sgn}[h'(s_0) p_0^{(1)}(i\omega_0)] > 0.$$

From Theorem 2 in Li *et al.* [86] it then follows that

$$\text{sgn}\left\{ \frac{d\text{Re}[\lambda(\tau)]}{d\tau}\bigg|_{\tau=\tau_0} \right\} > 0,$$

which suggests that the trivial steady state of the system (2.39) undergoes a Hopf bifurcation at $\tau = \tau_0$. □

In order to illustrate how the stability of the trivial steady state of the system (2.39) changes in the case of the weak gamma distribution kernel, we illustrate in Figure 2.6 the stability boundary for different values of $a_{12}a_{21}\beta^2$. In the case when $a_{12}a_{21}\beta^2 < -1$, the trivial steady state is stable inside the region bounded by the surface shown in Figure 2.6 (a) and unstable outside this region. For $-1 \leq a_{12}a_{21}\beta^2 \leq 1$, there are two non-overlapping surfaces, and the trivial steady state is stable for any parameter values lying inside the region bounded by these surfaces as shown in Figures 2.6 (b) and (c). For $a_{12}a_{21}\beta^2 > 1$, the trivial steady state is unstable for any $\tau \geq 0$, γ and α.

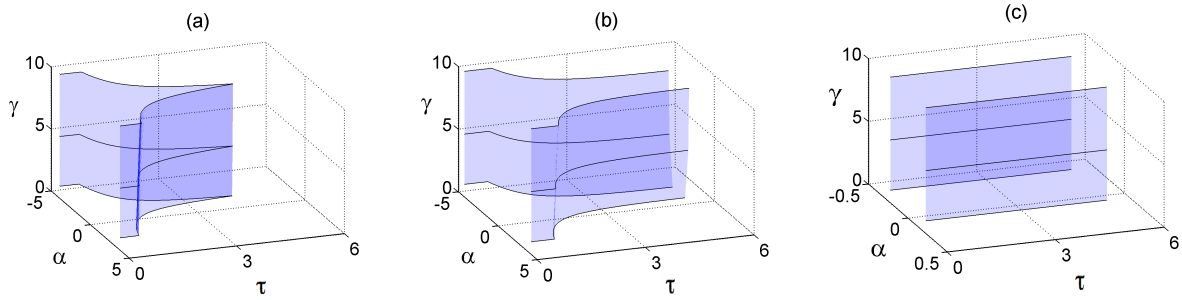

Figure 2.6: Stability boundary of the trivial steady state the system (2.2) with weak delay distribution kernel (1.7) ($r = 1$) and $a_{12} = 2$, $\beta = 1$. (a) $a_{12}a_{21}\beta^2 < -1$ with $a_{21} = -0.55$. (b) $-1 \leq a_{12}a_{21}\beta^2 < 0$ with $a_{21} = -0.45$. (c) $0 \leq a_{12}a_{21}\beta^2 \leq 1$ with $a_{21} = 0.45$. The trivial steady state is stable inside the region restricted by the boundaries and unstable outside this region.

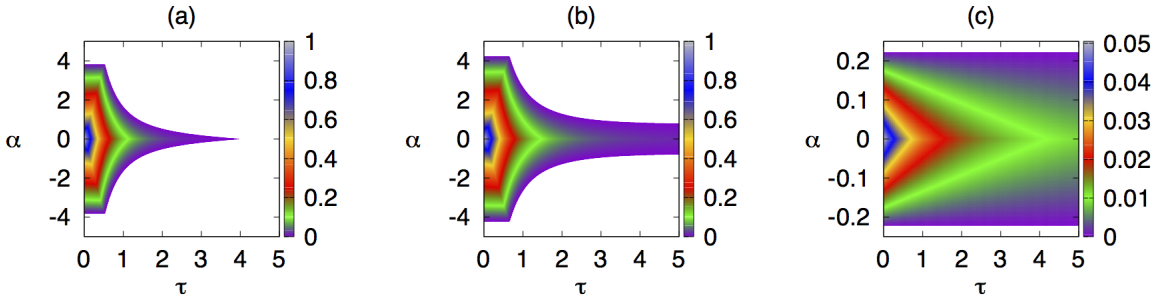

Figure 2.7: Stability region of the trivial steady state of the system (2.2) with weak delay distribution kernel (1.7) ($r = 1$) with $\gamma = 1$, $a_{12} = 2$, $\beta = 1$. (a) $a_{12}a_{21}\beta^2 < -1$ with $a_{21} = -0.55$. (b) $-1 \leq a_{12}a_{21}\beta^2 < 0$ with $a_{21} = -0.45$. (c) $0 \leq a_{12}a_{21}\beta^2 \leq 1$ with $a_{21} = 0.45$. Colour code denotes $[-\max\{\mathrm{Re}(\lambda)\}]$ for $\max\{\mathrm{Re}(\lambda)\} \leq 0$.

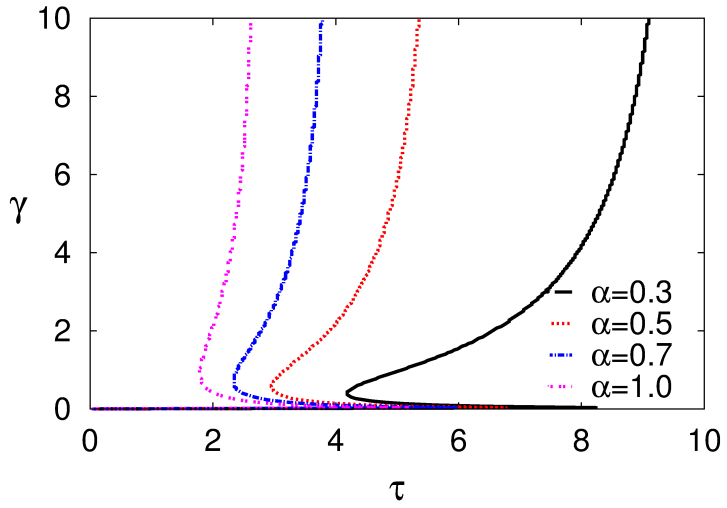

Figure 2.8: Boundary of stability in the τ-γ plane for the weak delay distribution kernel (1.7) ($r = 1$), for different values of α, $a_{12} = 2$, $a_{21} = -0.5$. The trivial steady state is stable to the left of the boundary and unstable to the right of it.

To get a better understanding of how eigenvalues are changing inside the stability region, we show in Figure 2.7 numerically computed eigenvalues of the characteristic equation for the cases shown in Figure 2.6 and one particular value of $\gamma = 1$. Figure 2.7 (a) shows that in the case when $a_{12}a_{21}\beta^2 < -1$, as the value of the discrete time delay increases, the stability region shrinks, and for sufficiently large values of the discrete time delay τ, the trivial steady state of the system (2.39) is unstable for any value of the coupling strength α. In the parameter region where $-1 \leq a_{12}a_{21}\beta^2 < 0$, as the discrete time delay increases, the stability region of the trivial steady state of the system (2.39) becomes smaller, but there is always a range of coupling strength values α, where the steady state is stable, as

shown in Figure 2.7 (b). In the case $0 \leq a_{12}a_{21}\beta^2 \leq 1$, the stability region is bounded by $|1 - a_{12}a_{21}\beta^2| = |a_{21}\alpha\beta^2|$ and is independent of τ and γ.

Figure 2.8 shows that as the coupling strength α between the two sub-networks is increased, in the case of the weak distribution kernel, the stability region of the trivial steady state becomes smaller in the $\gamma - \tau$ plane.

2.5.2 Strong gamma distributed delayed kernel

In this subsection, we consider the system (2.2) with a strong delay kernel, using the same procedure as we have done for weak delay kernel case. Introducing the new variables

$$\begin{aligned}
u_5(t) &= \int_0^\infty \gamma e^{-\gamma s} u_2(t-s)ds, \\
u_6(t) &= \int_0^\infty \gamma^2 s e^{-\gamma s} u_2(t-s)ds, \\
u_7(t) &= \int_0^\infty \gamma e^{-\gamma s} u_4(t-s)ds, \\
u_8(t) &= \int_0^\infty \gamma^2 s e^{-\gamma s} u_4(t-s)ds.
\end{aligned}$$

allows us to rewrite the system (2.1) as follows

$$\begin{cases}
\dot{u}_1(t) &= -u_1(t) + a_{12}\beta u_2(t-\tau) + \alpha\beta u_8(t), \\
\dot{u}_2(t) &= -u_2(t) + a_{21}\beta u_1(t-\tau), \\
\dot{u}_3(t) &= -u_3(t) + a_{12}\beta u_4(t-\tau) + \alpha\beta u_6(t), \\
\dot{u}_4(t) &= -u_4(t) + a_{21}\beta u_3(t-\tau), \\
\dot{u}_5(t) &= \gamma u_2(t) - \gamma u_5(t), \\
\dot{u}_6(t) &= \gamma u_5(t) - \gamma u_6(t), \\
\dot{u}_7(t) &= \gamma u_4(t) - \gamma u_7(t), \\
\dot{u}_8(t) &= \gamma u_7(t) - \gamma u_8(t).
\end{cases} \tag{2.54}$$

Substituting the Laplace transform (2.36) into the characteristic equation (2.6), or

using the system (2.54), we obtain a characteristic equation for the eigenvalues λ as follows

$$\det[\Delta(\tau,\lambda)] = \Delta_-(\tau,\lambda)\cdot\Delta_+(\tau,\lambda) = 0, \tag{2.55}$$

where

$$\Delta_-(\tau,\lambda) = (\lambda+\gamma)^2(\lambda+1)^2 - (\lambda+\gamma)^2 a_{12}a_{21}\beta^2 e^{-2\lambda\tau} - \gamma^2 a_{21}\alpha\beta^2 e^{-\lambda\tau}, \tag{2.56}$$

$$\Delta_+(\tau,\lambda) = (\lambda+\gamma)^2(\lambda+1)^2 - (\lambda+\gamma)^2 a_{12}a_{21}\beta^2 e^{-2\lambda\tau} + \gamma^2 a_{21}\alpha\beta^2 e^{-\lambda\tau}. \tag{2.57}$$

Lemma 2.5.4. *Let* $|1 - a_{12}a_{21}\beta^2| = |a_{21}\alpha\beta^2|$. *If*

$$-1 \le a_{12}a_{21}\beta^2 \le 1+\gamma \quad \textit{and} \quad a_{12}a_{21}\beta^2 \ne 1,$$

or

$$a_{12}a_{21}\beta^2 > 1+\gamma \quad \textit{or} \quad a_{12}a_{21}\beta^2 < -1 \quad \textit{and} \quad \tau \ne \tau_\gamma = \frac{2(a_{12}a_{21}\beta^2 - \gamma - 1)}{\gamma(1+a_{12}a_{21}\beta^2)},$$

then $\lambda = 0$ *is a simple root of the characteristic equation (2.55). If*

$$a_{12}a_{21}\beta^2 = 1,$$

or

$$a_{12}a_{21}\beta^2 > 1+\gamma \quad \textit{or} \quad a_{12}a_{21}\beta^2 < -1 \quad \textit{and} \quad \tau = \tau_\gamma,$$

then $\lambda = 0$ *is a double root of the characteristic equation (2.55).*

The proof of Lemma 2.5.4 is similar to the proof of Lemma 2.5.1.

Considering the case of the *strong* distribution kernel with $r = 2$ in Δ_- given by (2.56) (the analysis is similar for Δ_+ in (2.57)), we get a transcendental equation for eigenvalues λ:

$$(\lambda+\gamma)^2(\lambda+1)^2 - (\lambda+\gamma)^2 a_{12}a_{21}\beta^2 e^{-2\lambda\tau} - \gamma^2 a_{21}\alpha\beta^2 e^{-\lambda\tau} = 0. \tag{2.58}$$

When $\tau = 0$, the equation (2.58) becomes

$$\lambda^4 + (2+2\gamma)\lambda^3 + \left(-a_{12}a_{21}\beta^2 + 1 + 4\gamma + \gamma^2\right)\lambda^2 + \left(2\gamma - 2\gamma\, a_{12}a_{21}\beta^2 + 2\gamma^2\right)\lambda$$

$$+\gamma^2 - a_{12}a_{21}\beta^2\gamma^2 - \gamma^2 a_{21}\alpha\,\beta^2 = 0. \tag{2.59}$$

In view of the Routh-Hurwitz criterion, a set of the necessary and sufficient conditions for all roots of the equation (2.59) to have negative real part is

$$(H1)\begin{cases} a_{12}a_{21}\beta^2 < \gamma + 1, \\ a_{21}\alpha\beta^2 < 1 - a_{12}a_{21}\beta^2, \\ 2(\gamma+1)^2 a_{12}a_{21}\beta^2 < (\gamma+1)^4 + \gamma(\gamma+1)^2 a_{21}\alpha\beta^2 + a_{12}^2 a_{21}^2\beta^4. \end{cases} \tag{2.60}$$

Lemma 2.5.5. *Assume that (H1) holds. Then all the roots of equation (2.59) with $\tau = 0$ always have negative real part.*

Once again, when $\tau > 0$, we can use the same procedure as in the case of the delta distributed kernel in order to calculate $F(\omega)$ as follows:

$$\begin{aligned}
p_0^{(1)}((\omega) &= \left(\omega^4 - \left(1 + 4\,\gamma + \gamma^2\right)\omega^2 + \gamma^2\right)^2 + \left(2\,\left(1+\gamma\right)\omega^3 - 2\,\left(\gamma + \gamma^2\right)\omega\right)^2 \\
&\quad - \left(\gamma^2 + \omega^2\right)^2 {a_{12}}^2 {a_{21}}^2 \beta^4, \\
p_1^{(1)}((i\omega) &= -\gamma^2 a_{21}\alpha\,\beta^2\omega^4 + \gamma^2 a_{21}\alpha\,\beta^2\omega^2 + 4\,\gamma^3 a_{21}\alpha\,\beta^2\omega^2 + \gamma^4 a_{21}\alpha\,\beta^2\omega^2 \\
&\quad -\gamma^4 a_{21}\alpha\,\beta^2 - a_{12}{a_{21}}^2\beta^4\alpha\,\gamma^4 + a_{12}{a_{21}}^2\beta^4\alpha\,\gamma^2\omega^2 + i(-2\,\gamma^3 a_{21}\alpha\,\beta^2\omega^3 \\
&\quad -2\,\gamma^2 a_{21}\alpha\,\beta^2\omega^3 + 2\,\gamma^3 a_{21}\alpha\,\beta^2\omega + 2\,\gamma^4 a_{21}\alpha\,\beta^2\omega - 2\,a_{12}{a_{21}}^2\beta^4\alpha\,\gamma^3\omega).
\end{aligned} \tag{2.61}$$

$$F(\omega) = \omega^{16} + c_1\omega^{14} + c_2\omega^{12} + c_3\omega^{10} + c_4\omega^8 + c_5\omega^6 + c_6\omega^4 + c_7\omega^2 + c_8 \tag{2.62}$$

where

$$\begin{aligned}
c_1 &= 4\gamma^2 + 4, \quad c_2 = 16\,\gamma^2 - 2\,{a_{12}}^2{a_{21}}^2\beta^4 + 6\,\gamma^4 + 6, \\
c_3 &= 24\,\gamma^2 - 8\,\gamma^2{a_{12}}^2{a_{21}}^2\beta^4 + 24\,\gamma^4 - 4\,{a_{12}}^2{a_{21}}^2\beta^4 + 4\,\gamma^6 + 4, \\
c_4 &= {a_{12}}^4{a_{21}}^4\beta^8 + \gamma^8 - \gamma^4{a_{21}}^2\alpha^2\beta^4 + 36\,\gamma^4 + 16\,\gamma^2 - 2\,{a_{12}}^2{a_{21}}^2\beta^4 \\
&\quad +1 - 12\,{a_{12}}^2{a_{21}}^2\beta^4\gamma^4 - 16\,\gamma^2{a_{12}}^2{a_{21}}^2\beta^4 + 16\,\gamma^6, \\
c_5 &= 4\,\gamma^8 - 24\,{a_{12}}^2{a_{21}}^2\beta^4\gamma^4 + 24\,\gamma^4 - 2\,\gamma^6{a_{21}}^2\alpha^2\beta^4 - 8\,\gamma^6{a_{12}}^2{a_{21}}^2\beta^4 \\
&\quad +2\,\gamma^4{a_{21}}^3\alpha^2\beta^6 a_{12} + 4\,{a_{12}}^4{a_{21}}^4\beta^8\gamma^2 - 8\,\gamma^2{a_{12}}^2{a_{21}}^2\beta^4 + 24\,\gamma^6 \\
&\quad -2\,\gamma^4{a_{21}}^2\alpha^2\beta^4 + 4\,\gamma^2,
\end{aligned}$$

$$
\begin{aligned}
c_6 &= 6\,{a_{12}}^4{a_{21}}^4\beta^8\gamma^4 - 16\,\gamma^6{a_{12}}^2{a_{21}}^2\beta^4 - 2\,\gamma^4{a_{21}}^3\alpha^2\beta^6a_{12} \\
&\quad -\gamma^4{a_{21}}^4\alpha^2\beta^8{a_{12}}^2 + 6\,\gamma^4 - \gamma^4{a_{21}}^2\alpha^2\beta^4 - 12\,{a_{12}}^2{a_{21}}^2\beta^4\gamma^4 \\
&\quad -4\,\gamma^6{a_{21}}^2\alpha^2\beta^4 + 16\,\gamma^6 - \gamma^8{a_{21}}^2\alpha^2\beta^4 - 2\,\gamma^8{a_{12}}^2{a_{21}}^2\beta^4 \\
&\quad +6\,\gamma^8 - 12\,\gamma^6{a_{21}}^3\alpha^2\beta^6a_{12} - 16\,\gamma^5{a_{21}}^3\alpha^2\beta^6a_{12}, \\
c_7 &= 4\,\gamma^6 + 12\,\gamma^6{a_{21}}^3\alpha^2\beta^6a_{12} + 4\,\gamma^8 - 2\,\gamma^6{a_{21}}^2\alpha^2\beta^4 - 4\,\gamma^8{a_{12}}^2{a_{21}}^2\beta^4 \\
&\quad +2\,\gamma^8{a_{21}}^3\alpha^2\beta^6a_{12} - 2\,\gamma^6{a_{21}}^4\alpha^2\beta^8{a_{12}}^2 - 2\,\gamma^8{a_{21}}^2\alpha^2\beta^4 \\
&\quad -8\,\gamma^6{a_{12}}^2{a_{21}}^2\beta^4 + 4\,{a_{12}}^4{a_{21}}^4\beta^8\gamma^6 + 16\,\gamma^7{a_{21}}^3\alpha^2\beta^6a_{12}, \\
c_8 &= \gamma^8 - 2\,\gamma^8{a_{21}}^3\alpha^2\beta^6a_{12} - \gamma^8{a_{21}}^2\alpha^2\beta^4 - \gamma^8{a_{21}}^4\alpha^2\beta^8{a_{12}}^2 \\
&\quad -2\,\gamma^8{a_{12}}^2{a_{21}}^2\beta^4 + {a_{12}}^4{a_{21}}^4\beta^8\gamma^8.
\end{aligned}
$$

Lemma 2.5.6. *Assume that $c_8 < 0$. Then the equation $F(\omega) = 0$ has at least one positive root.*

Proof. Assumption $c_8 < 0$ implies that $F(0) = c_8 < 0$. Since $F(\omega)$ as defined by (2.62) is a continuous function of ω, and also $\lim_{\omega\to\infty} F(\omega) = \infty$, this means that there exists a positive root $\omega > 0$ of the equation $F(\omega) = 0$. □

Let $z = \omega^2$, then (2.62) becomes

$$h(z) = z^8 + c_1z^7 + c_2z^6 + c_3z^5 + c_4z^4 + c_5z^3 + c_6z^2 + c_7z + c_8 \tag{2.63}$$

Without loss of generality, suppose that the equation (2.63) has eight positive roots, denoted by z_i, $i = 1, \ldots, 8$. Then (2.62) should also have eight positive real roots

$$\omega_1 = \sqrt{z_1},\ \omega_2 = \sqrt{z_2},\ \omega_3 = \sqrt{z_3},\ \omega_4 = \sqrt{z_4},\ \omega_5 = \sqrt{z_5},\ \omega_6 = \sqrt{z_6},\ \omega_7 = \sqrt{z_7},\ \omega_8 = \sqrt{z_8}.$$

On the other hand, substituting $\lambda = i\omega$ for $\omega > 0$ into equation (2.20)

$$(i\omega+\gamma)^2(i\omega+1)^2 - \gamma^2a_{21}\alpha\beta^2e^{-i\omega\tau} - (i\omega+\gamma)^2a_{12}a_{21}\beta^2e^{-2i\omega\tau} = 0 \tag{2.64}$$

and separating into the real and imaginary part yields

$$\begin{aligned}
&\left(\gamma^2-\omega^2\right)\left(1-\omega^2\right)-4\,\omega^2\gamma-\gamma^2 a_{21}\alpha\,\beta^2\cos\left(\omega\,\tau\right)\\
&=\left(\gamma^2-\omega^2\right)a_{12}a_{21}\beta^2\cos\left(2\,\omega\,\tau\right)+2\,\gamma\,\omega\,a_{12}a_{21}\beta^2\sin\left(2\,\omega\,\tau\right),\\
&2\,\gamma\,\omega\,\left(1-\omega^2\right)+2\,\left(\gamma^2-\omega^2\right)\omega+\gamma^2 a_{21}\alpha\,\beta^2\sin\left(\omega\,\tau\right)\\
&=2\,\gamma\,\omega\,a_{12}a_{21}\beta^2\cos\left(2\,\omega\,\tau\right)-\left(\gamma^2-\omega^2\right)a_{12}a_{21}\beta^2\sin\left(2\,\omega\,\tau\right).
\end{aligned}\tag{2.65}$$

Using the trigonometric formulas $\cos(2\omega\tau)=2\cos^2(\omega\tau)-1$, $\cos(2\omega\tau)=1-2\sin^2(\omega\tau)$ and $\sin(2\omega\tau)=2\sin(\omega\tau)\cos(\omega\tau)$, the equation (2.65) can be rewritten as follows

$$\begin{aligned}
&\left(\gamma^2-\omega^2\right)\left(1-\omega^2+a_{12}a_{21}\beta^2\right)-4\,\omega^2\gamma\\
&=\{\gamma^2 a_{21}\alpha\beta^2+2(\gamma^2-\omega^2)a_{12}a_{21}\beta^2\cos(\omega\tau)+2\gamma\omega a_{12}a_{21}\beta^2\sin(\omega\tau)\}\cos(\omega\tau),\\
&2\,\gamma\,\omega\,\left(1-\omega^2-a_{12}a_{21}\beta^2\right)+2\,\left(\gamma^2-\omega^2\right)\omega\\
&=-\{\gamma^2 a_{21}\alpha\beta^2+2(\gamma^2-\omega^2)a_{12}a_{21}\beta^2\cos(\omega\tau)+2\gamma\omega a_{12}a_{21}\beta^2\sin(\omega\tau)\}\sin(\omega\tau).
\end{aligned}\tag{2.66}$$

Dividing the equations (2.66), one obtains

$$\tan(\omega\tau)=-\frac{2\,\gamma\,\omega\,\left(1-\omega^2-a_{12}a_{21}\beta^2\right)+2\,\left(\gamma^2-\omega^2\right)\omega}{\left(\gamma^2-\omega^2\right)\left(1-\omega^2+a_{12}a_{21}\beta^2\right)-4\,\omega^2\gamma}.\tag{2.67}$$

Let us define

$$\tau_k^j=\frac{1}{\omega_k}\left[\arctan\left(-\frac{2\,\gamma\,\omega_k\,\left(1-{\omega_k}^2-a_{12}a_{21}\beta^2\right)+2\,\left(\gamma^2-{\omega_k}^2\right)\omega_k}{\left(\gamma^2-{\omega_k}^2\right)\left(1-{\omega_k}^2+a_{12}a_{21}\beta^2\right)-4\,{\omega_k}^2\gamma}\right)+j\pi\right],\tag{2.68}$$

where $k=1,\ldots,8,\ j=0,1,2,\ldots$. Thus, (τ_k^j,ω_k) are solutions of the equation (2.64) and $\lambda=\pm i\omega_k$ are a pair of purely imaginary roots of (2.58) with $\tau=\tau_k^j$. If

$$\tau_0=\tau_{k_0}^0=\min_{1\le k\le 8}\{\tau_k^0\},\ \omega_0=\omega_{k_0},$$

where $k_0\in\{1,\ldots,8\}$, then τ_0 is the first value of τ such that the equation (2.58) has purely imaginary roots. Using the time delay τ as the bifurcation parameter, let $\lambda(\tau)=\alpha(\tau)\pm i\omega(\tau)$ be the root of the equation (2.58) near $\tau=\tau_0$ such that $\alpha(\tau_0)=0$, $\omega(\tau_0)=\omega_0$. Similar to the cases considered in the previous subsections, in order to show that we have a Hopf bifurcation at $\tau=\tau_0$, we have to establish that $d\mathrm{Re}[\lambda(\tau_0)]/d\tau>0$.

Theorem 2.5.2. *Suppose the conditions of Lemma 2.5.5 hold, and* $h'(s_0)p_0^{(1)}(i\omega_0) > 0$, *where* $p_0^{(1)}(i\omega)$ *and* $h(s)$ *are defined in (2.61) and (2.63), respectively, and* $s_0 = \omega_0^2$. *Then the trivial steady state of the system (2.54) is stable for* $\tau \in [0, \tau_0)$ *and undergoes a Hopf bifurcation at* $\tau = \tau_0$.

The proof of Theorem 2.5.2 is similar to the proof of Theorem 2.5.1.

Similar to the case of the weak gamma distribution kernel, we numerically compute the stability boundaries of the trivial steady state of the system (2.54) for the case of strong delay kernel. The boundary of the surface in Figure 2.9 shows the stable and unstable regions for different values of $a_{12}a_{21}\beta^2$. In the case when $a_{12}a_{21}\beta^2 < -1$, the trivial steady state is stable inside the region bounded by the surface shown in Figure 2.9 (a) and unstable outside this region. For $-1 \leq a_{12}a_{21}\beta^2 \leq 1$, there are two non-overlapping surfaces, and the trivial steady state is stable for any parameter values lying inside the region bounded by these surfaces as shown in Figures 2.9 (b) and (c). For $a_{12}a_{21}\beta^2 > 1$, the trivial steady state is always unstable for any $\tau \geq 0$, γ and α.

Figure 2.10 shows the stability region of the trivial steady state of the system (2.54) in the case of the strong delay kernel. Notably, the stability region for strong delay kernel looks qualitatively similar to the case for the weak delay kernel presented in Figure 2.7. Figure 2.10 (a) shows that in the case when $a_{12}a_{21}\beta^2 < -1$, as τ increases, the stability region becomes smaller and smaller, and for sufficiently large values of τ, the trivial steady state of the system (2.54) is unstable for any value of α.

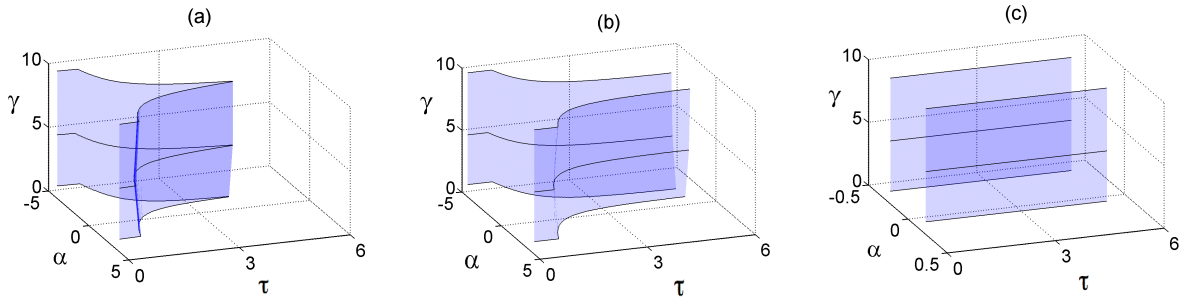

Figure 2.9: Stability boundary of the trivial steady state of the system (2.2) with strong delay distribution kernel (1.7) ($r = 2$) and $a_{12} = 2$, $\beta = 1$. (a) $a_{12}a_{21}\beta^2 < -1$ with $a_{21} = -0.55$. (b) $-1 \leq a_{12}a_{21}\beta^2 < 0$ with $a_{21} = -0.45$. (c) $0 \leq a_{12}a_{21}\beta^2 \leq 1$ with $a_{21} = 0.45$. The trivial steady state is stable inside the region restricted by the boundaries and unstable outside this region.

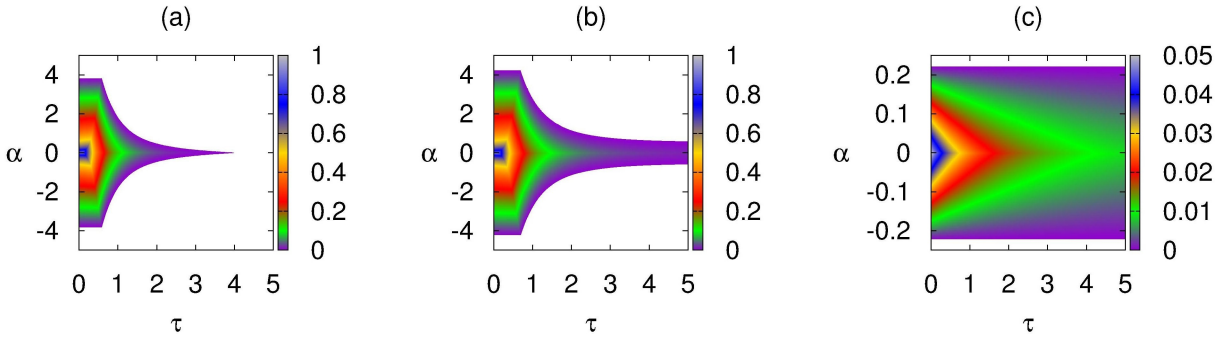

Figure 2.10: Stability region of the trivial steady state of the system (2.2) with strong delay distribution kernel (1.7) ($r = 2$) with $\gamma = 1$, $a_{12} = 2$, $\beta = 1$. (a) $a_{12}a_{21}\beta^2 < -1$ with $a_{21} = -0.55$. (b) $-1 \leq a_{12}a_{21}\beta^2 < 0$ with $a_{21} = -0.45$. (c) $0 \leq a_{12}a_{21}\beta^2 \leq 1$ with $a_{21} = 0.45$. Colour code denotes $[-\max\{\mathrm{Re}(\lambda)\}]$ for $\max\{\mathrm{Re}(\lambda)\} \leq 0$.

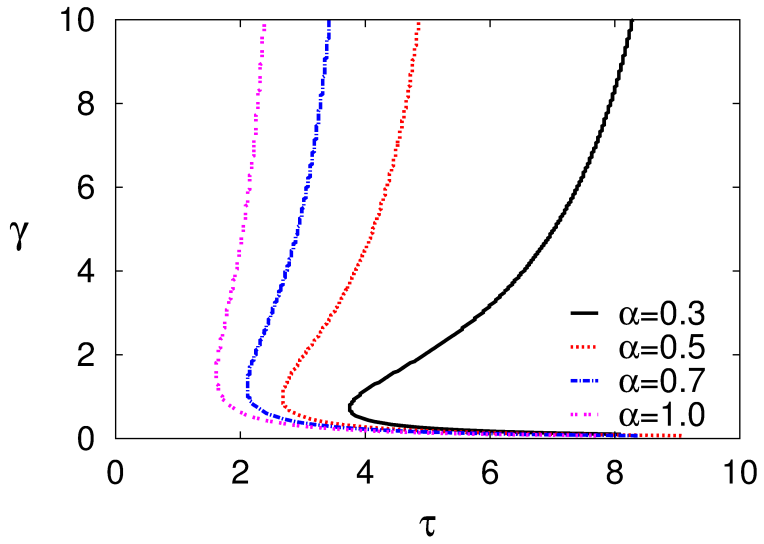

Figure 2.11: Boundary of stability in the τ-γ plane for the strong delay distribution kernel (1.7) ($r = 2$), for different values of α, $a_{12} = 2$, $a_{21} = -0.5$. The trivial steady state is stable to the left of the boundary and unstable to the right of it.

If parameter satisfy the condition $-1 \leq a_{12}a_{21}\beta^2 < 0$, the stability region of the trivial steady state of the system (2.54) shrinks with increasing τ, but there is always a range of coupling strength values α, where the steady state is stable, as shown in Figure 2.10 (b). In the case $0 \leq a_{12}a_{21}\beta^2 \leq 1$, the stable region is bounded by $|1 - a_{12}a_{21}\beta^2| = |a_{21}\alpha\beta^2|$ and is independent of τ and γ.

Figure 2.11 shows the stability region in τ and γ parameter space, and one can observe that as α gets larger, the stability region becomes smaller for strong delay kernel, and compared to the weak gamma kernel occupies a smaller region for the same parameter values.

2.6 Numerical simulations

This section presents the results of the numerical simulations of the system (2.2) using *dde23* suite in MATLAB. These simulations support theoretical results of the previous sections and also illustrate the stability of the trivial steady state of the system (2.2) in different parameter regimes. We consider four different cases, and for each of them we have three different intervals to consider. Firstly, we numerically find solutions of the system (2.2) with delta distribution kernel. Secondly, we use trapezoidal rule to treat the integral in system (2.2) for the uniform distribution case, and then show when solutions tend to the stable steady state, as well as the appearance of the periodic oscillations. In the last two subsections, we numerically solve the system (2.39) after using the linear chain trick to confirm the findings on the stability properties of the trivial steady state in cases of the weak and strong gamma distribution kernels.

2.6.1 Numerical simulations for the delta distribution kernel

In this subsection, we perform direct numerical simulations of the system (2.9) in the case of the delta distribution kernel $g(s) = \delta(s)$. Let $f(\cdot) = \tanh(\cdot)$, which implies that $\beta = f'(0) = 1$. Then the system (2.2) takes the form

$$\begin{aligned}
\dot{u}_1(t) &= -u_1(t) + a_{12}\tanh(u_2(t-\tau)) + \alpha\tanh(u_4(t)),\\
\dot{u}_2(t) &= -u_2(t) + a_{21}\tanh(u_1(t-\tau)),\\
\dot{u}_3(t) &= -u_3(t) + a_{12}\tanh(u_4(t-\tau)) + \alpha\tanh(u_2(t)),\\
\dot{u}_4(t) &= -u_4(t) + a_{21}\tanh(u_3(t-\tau)).
\end{aligned} \tag{2.69}$$

First, we consider the case when $a_{12}a_{21}\beta^2 < -1$ holds. For example, if $a_{12} = 2$, $a_{21} = -0.55$, and $\alpha = \pm 2$, then the expression (2.24) has the form

$$h(s) = s^4 + 4\,s^3 + 2.3700\,s^2 - 5.922\,s + 0.032.$$

In this case, $h(s) = 0$ has only one positive real root $s_0 = 0.882$, and $\omega_0 = 0.939$, $\tau_0 = 1.159$, $h'(s_0) = 10.331 > 0$, $p_0^{(1)}(i\omega_0) = 2.331 > 0$. Therefore, from Theorem 2.3.1, it follows that the trivial solution of the system (2.69) is stable when $0 \leq \tau < \tau_0$, and undergoes a Hopf bifurcation when τ crosses through the critical value of the time delay $\tau_0 = 1.159$, giving rise to a stable periodic solution, as illustrated in Figure 2.12 (a)-(f). In a similar manner,

when the parameter values of the system (2.2) satisfy $-1 \leq a_{12}a_{21}\beta^2 < 0$, i.e. for example, $a_{12} = 2, a_{21} = -0.45$ and $\alpha = \pm 2$, the expression (2.24) becomes

$$h(s) = s^4 + 4\,s^3 + 3.57\,s^2 - 2.318\,s + 0.028.$$

Hence, $h(s) = 0$ has one positive real root $s_0 = 0.416$, and $\omega_0 = 0.645$, $\tau_0 = 2.062$, $h'(s_0) = 3.02 > 0$, $p_0^{(1)}(i\omega_0) = 1.196 > 0$. Theorem 2.3.1 implies that the trivial solution of the system (2.69) is stable when $0 < \tau < \tau_0$ and undergoes a Hopf bifurcation at $\tau_0 = 2.062$, once again resulting in a stable periodic solution, as shown in Figure 2.13 (a)-(f).

In the case $0 \leq a_{12}a_{21}\beta^2 \leq 1$, the system (2.69) approaches the stable trivial steady state provided $|a_{21}\alpha\beta^2| < |1 - a_{12}a_{21}\beta^2|$ as illustrated in Figure 2.14 (a). If $|\alpha| > |\alpha_c|$, where α_c satisfies $|a_{21}\alpha_c\beta^2| = |1 - a_{12}a_{21}\beta^2|$, the trivial steady state is unstable via a steady-state bifurcation, and the system (2.69) tends to one of its stable non-trivial steady states, as shown in Figure 2.14 (b). One should note that it is possible for this system to simultaneously have multiple stable steady states for the same parameter values, and the solutions will approach one of them depending on the initial conditions. For $a_{12}a_{21}\beta^2 > 1$, the behaviour of the system (2.69) is similar to the case shown in Figure 2.14 (b).

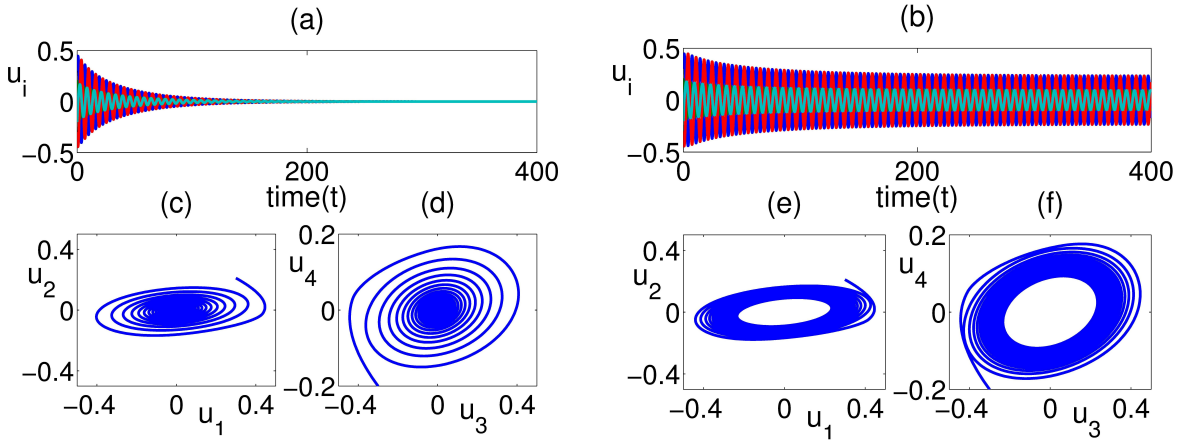

Figure 2.12: (a)-(f) Solution of the system (2.69) in the case when $a_{12}a_{21}\beta^2 < -1$. Parameter values are $a_{12} = 2$, $a_{21} = -0.55$, $\alpha = \pm 2$ and $\tau_0 = 1.159$. (a), (c)-(d) $0 < \tau = 1 < \tau_0$. (b), (e)-(f) $\tau = 1.2 > \tau_0$.

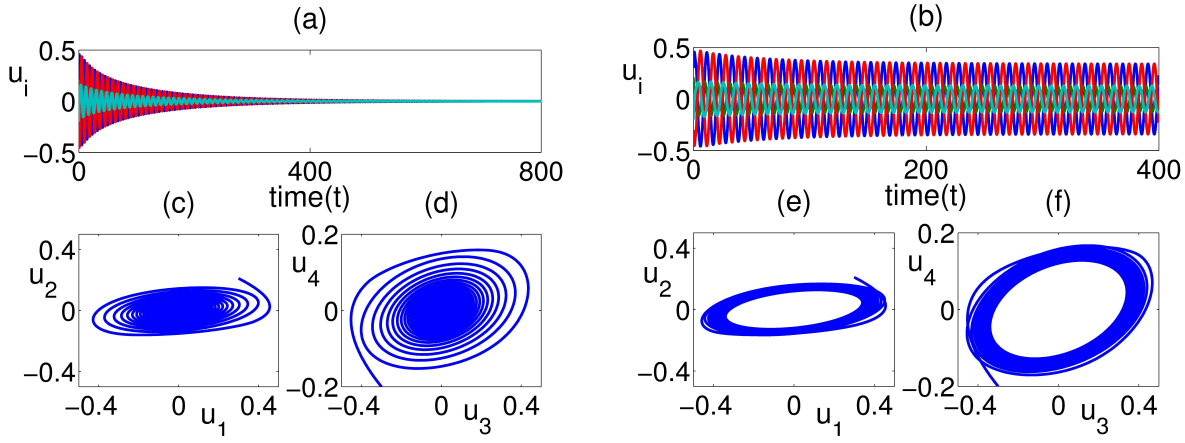

Figure 2.13: (a)-(f) Solution of the system (2.69) in the case when the condition $-1 \leq a_{12}a_{21}\beta^2 < 0$ holds. Parameter values are $a_{12} = 2$, $a_{21} = -0.45$, $\alpha = \pm 2$ and $\tau_0 = 2.062$. (a), (c)-(d) $0 < \tau = 1.8 < \tau_0$. (b), (e)-(f) $\tau = 2.4 > \tau_0$.

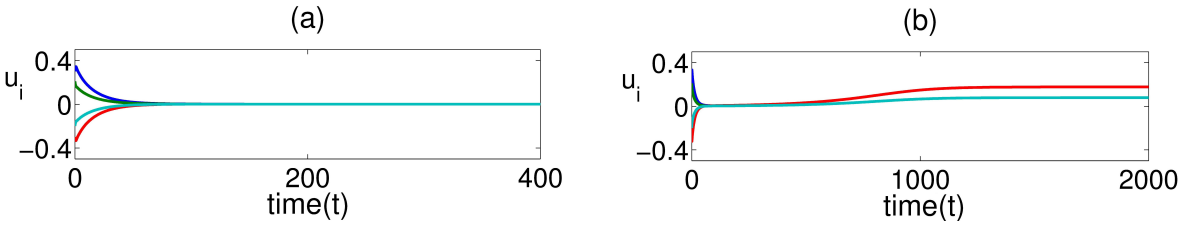

Figure 2.14: (a)-(b) Solution of the system (2.69) in the case when the condition $0 \leq a_{12}a_{21}\beta^2 \leq 1$ holds. Parameter values are $a_{12} = 2$, $a_{21} = 0.45$, $\tau = 0.5$. (a) $\alpha = 0.15$. (b) $\alpha = 0.25$.

2.6.2 Numerical simulations for the uniform distribution kernel

In this subsection, we numerically solve the nonlinear system (2.2) in the case of the uniformly distributed kernel by using a trapezoidal rule [29] to treat the integral as follows,

$$\int_a^b f(x)dx \approx \frac{(b-a)}{2}[f(a) + f(b)], \tag{2.70}$$

which yields

$$\begin{aligned}
\dot{u}_1(t) &= -u_1(t) + a_{12}\tanh(u_2(t-\tau)) + \frac{\alpha}{2}\tanh(u_4(t-(\tau+\sigma)) + u_4(t-(\tau-\sigma))),\\
\dot{u}_2(t) &= -u_2(t) + a_{21}\tanh(u_1(t-\tau)),\\
\dot{u}_3(t) &= -u_3(t) + a_{12}\tanh(u_4(t-\tau)) + \frac{\alpha}{2}\tanh(u_2(t-(\tau+\sigma)) + u_2(t-(\tau-\sigma))),\\
\dot{u}_4(t) &= -u_4(t) + a_{21}\tanh(u_3(t-\tau)).
\end{aligned} \tag{2.71}$$

We consider separately different values of $a_{12}a_{21}\beta^2$, and show the behaviour of the system (2.71) for $\sigma = 0.5$ and and different values of τ. First, we consider the case when $a_{12}a_{21}\beta^2 < -1$ is satisfied. For example, if $a_{12} = 2$, $a_{21} = -0.55$, and $\alpha = \pm 2$, the trivial steady state of the system (2.71) is stable when $0.5 \leq \tau < \tau_0$, where τ_0 satisfies the equation (2.34), and undergoes a Hopf bifurcation when τ crosses through the critical value $\tau_0 = 0.752$, giving rise to a stable periodic solution, as illustrated in Figure 2.15 (a)-(f). Similarly, when the parameter values of the system (2.71) satisfy $-1 \leq a_{12}a_{21}\beta^2 < 0$, i.e. for example, $a_{12} = 2, a_{21} = -0.45$ and $\alpha = \pm 2$, the trivial steady state of the system (2.71) is stable when $0.5 \leq \tau < \tau_0$, where τ_0 satisfies the equation (2.34), and undergoes a Hopf bifurcation when τ crosses through the critical value $\tau_0 = 0.93$, giving rise to a stable periodic solution, as illustrated in Figure 2.16 (a)-(f).

In the case $0 \leq a_{12}a_{21}\beta^2 \leq 1$, the system (2.69) approaches the stable trivial steady state provided $|a_{21}\alpha\beta^2| < |1 - a_{12}a_{21}\beta^2|$ as illustrated in Figure 2.17 (a). If $|\alpha| > |\alpha_c|$, where α_c satisfies $|a_{21}\alpha_c\beta^2| = |1 - a_{12}a_{21}\beta^2|$, the trivial steady state becomes unstable via a steady-state bifurcation, and the system (2.71) tends to one of its stable non-trivial steady states, as shown in Figure 2.17 (b). Similar to the previous case, it is possible for this system to simultaneously have multiple stable steady states for the same parameter values, and the solutions will approach one of them depending on the initial conditions. For $a_{12}a_{21}\beta^2 > 1$, the behaviour of the system (2.69) is similar to the case shown in Figure 2.17 (b).

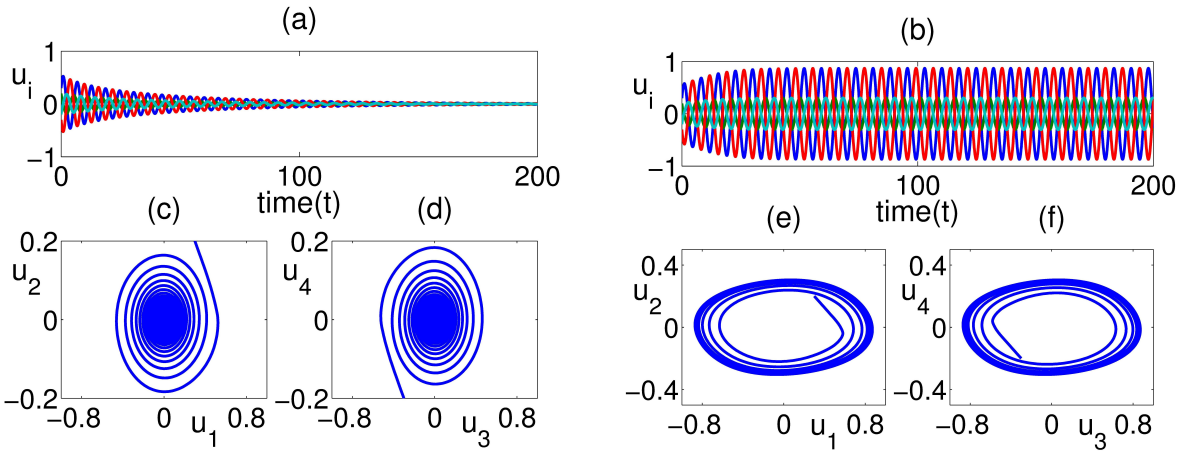

Figure 2.15: (a)-(f) Solution of the system (2.71) in the case when $a_{12}a_{21}\beta^2 < -1$. Parameter values are $a_{12} = 2$, $a_{21} = -0.55$, $\alpha = \pm 2$ and $\sigma = 0.5$. (a), (c)-(d) $0 < \tau = 0.7 < \tau_0$. (b), (e)-(f) $\tau = 1 > \tau_0$.

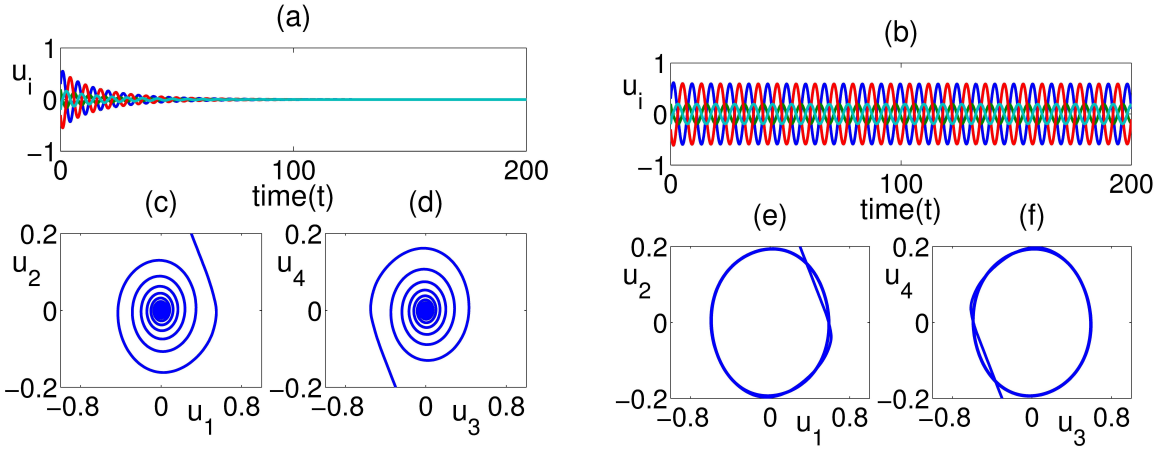

Figure 2.16: (a)-(f) Solution of the system (2.71) in the case when the condition $-1 \leq a_{12}a_{21}\beta^2 < 0$ holds. Parameter values are $a_{12} = 2$, $a_{21} = -0.45$, $\alpha = \pm 2$ and $\sigma = 0.5$. (a), (c)-(d) $0 < \tau = 0.8 < \tau_0$. (b), (e)-(f) $\tau = 1.2 > \tau_0$.

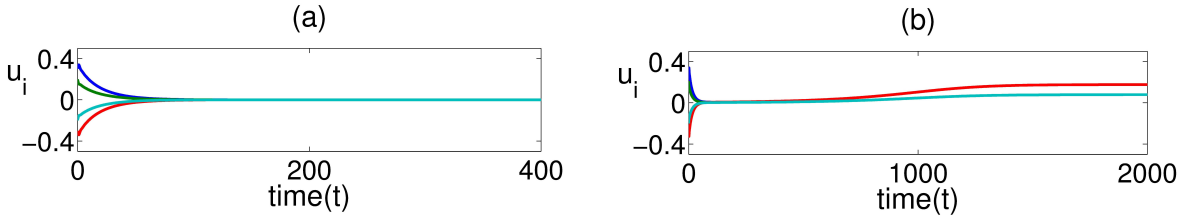

Figure 2.17: (a)-(b) Solution of the system (2.71) in the case when the condition $0 \leq a_{12}a_{21}\beta^2 \leq 1$ holds. Parameter values are $a_{12} = 2$, $a_{21} = 0.45$, $\sigma = 0.5$, $\tau = 0.8$. (a) $\alpha = 0.15$. (b) $\alpha = 0.25$.

2.6.3 Numerical simulations for the weak gamma distribution kernel

In order to illustrate the dynamics in the case of the weak gamma distribution kernel, we again take $f(\cdot) = \tanh(\cdot)$, $\beta = f'(0) = 1$, and rewrite the system (2.2) as

$$\begin{cases} \dot{u}_1(t) = -u_1(t) + a_{12}\tanh(u_2(t-\tau)) + \alpha\tanh(u_6(t)), \\ \dot{u}_2(t) = -u_2(t) + a_{21}\tanh(u_1(t-\tau)), \\ \dot{u}_3(t) = -u_3(t) + a_{12}\tanh(u_4(t-\tau)) + \alpha\tanh(u_5(t)), \\ \dot{u}_4(t) = -u_4(t) + a_{21}\tanh(u_3(t-\tau)), \\ \dot{u}_5(t) = \gamma u_2(t) - \gamma u_5(t), \\ \dot{u}_6(t) = \gamma u_4(t) - \gamma u_6(t). \end{cases} \tag{2.72}$$

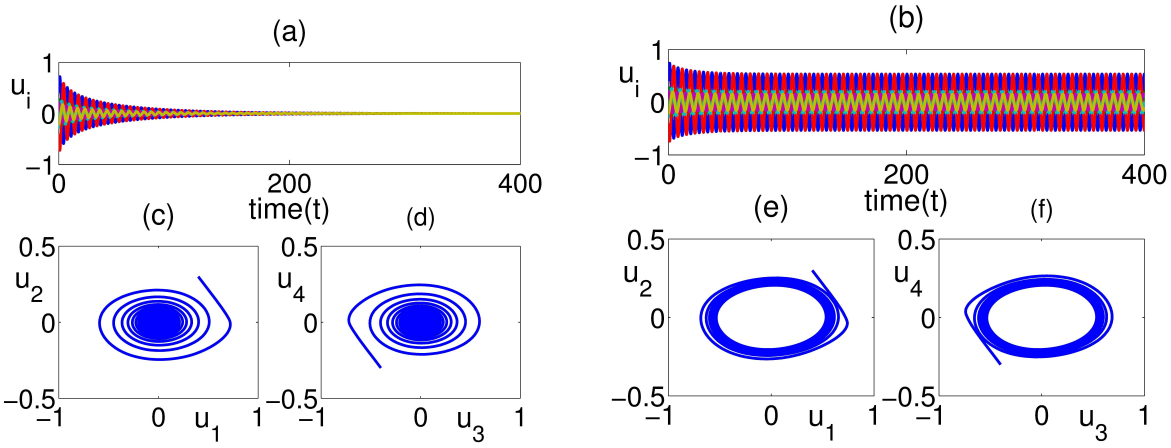

Figure 2.18: (a)-(f) Solution of the system (2.72) in the case when $a_{12}a_{21}\beta^2 < -1$. Parameter values are $a_{12} = 2$, $a_{21} = -0.55$, $\alpha = \pm 2$ and $\tau_0 = 0.873$. (a), (c)-(d) $0 < \tau = 0.8 < \tau_0$. (b), (e)-(f) $\tau = 1 > \tau_0$.

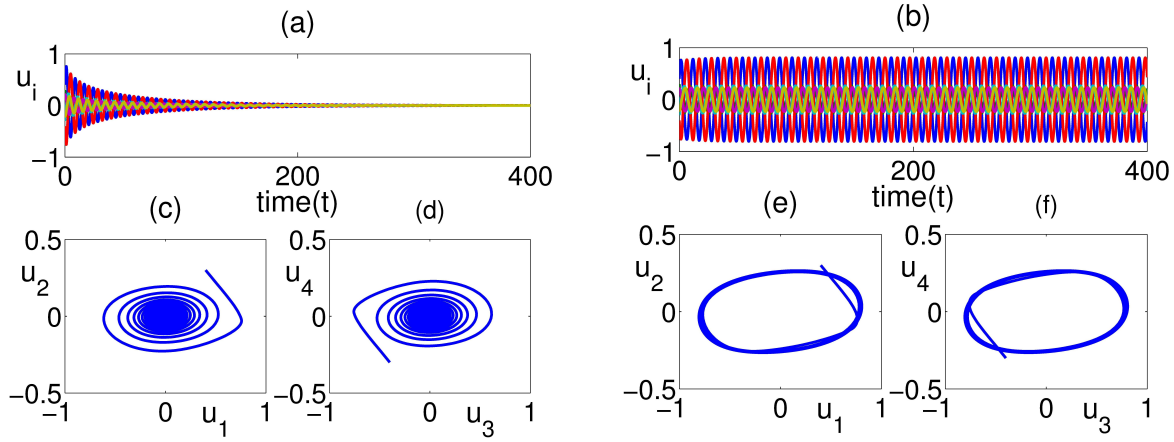

Figure 2.19: (a)-(f) Solution of the system (2.72) in the case when the condition $-1 \leq a_{12}a_{21}\beta^2 < 0$ holds. Parameter values are $a_{12} = 2$, $a_{21} = -0.45$, $\alpha = \pm 2$ and $\tau_0 = 1.286$. (a), (c)-(d) $0 < \tau = 1.2 < \tau_0$. (b), (e)-(f) $\tau = 2 > \tau_0$.

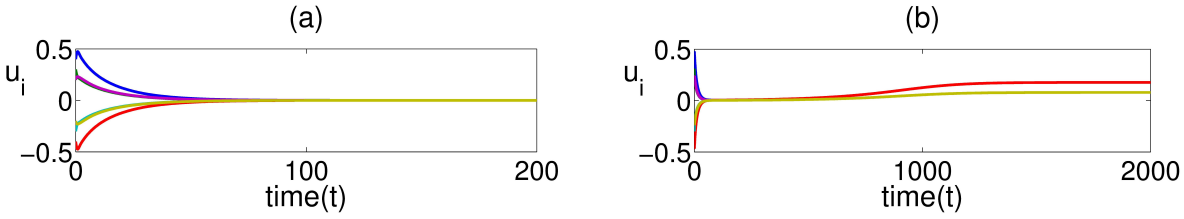

Figure 2.20: (a)-(b) Solution of the system (2.72) in the case when the condition $0 \leq a_{12}a_{21}\beta^2 \leq 1$ holds. Parameter values are $a_{12} = 2$, $a_{21} = 0.45$, $\tau = 0.5$. (a) $\alpha = 0.15$. (b) $\alpha = 0.25$.

In the case when $a_{12}a_{21}\beta^2 < -1$ (for example, $a_{12} = 2, a_{21} = -0.55$ and $\alpha = \pm 2$) we find $\omega_0 = 0.947$, $\tau_0 = 0.873$, $h'(s_0)p_0^{(1)}(i\omega_0) = 277.94 > 0$. Using Theorem 2.5.1,

one can conclude that the trivial steady state is stable when $0 < \tau < \tau_0$, illustrated in Figure 2.18 (a), (c)-(d), and at $\tau = \tau_0$ is loses stability via a Hopf bifurcation, which results in a stable periodic solution, as shown in Figure 2.18 (b), (e)-(f). In the same way, when parameters of the system (2.72) satisfy $-1 \leq a_{12}a_{21}\beta^2 < 0$, for example, $a_{12} = 2$, $a_{21} = -0.45$ and $\alpha = \pm 2$, we have $\omega_0 = 0.769$, $\tau_0 = 1.286$, $h'(s_0)p_0^{(1)}(i\omega_0) = 9.337 > 0$. It is possible to use Theorem 2.5.1 to conclude a Hopf bifurcation of the trivial steady state and a transition to a stable periodic solution at $\tau = \tau_0$, as illustrated in Figure 2.19 (a)-(f). Figures 2.20 (a)-(b) illustrate the case when $0 \leq a_{12}a_{21}\beta^2 \leq 1$, and we observe the loss of stability of the trivial steady state through a steady-state bifurcation, which results in a stable non-trivial equilibrium.

2.6.4 Numerical simulations for the strong gamma distribution kernel

In order to illustrate the dynamics in the case of the strong gamma distribution kernel, we again take $f(\cdot) = \tanh(\cdot)$, $\beta = f'(0) = 1$, and rewrite the system (2.2) as

$$\begin{cases} \dot{u}_1(t) = -u_1(t) + a_{12}\tanh(u_2(t-\tau)) + \alpha\tanh(u_8(t)), \\ \dot{u}_2(t) = -u_2(t) + a_{21}\tanh(u_1(t-\tau)), \\ \dot{u}_3(t) = -u_3(t) + a_{12}\tanh(u_4(t-\tau)) + \alpha\tanh(u_6(t)), \\ \dot{u}_4(t) = -u_4(t) + a_{21}\tanh(u_3(t-\tau)), \\ \dot{u}_5(t) = \gamma u_2(t) - \gamma u_5(t), \\ \dot{u}_6(t) = \gamma u_5(t) - \gamma u_6(t), \\ \dot{u}_7(t) = \gamma u_4(t) - \gamma u_7(t), \\ \dot{u}_8(t) = \gamma u_7(t) - \gamma u_8(t). \end{cases} \tag{2.73}$$

In the case when $a_{12}a_{21}\beta^2 < -1$ (for example, $a_{12} = 2, a_{21} = -0.55$ and $\alpha = \pm 2$) we find $\omega_0 = 0.733$, $\tau_0 = 1.20$, $h'(s_0)p_0^{(1)}(i\omega_0) = 351.87 > 0$. Using Theorem 2.5.2, one can conclude that the trivial steady state is stable when $0 < \tau < \tau_0$, illustrated in Figure 2.21 (a), (c)-(d), and at $\tau = \tau_0$ is loses stability via a Hopf bifurcation, which results in a stable periodic solution, as shown in Figure 2.21 (b), (e)-(f).

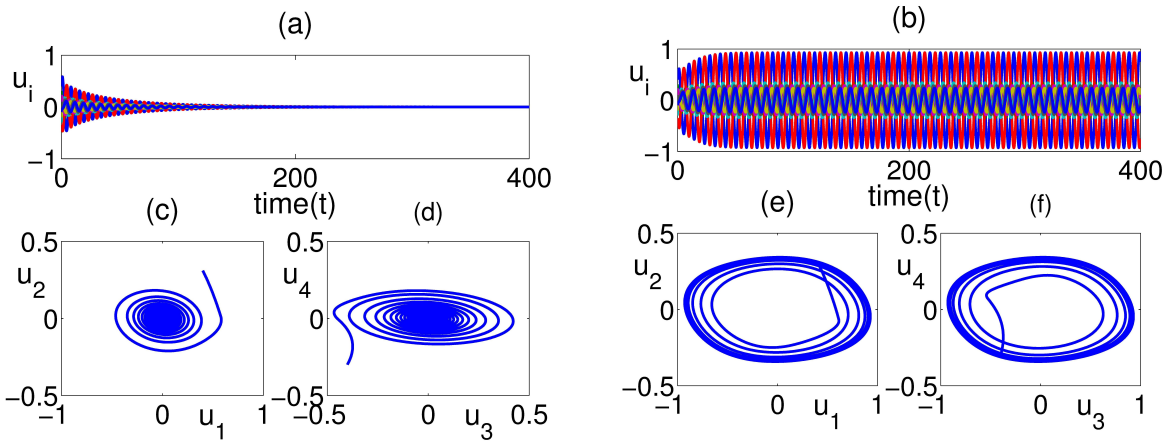

Figure 2.21: (a)-(f) Solution of the system (2.73) in the case when $a_{12}a_{21}\beta^2 < -1$. Parameter values are $a_{12} = 2$, $a_{21} = -0.55$, $\alpha = \pm 2$ and $\tau_0 = 1.20$. (a), (c)-(d) $0 < \tau = 0.9 < \tau_0$. (b), (e)-(f) $\tau = 1.3 > \tau_0$.

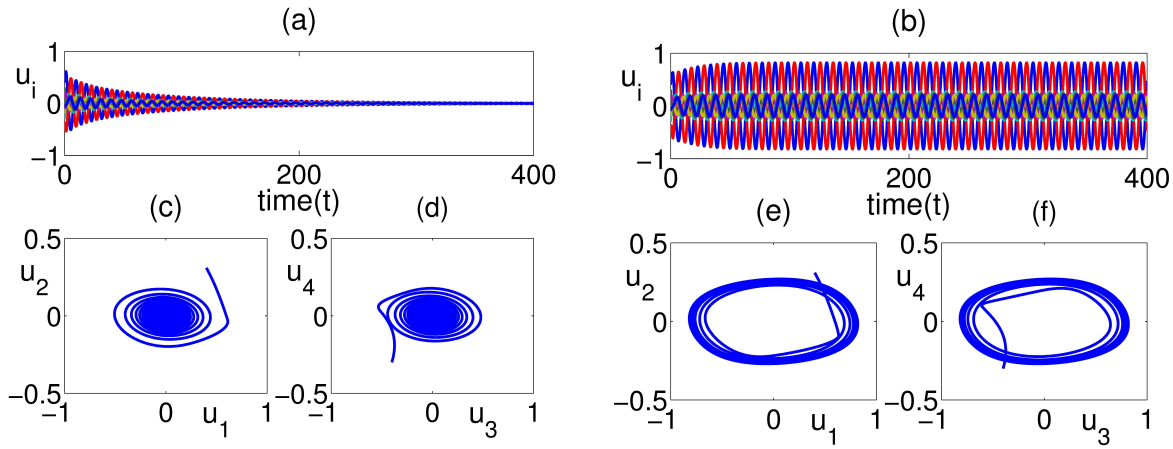

Figure 2.22: (a)-(f) Solution of the system (2.73) in the case when the condition $-1 \leq a_{12}a_{21}\beta^2 < 0$ holds. Parameter values are $a_{12} = 2$, $a_{21} = -0.45$, $\alpha = \pm 2$ and $\tau_0 = 1.66$. (a), (c)-(d) $0 < \tau = 1.2 < \tau_0$. (b), (e)-(f) $\tau = 1.8 > \tau_0$.

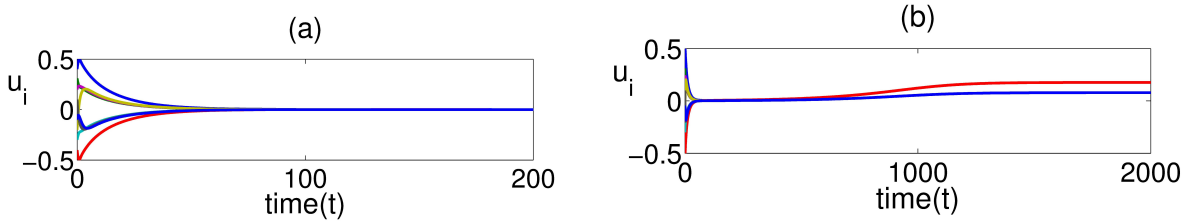

Figure 2.23: (a)-(b) Solution of the system (2.73) in the case when the condition $0 \leq a_{12}a_{21}\beta^2 \leq 1$ holds. Parameter values are $a_{12} = 2$, $a_{21} = 0.45$, $\tau = 0.5$. (a) $\alpha = 0.15$. (b) $\alpha = 0.25$.

In the same way, when parameters of the system (2.73) satisfy $-1 \leq a_{12}a_{21}\beta^2 < 0$,

for example, $a_{12} = 2$, $a_{21} = -0.45$ and $\alpha = \pm 2$, we have $\omega_0 = 0.606$, $\tau_0 = 1.667$, $h'(s_0)p_0^{(1)}(i\omega_0) = 115.93 > 0$. As shown in Figure 2.22 (a)-(f) the solutions of the system (2.2) tend to the stable trivial steady state and transition to a stable periodic solution at $\tau = \tau_0$. Figures 2.23 (a)-(b) show the case when $0 \leq a_{12}a_{21}\beta^2 \leq 1$, and one can see the loss of stability of the trivial steady state through a steady-state bifurcation, which results in a stable non-trivial equilibrium.

2.7 Discussion

In this chapter, we have analysed a generalised model of coupled neural networks with discrete and distributed time delays for a general distribution kernel. We have analytically obtained a characteristic equation determining the stability of the trivial steady state for any general distribution kernel. In order to further understand the dynamics of the system, we have studied in detail the cases of the three commonly used distribution kernels, i.e. delta, uniform and weak gamma distribution. For each of these distributions, we have obtained analytical conditions for stability of the null solution in terms of system parameters and the time delays. The results suggest that stability of the zero steady state depends on the synaptic weights, strength of the connection between the two sub-networks and time delays in the connection. In the case of the Dirac delta distribution kernel, the stability region of the trivial steady state becomes larger with increasing the product of the synaptic weights.

In the case of the uniformly distributed kernel, the stability properties of the trivial steady state strongly depend on the width of the distribution. In particular, as the width of the distribution becomes larger, the stability region shrinks and becomes an isolated bubble in the $\tau - \alpha$ plane. As one of the synaptic weights is increased, enlarging the distribution width leads to a smaller region of stability, but it never becomes an isolated island.

In the case of the weak gamma distribution kernel, we have obtained analytical and numerical results on the stability properties of the system, and have shown that the strength of the connection between the two sub-networks plays an important role. Increasing the coupling reduces the size of the stability region, where the trivial steady state is stable, and no oscillations are possible. We have also performed direct numerical simulations that confirm our analytical findings and illustrate the dynamics of the system inside and outside the stability regions for all distribution kernels presented in this chapter. Notably, for some parameter values, when the trivial steady state becomes unstable, the system

can support stable non-trivial steady states.

It is worth noting that while the cases of delta and weak gamma distribution exhibit a similar type of stability, in the case of the uniform distribution, it is not sufficient to consider only the mean time delay, as the width of the distribution also plays a profound role in defining the region of stability. Combination of discrete and distributed time delays considered in this chapter shows that stability regions for wider uniform distributions are characterised by smaller ranges of coupling strengths, which is in contrast to the results obtained in [7, 78, 79], where the authors observed an increase in the stability region for wider uniform distributions.

Neural networks are often used to model associative memories or pattern recognition, where information is represented by stable equilibria of the system. In order to retrieve a memory, the system should start with an initial condition lying within the basin of attraction of a stable steady state. If the steady state is unstable, this renders the retrieval of the memory impossible [60]. In the light of this observation, the results obtained in this chapter provide important insights into the circumstances where neural networks with discrete and distributed time delays can support a successful memory retrieval.

There are several directions in which work in this chapter can be extended to yield a better understanding of neural systems. One possibility would be to consider a large system of coupled neurons consisting of several sub-groups with different types of delayed connections within and between sub-groups. Such systems are known to be able to support rich dynamics including chimera states, where some nodes of the network have coherent dynamics, while others remain chaotic. The question of how such dynamics can be affected by the combination of discrete and distributed delays remains an open problem. Another practically important issue is that of dynamic synchronisation in systems with time-delayed connections. Kyrychko et al. have recently developed a formalism for analysis of synchronisation in systems with distributed delay coupling [80], and it would be insightful to generalise this approach to systems that include both discrete and distributed time delays between nodes.

An efficient pattern recognition relies on the presence of multistability in the system [25], and hence, requires a careful analysis of the basins of attraction of different steady states. Understanding the structure of these co-existing attractors in systems with discrete and distributed delays would explain how such neural networks perform the complex task of pattern recognition.

Chapter 3

Aging transition in system of oscillators with global distributed-delay coupling

In this chapter, an aging transition is analysed for high-dimensional globally coupled Stuart-Landau oscillators with distributed-delay coupling such that a random fraction of them become non-oscillators, as mentioned in subsection 1.3.3. We specify the most familiar distribution kernels such as uniform and gamma distribution kernels to find analytical expressions for stability regions. We also use a direct numerical method to confirm stability regions.

3.1 Model derivation

A system of N globally coupled Stuart-Landau oscillators with distributed-delay coupling can be written as follows

$$\dot{Z}_j(t) = (\alpha_j + i\omega)Z_j(t) - |Z_j(t)|^2 Z_j(t) + \frac{k}{N}\sum_{i=1}^{N}\left[\int_0^\infty g(t')Z_i(t-t')dt' - Z_j(t)\right] \\ -\frac{k}{N}\left[\int_0^\infty g(t')Z_j(t-t')dt' - Z_j(t)\right], \qquad j = 1, ..., N, \tag{3.1}$$

where $Z_j \in \mathbb{C}$, ω is the natural frequency of oscillations, α_j are bifurcation parameters that control whether in the absence of coupling the oscillator j exhibits a stable periodic solution ($\alpha_j > 0$) or converges to a stable trivial equilibrium ($\alpha_j < 0$), k is the coupling strength, and the last term in the right-hand side of (3.1) removes the self-coupling from

the system. The kernel g is taken to be positive-definite and normalised to unity, i.e.

$$g(u) \geq 0, \quad \int_0^\infty g(u)du = 1.$$

If the distribution kernel is taken in the form of the Dirac delta function $g(u) = \delta(u)$, one obtains a system of globally instantaneously coupled oscillators that has been extensively studied [3, 32, 98, 134, 162], while for $g(u) = \delta(u-\tau)$, the model (3.1) reduces to a system with a single discrete time delay studied in [153, 173]. By focusing on the dynamics of system (3.1), we extend the work of Thakur *et al.* [153] in the following directions. The first major difference is that we consider a more general and more realistic case of distributed delay. In order to gain a better understanding of the system behaviour inside the stability regions, we will numerically compute characteristic eigenvalues. By considering the important case of a gamma-distributed delay kernel we will show that it is not only the width of the distribution and the mean delay, but also the actual shape of the distribution that affects the stability region in systems with distributed delay coupling. Following Daido and Nakanishi [30], let p denote the fraction of inactive oscillators with the bifurcation parameter $\alpha_j = -b$ $(b > 0)$, and $q = 1 - p$ be the fraction of active oscillators with the bifurcation parameter $\alpha_j = a$ $(a > 0)$. To analyse the aging transition in the system (3.1) we use a mean-field approximation [30, 153] which assumes that all active and inactive oscillators achieve synchronization in their respective subpopulations (see [63] for further numerical evidence in support of this), i.e. we write $Z_j(t) = A(t)$ for all active elements and $Z_j(t) = I(t)$ for all inactive oscillators. This reduces the original high-dimensional system (3.1) to the following

$$\begin{aligned}
\dot{A}(t) = & \left[a - k\left(1 - \frac{1}{N}\right) + i\omega - |A(t)|^2\right] A(t) \\
& + k\left(q - \frac{1}{N}\right)\int_0^\infty g(t')A(t-t')dt' + kp\int_0^\infty g(t')I(t-t')dt', \\
\dot{I}(t) = & \left[-b - k\left(1 - \frac{1}{N}\right) + i\omega - |I(t)|^2\right] I(t) \\
& + k\left(p - \frac{1}{N}\right)\int_0^\infty g(t')I(t-t')dt' + kq\int_0^\infty g(t')A(t-t')dt'.
\end{aligned} \tag{3.2}$$

Linearisation of this system near the zero steady state $(A, I) = (0, 0)$ yields the following characteristic equation for eigenvalues λ

$$\begin{aligned}&\left[a - k\left(1 - \frac{1}{N}\right) + i\omega + k\left(q - \frac{1}{N}\right)\widehat{G}(\lambda) - \lambda\right]\\&\times\left[-b - k\left(1 - \frac{1}{N}\right) + i\omega + k\left(p - \frac{1}{N}\right)\widehat{G}(\lambda) - \lambda\right] - k^2pq\widehat{G}^2(\lambda) = 0,\end{aligned} \tag{3.3}$$

where

$$\widehat{G}(\lambda) = \int_0^\infty e^{-\lambda u}g(u)du,$$

is the Laplace transform of the function $g(u)$.

3.2 Uniform distribution kernel

To make analytical progress with analysis of the equation (3.3), we begin by considering the *uniformly-distributed delay kernel* (1.6). Laplace transform of the uniform distribution (1.6) can be readily found as

$$\widehat{G}(\lambda) = \frac{1}{2\sigma\lambda}e^{-\lambda\tau}(e^{\lambda\sigma} - e^{-\lambda\sigma}) = e^{-\lambda\tau}\frac{\sinh(\lambda\sigma)}{\lambda\sigma}. \tag{3.4}$$

Substituting this expression into the characteristic equation (3.3) and looking for characteristic roots in the form $\lambda = i\xi$, separating real and imaginary parts gives

$$\begin{aligned}&\left[a - k\left(1 - \frac{1}{N}\right) + k\left(q - \frac{1}{N}\right)\cos(\xi\tau)\gamma(\xi,\sigma)\right]\left[-b - k\left(1 - \frac{1}{N}\right) + k\left(p - \frac{1}{N}\right)\cos(\xi\tau)\gamma(\xi,\sigma)\right]\\&- \left[\omega - \xi + k\left(q - \frac{1}{N}\right)\sin(\xi\tau)\gamma(\xi,\sigma)\right]\times\left[\omega - \xi + k\left(p - \frac{1}{N}\right)\sin(\xi\tau)\gamma(\xi,\sigma)\right]\\&= k^2pq\cos(2\xi\tau)\gamma^2(\xi,\sigma),\\&\left[-b - k\left(1 - \frac{1}{N}\right) + k\left(p - \frac{1}{N}\right)\cos(\xi\tau)\gamma(\xi,\sigma)\right]\left[\omega - \xi + k\left(q - \frac{1}{N}\right)\sin(\xi\tau)\gamma(\xi,\sigma)\right]\\&+ \left[a - k\left(1 - \frac{1}{N}\right) + k\left(q - \frac{1}{N}\right)\cos(\xi\tau)\gamma(\xi,\sigma)\right]\times\left[\omega - \xi + k\left(p - \frac{1}{N}\right)\sin(\xi\tau)\gamma(\xi,\sigma)\right]\\&= -k^2pq\sin(2\xi\tau)\gamma^2(\xi,\sigma),\end{aligned} \tag{3.5}$$

where

$$\gamma(\xi,\sigma) = \frac{\sin(\xi\sigma)}{\xi\sigma}.$$

A solution of the system of equations (3.5) gives an implicit expression for the boundary of the amplitude death, i.e. the suppression of oscillations, in terms of system parameters. In order to better understand what is actually happening inside the corresponding stability regions, we use a pseudospectral method described in [19] and implemented in the traceDDE toolbox for MATLAB to numerically compute the characteristic eigenvalues of equation (3.3). To this end, we introduce auxiliary real variables $A = A_r + iA_i$ and $I = I_r + iI_i$, and rewrite the linearised system with uniformly-distributed delay kernel (1.6) as follows

$$\dot{\mathbf{z}}(t) = L_0\mathbf{z}(t) + \frac{1}{2\sigma}\int_{-(\tau+\sigma)}^{-(\tau-\sigma)} M\mathbf{z}(t+s)ds, \tag{3.6}$$

where $\mathbf{z} = (A_r, A_i, I_r, I_i)^T$,

$$L_0 = \begin{pmatrix} a - k\left(1 - \frac{1}{N}\right) & -\omega & 0 & 0 \\ \omega & a - k\left(1 - \frac{1}{N}\right) & 0 & 0 \\ 0 & 0 & -b - k\left(1 - \frac{1}{N}\right) & -\omega \\ 0 & 0 & \omega & -b - k\left(1 - \frac{1}{N}\right) \end{pmatrix},$$

and

$$M = \begin{pmatrix} k\left(q - \frac{1}{N}\right) & 0 & kp & 0 \\ 0 & k\left(q - \frac{1}{N}\right) & 0 & kp \\ kq & 0 & k\left(p - \frac{1}{N}\right) & 0 \\ 0 & kq & 0 & k\left(1 - \frac{1}{N}\right) \end{pmatrix}.$$

When $\sigma = 0$, the last term in the equation (3.6) turns into $M\mathbf{z}(t-\tau)$, and the system (3.2) reduces to the system with a single discrete time delay τ analysed in [153]. Figure 3.1 shows the regions of amplitude death together with the magnitude of the real part of the leading eigenvalue of the characteristic equation (3.5) in the (τ, k) parameter space for the case of a single discrete delay, i.e. $\sigma = 0$. One observes that increasing the natural frequency of oscillations ω or increasing the fraction of inactive oscillators leads to the increase in the number of stability islands and their size. Whilst Thakur et al. [153] have also noticed the increasing size of stability islands associated with increasing p, we also note the appearance of additional stability islands for higher values of time delays τ or for higher natural frequency ω.

To investigate the role of the width of uniform delay distribution σ, we now compare the results for the discrete and the uniformly-distributed delays with the same mean time delay τ. Figure 3.2 shows that as σ grows, this leads to an increase in the size of AD parameter regions, and the stability islands grow dramatically until they merge into a single continuous region along τ axis for higher proportions of the inactive oscillators p.

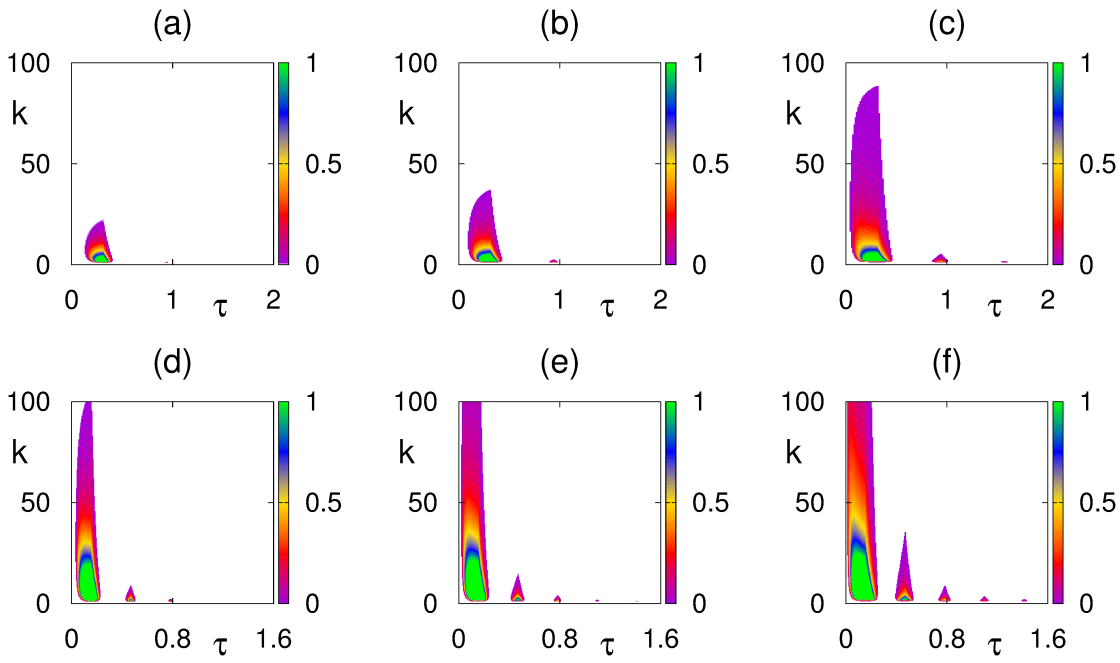

Figure 3.1: Regions of AD (aging transition) for the system (3.2) with uniform distribution kernel for $a = 2, b = 1, \sigma = 0, N = 500$, and $\omega = 10$ (a)-(c), or $\omega = 20$ (d)-(f). Colour code denotes $[-\max\{\mathrm{Re}(\lambda)\}]$ for $\max\{\mathrm{Re}(\lambda)\} \leq 0$. (a), (d) $p = 0.3$, (b), (e) $p = 0.4$, (c), (f) $p = 0.5$.

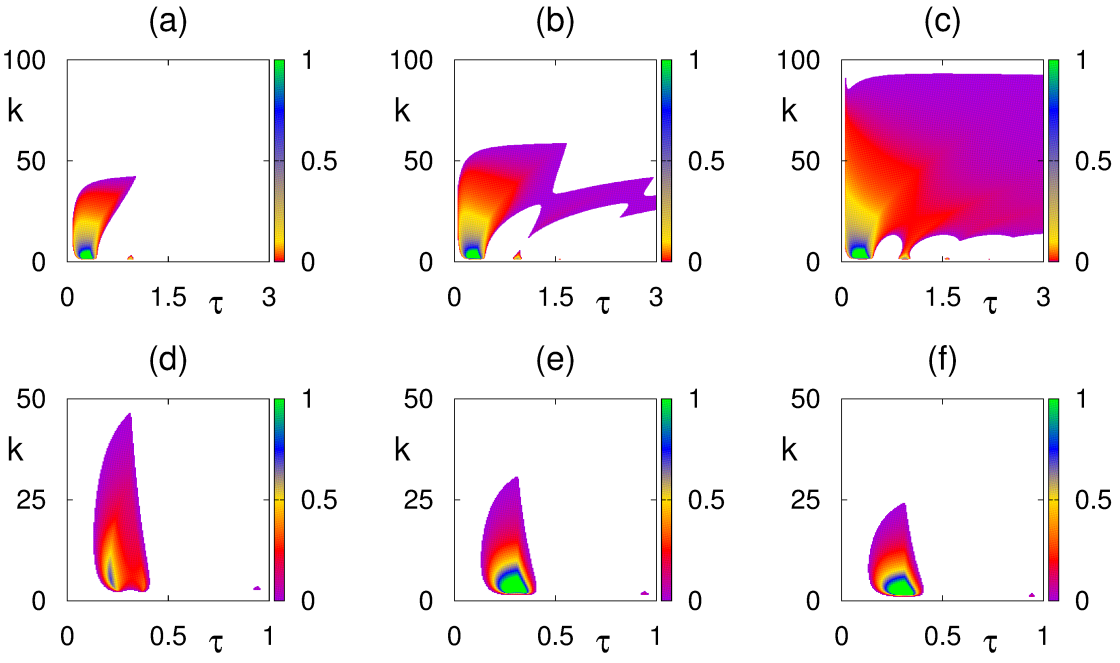

Figure 3.2: Regions of AD (aging transition) for the system (3.2) with uniform distribution kernel for $a = 2, b = 1, \omega = 10$. Colour code denotes $[-\max\{\mathrm{Re}(\lambda)\}]$ for $\max\{\mathrm{Re}(\lambda)\} \leq 0$. (a)-(c) $\sigma = 0.06$, $N = 500$; (d)-(f) $\sigma = 0$, $p = 0.1$. (a) $p = 0.3$, (b) $p = 0.4$, (c) $p = 0.5$, (d) $N = 2$, (e) $N = 4$, (f) $N = 20$.

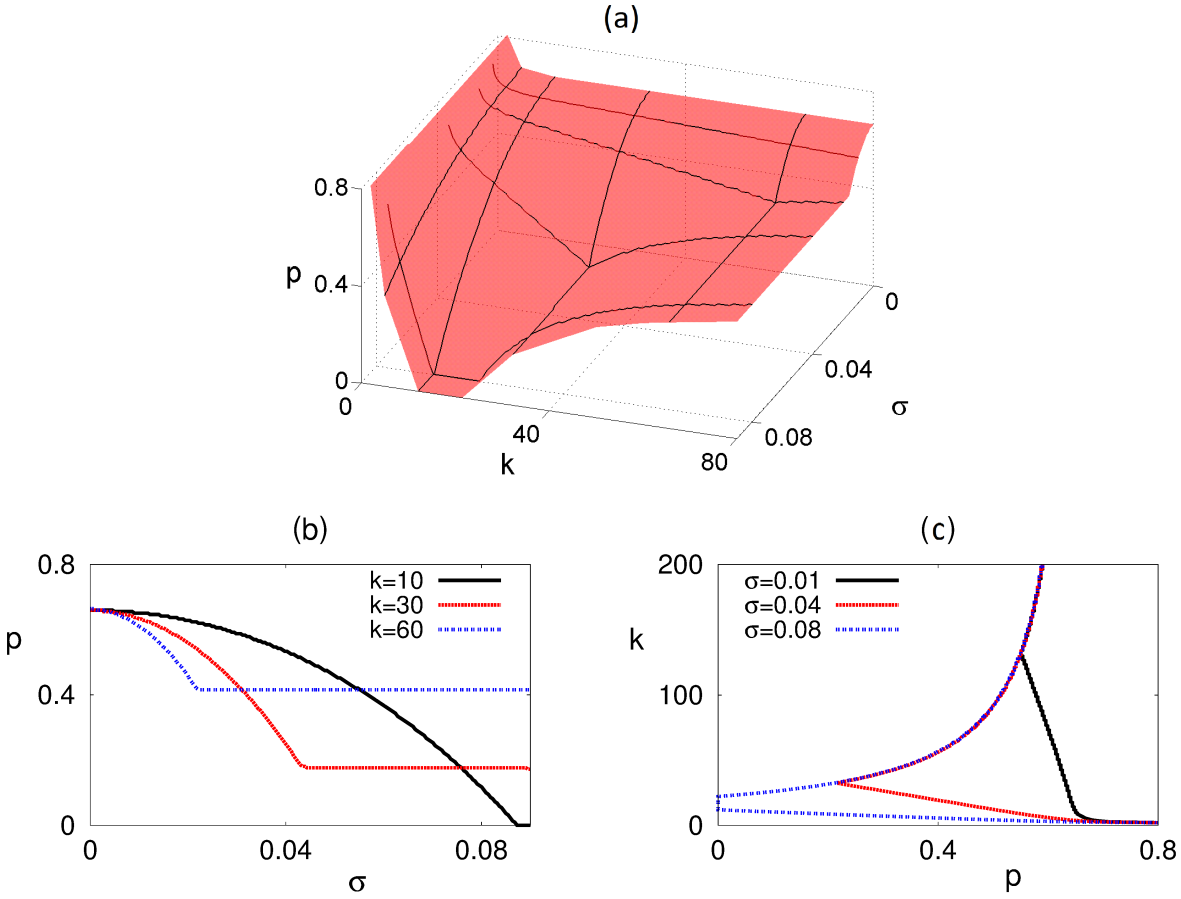

Figure 3.3: Regions of AD (aging transition) for the system (3.2) with uniform distribution kernel for $a = 2$, $b = 1$, $\omega = 10$, $\tau = 0.5$, $N = 500$. AD occurs inside of the surface in (a), above the curves in (b), and to the right of the boundary curves in (c).

One should note that while the difference between the delta- and uniformly-distributed delays is small for sufficiently small p, it becomes much more pronounced as p increases. Already in the case when exactly half of all oscillators are inactive ($p = 0.5$), whereas in Figure 3.1 (c) for $\sigma = 0$, $\omega = 10$, $p = 0.5$ there were still just three isolated death islands, for $\sigma = 0.06$ there is the whole range of coupling strengths where amplitude death can be achieved for an arbitrary value of the mean time delay τ, provided that it is greater than some minimum value. Figure 3.2 also illustrates that the stability regions shrink with the increasing number of oscillators N, until they reach some steady configuration beyond which they appear to be unaffected by further increases in N.

Figure 3.3 shows how the stability boundary of the trivial steady state depends on the parameters σ, p, and k. It is noteworthy that as the coupling strength increases, the size of AD regions in the σ-p plane decreases, and, in fact, AD happens for a smaller range of distribution widths for the same fraction of inactive oscillators p. Figure 3.3 (c) suggests

that as σ increases, AD occurs for smaller values of p for the same coupling strength k, thus implying that increasing the width of distribution for the same mean time delay can make the aging transition take place sooner that it would happen in the case of a discrete time delay.

3.3 Gamma distribution kernel

The second commonly used distribution in the literature is the gamma distribution (1.7). In this case, one can either use the Laplace transform of the distribution kernel

$$\widehat{G}(\lambda) = \left(\frac{\gamma}{\lambda+\gamma}\right)^r, \tag{3.7}$$

or apply the *linear chain trick* [91] that allows one to replace the original system with distributed delays by a system of $(r+1)$ ordinary differential equations. Considering the gamma distributed kernel in (3.2) with $r=1$ and introducing new variables

$$\begin{aligned} X_A(t) &= \int_0^\infty \gamma e^{-\gamma s} A(t-s)ds, \\ \\ X_I(t) &= \int_0^\infty \gamma e^{-\gamma s} I(t-s)ds, \end{aligned}$$

one can rewrite the system (3.2) as follows

$$\begin{cases} \dot{A}(t) &= \left[a - k\left(1-\frac{1}{N}\right) + i\omega\right] A(t) + k\left(q-\frac{1}{N}\right) X_A(t) + kpX_I(t), \\ \\ \dot{I}(t) &= \left[-b - k\left(1-\frac{1}{N}\right) + i\omega\right] I(t) + k\left(p-\frac{1}{N}\right) X_I(t) + kqX_A, \\ \\ \dot{X}_A(t) &= \gamma A(t) - \gamma X_A(t), \\ \\ \dot{X}_I(t) &= \gamma I(t) - \gamma X_I(t). \end{cases} \tag{3.8}$$

Substituting the Laplace transform (3.7) with $r=1$ into the characteristic equation (3.3), or linearising the system (3.8) near the trivial steady state $(0,0,0,0)$, gives the following characteristic equation for eigenvalues λ

$$\begin{aligned} &\left[(\lambda+\gamma)\left(a - k\left(1-\frac{1}{N}\right) + i\omega - \lambda\right) + \gamma k\left(q-\frac{1}{N}\right)\right] \\ \\ &\times \left[(\lambda+\gamma)\left(-b - k\left(1-\frac{1}{N}\right) + i\omega - \lambda\right) + \gamma k\left(p-\frac{1}{N}\right)\right] \\ \\ &-\gamma^2 k^2 pq = 0. \end{aligned} \tag{3.9}$$

This equation can be solved numerically to understand the role of different parameters in the aging transition for the case of the gamma distribution kernel.

Figure 3.4 illustrates the boundary of the amplitude death in terms of p, γ, k and ω for the weak delay distribution (1.7) with $r = 1$. For a fixed coupling strength k and sufficiently large natural frequency ω, the amplitude death can occur for an arbitrary fraction of inactive oscillators p, as long as γ is sufficiently small (which, in light of the relation (1.8), implies that the mean time delay τ_m should be sufficiently large). In this case, for larger values of γ there is a certain minimum p required for amplitude death, and the value of this critical p increases with γ.

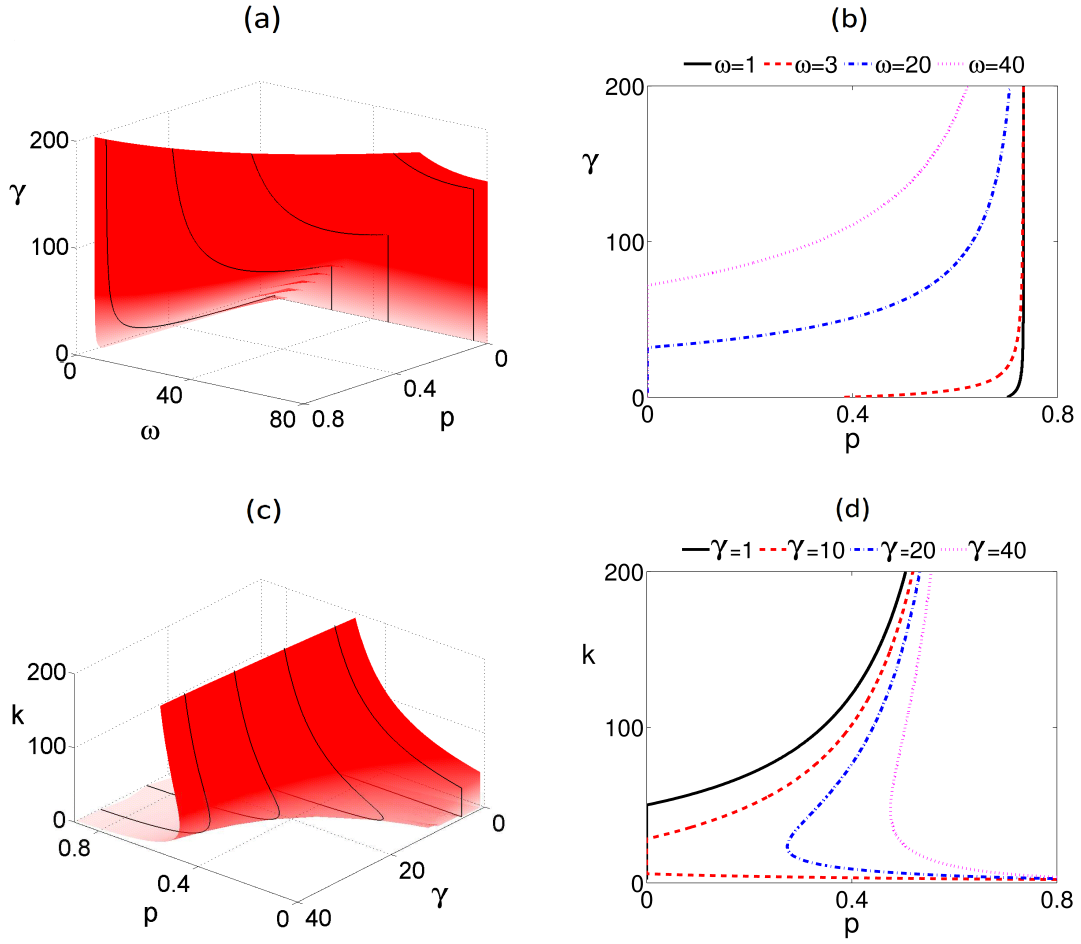

Figure 3.4: AD boundary of the system (3.8) with the weak delay distribution kernel for $a = 2, b = 1, N = 500$. (a)-(b) $k = 10$, (c)-(d) $\omega = 10$. AD occurs below and to the right of the surface in (a),(c), and to the right of the boundary curves in (b),(d).

For smaller values of ω, the amplitude death can only occur if p exceeds a certain threshold that again increases with γ until it reaches some value that is independent of γ if γ is sufficiently high. This means that if the mean time delay is reasonably small, the

threshold value of p becomes independent of τ_m. Similarly, for a fixed natural frequency ω and smaller values of γ, there is a range of coupling strengths k, for which the amplitude death can occur for an arbitrary proportion p of inactive oscillators. For higher γ (and, correspondingly, smaller mean time delay τ_m), the amplitude death can only take place for a sufficiently large value of p. Interestingly, this critical p initially decreases and then monotonically increases with k.

Considering the case of the *strong delay kernel* with $r = 2$, we use the same strategy as for the weak kernel and introduce new variables as follows

$$X_A(t) = \int_0^\infty \gamma e^{-\gamma s} A(t-s)ds, \quad Y_A(t) = \int_0^\infty \gamma^2 s e^{-\gamma s} A(t-s)ds,$$

$$X_I(t) = \int_0^\infty \gamma e^{-\gamma s} I(t-s)ds, \quad Y_I(t) = \int_0^\infty \gamma^2 s e^{-\gamma s} I(t-s)ds.$$

This allows one to rewrite the system (3.2) in the equivalent form

$$\begin{cases} \dot{A}(t) = \left[a - k\left(1 - \frac{1}{N}\right) + i\omega\right] A(t) + k\left(q - \frac{1}{N}\right) Y_A(t) + kpY_I(t), \\ \dot{I}(t) = \left[-b - k\left(1 - \frac{1}{N}\right) + i\omega\right] I(t) + k\left(p - \frac{1}{N}\right) Y_I(t) + kqY_A, \\ \dot{X}_A(t) = \gamma A(t) - \gamma X_A(t), \\ \dot{Y}_A(t) = \gamma X_A(t) - \gamma Y_A(t), \\ \dot{X}_I(t) = \gamma I(t) - \gamma X_I(t), \\ \dot{Y}_I(t) = \gamma X_I(t) - \gamma Y_I(t). \end{cases} \tag{3.10}$$

Linearising this system near the trivial steady state yields the following equation for characteristic eigenvalues λ

$$\begin{aligned} &\left[(\lambda+\gamma)^2\left(a - k\left(1 - \frac{1}{N}\right) + i\omega - \lambda\right) + \gamma^2 k\left(q - \frac{1}{N}\right)\right] \\ &\times \left[(\lambda+\gamma)^2\left(-b - k\left(1 - \frac{1}{N}\right) + i\omega - \lambda\right) + \gamma^2 k\left(p - \frac{1}{N}\right)\right] \\ &-\gamma^4 k^2 pq = 0. \end{aligned} \tag{3.11}$$

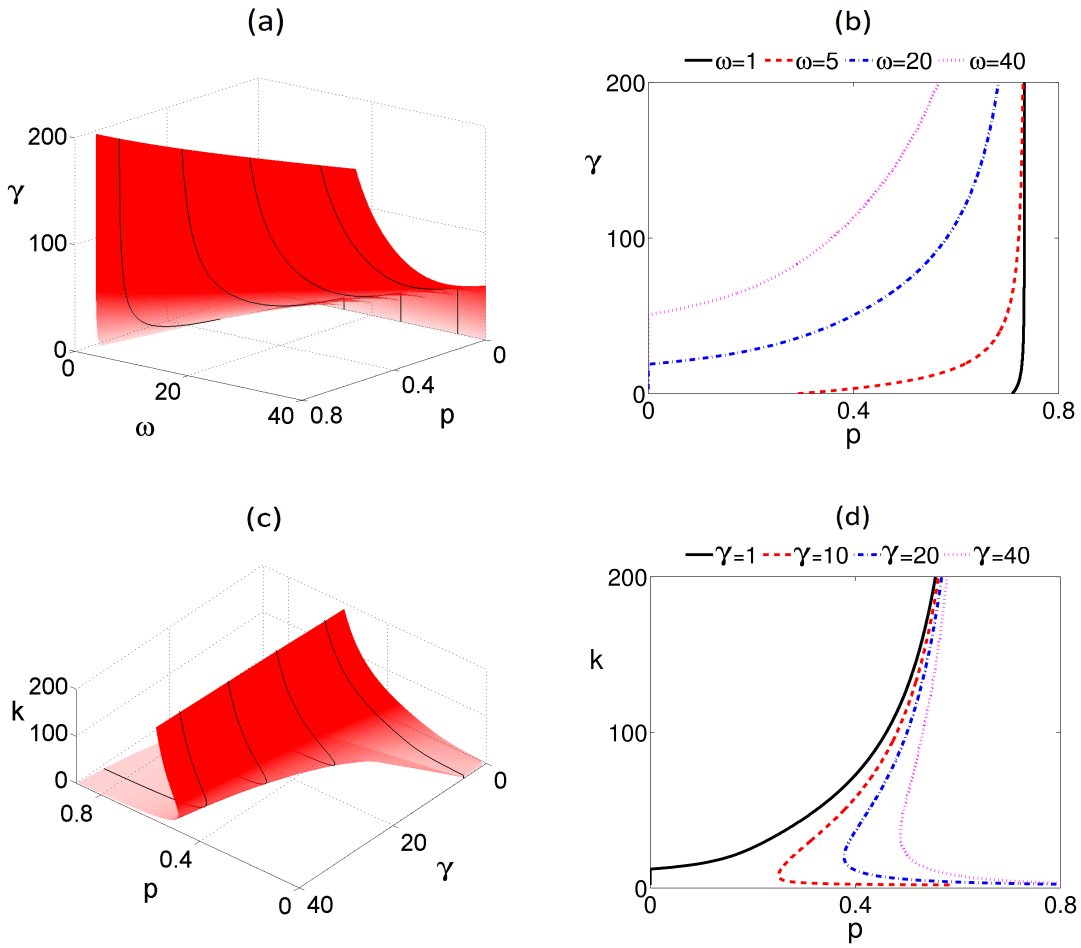

Figure 3.5: AD boundary of the system (3.10) with the strong delay distribution kernel for $a = 2$, $b = 1$, $N = 500$. (a)-(b) $k = 10$, (c)-(d) $\omega = 10$. AD occurs below and to the right of the surface in (a),(c), and to the right of the boundary curves in (b),(d).

Figure 3.5 illustrates AD regions for the strong delay distribution kernel (1.7) with $r = 2$. Boundaries of AD exhibit the behaviour qualitatively similar to that for the weak kernel, i.e. for the fixed coupling strength k increasing the natural frequency ω increases the range of γ, for which AD can occur with an arbitrary fraction of inactive oscillators p. However, one should note that for the same values of ω, aging transition in the case of the strong delay kernel takes place for much lower values of γ, i.e. for significantly higher values of the mean time delay τ_m than for the weak delay kernel. Furthermore, for a sufficiently small γ, whereas for the weak delay kernel it could be possible to achieve aging transition for an arbitrary value of p, in the case of the strong delay, there is a bound on the minimum value of p, and more generally for the same coupling strength and the same mean time delay, a higher p is required for AD.

3.4 Numerical simulations

In this section we perform the numerical simulations of the fully nonlinear system (3.2) to illustrate the stability of the trivial steady state in different parameter regimes. The results are shown for uniformly-distributed kernel in Figures 3.6 (a)-(b), for a weak delay kernel in Figures 3.6 (b)-(c), and for a strong delay kernel in Figures 3.6 (e)-(f). In all three cases, there is a stability switch, which gives rise to periodic oscillations, where the steady state loses its stability. The results of the numerical simulations fully agree with the stability analysis conducted in the previous section.

3.5 Discussion

In this chapter, we have studied aging transition in a system of globally coupled active and inactive oscillators with distributed-delay coupling. Using specific examples of uniform and gamma distributions, we have been able to analytically find boundaries of the amplitude death depending on the coupling parameters and the proportion of inactive oscillators, and we have also numerically computed characteristic eigenvalues in each scenario. For the case of uniform delay distribution, our results suggest that increasing the width of the distribution for the same mean time delay allows the system to achieve aging transition for a smaller coupling strength and a smaller proportion of inactive oscillators, and the largest proportion of inactive oscillators required for AD occurs for the discrete time delay. This highlights the fact that not only time delays can have a significant effect on aging transition, but also that the details of the delay distribution play an important role, since even for the same mean time delay, AD can occur or not depending on the width of the distribution.

In the case of the gamma distribution, provided the mean time delay is sufficiently large, there exists a range of coupling strengths, for which it is possible to achieve aging transition for any proportion of inactive oscillators, and the range of this coupling strength reduces with decreasing mean time delay. When one compares the behaviour of the system with a weak and strong distribution kernels, it becomes apparent that although AD regions exhibit qualitatively similar features for these two distributions, in the case of a strong distribution kernel aging transition occurs for higher values of the mean time delays and a higher proportion of inactive oscillators. This again reiterates the important role played by the delay distribution in quenching oscillations in coupled oscillator networks.

There are several possible ways how the work done in this chapter could be furthered.

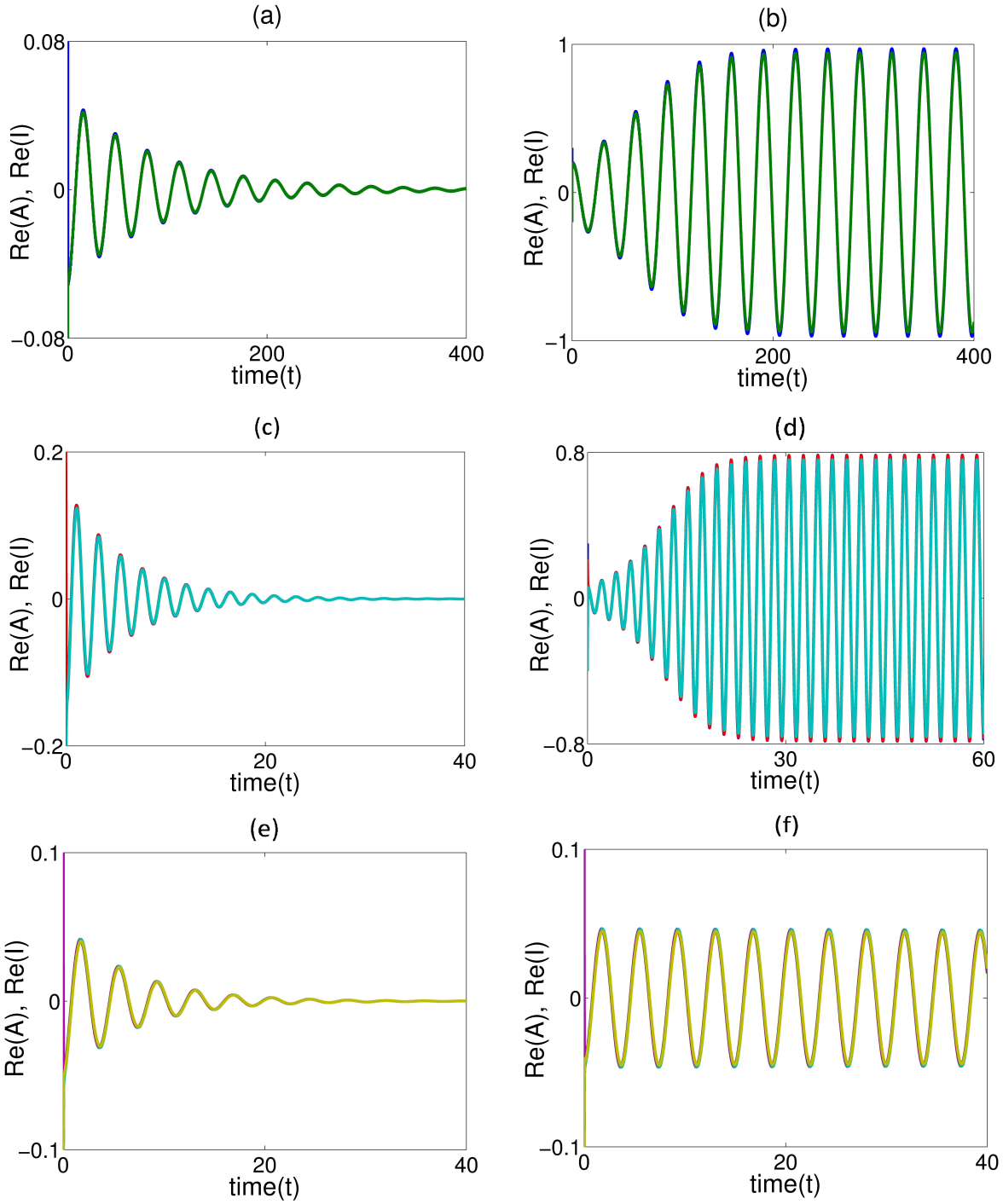

Figure 3.6: (a)-(b) Solutions of the system (3.2) with uniformly-distribution kernel for $\sigma = 0.01$. (c)-(d) Solutions of the system (3.8) with weak delay kernel for $\gamma = 40$. (e)-(f) Solutions of the system (3.10) with strong delay kernel for $\gamma = 40$. Other parameters, $a = 2$, $b = 1$, $\omega = 10$, $\tau = 0.5$, $N = 500$, $k = 100$. (a),(c),(e) $p = 0.8$. (b),(d),(f) $p = 0.2$.

One interesting and practically important problem concerns the analysis of aging transition in complex networks [59, 63, 129, 151], where the coupling is not global but is rather determined by a specific network topology, while distributed delays are to be expected due to the intricate nature of connections between nodes. In this respect, understanding the dynamics of interactions between network topology and distributed-delay coupling could provide significant insights into network behaviour and robustness. Quite often it may not be practically possible to fix a specific delay distribution for the coupling [12, 46, 47], systems may have combinations of discrete and distributed delays [119, 173], or delays can depend on the actual state of nodes [2, 65]. Hence, another important research direction would be to analyse aging transition in systems with mixed, stochastic, and state-dependent delays.

Chapter 4

Dynamics of subthalamic nucleus-globus palidus network with three delays

In this chapter, we analyse the stability of the system based on the original STN-GP model introduced by Nevado-Holgado *et al.* [106]. The stability analysis performed in [106] and its later modifications have made the following simplifications: it is assumed that the membrane time constants are exactly the same; the transmission delays in the neural populations are taken to be equal; nonlinear activation functions are replaced by linear functions. In this chapter, we concentrate on considering a general nonlinear class of activation functions. The activation functions are not necessarily just logistic curves, since the neural population might have more than a single inflexion point [158]. Moreover, the three time delays in the connections between the excitatory and inhibitory populations of neurons are taken to be different. Finally, the membrane time constants are taken to be different. In the next section, we introduce the model describing STN and GP neural populations. A time-shift transformation is used to reduce the number of time delays, prove positivity of solutions for all times, and implicitly calculate a steady state of the model. In Section 4.3 we derive analytical conditions for local stability of the steady state in the case of a non-zero delay in the self-interaction of the GP population, and an instant cross-interaction between GP and STN neural populations, and analyse the case when there is a delay in the cross-interaction between GP and STN populations, and an instant self-interaction in the GP population. In Section 4.4, we consider a general case and perform stability analysis of the system in the presence of a delayed self-interaction in the GP population and a delayed cross-interaction between STN and GP populations.

The chapter concludes with the summary of the results.

4.1 The model

Following Nevado-Holgado *et al.* [106], the mean firing rate model describing the temporal evolution of the firing rates of the excitatory population of neurons, STN, denoted by $S(t)$, and the inhibitory population of neurons, GP, denoted by $G(t)$, has the form

$$\begin{aligned} \tau_S S'(t) &= F_S(-w_{GS}G(t-T_{GS}) + w_{CS}Ctx) - S(t), \\ \tau_G G'(t) &= F_G(w_{SG}S(t-T_{SG}) - w_{GG}G(t-T_{GG}) - w_{XG}Str) - G(t), \end{aligned} \tag{4.1}$$

where $T_{GS} \geq 0$, $T_{SG} \geq 0$ and $T_{GG} \geq 0$ are the transmission time delays. In particular, T_{GS} is the transmission delay from GP to STN population, T_{SG} is the transmission delay from STN to GP population, and T_{GG} is an internal self-inhibition delay in the GP population. The constants τ_S and τ_G are the time membrane constants of neurons in STN and GP populations, while Ctx and Str represent a constant level of cortical and striatal excitation of the STN and GP populations, respectively. This system of equations represents a pair of reciprocally connected STN-GP sub-populations corresponding to one of many hypothesised basal ganglia information channels [95]. The synaptic weights w_{GS}, w_{CS}, w_{SG}, w_{GG}, and w_{XG} are all non-negative constants, and represent the strength of synaptic connectivity within and between the populations, where w_{xy} is the strength of the connection from population x to population y (e.g., w_{SG} is the synaptic connectivity from STN to GP). The functions F_S and F_G are the activation functions of the STN and GP neural populations, which describe their firing rate as a function of synaptic input, and are given by

$$\begin{aligned} F_S(\cdot) &= \frac{M_S}{1+\left(\frac{M_S-B_S}{B_S}\right)e^{\frac{-4(.)}{M_S}}}, \\ F_G(\cdot) &= \frac{M_G}{1+\left(\frac{M_G-B_G}{B_G}\right)e^{\frac{-4(.)}{M_G}}}, \end{aligned} \tag{4.2}$$

where M_S and M_G are the maximum firing rates of STN and GP populations, and B_S and B_G are the STN and GP firing rates in the absence of input. A schematic diagram of the model (4.1) representing the dynamics of STN-GP interactions is shown in Figure 4.1.

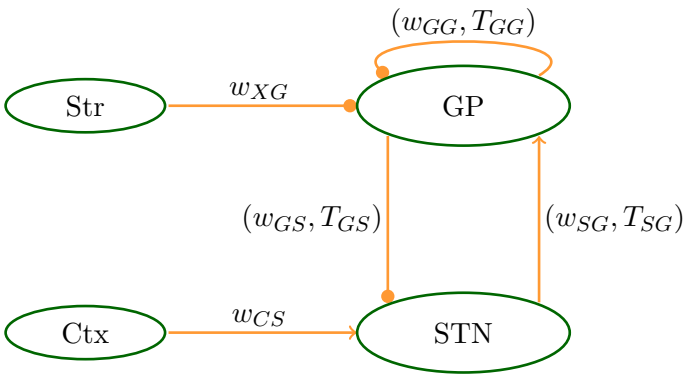

Figure 4.1: Diagrammatic sketch of the STN-GP model represented by the system (4.1).

Table 4.1: The parameters and their values used in the model together with their sources

Parameter	Value	Source
T_{SG}	6 ms	Kita *et al.* [73]
T_{GS}	6 ms	Fujimoto & Kita [41]
T_{GG}	4 ms	Nevado Holgado *et al.* [106]
τ_S	6 ms	Kita *et al.* [70], Nakanishi *et al.* [104], Paz *et al.* [115]
τ_G	14 ms	Kita & Kitai [71]
Ctx	27 spk/s	Lebedev & Wise [84]
Str	2 spk/s	Schultz & Romo [132]
M_S	300 spk/s	Hallworth *el al.* [57]
B_S	17 spk/s	Hallworth *el al.* [57]
M_G	400 spk/s	Kita *et al.* [73], Kita [69]
B_G	75 spk/s	Kita *et al.* [72], Kita [69]

The parameter values are summarised in Table 4.1, and are available in the literature (for details, see Nevado-Holgado *et al.* [106]). However, the synaptic weights w_{xy} were not available in the literature, but Nevado-Holgado *et al.* [106] found the values for which the model reproduced a wide range of experimental findings.

Before starting the stability analysis of the model (4.1), we can reduce the number of transmission delays by using a time-shift transformation in the firing rate $S(t)$ of the STN population [110, 111]. In order to do this, let us introduce a new variable $\tilde{S}(t)$ as follows

$$\tilde{S}(t) = S(t + T_{GS}) \quad \Longrightarrow \quad S(t) = \tilde{S}(t - T_{GS}). \tag{4.3}$$

Substituting the transformation (4.3) into the system (4.1) results in the following equi-

valent system

$$\begin{aligned} \tau_S \tilde{S}'(t) &= F_S(-w_{GS}G(t) + w_{CS}Ctx) - \tilde{S}(t), \\ \tau_G G'(t) &= F_G(w_{SG}\tilde{S}(t-T_1) - w_{GG}G(t-T_2) - w_{XG}Str) - G(t), \end{aligned} \tag{4.4}$$

where $T_1 = T_{GS} + T_{SG}$, $T_2 = T_{GG}$, and the new state variable $\tilde{S}(t)$ is time-shifted relative to the original state variable $S(t)$. It is clear that both systems (4.1) and (4.4) possess the same steady states and characteristic equations. From now on, all our analysis will be based on the model (4.4).

4.2 Positivity of firing rates

Since the model (4.4) describes the firing rates of the STN and GP populations, it is important to show that the solutions of this system are non-negative for all times $t > 0$. First, we shall start by proving that $\tilde{S}(t) \geq 0$ for all $t > 0$.

Lemma 4.2.1. *Let the function ϕ_S be the initial condition for $\tilde{S}(t)$, so that $\tilde{S}(s) = \phi_S(s)$ for $s \in (-T_1; 0)$. Let $\phi_S(s)$ be continuous and satisfy $0 \leq \phi_S(s) \leq M_S$ for $s \in (-T_1; 0)$, where $\phi_S(0) > 0$, and M_S is a positive constant. Then the solution $\tilde{S}(t)$ of the model (4.4) is always non-negative and satisfies $0 \leq \tilde{S}(t) \leq M_S$ for all $t \geq 0$.*

Proof. Suppose by contradiction that $\tilde{S}(t)$ can be negative. Assume that there exists a time instance t_1 such that $\tilde{S}(t_1) = 0$. It follows from the first equation of the system (4.4) that

$$\underbrace{\tau_S}_{>0} \tilde{S}'(t_1) = \underbrace{F_S(-w_{GS}G(t_1) + w_{CS}Ctx)}_{0<F_S<M_S} - \underbrace{\tilde{S}(t_1)}_{=0} > 0. \tag{4.5}$$

However, since $\tilde{S}(0) > 0$, for $\tilde{S}(t)$ to become negative after $t = t_1$ requires $\tilde{S}'(t_1) \leq 0$, which contradicts the expression (4.5). Furthermore, from (4.5), one can see that $\tilde{S}'(t_1) > 0$, which implies that $\tilde{S}(t)$ increases just for $t = t_1$. Since $\tilde{S}(0) = \phi_S(0)$ and by hypothesis $0 \leq \phi_S(t) \leq M_S$, it follows that $\tilde{S}(t)$ is bounded and $0 \leq \tilde{S}(t) \leq M_S$ for $t \geq 0$. Similar arguments can be used to show that $G(t)$ is non-negative and bounded by $0 \leq G(t) \leq M_G$ for $t \geq 0$, where M_G is a positive constant. □

The system (4.4) possesses a non-trivial steady state $E^* = (\tilde{S}^*, G^*)$, where $\tilde{S}^*$, G^* are

given implicitly by the solutions of

$$\begin{aligned} \tilde{S}^* &= F_S(-w_{GS}G^* + w_{CS}Ctx), \\ G^* &= F_G(w_{SG}\tilde{S}^* - w_{GG}G^* - w_{XG}Str). \end{aligned} \tag{4.6}$$

Note that $\tilde{S}^* > 0$, $G^* > 0$ by Lemma 4.2.1. In order to linearise the system (4.4) near the steady state $E^* = (\tilde{S}^*, G^*)$, let

$$\tilde{S} = \tilde{S}^* + X_S \quad \text{and} \quad G = G^* + X_G.$$

The linearised system for $\mathbf{X} = (\mathbf{X_S}, \mathbf{X_G})^\mathbf{T}$ can now be written in the form

$$\mathbf{X}'(t) = L_0\mathbf{X}(t) + L_1\mathbf{X}(t - T_1) + L_2\mathbf{X}(t - T_2), \tag{4.7}$$

where L_0, L_1 and L_2 are given by

$$L_0 = \begin{pmatrix} -\frac{1}{\tau_S} & -\frac{r_1 w_{GS}}{\tau_S} \\ 0 & -\frac{1}{\tau_G} \end{pmatrix}, \quad L_1 = \begin{pmatrix} 0 & 0 \\ \frac{r_2 w_{SG}}{\tau_G} & 0 \end{pmatrix} \quad \text{and} \quad L_2 = \begin{pmatrix} 0 & 0 \\ 0 & -\frac{r_2 w_{GG}}{\tau_G} \end{pmatrix},$$

where $r_1 = 4\tilde{S}^*(M_S - \tilde{S}^*)/M_S^2$ and $r_2 = 4G^*(M_G - G^*)/M_G^2$.

The associated characteristic matrix is

$$\Psi(\lambda, T_1, T_2) = \lambda I - L_0 - L_1 e^{-\lambda T_1} - L_2 e^{-\lambda T_2},$$

where I is the 2×2 identity matrix, and the corresponding characteristic equation becomes

$$\det[\Psi(\lambda, T_1, T_2)] \equiv \lambda^2 + p_1\lambda + p_2 + re^{-\lambda T_1} + (q_1\lambda + q_2)e^{-\lambda T_2} = 0, \tag{4.8}$$

where

$$p_1 = \frac{\tau_S + \tau_G}{\tau_S\tau_G}, \quad p_2 = \frac{1}{\tau_S\tau_G}, \quad r = \frac{r_1 r_2 w_{GS} w_{SG}}{\tau_S\tau_G}, \quad q_1 = \frac{r_2 w_{GG}}{\tau_G}, \quad \text{and} \quad q_2 = \frac{r_2 w_{GG}}{\tau_S\tau_G}. \tag{4.9}$$

The transcendental equation (4.8) determines the stability of the steady state E^*, and in order to analyse the characteristic equation (4.8) with two transmission delays, we consider three different cases. First, we assume that $T_1 = 0$ and $T_2 > 0$, and find stability conditions for E^*. Second, we take $T_2 = 0$ and $T_1 > 0$, and determine stability boundaries for E^* depending on the value of T_1. Finally, we analyse the stability properties of E^* in the general case when both time delays are present, i.e. $T_1 > 0$ and $T_2 > 0$.

4.3 Stability analysis: single time delay

In this section we consider the case when there is a delayed self-interaction in the GP population (i.e. $T_2 > 0$) and an instant cross-interaction between STN and GP populations (i.e. $T_1 = 0$). The characteristic equation (4.8) reduces to

$$\lambda^2 + p_1\lambda + p_2 + r + (q_1\lambda + q_2)e^{-\lambda T_2} = 0, \tag{4.10}$$

where p_i, q_i, $i = 1, 2$, and r are given by (4.9). Clearly, $\lambda = 0$ is not a root of the equation (4.10), so we look for solutions of (4.10) in the form $\lambda = i\xi$ ($\xi > 0$). This gives

$$-\xi^2 + p_1\xi i + p_2 + r + (q_1\xi i + q_2)(\cos\xi T_2 - i\sin\xi T_2) = 0, \tag{4.11}$$

and separating the real and imaginary parts of (4.11) yields

$$\begin{cases} \xi^2 - p_2 - r &= q_2\cos(\xi T_2) + q_1\xi\sin(\xi T_2), \\ p_1\xi &= q_2\sin(\xi T_2) - q_1\xi\cos(\xi T_2). \end{cases} \tag{4.12}$$

Upon squaring and adding the equations (4.12), one obtains a quartic equation in the form

$$\xi^4 - (q_1^2 + 2p_2 + 2r - p_1^2)\xi^2 + (p_2 + r)^2 - q_2^2 = 0. \tag{4.13}$$

The four roots of the equation (4.13) can be expressed as follows

$$\xi_\pm^2 = \frac{(q_1^2 + 2p_2 + 2r - p_1^2) \pm \sqrt{\Delta_1}}{2}, \tag{4.14}$$

where $\Delta_1 = (q_1^2+2p_2+2r-p_1^2)^2-4((p_2+r)^2-q_2^2)$. Depending on the values of p_i, q_i, $i = 1, 2$, and r, the equation (4.13) can have no, one or two positive roots. If $(p_2 + r)^2 - q_2^2 > 0$ and $q_1^2 + 2p_2 + 2r - p_1^2 < 0$ or $\Delta_1 < 0$, then the equation (4.13) has no positive roots. If $(p_2 + r)^2 - q_2^2 > 0$, $q_1^2 + 2p_2 + 2r - p_1^2 > 0$ and $\Delta_1 > 0$, then the equation (4.13) has two positive roots $\xi_\pm = \frac{\sqrt{2}}{2}[q_1^2 + 2p_2 + 2r - p_1^2 \pm \sqrt{\Delta_1}]^{\frac{1}{2}}$. If $(p_2 + r)^2 - q_2^2 < 0$ or $q_1^2 + 2p_2 + 2r - p_1^2 > 0$ and $\Delta_1 = 0$, then the equation (4.13) has one positive root ξ_+.

In either of the latter cases, the characteristic equation (4.10) has purely imaginary roots for some values of the time delay T_2. From equation (4.12) we have

$$\begin{aligned} \sin(\xi T_2) &= \frac{\xi(q_1\xi^2 + p_1q_2 - p_2q_1 - q_1r)}{q_1^2\xi^2 + q_2^2}, \\ \cos(\xi T_2) &= -\frac{p_1q_1\xi^2 - q_2\xi^2 + p2q_2 + q_2r}{q_1^2\xi^2 + q_2^2}, \end{aligned} \tag{4.15}$$

and dividing these two equations, the critical time delays can be found as

$$T_{2\pm}^j = \frac{1}{\xi_\pm}\left\{\tan^{-1}\left(-\frac{\xi_\pm(q_1\xi_\pm^2 + p_1q_2 - p_2q_1 - q_1r)}{p_1q_1\xi_\pm^2 - q_2\xi_\pm^2 + p_2q_2 + q_2r}\right) + j\pi\right\}, \qquad j = 0, 1, 2, \cdots. \tag{4.16}$$

It is worth noting that when $T_1 = T_2 = 0$, the system (4.4) becomes a system of ODEs with a characteristic equation

$$\lambda^2 + (p_1 + q_1)\lambda + p_2 + q_2 + r = 0. \tag{4.17}$$

which yields that whenever $p_1 + q_1 > 0$ and $p_2 + q_2 + r > 0$, all roots of the equation (4.17) with $T_1 = T_2 = 0$ always have negative real parts, and the steady state E^* is stable.

Summarising the above analysis and the results in [124, 142], we have the following lemma.

Lemma 4.3.1. *Suppose that $p_1 + q_1 > 0$ and $p_2 + q_2 + r > 0$, and that $\xi_\pm^2$ and $T_{2\pm}^j$ are defined by (4.14) and (4.16) respectively.*

(i) *If $(p_2 + r)^2 - q_2^2 > 0$ and $q_1^2 + 2p_2 + 2r - p_1^2 < 0$ or $\Delta_1 < 0$, then the number of roots in equations (4.10) and (4.17) is the same.*

(ii) *If $(p_2 + r)^2 - q_2^2 < 0$ or $q_1^2 + 2p_2 + 2r - p_1^2 > 0$ and $\Delta_1 = 0$, then the number of roots in equations (4.10) and (4.17) is the same for $T_2 \in [0, T_{2+}^0)$, and equation (4.10) has a pair of simple purely imaginary roots $\pm i\xi_+$ at $T_2 = T_{2+}^j$.*

(iii) *If $(p_2 + r)^2 - q_2^2 > 0$, $q_1^2 + 2p_2 + 2r - p_1^2 > 0$ and $\Delta_1 > 0$, then the number of roots in equations (4.10) and (4.17) is the same for $T_2 \in [0, T_2^0)$, where $T_2^0 = \min\{T_{2+}^0, T_{2-}^0\}$, and equation (4.10) has two pairs of simple purely imaginary roots $\pm i\xi_\pm$ at $T_2 = T_{2\pm}^j$.*

Under the assumption that $(p_2 + r)^2 - q_2^2 > 0$, $q_1^2 + 2p_2 + 2r - p_1^2 > 0$ and $\Delta_1 > 0$, the characteristic equation (4.10) has two purely imaginary solutions $i\xi_\pm$ with ξ_+ and ξ_- defined in (4.14). In order to determine the stability of the steady state (4.6) as T_2 varies, we calculate the sign of the derivative of $\mathrm{Re}(\lambda)$ at the points where $\lambda(T_2)$ is purely imaginary. Let $\lambda(T_2) = \eta(T_2) + i\xi(T_2)$ be the root of the equation (4.10) satisfying

$$\eta(T_{2\pm}^j) = 0, \quad \xi(T_{2\pm}^j) = \xi_\pm, \quad j = 0, 1, 2, \cdots.$$

Substituting $\lambda(T_2)$ into the equation (4.10) and taking the derivative with respect to T_2 gives

$$\left[\frac{d\lambda}{dT_2}\right]^{-1} = \frac{2\lambda+p_1+q_1e^{-\lambda T_2}-(q_1\lambda+q_2)T_1e^{-\lambda T_2}}{(q_1\lambda+q_2)\lambda e^{-\lambda T_2}} = \frac{(2\lambda+p_1)e^{\lambda T_2}+q_1-(q_1\lambda+q_2)T_2}{(q_1\lambda+q_2)\lambda}$$

$$= \frac{(2\lambda+p_1)e^{\lambda T_2}}{(q_1\lambda+q_2)\lambda} + \frac{q_1}{(q_1\lambda+q_2)\lambda} - \frac{T_2}{\lambda}.$$

Therefore,

$$\begin{aligned}\left[\frac{d\mathrm{Re}\{\lambda(T_2)\}}{dT_2}\right]^{-1}_{T_2=T^j_{2\pm}} &= \mathrm{Re}\left\{\frac{(2\lambda+p_1)e^{\lambda T_2}}{(q_1\lambda+q_2)\lambda}\right\}_{T_2=T^j_{2\pm}} + \mathrm{Re}\left\{\frac{q_1}{(q_1\lambda+q_2)\lambda}\right\}_{T_2=T^j_{2\pm}} - \mathrm{Re}\left\{\frac{T_2}{\lambda}\right\}_{T_2=T^j_{2\pm}} \\ &= \left\{\frac{(2q_2-p_1q_1)\xi\cos(\xi_\pm T^j_{2\pm})+(p_1q_2+2q_1\xi^2)\sin(\xi_\pm T^j_{2\pm})-q_1^2\xi_\pm}{(q_2^2+q_1^2\xi_\pm^2)\xi}\right\} \\ &= \frac{1}{q_2^2+q_1^2\xi^2}\left\{2\xi_\pm^2+(p_1^2-2p_2-2r-q_1^2)\right\} \\ &= \pm\sqrt{\Delta_1}\frac{1}{q_2^2+q_1^2\xi^2}.\end{aligned}$$

Hence, if $\Delta_1 \neq 0$, we have

$$\left[\frac{d\mathrm{Re}\{\lambda(T_2)\}}{dT_2}\right]_{T_2=T^j_{2+}} = \left[\frac{d\mathrm{Re}\{\lambda(T_2)\}}{dT_2}\right]^{-1}_{T_2=T^j_{2+}} = \frac{1}{q_2^2+q_1^2\xi^2}\sqrt{\Delta_1} > 0, \tag{4.18}$$

and

$$\left[\frac{d\mathrm{Re}\{\lambda(T_2)\}}{dT_2}\right]_{T_2=T^j_{2-}} = \left[\frac{d\mathrm{Re}\{\lambda(T_2)\}}{dT_2}\right]^{-1}_{T_2=T^j_{2-}} = -\frac{1}{q_2^2+q_1^2\xi^2}\sqrt{\Delta_1} < 0. \tag{4.19}$$

Combining the results of the Lemma 4.3.1 and the transversality conditions (4.18), (4.19) we have the following theorem regarding the stability of the steady state E^*.

Theorem 4.3.1. *For the system (4.4) with $T_1 = 0$ and $T_2 > 0$, suppose $p_1 + q_1 > 0$, $p_2 + q_2 + r > 0$ and $T^j_{2\pm}$ are defined by the equation (4.16). Then the following statements hold.*

(i) *If $(p_2+r)^2 - q_2^2 > 0$ and $q_1^2 + 2p_2 + 2r - p_1^2 < 0$ or $\Delta_1 < 0$, then the steady state E^* of the system (4.4) is stable for all $T_2 \geq 0$.*

(ii) *If $(p_2+r)^2 - q_2^2 < 0$ or $q_1^2 + 2p_2 + 2r - p_1^2 > 0$ and $\Delta_1 = 0$, then the steady state (4.6) of the system (4.4) is stable when $T_2 \in [0, T^0_{2+})$, undergoes a Hopf bifurcation when $T_2 = T^0_{2+}$, and is unstable when $T_2 > T^0_{2+}$.*

(iii) *If $(p_2+r)^2 - q_2^2 > 0$, $q_1^2 + 2p_2 + 2r - p_1^2 > 0$ and $\Delta_1 > 0$, then there is a positive integer k such that there are k switches from stability to instability. Furthermore, for the time delays defined as $T_2 \in \bigcup_{j=0}^{k}(T^{j-1}_{2-}, T^j_{2+})$, where $T^{-1}_{2-} = 0$, the steady state E^* of the system (4.4) is stable, and for the time delays $T_2 \in \bigcup_{j=0}^{k-1}(T^j_{2+}, T^j_{2-})$ and $T_2 > T^k_{2+}$, the steady state E^* of the system (4.4) is unstable.*

In order to gain a better understanding of the stability properties of the non-trivial steady state $E^* = (\tilde{S}^*, G^*)$ given by (4.6) for the system (4.7), we use a traceDDE suite

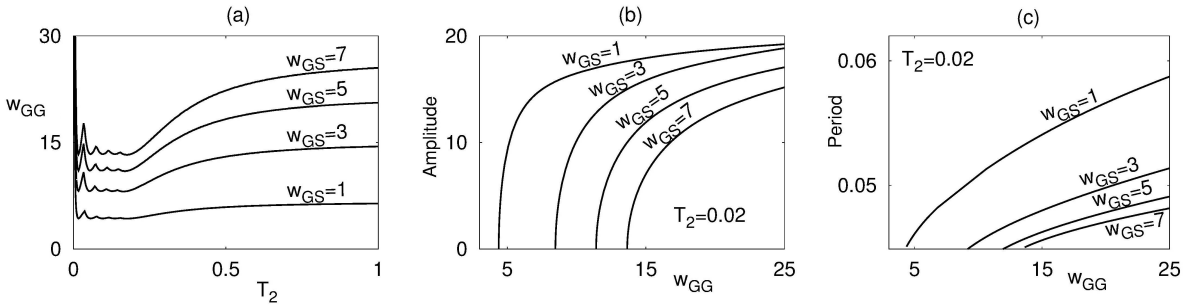

Figure 4.2: (a) Stability of the non-trivial steady state E^* of the system (4.4) in the parameter space of the time delay T_2 and the synaptic weight w_{GG} for different values of the synaptic weight w_{GS}. The non-trivial steady state E^* is stable below the stability boundaries. (b) Amplitude and (c) period of the periodic solutions for different values of w_{GS} and $T_2 = 0.02$.

in MATLAB [19, 90] to numerically calculate the stability boundaries for different values of the synaptic weights w_{GG}, w_{GS} and the time delay T_2.

Figure 4.2 (a) shows the stability boundary of the non-trivial steady state E^* for different values of the synaptic weight w_{GS}. The steady state is stable below the curves and unstable above them. As the value of the time delay T_2, which corresponds to the delayed self-interactions within the GP population, is increased, the steady state E^* undergoes a series of stability switches (as proved in Theorem 4.3.1), and for large values of the time delay T_2, the stability boundary becomes almost a constant independent of T_2. Increasing the synaptic weight w_{GS} does not change the shape of the stability boundary, however, for higher values of w_{GS}, the region where the steady state E^* is stable becomes larger. This suggests that the region of non-oscillatory behaviour, which corresponds to the healthy functioning of the STN-GP neural populations is larger for higher values of the synaptic connection between GP and STN populations. When the steady state E^* becomes unstable, it undergoes a Hopf bifurcation, which gives rise to stable periodic oscillations. In Figures 4.2 (b) and (c), we have plotted the amplitude and period of these periodic solutions for a fixed value of the time delay T_2 and several values of the synaptic weight w_{GS}. One can see that as the values of the synaptic weight w_{GS} are increased, this results in periodic oscillations with lower amplitude and a significantly lower period.

In the case of a delayed cross-interaction between GP and STN neural populations, i.e. $T_1 > 0$, and an instantaneous self-interaction, i.e. $T_2 = 0$, the characteristic equation (4.8) becomes

$$\lambda^2 + (p_1 + q_1)\lambda + (p_2 + q_2) + re^{-\lambda T_1} = 0. \tag{4.20}$$

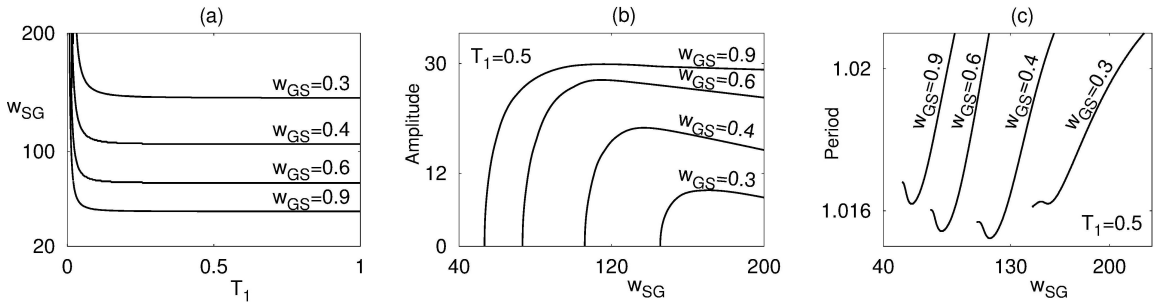

Figure 4.3: Stability of the non-trivial steady state E^* of the system (4.4) in the parameter space of time delay T_1 and the synaptic weight w_{SG} for different values of the synaptic weight w_{GS}. The non-trivial steady state E^* is stable below the stability boundaries. (b) Amplitude and (c) period of the periodic solutions for different values of w_{GS} and $T_1 = 0.5$.

The analysis of the characteristic equation (4.20) is similar to the analysis of characteristic equation (4.10), hence, the details are omitted here. Figure 4.3 (a) shows that the stability region of the steady state E^* in the (T_1, w_{SG}) plane, which is stable below the stability curves. The stability region increases for decreasing strength of the synaptic connection w_{GS} between GP and STN populations, but, unlike the case of $T_2 \neq 0$, there is just one stability switch from stable to unstable region with increasing T_1. Moreover, whilst the stability boundary for very small values of the time delay T_1 strongly depends on w_{SG}, it becomes a constant for larger values of T_1. Biologically, the region, where the steady state E^* is stable, corresponds to the healthy functioning of the GP-STN populations, and Figure 4.3 suggests that a stronger connection between GP and STN networks leads to a larger region of oscillations. In Figures 4.3 (b) and (c) we fix the value of the time delay T_1, and calculate amplitude and period of the periodic solutions, which arise after the steady state becomes unstable via a Hopf bifurcation. Figure 4.3 (b) shows that the amplitude of the oscillating solutions is increasing for small values of the synaptic weight w_{SG} between STN and GP populations and starts to drop slightly for very large w_{SG}, whereas higher values of the synaptic weight w_{GS} lead to a much higher amplitude of oscillations. The period of oscillations is shorter for small values of the synaptic weight w_{SG} and higher values of the synaptic weight w_{GS}, as illustrated in Figure 4.3 (c).

4.4 Stability analysis: two time delays

When $T_1 > 0$ and $T_2 > 0$, the characteristic equation (4.8) contains two transmission delays simultaneously present, which significantly complicates analytical calculations of the stability boundaries. We will follow the idea and method proposed in [18, 54]. One

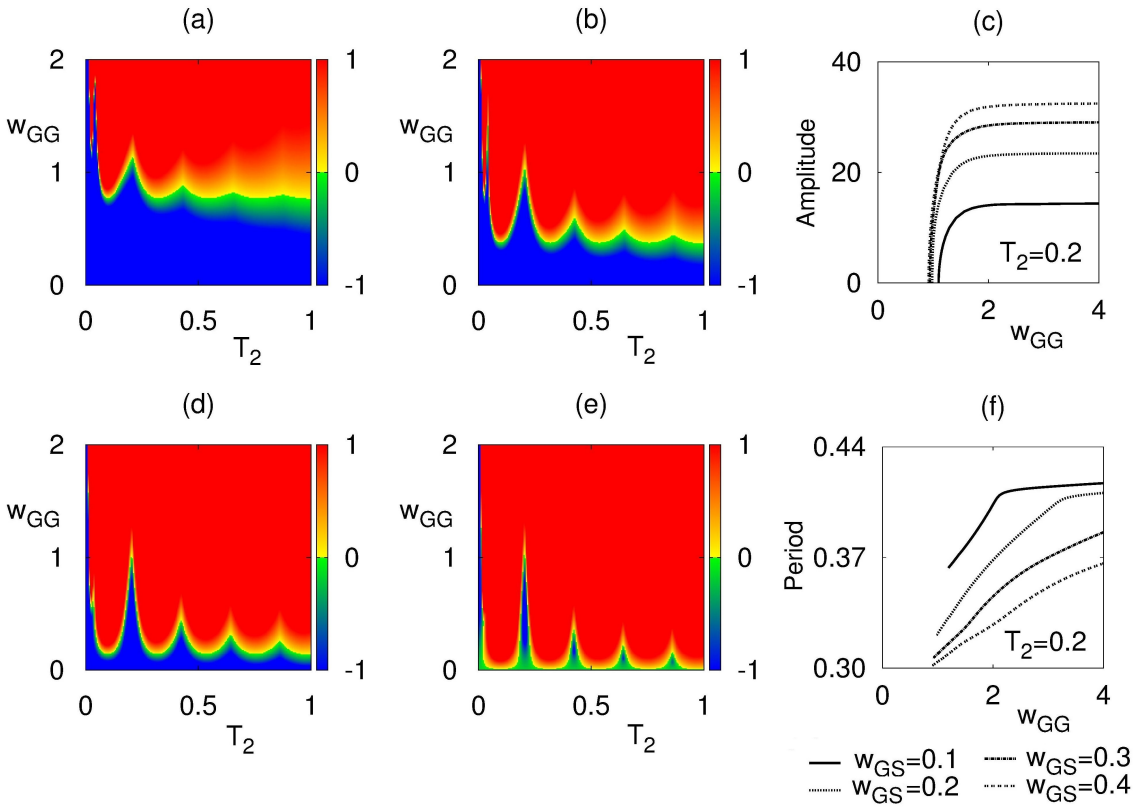

Figure 4.4: Real part of the leading eigenvalue of the characteristic equation (4.8) with $T_1 = 0.09$, $w_{SG} = 19$, and (a) $w_{GS} = 0.1$, (b) $w_{GS} = 0.2$, (c) $w_{GS} = 0.3$ and (d) $w_{GS} = 0.4$. Colour code denotes $[\max\{\mathrm{Re}(\lambda)\}]$. (c) Amplitude of the periodic solutions for different values of w_{GS} and $T_2 = 0.2$. (f) Period of the periodic solutions for different values of w_{GS} and $T_2 = 0.2$.

can rewrite characteristic equation (4.8) in an equivalent form as follows

$$1 + \rho_1(\lambda)e^{-\lambda T_1} + \rho_2(\lambda)e^{-\lambda T_2} = 0, \tag{4.21}$$

where

$$\rho_1(\lambda) = \frac{r}{\lambda^2 + p_1\lambda + p_2} \quad \text{and} \quad \rho_2(\lambda) = \frac{q_1\lambda + q_2}{\lambda^2 + p_1\lambda + p_2}.$$

Figures 4.4 (a), (b), (d) and (e) show numerically computed maximum real part of the eigenvalues of the characteristic equation (4.21) in the (T_2, w_{GG}) plane for a fixed value of the synaptic weight w_{SG} and different values of the synaptic weight w_{GS}. From these figures, one can see that there is a finite number of stability switches between stable and unstable regimes for the same values of w_{GG}, but increasing the strength of the synaptic connection w_{GS} between GP and STN populations significantly shrinks the stability region. Figures 4.4 (c) and (f) illustrate the amplitude and the period of the periodic solutions after the stability is lost for a fixed value of the time delay T_2. The amplitude

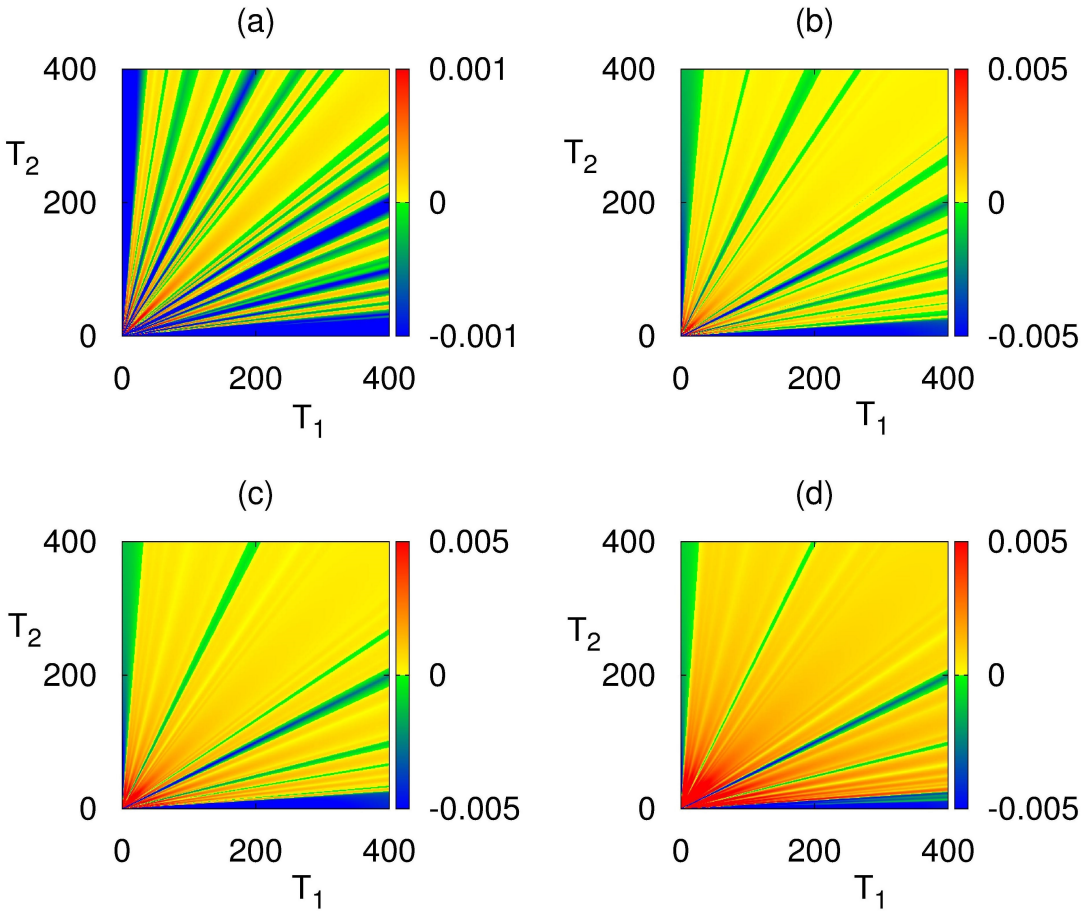

Figure 4.5: (a)-(d) Real part part of the leading eigenvalue of the characteristic equation (4.7) in the (T_1, T_2) plane for $w_{GS} = 1$, $w_{SG} = 3$, and (a) $w_{GG} = 1.6$, (b) $w_{GG} = 1.8$, (c) $w_{GG} = 2$ and (d) $w_{GG} = 2.4$. Colour code denotes $[\max\{\mathrm{Re}(\lambda)\}]$.

of oscillations grows for larger values of the synaptic weights w_{GG} and w_{GS}, whilst the period of oscillations becomes smaller for larger values of w_{GS} and grows with w_{GG}.

The stability boundary can now be parametrised using the Hopf frequency $\xi \in \Xi$, with $\Xi = \bigcup_{i=1}^{k} \Xi_k$ being composed of a finite number of intervals of finite length, and the critical time delays at the stability boundary in the (T_1, T_2) plane are given by

$$\begin{aligned} T_1 &= T_1^{u\pm}(\xi) = \tfrac{\mathrm{Arg}\,\rho_1(i\xi)+(2u-1)\pi\pm\phi_1}{\xi} \geq 0, \qquad u = u_0^{\pm}, u_0^{\pm}+1, u_0^{\pm}+2, \cdots \\ T_2 &= T_2^{v\pm}(\xi) = \tfrac{\mathrm{Arg}\,\rho_2(i\xi)+(2v-1)\pi\mp\phi_2}{\xi} \geq 0, \qquad v = v_0^{\pm}, v_0^{\pm}+1, v_0^{\pm}+2, \cdots \end{aligned} \tag{4.22}$$

where $\phi_1, \phi_2 \in [0, \pi]$ are found as follows

$$\begin{aligned} \phi_1 &= \cos^{-1}\left(\tfrac{1+|\rho_1(i\xi)|^2-|\rho_2(i\xi)|^2}{2|\rho_1(i\xi)}\right), \\ \phi_2 &= \cos^{-1}\left(\tfrac{1+|\rho_2(i\xi)|^2-|\rho_1(i\xi)|^2}{2|\rho_2(i\xi)}\right). \end{aligned} \tag{4.23}$$

and $u_0^+, u_0^-, v_0^+, v_0^-$ are the smallest positive integers for which the corresponding $T_1^{u_0^+}, T_1^{u_0^-}$, $T_2^{v_0^+}, T_2^{v_0^-}$ are all non-negative.

To better understand the stability changes in the presence of two time delays, we fixed w_{GS}, w_{SG}, varied the strength w_{GG} of the self-inhibitory connection of the GP population w_{GG} and numerically computed the maximum of the real part of the leading eigenvalue of the characteristic equation (4.21), as shown in Figure 4.5 (a)-(d). As the value of the self-inhibitory synaptic connection w_{GG} is increased, the number of open-ended curves (stable region) decreases. This means that in the presence of two time delays and high enough values of the synaptic weight w_{GG}, the model shows oscillatory behaviour for a wide range of T_1 and T_2 values.

We have performed numerical simulations of the full nonlinear system (4.4), and Figure 4.6 shows numerical solutions of the system (4.4) for different values of the synaptic weights and the time delays. In Figures 4.6 (a) and (b), the cross-interaction time delay T_1 between GP and STN populations is equal to zero, and the self-interaction time delay T_2 within the GP population is present; in Figures 4.6 (c) and (d), the cross-interaction time delay T_1 between GP and STN populations is present, and the self-interaction time delay T_2 within the GP population is equal to zero; and in Figures 4.6 (e) and (f), both time delays are present. In all three cases, there is a transition between the healthy firing of neurons, when after some short transient period, the solutions settle on the non-zero steady state E^*, and a Parkinsonian-type behaviour, where the steady state loses its stability, and this results in sustained periodic firing of both populations. The results of the numerical simulations fully agree with the stability analysis performed in the previous section, and show the predicted onset of oscillations as the steady state loses its stability.

4.5 Discussion

In this chapter, we have studied a general subthalamic nucleus (STN) and globus pallidus (GP) network with three distinct synaptic transmission delays. Using the time-shift transformation, we reduced the original system to an equivalent system with two time delays and showed the existence of a unique non-trivial steady state. The analysis in chapter 4 has concentrated on the stability properties of this steady state, since it has a profound effect on the dynamics of the neural populations. Biologically, the stable steady state corresponds to the healthy firing of the STN and GP populations, and if it is unstable, this results in periodic firing, which implies a Parkinsonian-type regime. To better understand the effects of different time delays on the overall stability of the system, we have divided

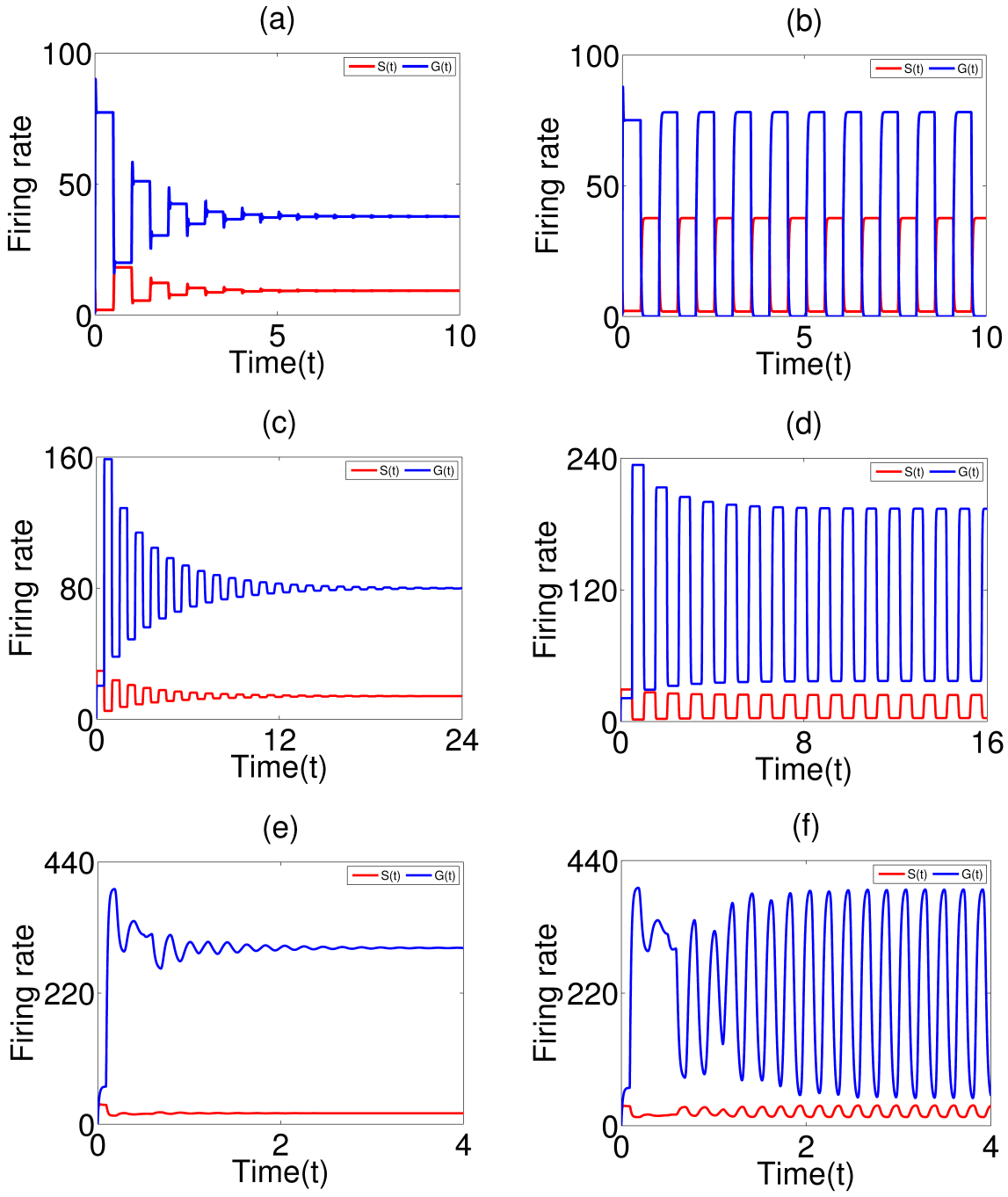

Figure 4.6: Numerical simulations of the full nonlinear system (4.4). Top panel: $w_{GS} = 3$, $w_{SG} = 19$, $T_2 = 0.5$, $T_1 = 0$ (a) $w_{GG} = 5$, (b) $w_{GG} = 15$. Middle panel: $w_{GS} = 1$, $w_{GG} = 6.6$, $T_1 = 0.5$, $T_2 = 0$, (c) $w_{SG} = 40$, (d) $w_{SG} = 60$. Bottom panel: $w_{GS} = 0.2$, $w_{SG} = 19$, $T_1 = 0.09$, $T_2 = 0.5$, (e) $w_{GG} = 0.3$, (f) $w_{GG} = 2$.

the analysis into three different cases: delayed self-interaction in the GP population only; delayed cross-interaction between GP and STN populations only; both interactions with time delays.

For the first two cases, we have analytically found the stability regions and have shown that the non-trivial steady state is stable below some critical value of the time delay, unstable when the time delay exceeds this critical value, and undergoes a Hopf bifurcation when the time delay is equal to the critical value. Furthermore, we have numerically computed eigenvalues of the corresponding characteristic equations for the three cases, showing that the strength of the synaptic connection from GP to STN population w_{GS} plays an important role in determining the stability of the steady state. In fact, when the time delay is only present in the self-interaction of the GP population, the stability region (healthy firing of neurons) increases with increasing w_{GS}, however, in the case when the time delay is only considered between STN and GP populations, the stability region gets larger for decreasing values of the synaptic weight w_{GS}. Moreover, the highest amplitude of oscillations in the case of the time delay being included in the self-interaction of the GP population corresponds to the lowest value of the synaptic strength w_{GS}, whilst if the time delay is only included into the interactions between STN and GP populations, the same effect on the amplitude of oscillations is observed for highest values of w_{GS}. In the case when both time delays are taken into account, the stability region shrinks if the synaptic weight w_{GS} is increased, leading to the smaller range of parameter values, where the healthy firing rate of neurons is possible, and the amplitude of oscillating solutions outside the stability region also grows for larger values synaptic weight w_{GS}. Numerical simulations performed for the fully nonlinear system agree with the stability analysis, and show the onset of sustained periodic calculations in all three cases.

Comparing the analysis done in this chapter to the previous work in [106], it is worth noting that we have considered the case when the activation functions are nonlinear, which gives a continuous derivative for the activation function, and rather than using the Taylor expansion under the assumption of small time delays, we have analysed stability of the system for arbitrary values of the three time delays.

Chapter 5

Dynamics of unidirectionally-coupled ring neural network with discrete and distributed delays

In this chapter, we consider a ring neural network with one-way distributed-delay coupling between the neurons and a discrete delayed self-feedback. In the general case of the distribution kernels, we are able to find a subset of the amplitude death regions depending on even (odd) number of neurons in the network. Furthermore, in order to show the full region of the amplitude death, we use particular delay distributions, including Dirac delta function and gamma distribution. Stability conditions for the trivial steady state are found in parameter spaces consisting of the synaptic weight of the self-feedback and the coupling strength between the neurons, as well as the delayed self-feedback and the coupling strength between the neurons. It is shown that both Hopf and steady-state bifurcations may occur when the steady state loses stability. We also perform numerical simulations of the fully nonlinear system to confirm theoretical findings.

We consider a Hopfield-type network of unidirectionally coupled neurons with a discrete delay self-feedback, and each i^{th} neuron receives a distributed delay signal from $(i-1)^{th}$ neuron as shown in Figure 5.1. The model can be written in the form

$$\dot{u}_i(t) \quad = -\kappa u_i(t) + af(u_i(t-\tau)) + b\int_0^\infty g(s)f(u_j(t-s))ds, \tag{5.1}$$

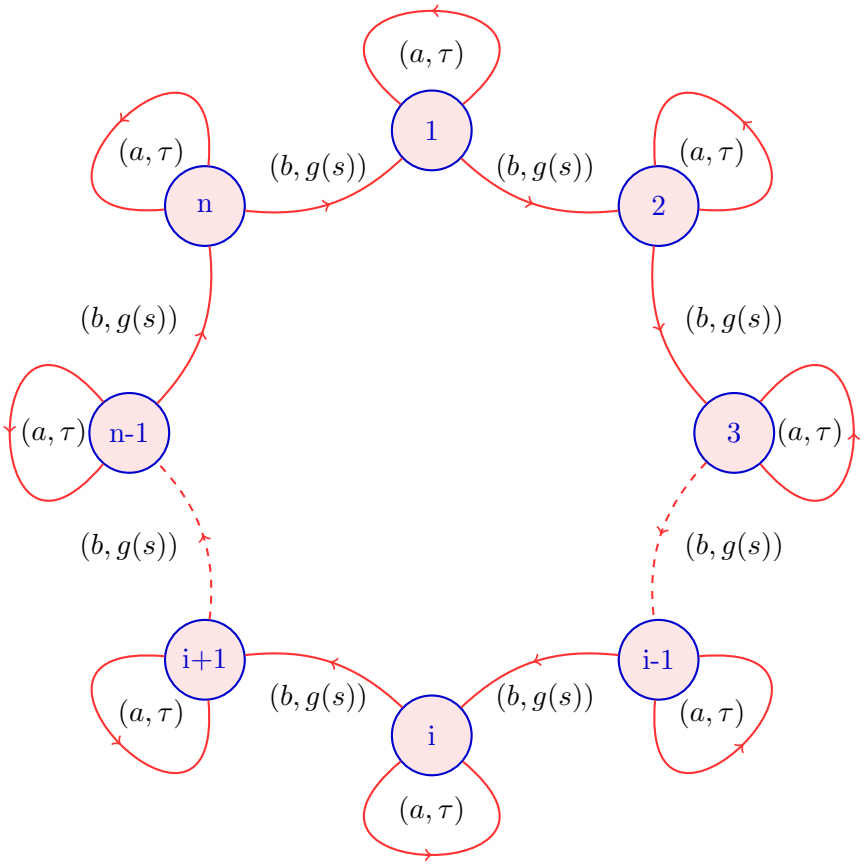

Figure 5.1: Schematic sketch of the unidirectionally coupled ring neural model with self-coupling described by the system (5.1).

where $i = 1, 2, \cdots, n$ and

$$j = \begin{cases} n & \text{for} \quad i = n, \\ i-1 & \text{for} \quad i = 2, 3, \cdots, n, \end{cases}$$

$\kappa > 0$, u_i denotes the voltage of the i^{th} neuron, a is the synaptic weight of the self-feedback and b denotes the coupling strength of the neuron's connection, which can be positive or negative. We assume that a neuron has a delayed self-feedback input represented by a discrete time delay, and the transmission delays between neurons are characterised by a distribution kernel $g(\cdot)$.

The transfer function $f : \mathbb{R} \to \mathbb{R}$ is assumed to be sigmoid and in $\mathcal{C}^1$. For the local stability analysis, we only require $f(0) = 0$, $f'(0) \neq 0$, and use a particular choice of $f(\cdot) = \tanh(\cdot)$ in the numerical simulations.

Without loss of generality, the distribution kernel $g(\cdot)$ is assumed to be normalised to unity and positive-definite, that is

$$\int_0^\infty g(s)ds = 1, \quad g(s) \geq 0.$$

In the case of the distribution kernel being a Dirac delta function, $g(s) = \delta(s-\sigma)$, the last term of the system (5.1) reduces to $bf(u(t-\sigma))$, which converts it to a unidirectionally-coupled ring neural system with discrete time delays in both self-feedback and in the connection between the neurons.

5.1 Stability Analysis

Under the assumption that $f(0) = 0$, the system (5.1) always possesses a trivial steady state $(u_1, u_2, \cdots, u_n) = (0, 0, \cdots, 0)$. Linearising the system (5.1) near the trivial steady state gives

$$\dot{\mathbf{u}}(t) = -\kappa I\mathbf{u}(t) + \alpha I\mathbf{u}(t-\tau) + \beta M\int_0^\infty g(s)\mathbf{u}(t-s)ds, \tag{5.2}$$

where $\mathbf{u} = (u_1, u_2, \cdots, u_n)$, I is an $n \times n$ identity matrix and M is given by

$$M = \begin{pmatrix} 0 & 0 & 0 & \cdots & 0 & 1 \\ 1 & 0 & 0 & \cdots & 0 & 0 \\ 0 & 1 & 0 & \cdots & 0 & 0 \\ : & : & : & \cdots & : & : \\ 0 & 0 & 0 & \cdots & 1 & 0 \end{pmatrix}_{n\times n},$$

where $\alpha = af'(0) \neq 0$ and $\beta = bf'(0) \neq 0$. The characteristic matrix can now be calculated as

$$\det[(\lambda + \kappa - \alpha e^{-\lambda\tau})I - \beta M\widehat{G}(\lambda)] = 0,$$

where

$$\widehat{G}(\lambda) = \int_0^\infty e^{-\lambda s}g(s)ds,$$

is the Laplace transform of the function $g(\cdot)$. The characteristic equation has the form

$$(\lambda + \kappa - \alpha e^{-\lambda\tau})^n = (\beta\widehat{G}(\lambda))^n, \tag{5.3}$$

with

$$\Delta(\tau,\lambda) = \begin{cases} \Delta_E(\tau,\lambda) & \text{if} \quad n \quad \text{is even}, \\ \Delta_O(\tau,\lambda) & \text{if} \quad n \quad \text{is odd}, \end{cases} \tag{5.4}$$

where $\Delta_E(\tau,\lambda)$ and $\Delta_O(\tau,\lambda)$ are

$$\Delta_E(\tau,\lambda) = \lambda + \kappa - \alpha e^{-\lambda\tau} \pm \beta\widehat{G}(\lambda) = 0 \tag{5.5}$$

and

$$\Delta_O(\tau,\lambda) = \lambda + \kappa - \alpha e^{-\lambda\tau} - \beta\widehat{G}(\lambda) = 0 \tag{5.6}$$

for even and odd n, respectively.

Lemma 5.1.1. *$\lambda = 0$ is a solution of characteristic equation (5.3) if and only if $|\beta| = \kappa - \alpha$ when n is even and $\beta = \kappa - \alpha$ when n odd.*

Proof. From the characteristic equations (5.5) and (5.6), computing $\widehat{G}(\lambda)$ at $\lambda = 0$ yields

$$\widehat{G}(0) = \int_0^\infty g(s)ds = 1.$$

Substituting this into $\Delta(\tau, 0) = 0$ given in (5.5), one has

$$\kappa - \alpha \pm \beta = 0,$$

and (5.6), yields

$$\kappa - \alpha - \beta = 0,$$

which completes the proof. □

Lemma 5.1.2. *Let $|\beta| = \kappa - \alpha$ when n is even and $\beta = \kappa - \alpha$ when n is odd. If the condition $E \neq \frac{\alpha\tau+1}{\alpha-\kappa}$ holds, then $\lambda = 0$ is a simple root of the characteristic equation (5.5) and (5.6) where $E = \int_0^\infty sg(s)ds > 0$.*

Proof. Recall from Lemma 5.1.1 that if the condition $|\beta| = \kappa - \alpha$ when n is even or the condition $\beta = \kappa - \alpha$ when n is odd hold, $\lambda = 0$ is a root of the characteristic equation (5.4). In order to determine the multiplicity of $\lambda = 0$, we compute the implicit derivative of the characteristic equations (5.5) and (5.6) with respect to λ. When n is even, this yields

$$\frac{d\Delta_E}{d\lambda} = 1 + \alpha\tau e^{-\lambda\tau} \mp \beta \int_0^\infty se^{\lambda s} g(s)ds,$$

and when n is odd, yields

$$\frac{d\Delta_O}{d\lambda} = 1 + \alpha\tau e^{-\lambda\tau} + \beta \int_0^\infty se^{\lambda s} g(s)ds.$$

Recalling that $|\beta| = \kappa - \alpha$ when n is even and $\beta = \kappa - \alpha$ when n is odd, and calculating the derivative at $\lambda = 0$, gives

$$\frac{d\Delta}{d\lambda}\Big|_{\lambda=0} = 1 + \alpha\tau + (\kappa - \alpha)E.$$

From the last expression, it is clear that if the condition $E \neq \frac{\alpha\tau+1}{\alpha-\kappa}$ is satisfied, then $\Delta(\tau, 0) \neq 0$, implying that $\lambda = 0$ is a simple root of the characteristic equation (5.4). □

It is well known that the trivial steady state $(u_1, u_2, \cdots, u_n) = (0, 0, \cdots, 0)$ is stable if and only if all roots of the characteristic equations (5.5) and (5.6) have negative real parts. We have the following result in a general case of the distribution kernel when all roots of the characteristic equations (5.5) and (5.6) have negative real parts.

Theorem 5.1.1. *If the parameters of system (5.2) satisfy* $|\beta| < \kappa - |\alpha|$ *and* $E = \int_0^\infty sg(s)ds > 0$ *then the trivial solution of (5.1) is stable for any distribution kernel and* $\tau \geq 0$.

Proof. Let $\lambda = \mu + i\omega$. Substituting this into the characteristic equation (5.5), then separating into real and imaginary part, yields

$$\begin{aligned} \mathrm{Re}(\mu,\omega) = &\quad \mu + \kappa - \alpha e^{-\mu\tau}\cos(\omega\tau) \pm \beta \int_0^\infty e^{-\mu s}\cos(\omega s)g(s)ds, \\ \Im(\mu,\omega) = &\quad \omega + \alpha e^{-\mu\tau}\sin(\omega\tau) \mp \beta \int_0^\infty e^{-\mu s}\sin(\omega s)g(s)ds. \end{aligned} \tag{5.7}$$

The real part in (5.7) satisfies

$$\mathrm{Re}(\mu,\omega) \geq \mathrm{Re}(\mu) = \mu + \kappa - |\alpha|e^{-\mu\tau} - |\beta| \int_0^\infty e^{-\mu s}g(s)ds, \tag{5.8}$$

since $|\beta| < \kappa - |\alpha|$. Furthermore,

$$\frac{d\mathrm{Re}(\mu)}{d\mu} = 1 + |\alpha|\tau e^{-\mu\tau} + |\beta| \int_0^\infty se^{-\mu s}g(s)ds,$$

where since $\mu \geq 0$, then $0 < e^{-\mu\tau} \leq 1$. Therefore,

$$\int_0^\infty se^{-\mu s}g(s)ds \leq |\int_0^\infty se^{-\mu s}g(s)ds| \leq \int_0^\infty s|e^{-\mu s}|g(s)ds \leq \int_0^\infty sg(s)ds = E > 0.$$

It follows that $\frac{d\mathrm{Re}(\mu)}{d\mu} > 0$. Hence $\mathrm{Re}(\mu) > 0$ for all $\mu \geq 0$, it follows from (5.8) that $\mathrm{Re}(\mu,\omega) > 0$ for all $\mu \geq 0$. Suppose that $\lambda = \mu + i\omega$ is a root of the characteristic equation (5.5). Then μ and ω must hold $\mathrm{Re}(\mu,\omega) = 0$ and $\Im(\mu,\omega) = 0$. From the above analysis, yields $\mu < 0$. Which implies that, all roots of the characteristic equation (5.5) have negative real part. □

Next, we are going to determine a region, where the trivial steady state is unstable for any distribution kernel $g(s)$ and $\tau \geq 0$.

Theorem 5.1.2. *The characteristic equation (5.4) has a root with positive real part for any distribution kernel and* $\tau \geq 0$ *if one of the following conditions is satisfied: (i)* $|\beta| > \kappa - \alpha$ *when* n *is even or* $\beta > \kappa - \alpha$ *when* n *is odd; or (ii)* $\alpha > \kappa$.

Proof. Substituting $\lambda = 0$ into the equations (5.5) and (5.6), gives

$$\Delta_E(\tau, 0) = \kappa - \alpha \pm \beta,$$

and

$$\Delta_O(\tau, 0) = \kappa - \alpha - \beta.$$

The assumptions (i) $|\beta| > \kappa - \alpha$ (n is even) or $\beta > \kappa - \alpha$ (n is odd) imply that $\Delta_E(\tau, 0) < 0$ and $\Delta_O(\tau, 0) < 0$, respectively. If the condition (ii) holds, then $\Delta_{E^-}(\tau, 0) =$

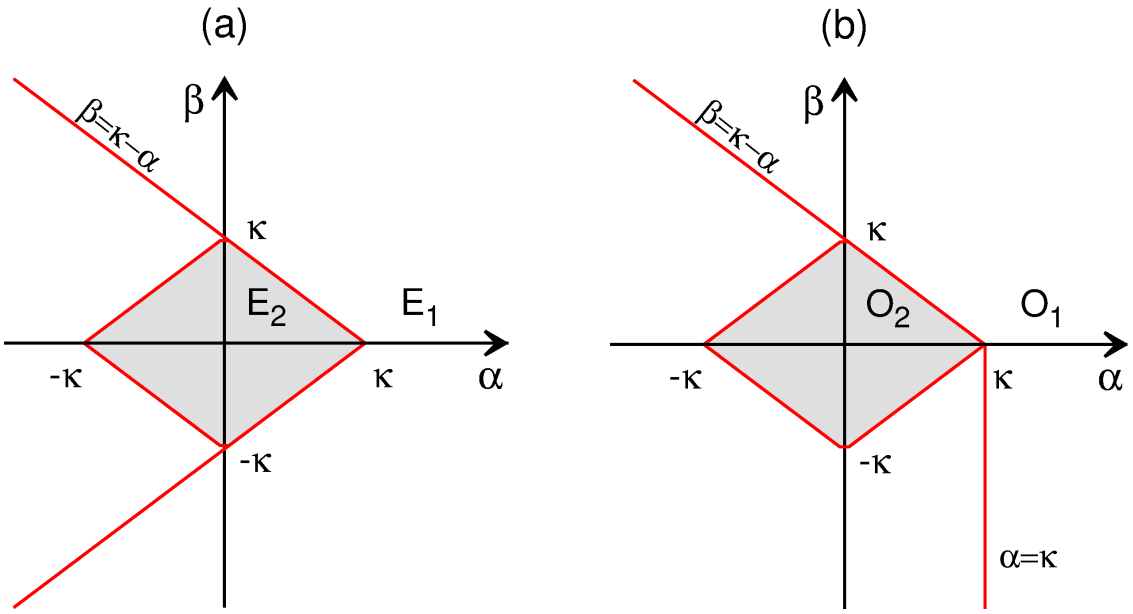

Figure 5.2: Stability region in the (α, β) parameter space of the trivial steady state of the system (5.1) for general distribution kernel. The regions (E_1) and (O_1) are unstable. The regions (E_2) and (O_2) are stable. (a) The case when n is even. (b) The case n is odd.

$\kappa-\alpha-\beta<0$ for $\beta \geq 0$, $\Delta_{E^+}(\tau,0)=\kappa-\alpha+\beta<0$ for $\beta \leq 0$ and $\Delta_O(\tau,0)=\kappa-\alpha-\beta<0$. On the other hand,

$$\lim_{\lambda\to\infty} \Delta_E(\tau,\lambda)=\infty, \qquad \lim_{\lambda\to\infty} \Delta_O(\tau,\lambda)=\infty.$$

Since $\Delta_E(\tau,\lambda)$ and $\Delta_O(\tau,\lambda)$ are continuous functions of λ, there exists $\lambda^*>0$ such that $\Delta_E(\tau,\lambda^*)=0$ and $\Delta_O(\tau,\lambda^*)=0$ for any $\tau \geq 0$, $|\beta|>\kappa-\alpha$ and $\beta>\kappa-\alpha$. Thus, the characteristic equations (5.5) and (5.6) have a root with positive real part, which completes the proof. □

So far, we have been able to obtain stability results for a general delay-distributed kernel. Figure 5.2 shows the subset of the stability region in the (α, β) plane, the shaded diamond-shaped domain is where the trivial steady state is stable whenever $|\beta|<\kappa-|\alpha|$ holds, and the size of the diamond depends on the parameter κ for both even and odd n as shown in Theorem 5.1.1. From Theorem 5.1.2, it follows that it is impossible to stabilise the unstable trivial steady state in E_1 in Figure 5.2 (a) and O_1 in Figure 5.2 (b) regions, if the parameters satisfy $|\beta|>\kappa-\alpha$ for even number of neurons or $\beta>\kappa-\alpha$ and $\alpha>\kappa$ for odd number of neurons.

Theorem 5.1.3. *On the lines $|\beta|=\kappa-\alpha$ when n is even, if $\tau<\frac{(\alpha-\kappa)E-1}{\alpha}$, then the trivial steady state becomes stable as β crosses both lines $\beta=\kappa-\alpha$ decreasingly and $\beta=-(\kappa-\alpha)$*

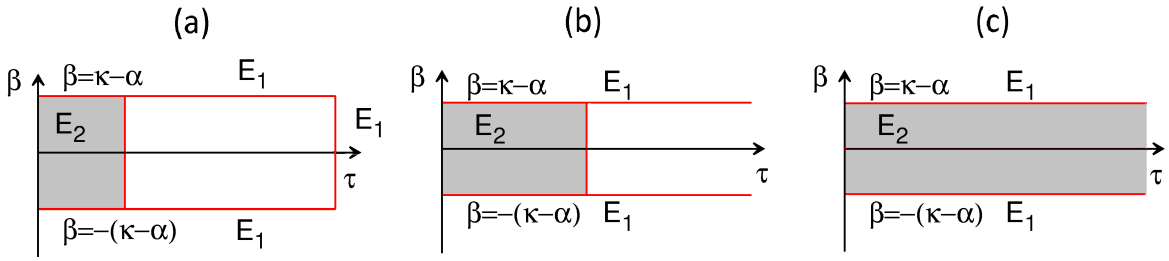

Figure 5.3: Stability boundary in the (τ, β) parameter space of the trivial steady state of the system (5.1) for general distribution kernel when n is even. The region E_1 is unstable. The region E_2 is stable when $\alpha < 0$ for $\tau < \frac{(\alpha-\kappa)E-1}{\alpha}$ and when $\alpha \geq 0$ for any τ. (a) $\alpha < -\kappa$. (b) $-\kappa \leq \alpha < 0$. (c) $0 \leq \alpha \leq \kappa$.

increasingly, where $E = \int_0^\infty sg(s)ds > 0$ *is the mean time delay.*

Proof. Recall that the $\lambda = 0$ lines are defined by the zero roots of $\Delta_E(\tau, \lambda) = 0$. Differentiating $\Delta_E(\tau, \lambda) = 0$ with respect to β, we obtain

$$\frac{d\mathrm{Re}(\lambda)}{d\beta} = \mathrm{Re}\left(\frac{\pm\int_0^\infty g(s)e^{-\lambda s}ds}{1+\alpha\tau e^{-\lambda\tau} \mp \beta\int_0^\infty se^{-\lambda s}g(s)ds}\right) = \mathrm{Re}\left(\frac{\pm\widehat{G}(\lambda)}{1+\alpha\tau e^{-\lambda\tau} \mp \beta\int_0^\infty se^{-\lambda s}g(s)ds}\right).$$

Therefore, at $|\beta| = \kappa - \alpha$ and $\lambda = 0$, one has

$$\frac{d\mathrm{Re}(\lambda)}{d\beta} = \frac{\pm 1}{1+\alpha\tau+(\kappa-\alpha)E}. \tag{5.9}$$

Hence, $\frac{d\mathrm{Re}(\lambda)}{d\beta} \lessgtr 0$, provided $\tau < \frac{(\alpha-\kappa)E-1}{\alpha}$, and the trivial steady state becomes stable as β decreases through the line $\beta = \kappa - \alpha$ and increases through the line $\beta = -(\kappa - \alpha)$, which completes the proof. □

Theorem 5.1.4. *On the line* $\beta = \kappa - \alpha$, $\beta > 0$ *when* n *is odd, if* $\tau < \frac{(\alpha-\kappa)E-1}{\alpha}$, *then the trivial steady state becomes stable as* β *crosses the line* $\beta = \kappa - \alpha$ *decreasingly, where* $E = \int_0^\infty sg(s)ds > 0$ *is the mean time delay.*

Proof. Recall that the $\lambda = 0$ line is defined by the zero roots of $\Delta_O(\tau, \lambda) = 0$.

Differentiating $\Delta_O(\tau, \lambda) = 0$ with respect to β, yields

$$\frac{d\mathrm{Re}(\lambda)}{d\beta} = \mathrm{Re}\left(\frac{\int_0^\infty g(s)e^{-\lambda s}ds}{1+\alpha\tau e^{-\lambda\tau}+\beta\int_0^\infty se^{-\lambda s}g(s)ds}\right) = \mathrm{Re}\left(\frac{\widehat{G}(\lambda)}{1+\alpha\tau e^{-\lambda\tau}+\beta\int_0^\infty se^{-\lambda s}g(s)ds}\right).$$

Then, when $\beta = \kappa - \alpha$ and $\lambda = 0$, we have

$$\frac{d\mathrm{Re}(\lambda)}{d\beta} = \frac{1}{1+\alpha\tau+(\kappa-\alpha)E}. \tag{5.10}$$

If $\tau < \frac{(\alpha-\kappa)E-1}{\alpha}$, this implies that $\frac{d\mathrm{Re}(\lambda)}{d\beta} < 0$, and, hence, the trivial steady state becomes stable as β decreases through the line $\beta = \kappa - \alpha$. This completes the proof. □

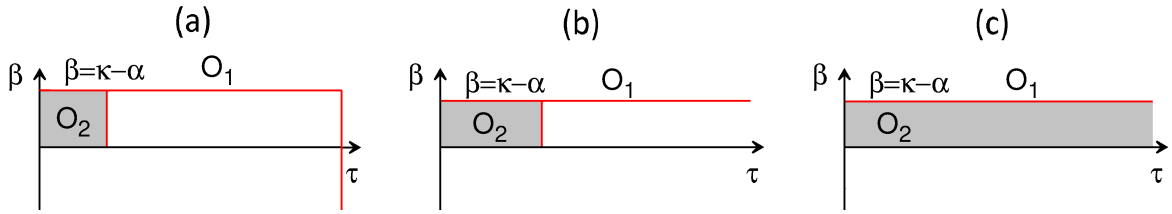

Figure 5.4: Stability boundary in the (τ, β) parameter space of the trivial steady state of the system (5.1) for general distribution kernel when n is odd. The region O_1 is unstable. The region O_2 is stable when $\alpha < 0$ for $\tau < \frac{(\alpha-\kappa)E-1}{\alpha}$ and when $\alpha \geq 0$ for any τ. (a) $\alpha < -\kappa$. (b) $-\kappa \leq \alpha < 0$. (c) $0 \leq \alpha \leq \kappa$.

Remark 5.1.1. *From Theorem 5.1.3, if* $0 \leq \alpha \leq \kappa$, *then* $\frac{d\mathrm{Re}(\lambda)}{d\beta} \gtrless 0$ *in (5.9), regardless of the distribution kernel and the time delay* $\tau \geq 0$. *Thus, the trivial steady state loses stability via a steady-state bifurcation by increasing* β *through the line* $\beta = \kappa - \alpha$ *and decreasing* β *through the line* $\beta = -(\kappa - \alpha)$.

Remark 5.1.2. *From Theorem 5.1.4, if* $0 \leq \alpha \leq \kappa$, *then* $\frac{d\mathrm{Re}(\lambda)}{d\beta} > 0$ *in (5.10) regardless of the distribution kernel and the time delay* $\tau \geq 0$. *Thus, the trivial steady state loses stability via a steady-state bifurcation by increasing* β *through the line* $\beta = \kappa - \alpha$.

Remark 5.1.3. *For a fixed value of* α *and for any kernel distribution, if* $|\alpha| < \kappa$, *then* $\beta \neq 0$ *for any* $\tau \geq 0$. *Furthermore, if* $|\alpha| > \kappa$, *then there exists* τ_0 *such that* $\beta = 0$ *for* $\tau = \tau_0$.

Proof. In order to find τ when $\beta = 0$ in Remark 5.1.3, let us assume that $\beta = 0$ in both characteristic equations (5.5) and (5.6), which yields

$$\lambda + \kappa - \alpha e^{-\lambda\tau} = 0. \tag{5.11}$$

Substituting $\lambda = i\omega$, $(\omega > 0)$ into (5.11) and separating into real and imaginary parts, we get

$$\kappa = \alpha \cos(\omega\tau), \qquad -\omega = \alpha \sin(\omega\tau). \tag{5.12}$$

It can be easily seen that the equations (5.12) can only be satisfied, if $|\alpha| > \kappa$. Under this assumption, squaring and adding (5.12) gives an expression for the Hopf frequency ω in the form $\omega = \sqrt{\alpha^2 - \kappa^2}$. Moreover, from the system (5.12), substituting ω, we can find the expressions for the time delay τ as follows

$$\tau \backsimeq \tau_j = \frac{1}{\sqrt{\alpha^2 - \kappa^2}} \begin{cases} (2j+1)\pi - \cos^{-1}(\frac{\kappa}{\alpha}) & \text{for } 0 < \kappa < \alpha, \\ \\ 2j\pi + \cos^{-1}(\frac{\kappa}{\alpha}) & \text{for } \alpha < -\kappa < 0, \end{cases} \tag{5.13}$$

where $j = 0, 1, \ldots$. Since the trivial steady state is unstable for $\alpha > \kappa$, we are only interested in the case when $\alpha < -\kappa$. This simplifies the equation (5.13) as

$$\tau_0 = \frac{\cos^{-1}\left(\frac{\kappa}{\alpha}\right)}{\sqrt{\alpha^2 - \kappa^2}} \text{ for } \alpha < -\kappa < 0,$$

where $\cos^{-1}(\cdot)$ is the principal branch of the inverse $\cos(\cdot)$ function, which has the range $[0, \pi]$. □

Figure 5.3 illustrates a part of a stability region in (τ, β) plane for even n and a general distribution kernel $g(s)$. The shaded area E_2 in Figures 5.3 (a) and (b) indicate that the trivial steady state is stable if both conditions $\tau < \frac{(\alpha-\kappa)E-1}{\alpha}$ and $\alpha < 0$ are satisfied. This is in the full agreement with Theorem 5.1.3, which states that if β increases through the line $\beta = \kappa - \alpha$ and decreases through the line $\beta = -(\kappa - \alpha)$, then the characteristic equation (5.4) has a positive real root. The closure in Figure 5.3 (a) reveals that for large enough values of the time delay τ and $\alpha < -\kappa$, the trivial steady state becomes unstable independently of the parameter β as stated in Remark 5.1.3. In Figure 5.3 (c), if $0 \leq \alpha \leq \kappa$, the trivial steady state can only lose its stability through the lines $|\beta| = \kappa - \alpha$. Finally, for $\alpha > \kappa$, the zero steady state is always unstable for $\tau \geq 0$, following the results of Theorem 5.1.2 (ii).

Figure 5.4 shows the stability regions for an odd number of neurons and different values of α. For all the three cases, form Theorem 5.1.4 it follows that the trivial steady state becomes stable as β passes through the line $\beta = \kappa - \alpha$ decreasingly. The shaded area O_2 in Figures 5.4 (a) and (b) indicate the region where that the trivial steady state is stable, provided $\tau < \frac{(\alpha-\kappa)E-1}{\alpha}$ and $\alpha < 0$ hold. The shaded area O_2 in Figure 5.4 (c) is a stability region for $\alpha > 0$ as stated in Remark 5.1.2. For both even and odd number of neurons Theorem 5.1.2 (ii) shows that if $\alpha > \kappa$, then the trivial steady state is always unstable independently of the time delay τ. It is noteworthy to mention that the trivial steady state undergoes a steady-state bifurcation through the horizontal lines $|\beta| = \kappa - \alpha$ when n is even and $\beta = \kappa - \alpha$ when n is odd as illustrated in Figures 5.3 and 5.4, and stated in Lemma 5.1.2.

Due to the complexity of the system, it is not possible to find the full stability region for a general distribution kernel. Therefore, we choose specific delay kernel distributions to obtain further analytical results and find the complete stability region for a trivial steady state.

5.2 Dirac delta function

When the delay distribution kernel is chosen as a Dirac delta function, as we discussed in subsection 1.3.1, then there are two possibilities. First, if $g(s) = \delta(s-\sigma)$, then the system (5.1) reduces to the system with two distinct discrete time delays. This case has been considered in a system of two neurons in [133], tri-neural network in [164], four neurons system in [157], and a ring of n neurons network in [23, 99].

Let us consider the distribution kernel of the form $g(s) = \delta(s)$, i.e

$$\int_0^\infty f(\mathbf{u}(t-s))\delta(s)ds = f(\mathbf{u}(t)). \tag{5.14}$$

In this case, the linearised model (5.2) becomes a system with a discrete time delay only, and has the form

$$\dot{\mathbf{u}}(t) = (-\kappa I + \beta M)\mathbf{u}(t) + \alpha I\mathbf{u}(t-\tau), \tag{5.15}$$

where $\mathbf{u} = (u_1, u_2, \cdots, u_n)$, I is an $n \times n$ identity matrix and M is defined in (5.2). The corresponding characteristic equations for even and odd n, respectively, are

$$\Delta_E(\tau, \lambda) = \lambda + \kappa \pm \beta - \alpha e^{-\lambda\tau} = 0 \tag{5.16}$$

and

$$\Delta_O(\tau, \lambda) = \lambda + \kappa - \beta - \alpha e^{-\lambda\tau} = 0. \tag{5.17}$$

In Section 5.1, we have analysed the characteristic equation for any general distribution kernel and we have obtained a subset of stability boundary in both (α, β) and (τ, β) parameter spaces. In the following we consider the same parameter spaces to determine the complete stability region in the case $g(s) = \delta(s)$.

Theorem 5.2.1. *For the system (5.1) with delta distributed kernel $g(s) = \delta(s)$ and even n, the following holds.*

(i) *The trivial steady state is unstable if $|\beta| > \kappa - \alpha$.*

(ii) *The trivial steady state is stable if $|\beta| < \kappa - |\alpha|$.*

(iii) *The trivial steady state is stable if $\kappa + \alpha < |\beta| < \kappa - \alpha$ and $\tau \in [0, \tau_{even})$, Hopf bifurcation occurs at $\tau = \tau_{even}$, and the steady state is unstable if $\tau > \tau_{even}$, where τ_{even} is the first critical time delay given by $\tau_{even} = \min\{\tau_0^-, \tau_0^+\}$ and*

$$\tau_0^\pm = \frac{\cos^{-1}(\frac{\kappa \pm \beta}{\alpha})}{\sqrt{\alpha^2 - (\kappa \pm \beta)^2}}.$$

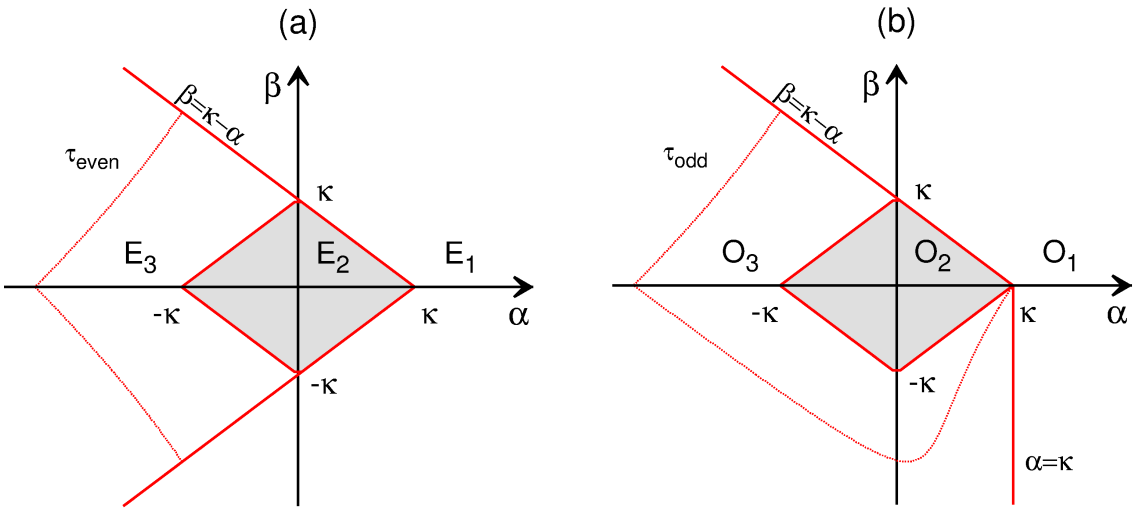

Figure 5.5: Stability boundary in (α, β) parameter space of the trivial steady state of the system (5.1) with delta distribution kernel. (a) When n is even, the region E_1 corresponds to the unstable trivial steady state, the region E_2 indicates the area where the trivial steady state is stable, and the region E_3 shows a stability region when $\tau \in [0, \tau_{even})$. (b) When n is odd, the region O_1 illustrates the unstable trivial steady state, the region O_2 shows where the trivial steady state is stable, and the region O_3 a stability region when $\tau \in [0, \tau_{odd})$.

Proof. Results (i) and (ii) immediately follow from Theorem 5.1.1 and 5.1.2. In (iii), assume the condition $\kappa + \alpha < |\beta| < \kappa - \alpha$ is satisfied. First, for $\tau = 0$, the characteristic equation (5.16) becomes $\Delta_E(0, \lambda) = \lambda + \kappa \pm \beta - \alpha$, with the eigenvalues given as $\lambda^* = -(\kappa \pm \beta - \alpha)$. Since $|\beta| < \kappa - \alpha$, $\lambda^* < 0$, and, therefore, the trivial steady state is stable. Now, we consider the case when $\tau > 0$ and look for the eigenvalues in the form $\lambda = i\omega$, $\omega > 0$. Substituting $\lambda = i\omega$ into (5.16), and separating into real and imaginary parts, we get

$$\begin{aligned} \kappa \pm \beta - \alpha \cos(\omega\tau) &= 0, \\ \omega + \alpha \sin(\omega\tau) &= 0. \end{aligned} \tag{5.18}$$

Upon squaring and adding the two equations (5.18), one obtains

$$\omega^2 = \alpha^2 - (\kappa \pm \beta)^2, \tag{5.19}$$

and from the first equation of the system (5.18) it follows that

$$\tau_j^{\pm} = \frac{1}{\sqrt{\alpha^2 - (\kappa \pm \beta)^2}} \begin{cases} (2j+1)\pi - \cos^{-1}\left(\dfrac{\kappa \pm \beta}{\alpha}\right) & \text{for } 0 < \kappa \pm \beta < \alpha, \\ 2j\pi + \cos^{-1}\left(\dfrac{\kappa \pm \beta}{\alpha}\right) & \text{for } \alpha < -(\kappa \pm \beta) < 0. \end{cases} \tag{5.20}$$

Since $|\beta| < \kappa - \alpha$, the latter expression for $\tau_j^{\pm}$ becomes

$$\tau_j^{\pm} = \frac{\cos^{-1}(\frac{\kappa \pm \beta}{\alpha}) + 2j\pi}{\sqrt{\alpha^2 - (\kappa \pm \beta)^2}}, \tag{5.21}$$

where $j = 0, 1, 2, ...$ Now we have to show that a Hopf bifurcation occurs when $\tau = \tau_{even}$. The solutions of the equation (5.19) are pairs $(\tau_j^{\pm}, \omega)$, where $\lambda = \pm i\omega$ are pairs of purely imaginary roots of (5.16) with $\tau = \tau_j^{\pm}$. Define

$$\tau_{even} = \min\{\tau_0^-, \tau_0^+\},$$

where τ_{even} is the first critical value of the time delay τ, for which the roots of equation (5.16) cross the imaginary axis. In order to determine the direction of the root crossing, we differentiate the characteristic equation (5.16) with respect to α:

$$\frac{d\lambda}{d\alpha} = \frac{e^{-\lambda\tau}}{1 + \alpha\tau e^{-\lambda\tau}} = \frac{1}{e^{\lambda\tau} + \alpha\tau}. \tag{5.22}$$

From (5.22) it follows that

$$\frac{d\mathrm{Re}(\lambda)}{d\alpha} = \frac{\alpha\tau + \cos(\omega\tau)}{(\alpha\tau + \cos(\omega\tau))^2 + (\sin(\omega\tau))^2}. \tag{5.23}$$

Using the first equation of (5.18), we obtain

$$\alpha\tau + \cos(\omega\tau) = \alpha\tau + \frac{\kappa \pm \beta}{\alpha} > \alpha\tau + \frac{\alpha}{\alpha} = \alpha\tau + 1,$$

which implies that $\alpha\tau + 1 < 0$ if $\alpha < -\frac{1}{\tau}$. This completes the proof. □

Theorem 5.2.2. *For the system (5.1) with delta distributed kernel $g(s) = \delta(s)$ and odd n, the following holds.*

(i) *The trivial steady state is unstable if $\beta > \kappa - \alpha$ and $\alpha > \kappa$.*

(ii) *The trivial steady state is stable if $|\beta| < \kappa - |\alpha|$.*

(iii) *The trivial steady state is stable if $\beta < \kappa - \alpha$, $\alpha < \kappa$ and $\tau \in [0, \tau_{odd})$, a Hopf bifurcation occurs at $\tau = \tau_{odd}$, and the steady state is unstable for all $\tau > \tau_{odd}$, where τ_{odd} is the first critical time delay given by*

$$\tau_{odd} = \frac{\cos^{-1}(\frac{\kappa - \beta}{\alpha})}{\sqrt{\alpha^2 - (\kappa - \beta)^2}}.$$

Proof. The proof of this theorem is similar to the proof of Theorem 5.2.1. In order to find τ_{odd}, we look for eigenvalues of the characteristic equation in the form $\lambda = i\omega$, substitute this into (5.16), and separating into real and imaginary parts, we get

$$\begin{aligned} \kappa - \beta - \alpha\cos(\omega\tau) &= 0, \\ \omega + \alpha\sin(\omega\tau) &= 0. \end{aligned} \tag{5.24}$$

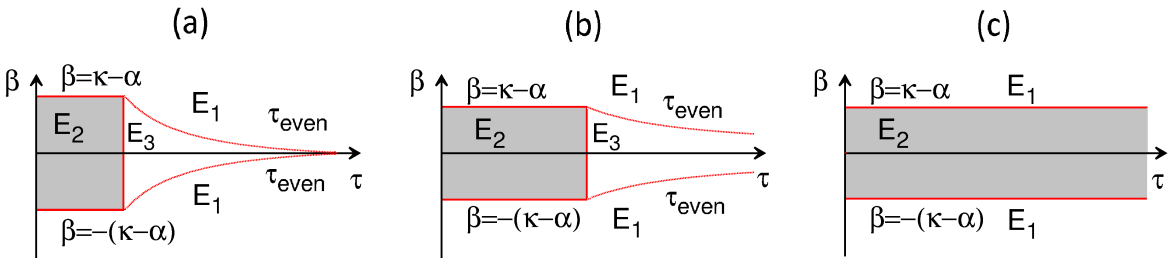

Figure 5.6: Stability boundary in (τ, β) parameter space of the trivial steady state of the system (5.1) for delta distributed kernel when n is even. The region E_1 corresponds to the unstable trivial steady state. The region E_2 is where the trivial steady state is stable when $\alpha < 0$ for $\tau < -\frac{1}{\alpha}$ and when $\alpha \geq 0$ for any τ. The region E_3 shows the stable region for $-\frac{1}{\alpha} \leq \tau < \tau_{even}$. (a) $\alpha < -\kappa$. (b) $-\kappa \leq \alpha < 0$. (c) $0 \leq \alpha \leq \kappa$.

Squaring and adding the equations (5.24), yields

$$\omega^2 = \alpha^2 - (\kappa - \beta)^2, \tag{5.25}$$

and from the first equation of the system (5.24), one obtains

$$\tau_j^- = \frac{1}{\sqrt{\alpha^2 - (\kappa-\beta)^2}} \begin{cases} (2j+1)\pi - \cos^{-1}\left(\dfrac{\kappa-\beta}{\alpha}\right) & \text{for } 0 < \kappa - \beta < \alpha, \\ 2j\pi + \cos^{-1}\left(\dfrac{\kappa-\beta}{\alpha}\right) & \text{for } \alpha < -(\kappa-\beta) < 0, \end{cases} \tag{5.26}$$

where $\tau_{odd} = \tau_0^-$ is the first critical time delay, when the trivial steady state loses its stability. This completes the proof. □

Theorems 5.2.1 and 5.2.2 give the stability properties of the trivial steady state in (α, β) parameter space when the delay distribution kernel $g(s) = \delta(s)$. When n is even, in Figure 5.5 (a), the stability region bounded by the lines $|\beta| = \kappa - \alpha$ to the left of the shaded diamond, and remains symmetric with respect to α-axis. Figure 5.5 (b) shows the stability boundary when n is odd. In this case, the stability region is enlarged towards down-left of the shaded diamond. It is worth noting, that unlike the case when n is even, for an odd n, the stability region becomes asymmetric.

Next, we analyse the stability properties of the trivial steady state of the system (5.2) in (τ, β) plane with delta distributed kernel.

Theorem 5.2.3. *For the system (5.1) with delta distributed kernel $g(s) = \delta(s)$ and even n, the following statements hold.*

(i) *For $\alpha < 0$, the trivial steady state is stable if $|\beta| < \kappa - \alpha$ and $\tau < -\frac{1}{\alpha}$. By increasing (decreasing) β through the line $|\beta| = \kappa - \alpha$, the trivial steady state loses its stability*

via a steady-state bifurcation occurs. The trivial steady state is stable if $|\beta| < \kappa - \alpha$ *and* $\tau \in [-\frac{1}{\alpha}, \tau_{even})$*, a Hopf bifurcation occurs at* $\tau = \tau_{even}$*. The trivial steady state unstable if* $\tau > \tau_{even}$*. For* $\alpha < -\kappa$*, the trivial steady state is unstable independent of* β *for* $\tau > \tau_0 = \frac{\cos^{-1}(\frac{\kappa}{\alpha})}{\sqrt{\alpha^2-\kappa^2}}$.

(ii) *For* $0 \leq \alpha \leq \kappa$*, the trivial steady state is stable if* $|\beta| < \kappa - \alpha$ *increasing(decreasing)* β *through the line* $|\beta| = \kappa - \alpha$ *steady-state bifurcation occurs, independent of time delay* τ*. The trivial steady state is unstable if* $|\beta| > \kappa - \alpha$.

Proof. Following the stability results in the case of the general distribution kernel stated in Theorem 5.1.3 and Remark 5.1.1, we have proved the results in (i) and (ii) that are related to the appearance of the steady-state bifurcation. We have also shown the trivial steady state is unstable independent of β in Remark 5.1.3 for $\alpha < -\kappa$. In order to show the occurrence of a Hopf bifurcation in (i) and (ii), when $\tau = \tau_{even}$, differentiating implicitly (5.16) with respect to τ we find that

$$\frac{d\lambda}{d\tau} = \frac{1}{1 + \alpha\tau e^{-\lambda\tau}}. \tag{5.27}$$

Substituting $\lambda = i\omega$ into (5.27), and taking real part, one has

$$\frac{d\mathrm{Re}(\lambda)}{d\tau} = \frac{1 + \alpha\tau\cos(\omega\tau)}{(1 + \alpha\tau\cos(\omega\tau))^2 + (\alpha\tau\sin(\omega\tau))^2}. \tag{5.28}$$

Using the first equation of (5.18) yields,

$$1 + \alpha\tau\cos(\omega\tau) = 1 + \tau(\kappa \pm \beta) > 1 + \tau\alpha,$$

which implies that $1 + \tau\alpha > 0$ if $\tau > -\frac{1}{\alpha}$, and we conclude that for $\tau = \tau_{even}$ there is a root $\lambda = \lambda(\tau) = \alpha(\tau) \pm i\omega(\tau)$ satisfying $\alpha(\tau_{even}) = 0$, $\omega(\tau_{even}) = \omega$ and $\frac{d\mathrm{Re}(\lambda)}{d\tau}|_{\tau=\tau_{even}} > 0$. This root crosses the imaginary axis at $\tau = \tau_{even}$ from left to right if $\tau > -\frac{1}{\alpha}$, which completes proof. □

Theorem 5.2.4. *For the system (5.1) with delta function* $g(s) = \delta(s)$ *when* n *is odd, the following statements hold.*

(i) *For* $\alpha < 0$ *and* $\beta > 0$*, the trivial steady state is stable if* $\beta < \kappa - \alpha$ *and* $\tau < -\frac{1}{\alpha}$*, increasing* β *through the line* $\beta = \kappa - \alpha$ *a steady-state bifurcation occurs. The trivial steady state is stable if* $\beta < \kappa - \alpha$ *and* $\tau \in [-\frac{1}{\alpha}, \tau_{odd})$*, Hopf bifurcation occurs at* $\tau = \tau_{odd}$*. The trivial steady state is unstable if* $\tau > \tau_{odd}$*. For* $\alpha < 0$ *and* $\beta < 0$*, the trivial steady state is stable if* $\tau \in [0, \tau_{odd})$*, Hopf bifurcation occurs at* $\tau = \tau_{odd}$*. The trivial steady state unstable if* $\tau > \tau_{odd}$*. For* $\alpha < -\kappa$*, the trivial steady state is unstable independent of* β *for* $\tau > \tau_0 = \frac{\cos^{-1}(\frac{\kappa}{\alpha})}{\sqrt{\alpha^2-\kappa^2}}$.

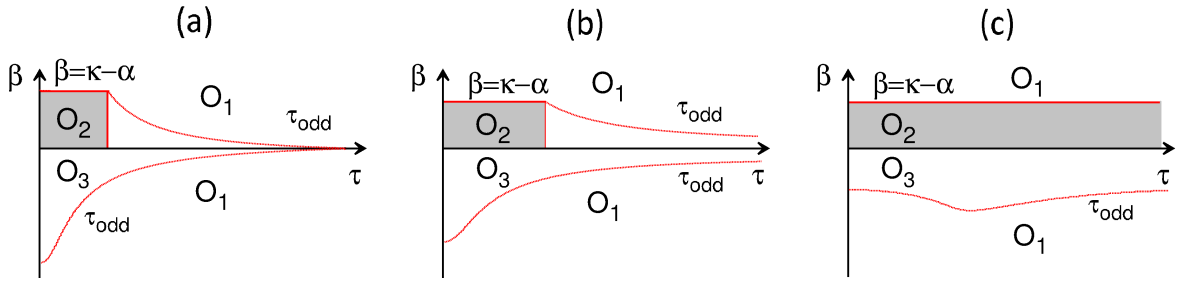

Figure 5.7: Stability boundary in the (τ, β) plane of the trivial steady state of the system (5.1) for general distribution kernel when n is odd. The region O_1 is unstable. The region O_2 is stable when $\alpha < 0$ for $\tau < -\frac{1}{\alpha}$ and when $\alpha \geq 0$ for any τ. The region O_3 is stable for $\tau < \tau_{odd}$. (a) $\alpha < -\kappa$. (b) $-\kappa \leq \alpha < 0$. (c) $0 \leq \alpha \leq \kappa$.

(ii) *For $0 \leq \alpha \leq \kappa$ and $\beta > 0$, the trivial steady state is stable if $\beta < \kappa - \alpha$. With increasing β through the line $\beta = \kappa - \alpha$, the steady state undergoes a steady-state bifurcation, independent of the time delay τ. The trivial steady state is unstable if $\beta > \kappa - \alpha$. For $0 < \alpha \leq \kappa$ and $\beta < 0$, the trivial steady state is stable if $\tau \in [0, \tau_{odd})$, Hopf bifurcation occurs at $\tau = \tau_{odd}$. The trivial steady state unstable if $\tau > \tau_{odd}$.*

Proof. Similar to the proof of Theorem 5.2.3, following the stability results for a general distribution kernel stated in Theorem 5.1.4 and Remarks 5.1.2 and 5.1.3, we have shown the existence of the steady-state bifurcation. In order to show the occurrence of a Hopf bifurcation in (i) and (ii), when $\tau = \tau_{even}$, differentiating implicitly (5.17) with respect to τ we find that

$$\frac{d\lambda}{d\tau} = \frac{1}{1 + \alpha\tau e^{-\lambda\tau}}. \tag{5.29}$$

It follows from (5.29) that

$$\frac{d\mathrm{Re}(\lambda)}{d\tau} = \frac{1 + \alpha\tau\cos(\omega\tau)}{(1 + \alpha\tau\cos(\omega\tau))^2 + (\alpha\tau\sin(\omega\tau))^2}. \tag{5.30}$$

For $0 < \beta < \kappa - \alpha$, using the first equation of (5.24) we obtain, $1 + \alpha\tau\cos(\omega\tau) = 1 + \tau(\kappa - \beta) > 1 + \tau\alpha > 0$ if $\tau > -\frac{1}{\alpha}$. For $\beta < 0$, this implies that $1 + \alpha\tau\cos(\omega\tau) = 1 + \tau(\kappa - \beta) > 0$, which completes the proof. □

Theorem 5.2.3 and 5.2.4, illustrate the full stability region in (τ, β) parameter space. After specify the distributed delay by delta function $g(s) = \delta(s)$ the condition for a general distributed kernel $\tau < \frac{(\kappa-\alpha)E-1}{\alpha}$ reduces to $\tau < -\frac{1}{\alpha}$. The stability region splits into three different shapes depends on the conditions on the parameter space. When n is even and $\alpha < 0$ in Figure 5.6 (a) and (b), the trivial steady state is stable if $|\beta| = \kappa - \alpha$ and $\tau < -\frac{1}{\alpha}$, the trivial steady state is stable for $\tau \in [-\frac{1}{\alpha}, \tau_{even})$ and undergoes Hopf

bifurcation at $\tau = \tau_{even}$. As we discussed in previous section and shown in Figure 5.6 (a), if $\alpha < -\kappa$ then the trivial steady state unstable independently of β for large enough of τ. When $0 \leq \alpha \leq \kappa$ as shown in Figure 5.6 (c), the delta function does not have any effect compared with a general distribution. When n is odd, again it gives three boundary regions. The upper shapes are similar to the case when n is even and also the theoretical analysis remain the same for $\beta > 0$. The asymmetry shape arises when $\beta < 0$ for all three different conditions on parameter region as shown in Figure 5.7, which is the trivial steady state is stable if $\tau \in [0, \tau_{odd})$, Hopf bifurcation occurs at $\tau = \tau_{odd}$. The trivial steady state unstable if $\tau > \tau_{odd}$.

5.3 Weak gamma distributed delayed kernel

In this section we consider the case when the delay distribution kernel is taken as gamma distribution. Following the same technique as in Section 2.5, substituting the Laplace transform (2.36) with $r = 1$ into (5.4), the characteristic equation becomes

$$\lambda^2 + p_1\lambda + p_2 + (q_1\lambda + q_2)e^{-\lambda\tau} = 0, \tag{5.31}$$

where

$$p_1 = \gamma + \kappa, \quad p_2 = \begin{cases} (\kappa \pm \beta)\gamma & \text{if} \quad n \quad \text{is even}, \\ (\kappa - \beta)\gamma & \text{if} \quad n \quad \text{is odd}, \end{cases} \quad q_1 = -\alpha, \quad q_2 = -\alpha\gamma. \tag{5.32}$$

In order to determine the stability of the trivial steady state of the system (5.1), we investigate the distribution of roots of characteristic equation (5.31). The boundary of the stability region consists of points such that (5.31) has roots with zero real part. This can happen either when $\lambda = 0$ or $\lambda = i\omega\,(\omega > 0)$. As shown in Lemma 5.1.1 for any distribution kernel, $\lambda = 0$ is a solution of the characteristic equation (5.31) if and only if $|\beta| = \kappa - \alpha$ when n is even and $\beta = \kappa - \alpha$ when n is odd. In order to find the boundaries of the stability region, we look at the case when the characteristic equation has a pair of purely imaginary roots. Looking eigenvalues of the characteristic equation in the form $\lambda = i\omega$, substituting this form into (5.31) gives the following equation

$$-\omega^2 + p_1\omega i + p_2 + (q_1\omega i + q_2)(\cos(\omega\tau) - i\sin(\omega\tau)) = 0. \tag{5.33}$$

Separating the real and imaginary parts of (5.33) yields

$$\begin{cases} \omega^2 - p_2 &= q_2\cos(\omega\tau) + q_1\omega\sin(\omega\tau), \\ p_1\omega &= q_2\sin(\omega\tau) - q_1\omega\cos(\omega\tau). \end{cases} \tag{5.34}$$

Squaring and adding the two equations in (5.34), one obtains a quartic equation

$$\omega^4 - (q_1^2 + 2p_2 - p_1^2)\omega^2 + p_2^2 - q_2^2 = 0, \tag{5.35}$$

which solutions can be found as

$$\omega_\pm^2 = \frac{(q_1^2 + 2p_2 - p_1^2) \pm \sqrt{(q_1^2 + 2p_2 - p_1^2)^2 - 4(p_2^2 - q_2^2)}}{2}. \tag{5.36}$$

Let $\Phi = (q_1^2 + 2p_2 - p_1^2)^2 - 4(p_2^2 - q_2^2) < 0$. If (H1) $p_2^2 - q_2^2 > 0$ and $q_1^2 + 2p_2 - p_1^2 < 0$ or $\Phi < 0$, then the equation (5.35) has no real roots. If (H2) $p_2^2 - q_2^2 < 0$ or $q_1^2 + 2p_2 - p_1^2 > 0$ and $\Phi = 0$, then the equation (5.35) has one positive root ω_+ given by

$$\omega_+ = \frac{\sqrt{2}}{2}[q_1^2 + 2p_2 - p_1^2 + \sqrt{\Phi}]^{\frac{1}{2}}.$$

If (H3) $p_2^2 - q_2^2 > 0$, $q_1^2 + 2p_2 - p_1^2 > 0$ and $\Phi > 0$, then the equation (5.35) has two positive roots $\omega_\pm = \frac{\sqrt{2}}{2}[q_1^2 + 2p_2 - p_1^2 \pm \sqrt{\Phi}]^{\frac{1}{2}}$.

If either of the hypotheses (H2) or (H3) holds, the equation (5.31) has purely imaginary roots after τ takes certain values. These values $\tau = \tau_j^\pm$ can be found as follows. We can find $\sin(\omega\tau)$ and $\cos(\omega\tau)$ from a pair of equation (5.34) as

$$\begin{aligned} \sin(\omega\tau) &= \frac{\omega(q_1\omega^2 + p_1q_2 - p_2q_1)}{q_1^2\omega^2 + q_2^2}, \\ \cos(\omega\tau) &= -\frac{p_1q_1\omega^2 - q_2\omega^2 + p_2q_2}{q_1^2\omega^2 + q_2^2}. \end{aligned} \tag{5.37}$$

Dividing $\sin(\omega\tau)$ by $\cos(\omega\tau)$, the critical time delays can be expressed as

$$\tau_j^\pm = \frac{1}{\omega_\pm}\left\{\tan^{-1}\left(-\frac{\omega_\pm(q_1\omega_\pm^2 + p_1q_2 - p_2q_1)}{p_1q_1\omega_\pm^2 - q_2\omega_\pm^2 + p_2q_2}\right) + j\pi\right\}, \qquad j = 0, 1, 2, \cdots. \tag{5.38}$$

Here we define

$$\tau_{weak} = \min\{\tau_0^-, \tau_0^+\}$$

as the first critical time delay. Note that when $\tau = 0$, then the system (5.1) with gamma distribution (1.7) becomes a system of ODEs with a characteristic equation

$$\lambda^2 + (p_1 + q_1)\lambda + p_2 + q_2 = 0. \tag{5.39}$$

Lemma 5.3.1. *Assume that (H4) $p_1 + q_1 > 0$ and $p_2 + q_2 > 0$, then all roots of the equation (5.39) with $\tau = 0$ always have negative real parts.*

Lemma 5.3.2. *Suppose that (H4) holds and $\omega_\pm^2$ and $\tau_j^\pm$ are defined by equations (5.36) and (5.38) respectively.*

(i) *If (H1) is satisfied, then the number of positive real roots in equations (5.31) and (5.39) is the same.*

(ii) *If (H2) is satisfied, then the number of positive real roots in equations (5.31) and (5.39) is the same for $\tau \in [0, \tau_{weak})$ and the equation (5.31) has a simple pair of purely imaginary roots $\pm i\omega_+$ at $\tau = \tau_{j^+}$.*

(iii) *If (H3) is satisfied, then the number of positive real roots in equations (5.31) and (5.39) is the same for $\tau \in [0, \tau_{weak})$, and the equations (5.31) has two pairs of simple purely imaginary roots $\pm i\omega_\pm$ at $\tau = \tau_j^\pm$.*

Under the hypothesis (H3), the characteristic equation (5.31) has two imaginary solutions $i\omega_\pm$ with $\omega_+ > \omega_- > 0$ defined by (5.36). In order to determine the stability of the steady state as τ varies, we calculate the sign of the derivative of $\mathrm{Re}(\lambda)$ at the points where $\lambda(\tau)$ is purely imaginary.

Lemma 5.3.3. *The following transversality conditions are satisfied*

$$\left[\frac{d\mathrm{Re}\{\lambda(\tau)\}}{d\tau}\right]_{\tau=\tau_j^+} > 0, \quad \left[\frac{d\mathrm{Re}\{\lambda(\tau)\}}{d\tau}\right]_{\tau=\tau_j^-} < 0.$$

Following the above analysis, we can investigate the stability of the trivial solution of the system (5.1) with weak distribution kernel (1.7) ($r = 1$). When $\tau = 0$, all roots of (5.39) have negative real parts if and only if (H4) is satisfied. Substituting (5.32) into $p_2 + q_2 > 0$, one obtains

$$\begin{cases} \gamma(\kappa - \beta) - \alpha\gamma > 0 \Rightarrow \alpha < \kappa - \beta \quad \text{if} \quad n \quad \text{is odd}, \\ \\ \gamma(\kappa \pm \beta) - \alpha\gamma > 0 \Rightarrow \alpha < \kappa + |\beta| \quad \text{if} \quad n \quad \text{is even}. \end{cases} \tag{5.40}$$

It follows that the trivial steady state of a ring neuron system (5.1) without self-connection delay is stable if and only if (5.40) is satisfied. Now we consider the effect of the self-connection delay in the ring neural system (5.1). Lets us check the hypothesise (H1-H3) by substituting p_1, p_2, q_1, and q_2.

First, substituting the parameters (5.32) into (H1) $p_2^2 - q_2^2 > 0$ and $q_1^2 + 2p_1 - p_1^2 < 0$, respectively yields,

$$\begin{cases} \gamma^2(\kappa - \beta)^2 - \alpha^2\gamma^2 > 0 \Rightarrow \alpha < |\kappa - \beta| < \kappa + |\beta| \quad \text{if} \quad n \quad \text{is odd}, \\ \\ \gamma^2(\kappa \pm \beta)^2 - \alpha^2\gamma^2 > 0 \Rightarrow \alpha < |\kappa \pm \beta| < \kappa + |\beta| \quad \text{if} \quad n \quad \text{is even}, \end{cases} \tag{5.41}$$

and

$$\begin{cases} \alpha^2-\kappa^2-\gamma(2\beta+\gamma)<0 \Rightarrow |\alpha|<\kappa \text{ and } \beta>-\frac{\gamma}{2} & \text{if } \quad n \quad \text{is odd,} \\ \\ \alpha^2-\kappa^2+\gamma(\pm 2\beta-\gamma)<0 \Rightarrow |\alpha|<\kappa \text{ and } |\beta|>-\frac{\gamma}{2} & \text{if } \quad n \quad \text{is even.} \end{cases} \tag{5.42}$$

Now, substituting (5.32) into (H2) $p_2^2-q_2^2<0$, yields

$$\begin{cases} \gamma^2(\kappa-\beta)^2-\alpha^2\gamma^2<0 \Rightarrow \alpha>|\kappa-\beta| & \text{if } \quad n \quad \text{is odd,} \\ \\ \gamma^2(\kappa\pm\beta)^2-\alpha^2\gamma^2<0 \Rightarrow \alpha>|\kappa\pm\beta| & \text{if } \quad n \quad \text{is even.} \end{cases} \tag{5.43}$$

Finally, in (H3) we have condition $p_2^2-q_2^2>0$, which is the same as in (5.41), and $q_1^2+2p_1-p_1^2>0$, $\Phi>0$ gives to

$$\begin{cases} \alpha^2-\kappa^2-\gamma(2\beta+\gamma)>0 \Rightarrow |\alpha|>\kappa \text{ and } \beta<-\frac{\gamma}{2} & \text{if } \quad n \quad \text{is odd,} \\ \\ \alpha^2-\kappa^2+\gamma(\pm 2\beta-\gamma)>0 \Rightarrow |\alpha|>\kappa \text{ and } |\beta|<-\frac{\gamma}{2} & \text{if } \quad n \quad \text{is even,} \end{cases} \tag{5.44}$$

and

$$\begin{cases} (\alpha^2+2\gamma(\kappa-\beta)-(\gamma+\kappa)^2)^2-4(\gamma^2(\kappa-\beta)^2-\alpha^2\gamma^2)>0 \Rightarrow \alpha>|\kappa-\beta| & \text{if } \quad n \quad \text{is odd,} \\ \\ (\alpha^2+2\gamma(\kappa\pm\beta)-(\gamma+\kappa)^2)^2-4(\gamma^2(\kappa\pm\beta)^2-\alpha^2\gamma^2)>0 \Rightarrow \alpha>|\kappa\pm\beta| & \text{if } \quad n \quad \text{is even.} \end{cases} \tag{5.45}$$

From the above analysis and using Lemma 5.3.2 and Lemma 5.3.3, one has the following theorems on the distribution of the roots of the characteristic equation (5.31).

Theorem 5.3.1. *For the system (5.1) with gamma distributed delayed kernel (1.7) when n is even and $\tau_j^{\pm}$ defined in (5.38), the following statements hold.*

(i) *The trivial steady state is unstable if $|\beta|>\kappa-\alpha$.*

(ii) *The trivial steady state is stable if $\alpha<\kappa+|\beta|$ and $|\alpha|<\kappa$.*

(iii) *The trivial steady state is stable if $\alpha<\kappa+|\beta|$, $\alpha>-\kappa$ and $\tau\in[0,\tau_{weak})$, a Hopf bifurcation occurs at $\tau=\tau_{weak}$, and the steady state is unstable if $\tau>\tau_{weak}$.*

Theorem 5.3.2. *For the system (5.1) with gamma distributed delayed kernel (1.7) with odd n and $\tau_j^{\pm}$ defined in (5.38), the following statements hold.*

(i) *The trivial steady state is unstable if $\beta>\kappa-\alpha$ and $\alpha>\kappa$.*

(ii) *The trivial steady state is stable if $\alpha<\kappa+|\beta|$ and $|\alpha|<\kappa$.*

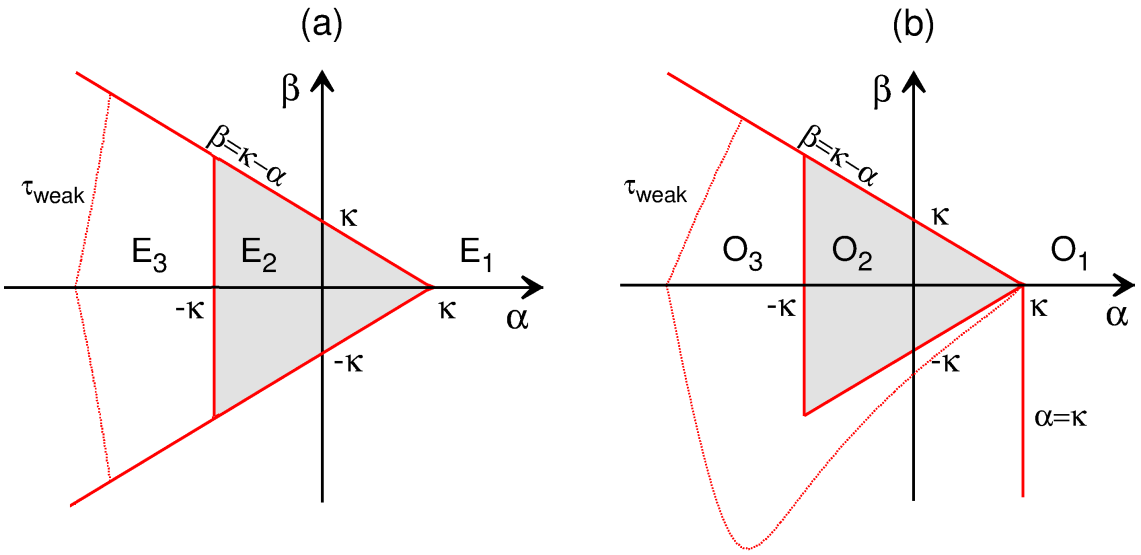

Figure 5.8: Stability boundary of the trivial steady state of the system (5.1) for weak gamma distributed kernel. The trivial steady state is unstable in the regions E_1 and O_1. The trivial steady state is stable in the regions E_2 and O_2. In the regions E_3 and O_3, the trivial steady state is stable for $\tau \in [0, \tau_{weak})$. (a) n is even. (b) n is odd.

(iii) *The trivial steady state is stable if* $\beta < \kappa - \alpha$ *and* $\alpha < \kappa$ *and* $\tau \in [0, \tau_{weak})$*, a Hopf bifurcation occurs at* $\tau = \tau_{weak}$*, and the steady state is unstable if* $\tau > \tau_{weak}$*.*

Figure 5.8 illustrates the stability of the trivial steady state of the system (5.1) in the case when the distribution kernel is chosen as a weak gamma distribution. Inside the shaded-triangle regions E_2 and O_2, the trivial steady state is stable. In this case, the regions are larger in comparison to the case of the delta distributed kernel. Similar to the case of the delta distribution kernel, the stability region extends to the left of the triangle and remains symmetric along α-axis for an even number of neurons, as shown in Figure 5.8 (a). When n is odd, the shape of stability loses its symmetry property as the stability region grows from both down and left of the triangle as shown in Figure 5.8 (b).

Theorem 5.3.3. *For the system (5.1) with the gamma distribution kernel (1.7) when* n *is even and* $\tau_j^{\pm}$ *defined in (5.38), the following statements hold.*

(i) *For* $\alpha < 0$*, the trivial steady state is stable if* $|\beta| < \kappa - \alpha$ *and* $\tau < \frac{\alpha-\kappa-\gamma}{\alpha\gamma}$*, and by increasing (decreasing)* β *through the line* $|\beta| = \kappa - \alpha$*, it loses its stability through a steady-state bifurcation. Furthermore, the trivial steady state is stable if* $|\beta| < \kappa - \alpha$ *and* $\tau \in [\frac{\alpha-\kappa-\gamma}{\alpha\gamma}, \tau_{weak})$*, and a Hopf bifurcation occurs at* $\tau = \tau_{weak}$*. The trivial steady state is unstable* $\tau > \tau_{weak}$*. For* $\alpha < -\kappa$*, the trivial steady state is unstable independent of* β *for* $\tau > \tau_0 = \frac{\cos^{-1}(\frac{\kappa}{\alpha})}{\sqrt{\alpha^2-\kappa^2}}$*.*

(ii) *For $0 \leq \alpha \leq \kappa$, the trivial steady state is stable if $|\beta| < \kappa - \alpha$, and with increasing (decreasing) β through the line $|\beta| = \kappa - \alpha$, it undergoes a steady-state bifurcation, independently of the time delay τ. The trivial steady state unstable for $|\beta| > \kappa - \alpha$.*

Theorem 5.3.4. *For the system (5.1) with the gamma distribution kernel (1.7) when n is odd and $\tau_j^{\pm}$ defined in (5.38), the following statements hold.*

(i) *For $\alpha < -\kappa$ and $\beta > 0$, the trivial steady state is stable if $\beta < \kappa - \alpha$ and $\tau < \frac{\alpha-\kappa-\gamma}{\alpha\gamma}$, and by increasing β through the line $\beta = \kappa - \alpha$, it loses its stability via a steady-state bifurcation. The trivial steady state is stable if $\beta < \kappa - \alpha$ and $\tau \in [\frac{\alpha-\kappa-\gamma}{\alpha\gamma}, \tau_{weak})$, a Hopf bifurcation occurs at $\tau = \tau_{weak}$. The trivial steady state is unstable if $\tau > \tau_{weak}$. For $\alpha < 0$ and $\beta < 0$, the trivial steady state is stable if $\tau \in [0, \tau_{weak})$, a Hopf bifurcation occurs at $\tau = \tau_{weak}$. The trivial steady state unstable if $\tau > \tau_{weak}$. For $\alpha < -\kappa$, the trivial steady state is unstable independent of β for $\tau > \tau_0 = \frac{\cos^{-1}(\frac{\kappa}{\alpha})}{\sqrt{\alpha^2-\kappa^2}}$.*

(ii) *For $0 \leq \alpha \leq \kappa$ and $\beta > 0$, the trivial steady state is stable if $\beta < \kappa - \alpha$, and by increasing β through the line $\beta = \kappa - \alpha$, it undergoes a steady-state bifurcation, independent of the time delay τ. The trivial steady state unstable if $\beta > \kappa - \alpha$. For $0 < \alpha \leq \kappa$ and $\beta < 0$, the trivial steady state is stable if $\tau \in [0, \tau_{weak})$, a Hopf bifurcation occurs at $\tau = \tau_{weak}$. The trivial steady state unstable if $\tau > \tau_{weak}$.*

Similar to the case of the general distribution kernel and delta distributed kernel, the stability boundary in (τ, β) is similar to Figure 5.6 and 5.7 for even and odd n, respectively. If we substitute the mean time delay $E = \frac{1}{\gamma}$ into the condition $\tau < \frac{(\kappa-\alpha)E-1}{\alpha}$, it becomes $\tau < \frac{\alpha-\kappa-\gamma}{\alpha\gamma}$ which is now the length of horizontal line, and now it depends not only on α but also on γ and κ.

In next section, we give two examples to support our analytical results.

5.4 Examples and numerical simulations

In order to confirm our analytical findings, in this section, we consider two examples when n is even and n is odd in (5.1) for the cases when the delay-distribution kernel is taken as Dirac delta function and in the form of a weak gamma distribution. We shall use traceDDE toolbox to compute the characteristic roots and stability regions for the trivial steady state of the system (5.1). We will also perform direct numerical simulations of the fully nonlinear system using *dde23* suite in Matlab.

5.4.1 Example: even number of ring-coupled neurons

We consider the system (5.1) with $n = 2$, which is shown schematically in Figure 5.9.

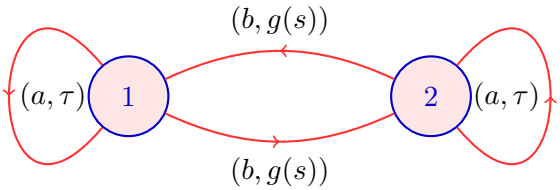

Figure 5.9: A schematic sketch of the unidirectionally coupled two neurons with distributed delays and a discrete-delayed self-connection.

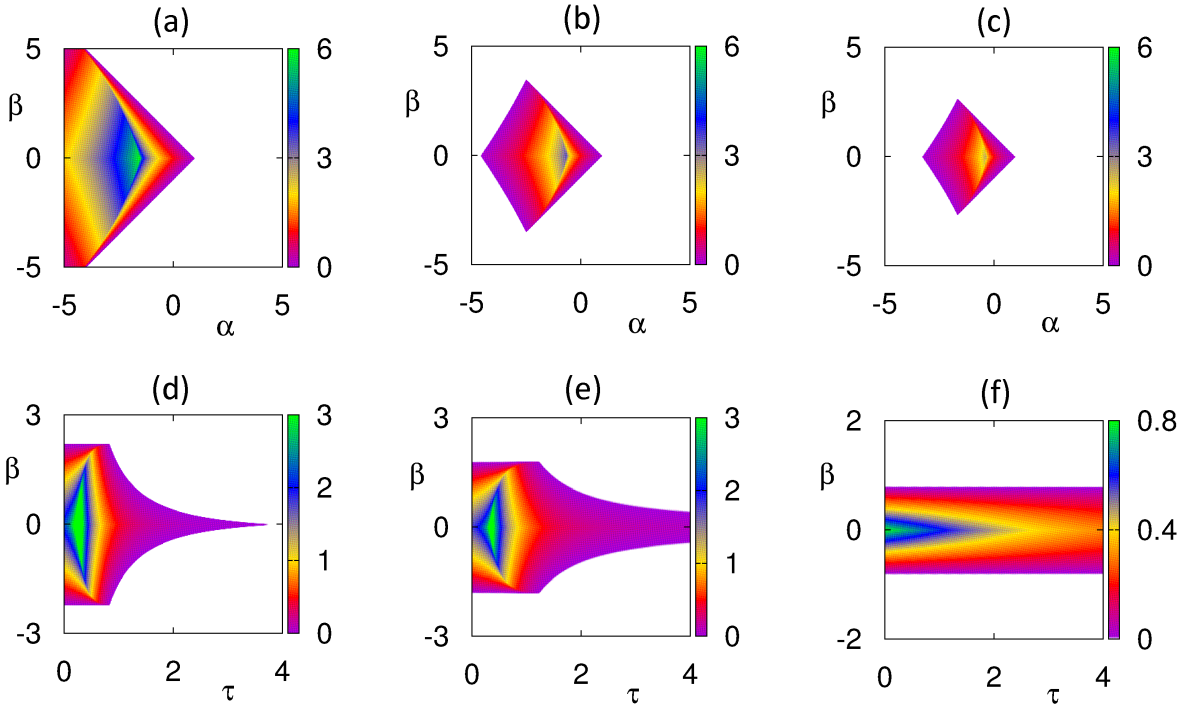

Figure 5.10: Stability region for the trivial steady state of the system (5.1) with delta distributed kernel $g(s) = \delta(s)$ and $n = 2$. Colour code denotes $[-\max\{\mathrm{Re}(\lambda)\}]$ for $\max\{\mathrm{Re}(\lambda)\} \leq 0$. (a)-(c) $\kappa = 1$. (a) $\tau = 0.2$. (b) $\tau = 0.4$. (c) $\tau = 0.6$. (d)-(f) $\kappa = 1$. (d) $\alpha = -1.2\,(\alpha < -\kappa)$. (e) $\alpha = -0.8\,(-\kappa \leq \alpha < 0)$. (f) $\alpha = 0.2\,(0 \leq \alpha \leq \kappa)$.

Figures 5.10 (a)-(c) show the numerically computed stability regions for the trivial steady state of the system (5.1) with delta distributed kernel and $n = 2$ in the (α, β) plane. The colour represents $[-\max\{\mathrm{Re}(\lambda)\}]$. It can been seen that the shape of the stability area is symmetric with respect to the α-axis, which is in direct agreement with Theorem 5.2.1. As time delay τ is increased, the stability region detaches from the $\alpha-$axis, and becomes a small island for larger values of τ. In Figure 5.10 (d)-(f), the stability area is computed in the (τ, β) plane and several values of α. For negative values of α, the steady

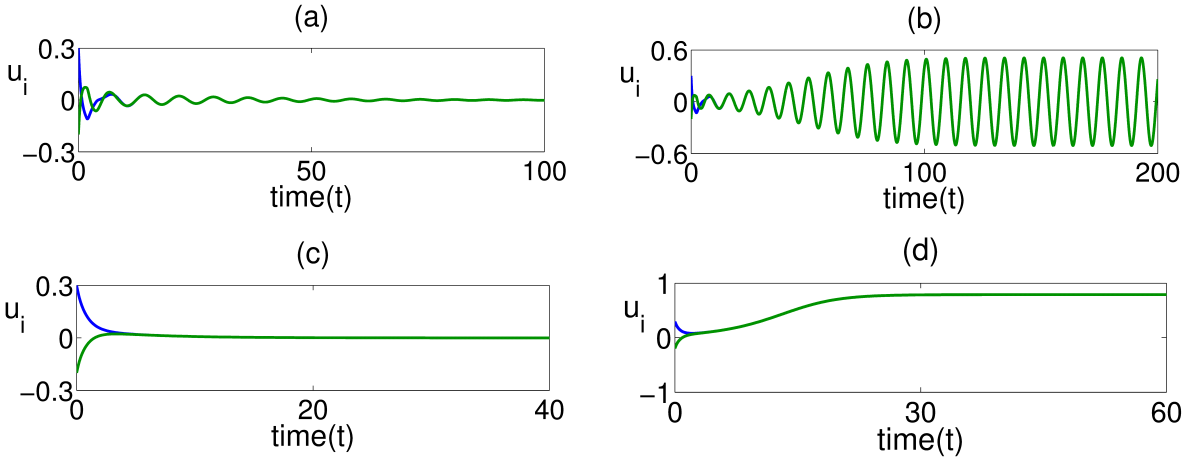

Figure 5.11: (a)-(b) Solution of the system (5.46) in the case when $\alpha < 0$. Parameter values are $\kappa = 1$, $b = 1$, $a = -0.8$ and $\tau_{even} = 1.96$. (a) $0 < \tau = 1.8 < \tau_{even}$. (b) $\tau = 2.2 > \tau_{even}$. (c)-(d) Solution of the system (5.46) in the case when $\alpha \geq 0$. Parameter values are $\kappa = 1$, $a = 0.2$, $\tau = 0.5$. (c) $b = 0.6$. (d) $b = 1$.

state undergoes both Hopf and steady state bifurcations (shown in Figure 5.10 (d)-(e)) when it loses its stability, which is in agreement with Theorem 5.1.3 and Theorem 5.2.3. Figure 5.10 (f) corresponds to the case of positive values of $\alpha \in [0, \kappa]$, where the steady state can only undergo a steady-state bifurcation (as shown in Remark 5.1.1).

We also perform direct numerical simulations of the full nonlinear system (5.1) with $n = 2$ and a delta distributed kernel. Let $f(\cdot) = \tanh(\cdot)$, which implies that $f'(0) = 1$. We can rewrite system (5.1) for $n = 2$ and $g(s) = \delta(s)$ as follows

$$\begin{aligned} \dot{u}_1(t) &= -\kappa u_1(t) + a\tanh(u_1(t-\tau)) + b\tanh(u_2(t)), \\ \dot{u}_2(t) &= -\kappa u_2(t) + a\tanh(u_2(t-\tau)) + b\tanh(u_1(t)). \end{aligned} \tag{5.46}$$

From Theorem 5.2.3 (i) and (ii), it follows that whenever $\alpha < 0$, the trivial steady state is stable if $|\beta| < \kappa - \alpha$ and $\tau \in [-\frac{1}{\alpha}, \tau_{even})$. Here, we take $\kappa = 1$, $b = \pm 1$, $a = -0.8$, which gives the first critical value of the time delay $\tau_{even} = 1.96$, where the trivial steady state loses its stability. In Figure 5.11 (a) and Figure 5.12 (a), the trivial steady state is stable for $1.25 \leq \tau < 1.96$, and undergoes a Hopf bifurcation at $\tau_{even} = 1.96$, giving rise to a stable periodic solution, as plotted in Figure 5.11 (b) and Figure 5.12 (b). Note that when $\beta > 0$ and $\tau > \tau_{even}$, we observe an isochronal synchronous state, as shown in Figure 5.11 (b), while $\beta < 0$ and $\tau > \tau_{even}$, there is an anti-phase synchronous state, as illustrated in Figure 5.12 (b).

Following Theorem 5.2.3 (iii), when $0 \leq \alpha \leq \kappa$, the trivial steady state is stable if $|\beta| < \kappa - \alpha$, which is satisfied for parameters $\kappa = 1$, $a = 0.2$, $b = \pm 0.6$, and the solutions

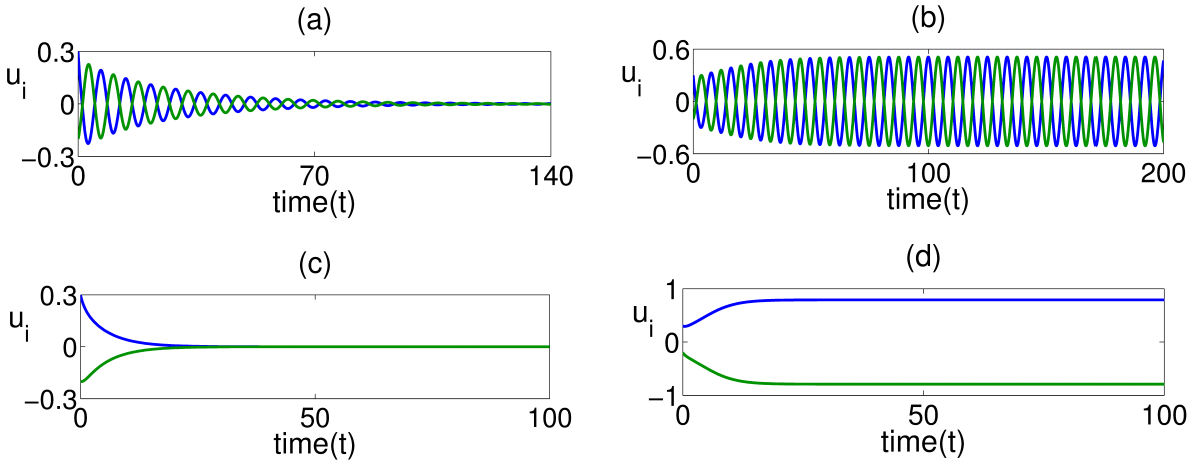

Figure 5.12: (a)-(b) Solution of the system (5.46) in the case when $\alpha < 0$. Parameter values are $\kappa = 1$, $b = -1$, $a = -0.8$ and $\tau_{even} = 1.96$. (a) $0 < \tau = 1.8 < \tau_{even}$. (b) $\tau = 2.2 > \tau_{even}$. (c)-(d) Solution of the system (5.46) in the case when $\alpha \geq 0$. Parameter values are $\kappa = 1$, $a = 0.2$, $\tau = 0.5$. (c) $b = -0.6$. (d) $b = -1$.

are shown in Figure 5.11 (c) and Figure 5.12 (c). If $\beta > \beta_c$, where β_c satisfies $|\beta_c| = \kappa - \alpha$, then the trivial steady state is a repeller, and there exists stable non-trivial steady states, as plotted in Figure 5.11 (d) and Figure 5.12 (d).

Next, we perform numerical simulations for the system (5.1) with weak gamma distributed kernel and $n = 2$. Introducing two new variables

$$u_3(t) = \int_0^\infty \gamma e^{-\gamma s} u_1(t-s)ds,$$

$$u_4(t) = \int_0^\infty \gamma e^{-\gamma s} u_2(t-s)ds,$$

allows one rewrite the system 5.1 with $n = 2$ as follows

$$\begin{aligned}
\dot{u}_1(t) &= -\kappa u_1(t) + a\tanh(u_1(t-\tau)) + b\tanh(u_4(t)),\\
\dot{u}_2(t) &= -\kappa u_2(t) + a\tanh(u_2(t-\tau)) + b\tanh(u_3(t)),\\
\dot{u}_3(t) &= \gamma u_1(t) - \gamma u_3(t),\\
\dot{u}_4(t) &= \gamma u_2(t) - \gamma u_4(t).
\end{aligned} \tag{5.47}$$

The stability region in (α, β) plane for weak gamma distributed delay kernel is larger compare to the case of the delta distributed kernel for larger values of τ, and with increasing τ, it shrinks and becomes an isolated island, as shown in Figure 5.13 (b)-(c). The stability region has a symmetry with respect to α-axis as illustrated in Figure 5.13 (a)-(c). Similar

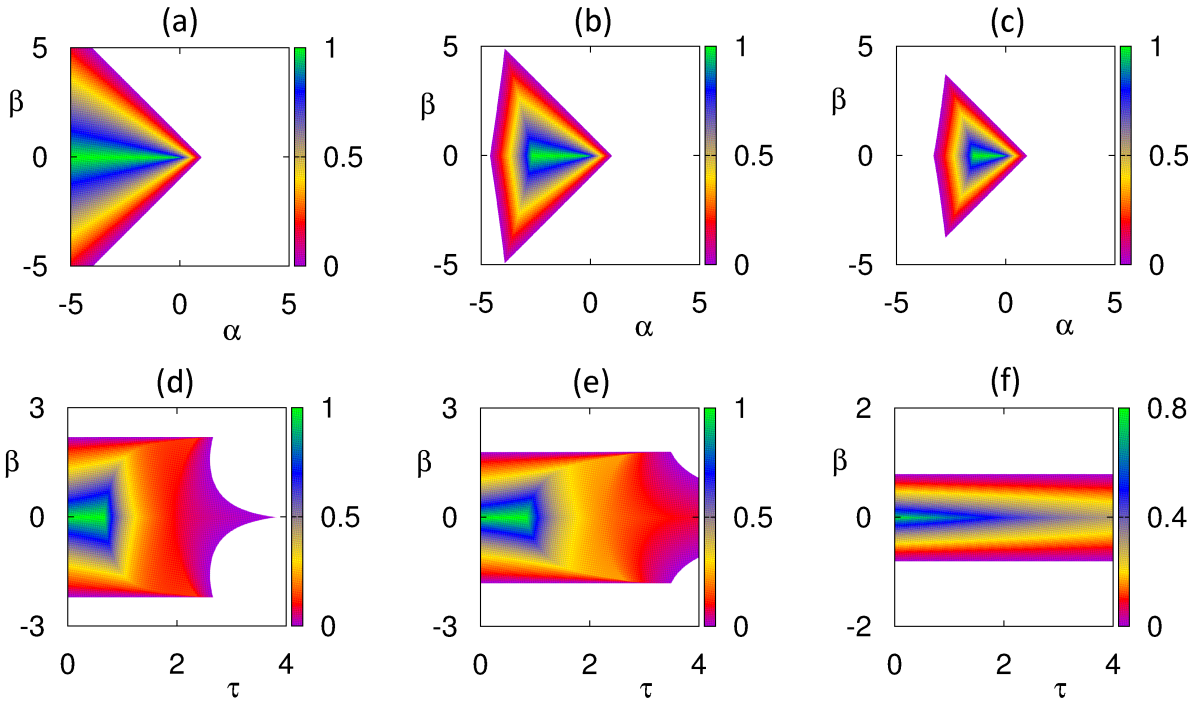

Figure 5.13: Stability of the trivial steady state of the system (5.1) with weak gamma distributed kernel and $n = 2$. Colour code denotes $[-\max\{\mathrm{Re}(\lambda)\}]$ for $\max\{\mathrm{Re}(\lambda)\} \leq 0$. (a)-(c) Stability region in (α, β), for parameters $\kappa = 1$, $\gamma = 1$. (a) $\tau = 0.2$. (b) $\tau = 0.4$. (c) $\tau = 0.6$. (d)-(f) Stability region in (τ, β), for parameters $\kappa = 1$, $\gamma = 1$. (d) $\alpha = -1.2\,(\alpha < -\kappa)$. (e) $\alpha = -0.8\,(-\kappa \leq \alpha < 0)$. (f) $\alpha = 0.2\,(0 \leq \alpha \leq \kappa)$.

to the case of the delta distributed kernel, in this case, there are three different boundary regions in (τ, β) parameter space depending on the values of α, and they are all symmetric with respect to the α-axis as plotted in Figure 5.13 (d)-(f). The trivial steady state can lose its stability via a steady-state bifurcation as well as Hopf bifurcation for negative values of α, shown in Figure 5.13 (d)-(e) and it undergoes a steady state bifurcation for $0 \leq \alpha \leq \kappa$ (Figure 5.13 (f)). Figure 5.14 illustrates the boundary of the stability region of the trivial steady state in β, τ and γ parameter space for the weak distribution kernel. If $\kappa = 1$ and $\alpha = -1$, then $-\kappa \leq \alpha < 0$ is satisfied, which means that the trivial steady state is stable inside the region bounded by the symmetric surfaces shown in Figure 5.14 (a) and unstable outside this region. It can be observed in Figure 5.14 (b) that as long as the coupling strength β between the two neurons decreases, the stability region of the trivial steady becomes larger.

From Theorem 5.3.3, when $\alpha < 0$, then the trivial steady state is stable if $|\beta| < \kappa - \alpha$ and $\tau \in [\frac{\alpha-\kappa-\gamma}{\alpha\gamma}, \tau_{weak})$. For parameter values $\kappa = 1$, $b = \pm 1$, $a = -0.8$, $\gamma = 1$, the first critical time delay in (5.38) is $\tau_{weak} = 4.14$. Thus, for $\tau \in [3.5, 4.14)$ the trivial steady

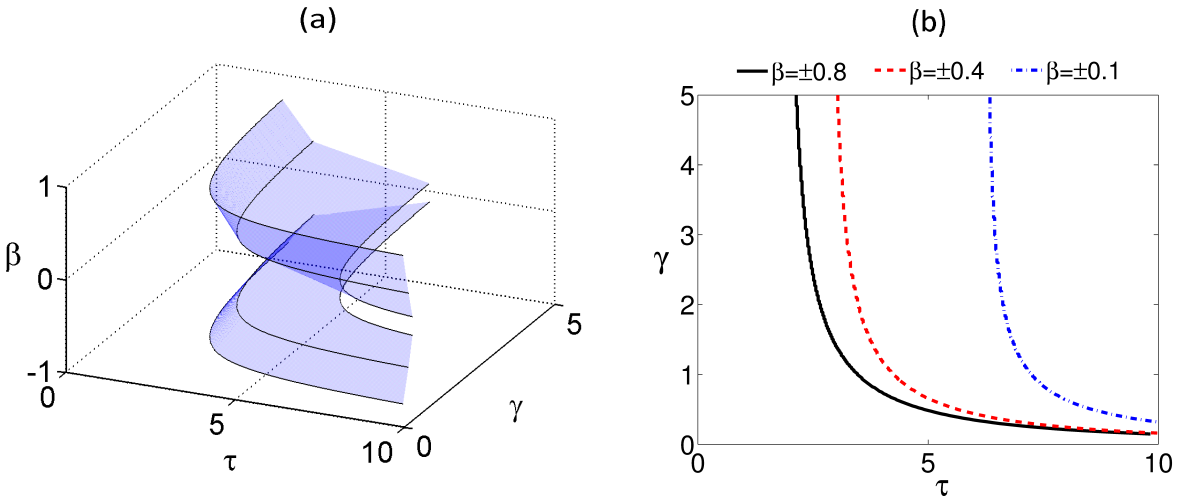

Figure 5.14: Stability boundaries of the trivial steady state of the system (5.1) with weak gamma distributed kernel and $n = 2$. Parameter values are $\kappa = 1$, $\alpha = -1$. The trivial steady state is stable inside the region restricted by the boundaries in (a), and to the left of the boundary curves in (b).

state is stable, as shown in Figure 5.15 (a) and Figure 5.16 (a), Hopf bifurcation occurs at $\tau_{weak} = 4.14$, and periodic oscillations exist for $\tau_{weak} > 4.14$.

Moreover, similar to the delta distribution kernel, Figure 5.15 (b) and Figure 5.16 (b) show the isochronal and the anti-phase synchrony states, respectively. If $\kappa = 1$, $a = 0.2$, $b = \pm 0.6$, then $0 \leq \alpha \leq \kappa$ and $|\beta| < \kappa - \alpha$ are satisfied as required by Theorem 5.2.3 (iii) to ensure the stability of the trivial steady state, and this is illustrated in Figure 5.15 (c) and Figure 5.16 (c). If $\kappa = 1$, $a = 0.2$, $b = \pm 0.6$, and $\beta \geq \pm 0.8$, then the condition $|\beta| \geq \kappa - \alpha$ is satisfied, and the trivial steady state becomes unstable through a steady-state bifurcation, and the system (5.47) tends to one of its stable non-trivial steady states, as shown in Figure 5.15 (d) and Figure 5.16 (d). One should note that it is possible for this system to simultaneously have multiple stable steady states for the same parameter values, and the solutions will approach one of them depending on the initial conditions.

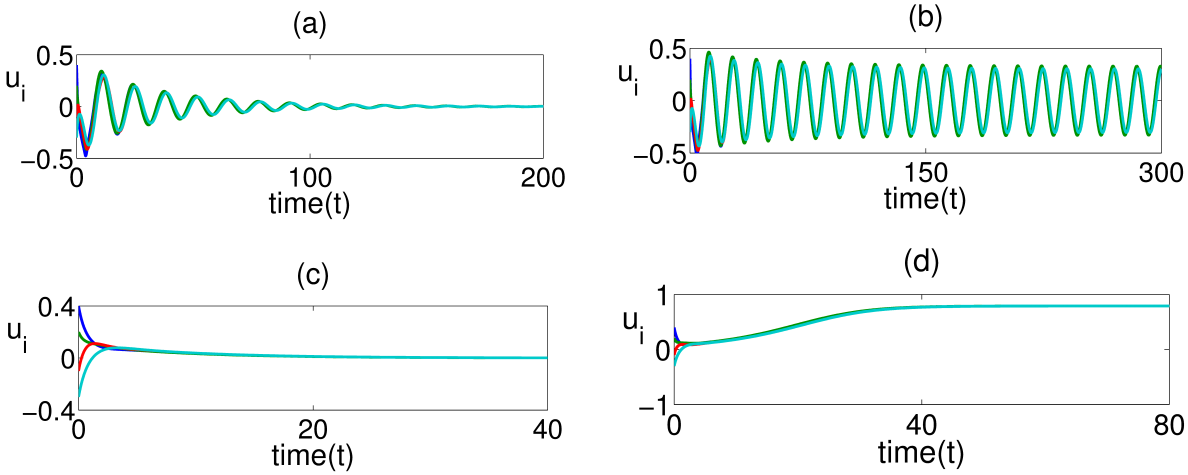

Figure 5.15: (a)-(b) Solution of the system (5.47) in the case when $\alpha < 0$. Parameter values are $\kappa = 1$, $b = 1$, $a = -0.8$, $\gamma = 1$ and $\tau_{weak} = 4.14$. (a) $0 < \tau = 3.8 < \tau_{weak}$. (b) $\tau = 4.3 > \tau_{weak}$. (c)-(d) Solution of the system (5.47) in the case when $\alpha \geq 0$. Parameter values are $\kappa = 1$, $a = 0.2$, $\gamma = 1$, $\tau = 0.5$. (c) $b = 0.6$. (d) $b = 1$.

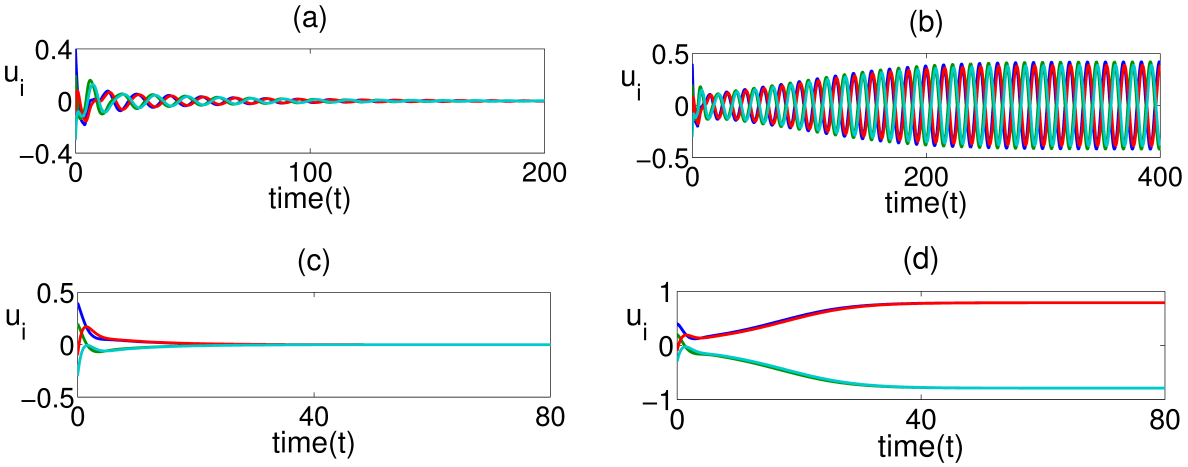

Figure 5.16: (a)-(b) Solution of the system (5.47) in the case when $\alpha < 0$. Parameter values are $\kappa = 1$, $b = -1$, $a = -0.8$, $\gamma = 1$ and $\tau_{weak} = 4.14$. (a) $0 < \tau = 3.8 < \tau_{weak}$. (b) $\tau = 4.3 > \tau_{weak}$. (c)-(d) Solution of the system (5.47) in the case when $\alpha \geq 0$. Parameter values are $\kappa = 1$, $a = 0.2$, $\gamma = 1$, $\tau = 0.5$. (c) $b = -0.6$. (d) $b = -1$.

5.4.2 Example: odd number of ring-coupled neurons

For the second example, we consider three unidirectionally coupled neurons with self-connections as shown in the diagrammatic sketch 5.17. If the distribution kernel is chosen as a delta function, i.e. $g(s) = \delta(s)$, then the system (5.1) can be written as follows

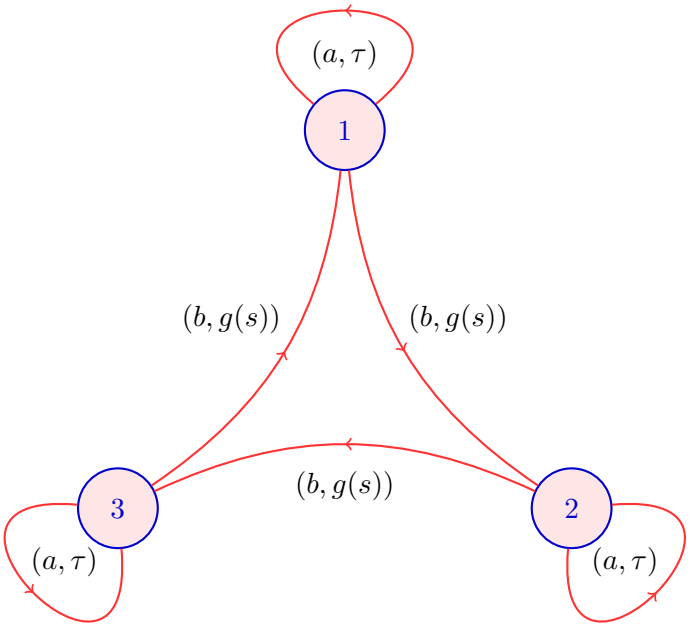

Figure 5.17: A diagrammatic sketch of the unidirectionally coupled three neurons with distributed delays and a discrete-delayed self-connection.

$$\begin{aligned}
\dot{u}_1(t) &= -\kappa u_1(t) + a\tanh(u_1(t-\tau)) + b\tanh(u_3(t)),\\
\dot{u}_2(t) &= -\kappa u_2(t) + a\tanh(u_2(t-\tau)) + b\tanh(u_2(t)),\\
\dot{u}_3(t) &= -\kappa u_3(t) + a\tanh(u_3(t-\tau)) + b\tanh(u_1(t)).
\end{aligned} \tag{5.48}$$

Figures 5.18 (a)-(c) show the stability region of the trivial steady state for delta distributed kernle $g(s) = \delta(s)$ in (α, β) plane when $n = 3$. Similar to the case of delta function when $n = 2$, the stability region becomes smaller with increasing time delay τ, but unlike the case of the even number of neurons, here the stability region is asymmetric with respect to α-axis. Figures 5.18 (d)-(f) illustrate three different stability boundaries of the trivial steady state (τ, β) plane for $n = 3$ and different values of α.

In Figures 5.18 (d)-(e), when α is negative and β is positive, similar to the case when $n = 2$, the boundary of stability region consists to two parts for which trivial steady state can lose its stability via a steady-state and a Hopf bifurcation. In Figure 5.18 (f), for positive values α and β, the trivial steady state undergoes a steady-state bifurcation only. In contrast to the case of the even number of neurons, the steady state can lose its stability via a Hopf bifurcation only when $\beta < 0$, which makes the stability area asymmetric with respect to α-axis.

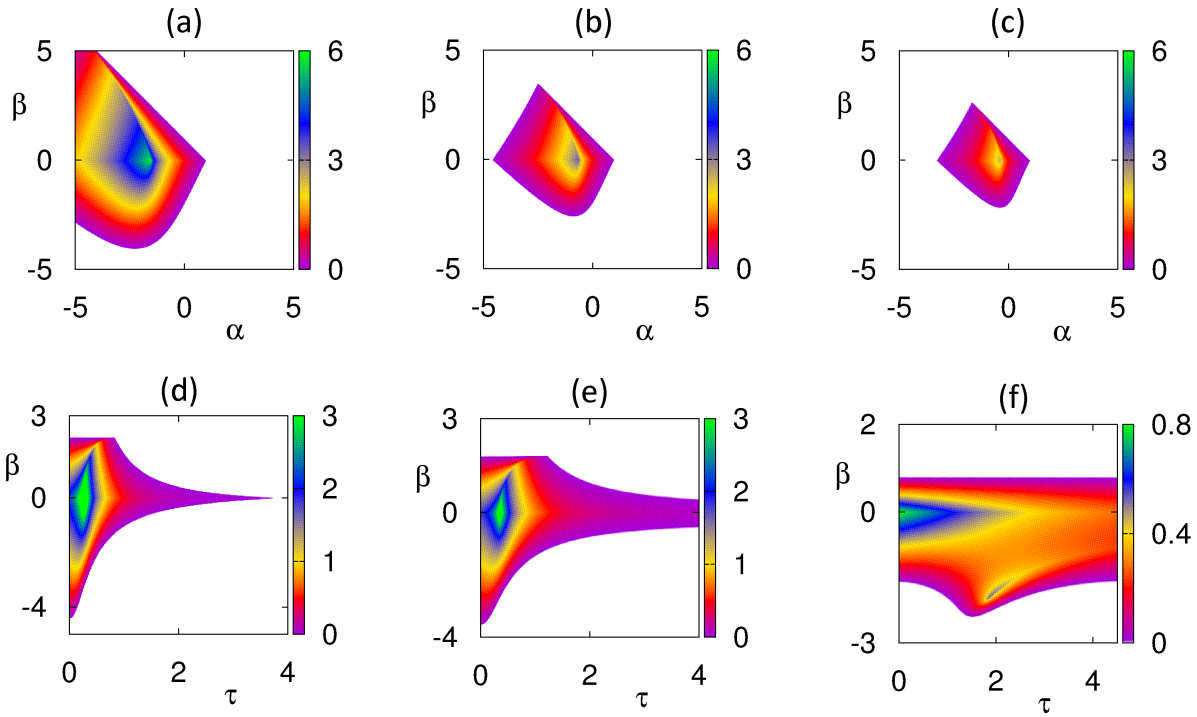

Figure 5.18: Stability boundary of the trivial steady state of the system (5.1) delta distributed kernel $g(s) = \delta(s)$ and $n = 3$. Colour code denotes $[-\max\{\mathrm{Re}(\lambda)\}]$ for $\max\{\mathrm{Re}(\lambda)\} \leq 0$. (a)-(c) Stability region in (α, β), for parameters $\kappa = 1$. (a) $\tau = 0.2$. (b) $\tau = 0.4$. (c) $\tau = 0.6$. (d)-(f) Stability region in (τ, β), for parameters $\kappa = 1$. (d) $\alpha = -1.2\,(\alpha < -\kappa)$. (e) $\alpha = -0.8\,(-\kappa \leq \alpha < 0)$. (f) $\alpha = 0.2\,(0 \leq \alpha \leq \kappa)$.

From the analysis in Section 5.2 for odd number of neurons, the stability of the trivial steady state depends on whether the coupling strength β is positive or negative. For $\beta > 0$ the analysis is similar to that in the case of the even number of neurons. If $\alpha = af'(0) = -0.8 < 0$, $\beta = bf'(0) = 1 > 0$, $\kappa = 1$, then from equation (5.26), we have $\tau_{odd} = 1.96$, which means that the condition $\beta < \kappa - \alpha$ is satisfied. This, in turn, means that for $\tau \in [0, \tau_{odd})$ the trivial steady state is stable as shown in Figure 5.19 (a), and display an isochronally synchronised periodic oscillations for $\tau > \tau_{odd}$, as illustrated in Figure 5.19 (b).

In the case when $\kappa = 1$, $a = 0.2$, the condition $0 \leq \alpha \leq \kappa$ holds, and for $b = 0.9$, the solutions tend to the trivial steady state, as illustrated in Figure 5.19 (c), while for $b = 1$, the solutions converge to a non-trivial steady state, as shown in Figure 5.19 (d). Next, we consider negative values of β. If $\kappa = 1$, $b = -1$, $a = -0.8$, then $\tau_{odd} = 1.56$, and the trivial steady state is stable for $0 \leq \tau < \tau_{odd}$, as displayed in Figure 5.20 (a), and $\tau > \tau_{odd}$, a splay-phase synchronous periodic state appears, as shown in Figure 5.20 (b).

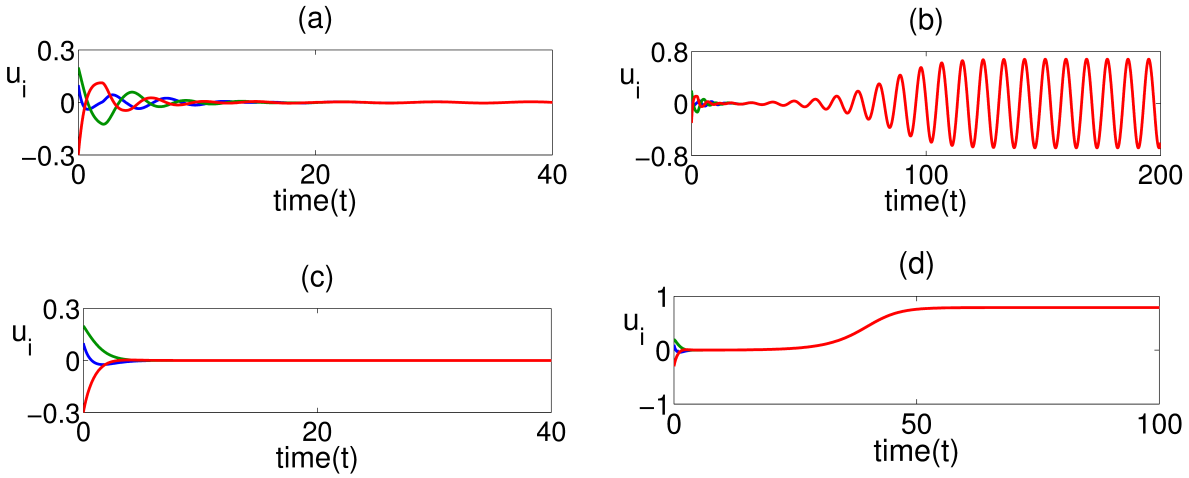

Figure 5.19: (a)-(b) Solution of the system (5.48) in the case when $\alpha < 0$. Parameter values are $\kappa = 1$, $b = 1$, $a = -0.8$ and $\tau_{odd} = 1.96$. (a) $0 < \tau = 1.8 < \tau_{odd}$. (b) $\tau = 2.2 > \tau_{odd}$. (c)-(d) Solution of the system (5.48) in the case when $\alpha \geq 0$. Parameter values are $\kappa = 1$, $\tau = 0.5$, $a = 0.2$. (c) $b = 0.9$. (d) $b = 1.3$.

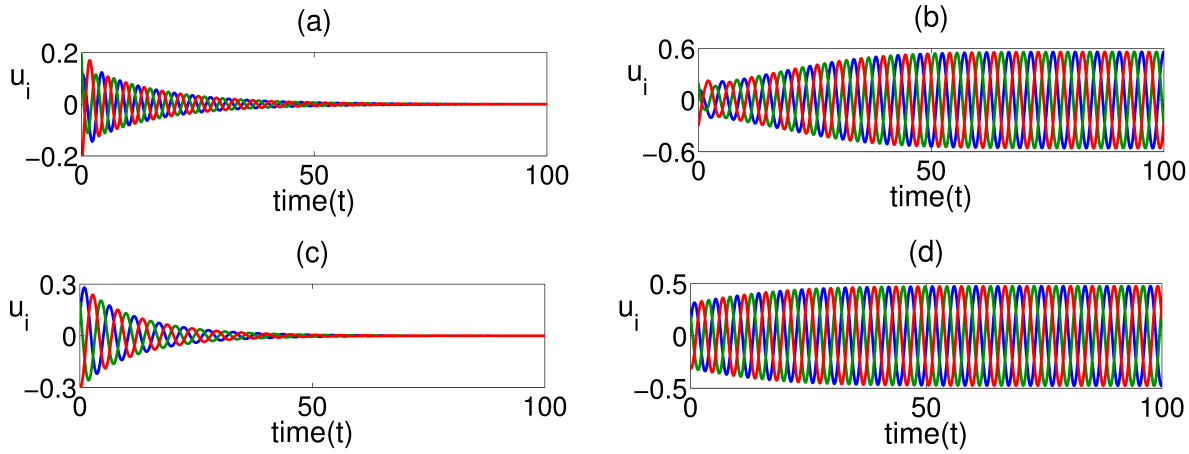

Figure 5.20: (a)-(b) Solution of the system (5.48) in the case when $\alpha < 0$. Parameter values are $\kappa = 1$, $b = -1$, $a = -0.8$ and $\tau_{odd} = 1.56$. (a) $0 < \tau = 1.3 < \tau_{odd}$. (b) $\tau = 1.8 > \tau_{odd}$. (c)-(d) Solution of the system (5.48) in the case when $\alpha \geq 0$. Parameter values are $\kappa = 1$, $\tau = 0.5$, $a = 0.2$. (c) $b = -1.5$. (d) $b = -1.8$.

For $\alpha \geq 0$, $\kappa = 1$, $a = 0.2$, the solutions approach the trivial steady state for $b = -1.5$, as in Figure 5.20 (c), with periodic oscillations around the trivial steady state for $b = -1.8$. Unlike the case of the delta distributed kernel for $n = 2$, here the period oscillations are in the form of a splay-phase synchronous solutions, as illustrated in Figure 5.20 (d).

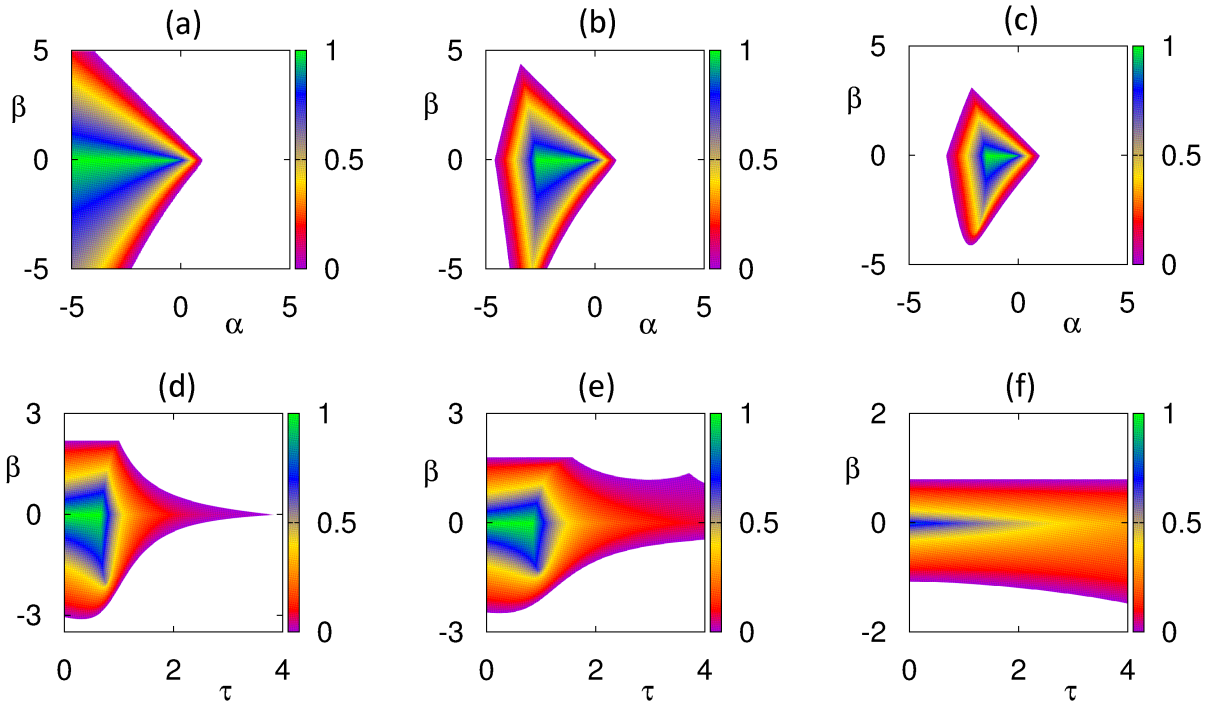

Figure 5.21: Stability of the trivial steady state of the system (5.1) with weak gamma distributed kernel and $n = 3$. Colour code denotes $[-\max\{\mathrm{Re}(\lambda)\}]$ for $\max\{\mathrm{Re}(\lambda)\} \leq 0$. (a)-(c) Stability region in (α, β), for parameters $\kappa = 1$, $\gamma = 1$. (a) $\tau = 0.2$. (b) $\tau = 0.4$. (c) $\tau = 0.6$. (d)-(f) Stability region in (τ, β), for parameters $\kappa = 1$, $\gamma = 1$. (d) $\alpha = -1.2\,(\alpha < -\kappa)$. (e) $\alpha = -0.8\,(-\kappa \leq \alpha < 0)$. (f) $\alpha = 0.2\,(0 \leq \alpha \leq \kappa)$.

By using the same process as for $n = 2$ in the case of the weak gamma distributed kernel, we can introduce the new variables

$$u_4(t) = \int_0^\infty \gamma e^{-\gamma s} u_1(t-s)ds,$$

$$u_5(t) = \int_0^\infty \gamma e^{-\gamma s} u_2(t-s)ds,$$

$$u_6(t) = \int_0^\infty \gamma e^{-\gamma s} u_3(t-s)ds,$$

and replace the system (5.1) with $n = 3$ by an equivalent 6-dimensional system with discrete time delays only as follows,

$$
\begin{aligned}
\dot{u}_1(t) &= -\kappa u_1(t) + a\tanh(u_1(t-\tau)) + b\tanh(u_6(t)),\\
\dot{u}_2(t) &= -\kappa u_2(t) + a\tanh(u_2(t-\tau)) + b\tanh(u_5(t)),\\
\dot{u}_3(t) &= -\kappa u_3(t) + a\tanh(u_3(t-\tau)) + b\tanh(u_4(t)),\\
\dot{u}_4(t) &= \gamma u_1(t) - \gamma u_4(t),\\
\dot{u}_5(t) &= \gamma u_2(t) - \gamma u_5(t),\\
\dot{u}_6(t) &= \gamma u_3(t) - \gamma u_6(t).
\end{aligned}
\tag{5.49}
$$

Figures 5.21 (a)-(c) show the stability region of the trivial steady state for weak gamma distributed delay kernel in (α, β) plane. Similar to the case of $n = 2$, increasing the time delay τ makes the stability region smaller, but it loses its symmetry property with respect to the α-axis for an odd number of neurons. Figures 5.21 (d)-(f) demonstrate the stability regions of the trivial steady state with gamma distributed kernel with $n = 3$ in the (τ, β) plane for different values of α. By changing α form negative to positive, it is possible for a trivial steady state to undergo both steady-state and Hopf bifurcation, as shown in Figures 5.21 (d)-(e), and a steady-state bifurcation only, as shown in Figure 5.21 (f).

Figure 5.22 illustrates the stability region in the β, τ, and γ parameter space for the weak gamma distributed kernel for odd number of neurons. The steady state is stable between the two surfaces in Figure 5.22 (a), and unstable everywhere else. Figures 5.22 (b)-(c) illustrate the stability region in (τ, γ) plane, the stability area grows as the coupling strength $\beta > 0$ is decreased, or $\beta < 0$ is increased.

As can be seen in Figure 5.23 (a) and Figure 5.24 (a), the trivial steady is stable, and solutions tend to this steady state. For $\tau > \tau_{weak}$, Figure 5.23 (b) and Figure 5.24 (b) display an isochronal synchronous and splay-phase oscillatory states, respectively. It is worth noting that if $\alpha \geq 0$, the solutions of the system (5.49) approach a trivial steady states for $\beta = 0.6$, as in Figure 5.23 (c), and they settle on a stable non-trivial steady state for $\beta = 1$, while in Figure 5.23 (d), the trivial steady state is stable for $\beta = -0.9$, as in Figure 5.24 (c), and for $\beta = -1.2$, there are periodic oscillations around the zero steady state, as shown in Figure 5.24 (d).

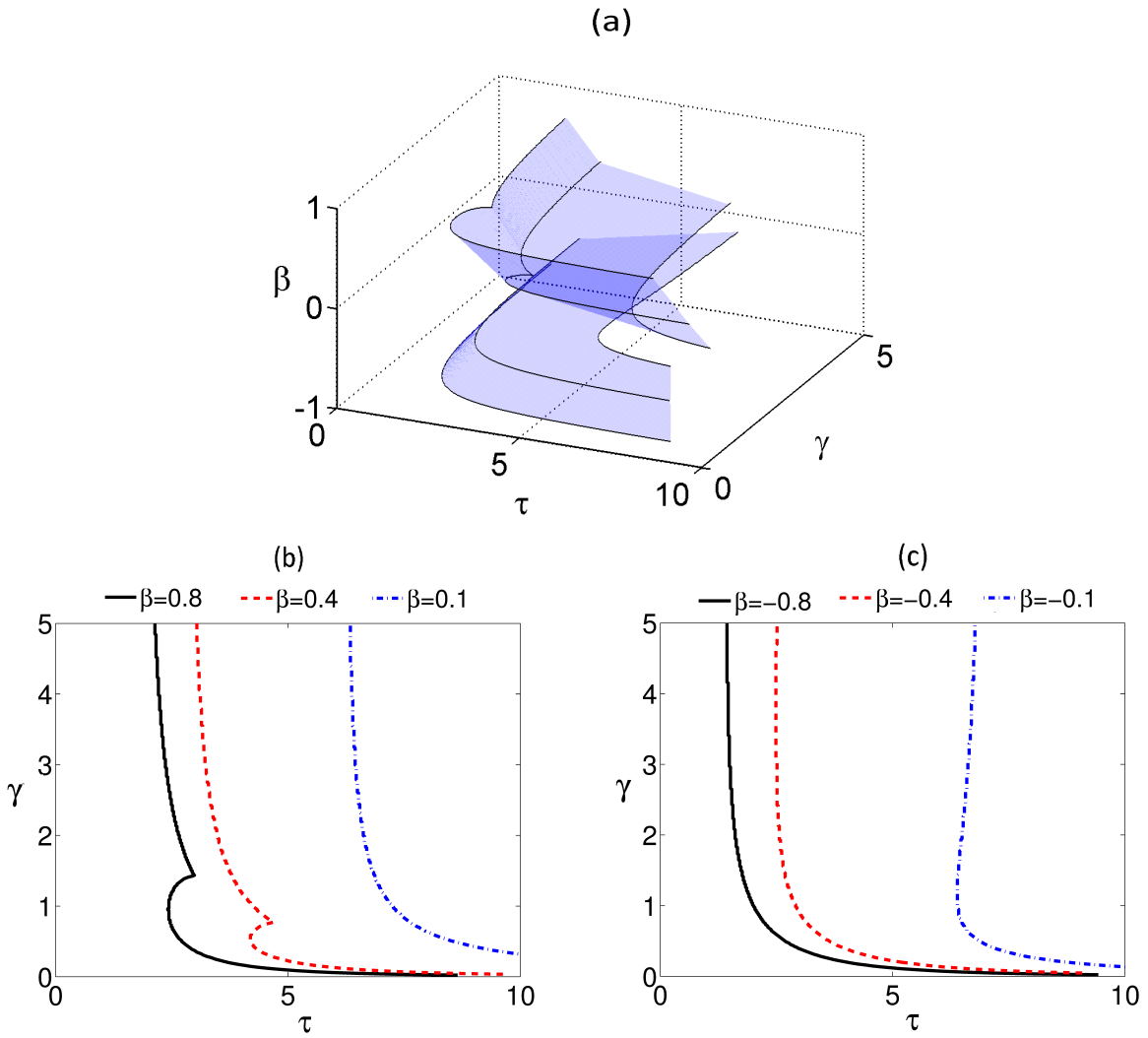

Figure 5.22: Stability boundary for the trivial steady state of the system (5.1) with weak gamma distributed kernel and $n = 3$. Parameter values are $\kappa = 1$, $\alpha = -1$. The trivial steady state is stable inside the region restricted by the boundaries in (a), and to the left of the boundary curves in (b), (c).

5.5 Discussion

In this chapter, we have considered a unidirectionally-coupled ring neural network with discrete and distributed time delays in the connections between neurons. In particular, we have focussed on the analysis of the characteristic equation of the linearised model with a general delay-distributed kernel. For a general delay-distributed kernel, we have analytically found a subset of stability regions for the trivial steady state for both odd and even numbers of neurons. We have shown that for negative values of the synaptic weight α, the time delay τ has a significant effect on the stability of the zero steady state. Whenever the condition $\tau < \frac{(\kappa-\alpha)E-1}{\alpha}$ is satisfied, the area between the horizontal lines $|\beta| = \kappa - \alpha$

in the case of an even number of neurons, and the area below the line $\beta = \kappa - \alpha$ in the case of odd number of neurons, is where the trivial steady state is stable. In contrast, the time delay does not affect the stability of the trivial steady state when $\alpha \geq 0$ for even n, and $\alpha \geq 0$ and $\beta > 0$ for odd n.

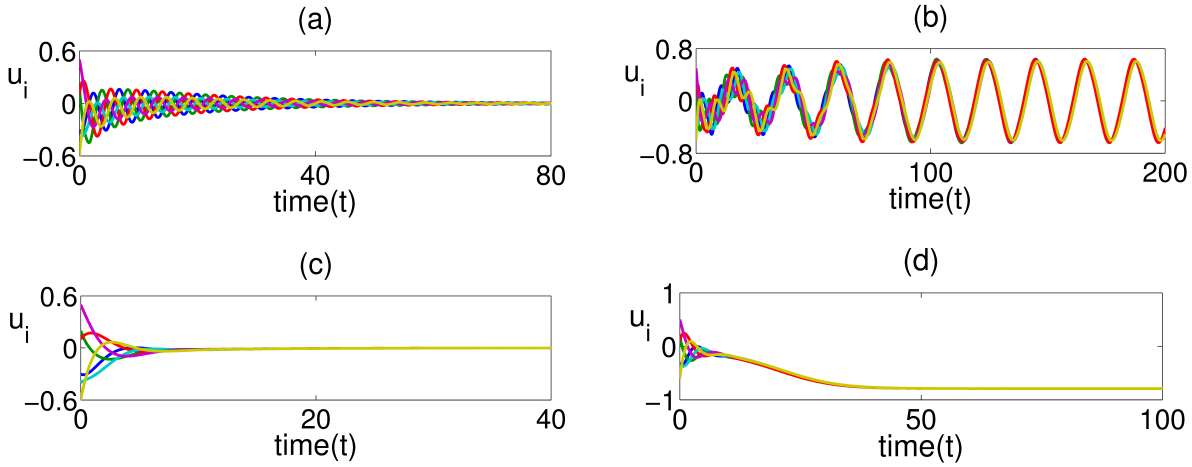

Figure 5.23: (a)-(b) Solution of the system (5.49) in the case when $\alpha < 0$. Parameter values are $\kappa = 1$, $b = 1.5$, $a = -0.8$, $\gamma = 1$ and $\tau_{weak} = 1.87$. (a) $0 < \tau = 1.5 < \tau_{weak}$. (b) $\tau = 4 > \tau_{weak}$. (c)-(d) Solution of the system (5.49) in the case when $\alpha \geq 0$. Parameter values are $\kappa = 1$, $\gamma = 1$, $\tau = 0.5$, $a = 0.2$. (c) $b = 0.6$. (d) $b = 1$.

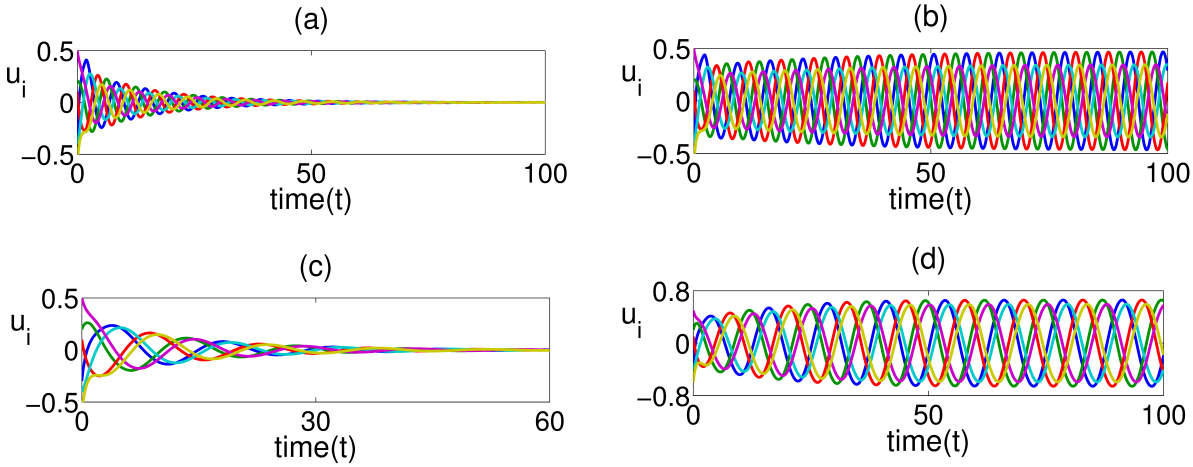

Figure 5.24: (a)-(b) Solution of the system (5.49) in the case when $\alpha < 0$. Parameter values are $\kappa = 1$, $b = -1$, $a = -0.8$, $\gamma = 1$ and $\tau_{weak} = 2.13$. (a) $0 < \tau = 1.8 < \tau_{weak}$. (b) $\tau = 2.2 > \tau_{weak}$. (c)-(d) Solution of the system (5.49) in the case when $\alpha \geq 0$. Parameter values are $\kappa = 1$, $\gamma = 1$, $\tau = 0.5$, $a = 0.2$. (c) $b = -0.9$. (d) $b = -1.2$.

In order to get deeper insights into the dynamics of the system (5.1), we have used two particular types of the distribution kernel, namely, delta function and weak gamma distribution. For both of these distributions, we have analytically found the conditions for

the stability of the zero steady state, which depend on κ, α, β, and τ. In the case of the delta distributed kernel, the stability region E_3 and O_3 (Figure 5.5) in the (α, β) parameter space extends to the left of the diamond-shaped stability boundary symmetrically for even n, and to the down-left of the diamond-shaped stability boundary for n is odd. In both cases, these regions become smaller with increasing time delay τ.

In the case of the weak gamma distributed kernel, the stability region is larger (shaded triangle-shaped areas in E_2 and O_2 shown in Figure 5.8) compared to the case of the delta distributed kernel. Increasing the time delay τ reduces the stability region, and it is symmetric with respect to the α axis for even number of neurons, and is asymmetric if the number of neurons is odd. As shown in Figures 5.14-5.21, the trivial steady state can lose its stability via a steady-state and Hopf bifurcations, or via a steady state bifurcation only, depending on the sign of α.

We have also performed direct numerical simulations of the full nonlinear system to illustrate the dynamics for both delta and weak gamma distributions. The numerical simulations support our analytical findings and show convergence of solutions to a trivial steady state (when it is stable), as well as the regime of sustained periodic oscillations, when the trivial steady state undergoes a Hopf bifurcation. For some parameter values, when the trivial steady state becomes unstable, the system (5.1) possesses non-trivial steady states, which are stable.

There are several directions in which an n unidirectionally-coupled neurons model can be extended. For example, by considering the same architecture with bidirectional delay-distributed coupling between neurons, would generalise the work of systems considered in [24, 62, 161, 166]. Another possibility is to extend systems in [92, 93] by coupling two or more unidirectionally-coupled ring neural systems of the form (5.1) between themselves.

Chapter 6

Conclusions

In this thesis, we have considered four neural networks models, including a system of coupled two sub-networks with both discrete and distributed delay in the connections, a model of N globally coupled Stuart-Landau oscillators with distributed delay, an STN-GP neural network with three independent time delays, and a unidirectionally-coupled ring of n neurons networks with a combination of both discrete and distributed delays. In the first chapter, we have presented an overview of the existing literature on the subject, and have discussed the significance of including time delays when modelling various physical and biological phenomena.

In Chapter 2, we have analysed a generalised model of coupled neural networks with discrete and distributed time delays for a general distribution kernel. We have analytically obtained a characteristic equation determining the stability of the trivial steady state for any general distribution kernel. In order to further understand the dynamics of the system, we have studied in detail the cases of the three commonly used distribution kernels, i.e. delta, uniform, strong and weak gamma distribution. For each of these distributions, we have obtained analytical conditions for stability of the null solution in terms of system parameters and the time delays. The results suggest that stability of the zero steady state depends on the synaptic weights, strength of the connection between the two sub-networks and time delays in the connection.

In the case of the Dirac delta distribution kernel, the stability region of the trivial steady state becomes larger with increasing the product of the synaptic weights. In the case of the uniformly distributed kernel, the stability properties of the trivial steady state strongly depend on the width of the distribution. In particular, as the width of the distribution becomes larger, the stability region shrinks and becomes an isolated bubble in the $\tau - \alpha$ plane. As one of the synaptic weights is increased, enlarging the distribution

width leads to a smaller region of stability, but it never becomes an isolated island. In the case of the weak and strong gamma distribution kernel, we have obtained analytical and numerical results on the stability properties of the system, and have shown that the strength of the connection between the two sub-networks plays an important role. Increasing the coupling reduces the size of the stability region, where the trivial steady state is stable, and no oscillations are possible. We have also performed direct numerical simulations that confirm our analytical findings.

In Chapter 3, we have studied aging transition in a system of globally coupled active and inactive oscillators with distributed-delay coupling. Using specific examples of uniform and gamma distributions, we have been able to analytically find boundaries of the amplitude death depending on the coupling parameters and the proportion of inactive oscillators, and we have also numerically computed characteristic eigenvalues in each scenario. For the case of uniform delay distribution, our results suggest that increasing the width of the distribution for the same mean time delay allows the system to achieve aging transition for a smaller coupling strength and a smaller proportion of inactive oscillators, and the largest proportion of inactive oscillators required for AD occurs for the discrete time delay. This highlights the fact that not only time delays can have a significant effect on aging transition, but also that the details of the delay distribution play an important role, since even for the same mean time delay, AD can occur or not depending on the width of the distribution.

In the case of the gamma distribution, provided the mean time delay is sufficiently large, there exists a range of coupling strengths, for which it is possible to achieve aging transition for any proportion of inactive oscillators, and the range of this coupling strength reduces with decreasing mean time delay. When one compares the behaviour of the system with weak and strong distribution kernels, it becomes apparent that although AD regions exhibit qualitatively similar features for these two distributions, in the case of a strong distribution kernel aging transition occurs for higher values of the mean time delays and a higher proportion of inactive oscillators. This again reiterates the important role played by the delay distribution in quenching oscillations in coupled oscillator networks.

Chapter 4 was devoted to the analysis of a general subthalamic nucleus (STN) and globus pallidus (GP) network with three distinct synaptic transmission delays. Using the time-shift transformation, we reduced the original system to an equivalent system with two time delays and showed the existence of a unique non-trivial steady state. The analysis in this chapter has concentrated on the stability properties of this steady state, since it

has a profound effect on the dynamics of the neural populations. Biologically, the stable steady state corresponds to the healthy firing of the STN and GP populations, and if it is unstable, this results in periodic firing, which imply a Parkinsonian-type regime. To better understand the effects of different time delays on the overall stability of the system, we have divided the analysis into three different cases: the delayed self-interaction in the GP population only; the delayed cross-interaction between GP and STN populations only; both interactions happen with time delays.

For the first two cases, we have analytically found the stability regions and have shown that the non-trivial steady state is stable below some critical value of the time delay, unstable when the time delay exceeds this critical value, and undergoes a Hopf bifurcation when the time delay is equal to the critical value. Furthermore, we have numerically computed eigenvalues of the corresponding characteristic equations for the three cases, showing that the strength of the synaptic connection from GP to STN population w_{GS} plays an important role in determining the stability of the steady state. In fact, when the time delay is only present in the self-interaction of the GP population, the stability region (healthy firing of neurons) increases with increasing w_{GS}, however, in the case when the time delay is only considered between STN and GP populations, the stability region gets larger for decreasing values of the synaptic weight w_{GS}. Moreover, the highest amplitude of oscillations in the case of the time delay being included in the self-interaction of the GP population corresponds to the lowest value of the synaptic strength w_{GS}, whilst if the time delay is only included into the interactions between STN and GP populations, the same effect on the amplitude of oscillations is observed for highest values of w_{GS}. In the case when both time delays are taken into account, the stability region shrinks if the synaptic weight w_{GS} is increased, leading to the smaller range of parameter values, where the healthy firing rate of neurons is possible, and the amplitude of oscillating solutions outside the stability region also grows for larger values synaptic weight w_{GS}.

In Chapter 5, we analysed a unidirectionally-coupled ring neural network with n neurons with delay-distributed connections between neurons and a discrete-delayed self-feedback. We have analytically analysed the stability properties of the trivial steady state of the system in the case of a general distribution kernel, considering separately the cases of odd and even number of neurons in the system. We have been able to identify subsets of the stability regions, and in order make further analytical progress and understand the dynamical behaviour of the system, we have studied in detail the cases of delta and weak gamma distributed kernels.

In the case of the Dirac delta distribution kernel, we have obtained analytical conditions on the stability of the trivial steady state in terms of κ, α, β, and τ. For an even (odd) number of neurons, the stability region of the trivial solution reduces symmetrically (asymmetrically) along α-axis with increasing time delay τ in the $\alpha - \beta$ plane. In the case of the weak gamma distribution kernel, the stability region occupies a larger area in the $\alpha - \beta$ parameter plane compared to the case of the delta distributed kernel. In the $\tau - \beta$ parameter space, changing the sign of the synaptic weight α can cause the trivial steady state to lose its stability via steady-state bifurcation giving rise to stable non-trivial steady state and/or via a Hopf bifurcation giving rise to a stable periodic solution.

Bibliography

[1] F. Ahmadkhanlou and H. Adeli. Optimum cost design of reinforced concrete slabs using neural dynamics model. *Engineering Applications of Artificial Intelligence*, 18(1):65–72, 2005. 1

[2] W.G. Aiello, H.I. Freedman, and J. Wu. Analysis of a model representing stage-structured population growth with state-dependent time delay. *SIAM J. Appl. Math.*, 52:855–869, 1992. 71

[3] Y. Aizawa. Synergetic approach to the phenomena of mode-locking in nonlinear systems. *Prog. Theor. Phys.*, 56(3):703–716, 1976. 60

[4] S. Amari and A. Cichocki. Adaptive blind signal processing-neural network approaches. *Proceedings of the IEEE*, 86(10):2026–2048, 1998. 1

[5] J.A. Anderson. *Neurocomputing*, volume 2. MIT press, 1993. 3

[6] D.G. Aronson, G.B. Ermentrout, and N. Kopell. Amplitude response of coupled oscillators. *Physica D*, 41:403–449, 1990. 14

[7] F.M. Atay. Distributed delays facilitate amplitude death of coupled oscillators. *Phys. Rev. Lett.*, 91(9):094101, 2003. 9, 14, 58

[8] F.M. Atay. *Complex time-delay systems: theory and applications*. Springer, 2010. 5

[9] F.M. Atay and A. Hutt. Neural fields with distributed transmission speeds and long-range feedback delays. *SIAM Journal on Applied Dynamical Systems*, 5(4):670–698, 2006. 6

[10] S.J. Aton and E.D. Herzog. Come together, right... now: synchronization of rhythms in a mammalian circadian clock. *Neuron*, 48(4):531–534, 2005. 2, 14

[11] P. Baldi and A.F. Atiya. How delays affect neural dynamics and learning. *Neural Networks, IEEE Transactions on*, 5(4):612–621, 1994. 12, 13

[12] M. Barrio, K. Burrage, A. Leier, and T. Tian. Oscillatory regulation of hes1: discrete stochastic delay modelling and simulation. *PLoS Computational Biology*, 2:e117, 2006. 7, 71

[13] J. Bélair, S.A. Campbell, and P Van Den Driessche. Frustration, stability, and delay-induced oscillations in a neural network model. *SIAM Journal on Applied Mathematics*, 56(1):245–255, 1996. 5, 21, 22

[14] S. Bernard, J. Bélair, and M.C. Mackey. Sufficient conditions for stability of linear differential equations with distributed delay. *Discrete and Continuous Dynamical Systems Series B*, 1(2):233–256, 2001. 2, 9

[15] S. Bernard and F. Crauste. Optimal linear stability condition for scalar differential equations with distributed delay. *arXiv preprint arXiv:1405.7333*, 2014. 9

[16] S. Bernard, D. Gonze, B. Čajavec, H. Herzel, and A. Kramer. Synchronization-induced rhythmicity of circadian oscillators in the suprachiasmatic nucleus. *PLoS Computational Biology*, 3:e68, 2007. 2

[17] S.P. Blythe, R.M. Nisbet, W.S. Gurney, and N. MacDonald. Stability switches in distributed delay models. *J. Math. Anal. Appl.*, 109:388–396, 1985. 8

[18] K.B. Blyuss, Y.N. Kyrychko, P. Hövel, and E. Schöll. Control of unstable steady states in neutral time-delayed systems. *The European Physical Journal B*, 65(4):571–576, 2008. 81

[19] D. Breda, S. Maset, and R. Vermiglio. Pseudospectral approximation of eigenvalues of derivative operators with non-local boundary conditions. *Applied Numerical Mathematics*, 56(3):318–331, 2006. 30, 33, 62, 80

[20] C. Cakan, J. Lehnert, and E. Schöll. Heterogeneous delays in neural networks. *arXiv preprint arXiv:1311.1919*, 2013. 14

[21] S.A. Campbell, R. Edwards, and P. van den Driessche. Delayed coupling between two neural network loops. *SIAM Journal on Applied Mathematics*, 65(1):316–335, 2004. 12, 20

[22] S.A. Campbell and R. Jessop. Approximating the stability region for a differential equation with a distributed delay. *Mathematical Modelling of Natural Phenomena*, 4(02):1–27, 2009. 2, 10

[23] S.A. Campbell, S. Ruan, G. Wolkowicz, and J. Wu. Stability and bifurcation of a simple neural network with multiple time delays. *Fields Inst. Commun*, 21(4):65–79, 1999. 13, 96

[24] S.A. Campbell, Y. Yuan, and S.D. Bungay. Equivariant hopf bifurcation in a ring of identical cells with delayed coupling. *Nonlinearity*, 18(6):2827, 2005. 121

[25] C.-Y. Cheng, K.-H. Lin, and C.-W. Shih. Multistability in recurrent neural networks. *SIAM Journal on Applied Mathematics*, 66(4):1301–1320, 2006. 58

[26] K.L. Cooke and Z. Grossman. Discrete delay, distributed delay and stability switches. *Journal of Mathematical Analysis and Applications*, 86(2):592–627, 1982. 2, 8, 9

[27] S. Coombes and C. Laing. Delays in activity-based neural networks. *Philosophical Transactions of the Royal Society A: Mathematical, Physical and Engineering Sciences*, 367(1891):1117–1129, 2009. 16

[28] J.D. Cowan. A statistical mechanics of neuron activity. *Some Mathematical Questions in Biology, American Mathematical Society, Providence, RI*, pages 1–58, 1970. 11

[29] G. Dahlquist and Å. Björck. Numerical methods in scientific computing, volume i. *SIAM, Philadelphia*, 2007. 51

[30] H. Daido and K. Nakanishi. Aging transition and universal scaling in oscillator networks. *Phys. Rev. Lett.*, 93(10):104101, 2004. 2, 13, 60

[31] W. Dauer and S. Przedborski. Parkinson's disease: mechanisms and models. *Neuron*, 39(6):889–909, 2003. 15

[32] G.B. Ermentrout. Oscillator death in populations of "all-to all" coupled nonlinear oscillators. *Physica D*, 41(2):219–231, 1990. 60

[33] G.B. Ermentrout and J.D. Cowan. A mathematical theory of visual hallucination patterns. *Biological Cybernetics*, 34(3):137–150, 1979. 15

[34] T. Erneux. *Applied delay differential equations*, volume 3. Springer Science & Business Media, 2009. 2, 16

[35] T. Faria. On a planar system modelling a neuron network with memory. *Journal of Differential Equations*, 168(1):129–149, 2000. 20

[36] C. Feng. Oscillatory behavior on a three-node neural network model with discrete and distributed delays. *Advances in Artificial Neural Systems*, 2014:1, 2014. 12

[37] P. Feng. Dynamics of a segmentation clock model with discrete and distributed delays. *International Journal of Biomathematics*, 3(04):399–416, 2010. 2, 11

[38] V. Flunkert, I. Fischer, and E. Schöll. Dynamics, control and information in delay-coupled systems: an overview, 2013. 5

[39] V. Flunkert, S. Yanchuk, T. Dahms, and E. Schöll. Synchronizing distant nodes: a universal classification of networks. *Phys. Rev. Lett.*, 105(25):254101, 2010. 5

[40] M. Forti and A. Tesi. New conditions for global stability of neural networks with application to linear and quadratic programming problems. *Circuits and Systems I: Fundamental Theory and Applications, IEEE Transactions on*, 42(7):354–366, 1995. 1

[41] K. Fujimoto and H. Kita. Response characteristics of subthalamic neurons to the stimulation of the sensorimotor cortex in the rat. *Brain Research*, 609(1):185–192, 1993. 16, 74

[42] H. Fukuda, N. Nakamichi, M. Hisatsune, H. Murase, and T. Mizuno. Synchronization of plant circadian oscillators with a phase delay effect of the vein network. *Phys. Rev. Lett.*, 99:098102, 2007. 2

[43] P. Gatev, O. Darbin, and T. Wichmann. Oscillations in the basal ganglia under normal conditions and in movement disorders. *Movement Disorders*, 21(10):1566–1577, 2006. 15

[44] J. Ge and J. Xu. Stability switches and bifurcation analysis in a coupled neural system with multiple delays. *Science China Technological Sciences*, 59(6):920–931, 2016. 12

[45] A. Gillies, D. Willshaw, and Z. Li. Subthalamic–pallidal interactions are critical in determining normal and abnormal functioning of the basal ganglia. *Proceedings of the Royal Society of London. Series B: Biological Sciences*, 269(1491):545–551, 2002. 16

[46] A. Gjurchinovski and V. Urumov. Stabilization of unstable steady states by variable-delay feedback control. *EPL*, 84(4):40013, 2008. 71

[47] A. Gjurchinovski and V. Urumov. Variable-delay feedback control of unstable steady states in retarded time-delayed systems. *Physical Review E*, 81(1):016209, 2010. 2, 6, 71

[48] A. Gjurchinovski, A. Zakharova, and E. Schöll. Amplitude death in oscillator networks with variable-delay coupling. *Physical Review E*, 89(3):032915, 2014. 6

[49] L. Glass. Synchronization and rhythmic processes in physiology. *Nature*, 410:277–284, 2001. 2

[50] K. Gopalsamy and X.-Z. He. Stability in asymmetric hopfield nets with transmission delays. *Physica D: Nonlinear Phenomena*, 76(4):344–358, 1994. 10

[51] J. Götz, N. Schonrock, B. Vissel, and L.M. Ittner. Alzheimer's disease selective vulnerability and modeling in transgenic mice. *Journal of Alzheimer's Disease*, 18(2):243–251, 2009. 15

[52] S.A. Gourley and J.H. So. Extinction and wavefront propagation in a reaction-diffusion model of a structured population with distributed maturation delay. *Proceedings of the Royal Society of Edinburgh: Section A Mathematics*, 133(03):527–548, 2003. 2, 6

[53] K. Gu, J. Chen, and V.L. Kharitonov. *Stability of time-delay systems*. Springer Science & Business Media, 2003. 2, 27

[54] K. Gu, S.-I. Niculescu, and J. Chen. On stability crossing curves for general systems with two delays. *Journal of Mathematical Analysis and Applications*, 311(1):231–253, 2005. 81

[55] P.D. Gupta, N.C. Majee, and A.B. Roy. Stability and hopf-bifurcation analysis of delayed bam neural network under dynamic thresholds. *Nonlinear Analysis*, 14(4):435–461, 2009. 11

[56] V. Gupta and K.V. Kadambari. Neuronal model with distributed delay: analysis and simulation study for gamma distribution memory kernel. *Biological Cybernetics*, 104(6):369–383, 2011. 8

[57] N.E. Hallworth, C.J. Wilson, and M.D. Bevan. Apamin-sensitive small conductance calcium-activated potassium channels, through their selective coupling to voltage-gated calcium channels, are critical determinants of the precision, pace, and pattern

of action potential generation in rat subthalamic nucleus neurons in vitro. *The Journal of Neuroscience*, 23(20):7525–7542, 2003. 74

[58] Y. Han and Y. Song. Stability and hopf bifurcation in a three-neuron unidirectional ring with distributed delays. *Nonlinear Dynamics*, 69(1-2):357–370, 2012. 11

[59] Z. He, S. Liu, and M. Zhan. Dynamical robustness analysis of weighted complex networks. *Physica A*, 392(18):4181–4191, 2013. 14, 71

[60] J.J. Hopfield. Neurons with graded response have collective computational properties like those of two-state neurons. *Proceedings of the National Academy of Sciences*, 81(10):3088–3092, 1984. 5, 20, 58

[61] C.-H. Hsu and T.-S. Yang. Periodic oscillations arising and death in delay-coupled neural loops. *International Journal of Bifurcation and Chaos*, 17(11):4015–4032, 2007. 12

[62] L. Huang and J. Wu. Nonlinear waves in networks of neurons with delayed feedback: pattern formation and continuation. *SIAM Journal on Mathematical Analysis*, 34(4):836–860, 2003. 121

[63] W. Huang, X. Zhang, X. Hu, Y. Zou, Z. Liu, and S. Guan. Variation of critical point of aging transition in a networked oscillators system. *Chaos*, 24:023122, 2014. 60, 71

[64] A. Hutt and L. Zhang. Distributed nonlocal feedback delays may destabilize fronts in neural fields, distributed transmission delays do not. *The Journal of Mathematical Neuroscience*, 3(9):1–21, 2013. 6

[65] T. Insperger, G. Stépán, and J. Turi. State-dependent delay in regenerative turning processes. *Nonl. Dyn.*, 47:275–283, 2007. 71

[66] V.K. Jirsa and M. Ding. Will a large complex system with time delays be stable? *Phys. Rev. Lett.*, 93(7):070602, 2004. 2, 9

[67] W. Just, A. Pelster, M. Schanz, and E. Schöll. Delayed complex systems: an overview, 2010. 5

[68] C. Kim and D.Q. Nykamp. Dynamics of a network of excitatory and inhibitory neurons induced by depolarization block. *BMC Neuroscience*, 15(Suppl 1):P76, 2014. 15

[69] H. Kita. Globus pallidus external segment. *Progress in Brain Research*, 160:111–133, 2007. 74

[70] H. Kita, H.T. Chang, and S.T. Kitai. Pallidal inputs to subthalamus: intracellular analysis. *Brain Research*, 264(2):255–265, 1983. 74

[71] H. Kita and S.T. Kitai. Intracellular study of rat globus pallidus neurons: membrane properties and responses to neostriatal, subthalamic and nigral stimulation. *Brain Research*, 564(2):296–305, 1991. 74

[72] H. Kita, A. Nambu, K. Kaneda, Y. Tachibana, and M. Takada. Role of ionotropic glutamatergic and gabaergic inputs on the firing activity of neurons in the external pallidum in awake monkeys. *Journal of Neurophysiology*, 92(5):3069–3084, 2004. 74

[73] H. Kita, Y. Tachibana, A. Nambu, and S. Chiken. Balance of monosynaptic excitatory and disynaptic inhibitory responses of the globus pallidus induced after stimulation of the subthalamic nucleus in the monkey. *The Journal of Neuroscience*, 25(38):8611–8619, 2005. 16, 74

[74] A. Koseska, E. Volkov, and J. Kurths. Detuning-dependent dominance of oscillation death in globally coupled synthetic genetic oscillators. *EPL*, 85:28002, 2009. 14

[75] A. Koseska, E. Volkov, and J. Kurths. Parameter mismatches and oscillation death in coupled oscillators. *Chaos*, 20:023132, 2010. 14

[76] A.K. Kryukov, V.S. Petrov, L.S. Averyanova, G.V. Osipov, W. Chen, O. Drugova, and C.K. Chan. Synchronization phenomena in mixed media of passive, excitable, and oscillatory cells. *Chaos*, 18(3):037129, 2008. 14

[77] Y. Kuang. *Delay differential equations: with applications in population dynamics*. Academic Press, 1993. 27

[78] Y.N. Kyrychko, K.B. Blyuss, and E. Schöll. Amplitude death in systems of coupled oscillators with distributed-delay coupling. *Eur. Phys. J. B*, 84(2):307–315, 2011. 14, 58

[79] Y.N. Kyrychko, K.B. Blyuss, and E. Schöll. Amplitude and phase dynamics in oscillators with distributed-delay coupling. *Phil. Trans. R. Soc. London, Ser. A*, 371(1999):20120466, 2013. 14, 58

[80] Y.N. Kyrychko, K.B. Blyuss, and E. Schöll. Synchronization of networks of oscillators with distributed delay coupling. *Chaos*, 24:043117, 2014. 2, 14, 58

[81] Y.N. Kyrychko and S.J. Hogan. On the use of delay equations in engineering applications. *Journal of Vibration and Control*, 2010. 5

[82] Q. Lai, B. Hu, Z.-H. Guan, T. Li, D.-F. Zheng, and Y.-H. Wu. Multistability and bifurcation in a delayed neural network. *Neurocomputing*, 2016. 13

[83] C.R. Laing and A. Longtin. Dynamics of deterministic and stochastic paired excitatory—inhibitory delayed feedback. *Neural Computation*, 15(12):2779–2822, 2003. 16

[84] M.A. Lebedev and S.P. Wise. Oscillations in the premotor cortex: single-unit activity from awake, behaving monkeys. *Experimental Brain Research*, 130(2):195–215, 2000. 74

[85] E. Ledoux and N. Brunel. Dynamics of networks of excitatory and inhibitory neurons in response to time-dependent inputs. *Frontiers in Computational Neuroscience*, 5, 2011. 16

[86] J. Li, L. Zhang, and Z. Wang. Two effective stability criteria for linear time-delay systems with complex coefficients. *Journal of Systems Science and Complexity*, 24(5):835–849, 2011. 27, 40

[87] Z. Li and J.J. Hopfield. Modeling the olfactory bulb and its neural oscillatory processings. *Biological Cybernetics*, 61(5):379–392, 1989. 15

[88] X. Liao, K.-W. Wong, and Z. Wu. Bifurcation analysis on a two-neuron system with distributed delays. *Physica D: Nonlinear Phenomena*, 149(1):123–141, 2001. 11

[89] S. Little and P. Brown. The functional role of beta oscillations in Parkinson's disease. *Parkinsonism & Related Disorders*, 20:S44–S48, 2014. 15

[90] J.J. Loiseau, W. Michiels, S.-I. Niculescu, and R. Sipahi. *Topics in time delay systems: analysis, algorithms and control*, volume 388. Springer, 2009. 80

[91] N. MacDonald. Time lags in biological systems. 1978. 8, 35, 65

[92] X. Mao. Stability and hopf bifurcation analysis of a pair of three-neuron loops with time delays. *Nonlinear Dynamics*, 68(1-2):151–159, 2012. 12, 121

[93] X. Mao and Z. Wang. Stability switches and bifurcation in a system of four coupled neural networks with multiple time delays. *Nonlinear Dynamics*, 82(3):1551–1567, 2015. 12, 121

[94] C.M. Marcus and R.M. Westervelt. Stability of analog neural networks with delay. *Physical Review A*, 39(1):347, 1989. 2, 5, 10, 20, 21

[95] R. Merrison-Hort, N. Yousif, F. Njap, U.G. Hofmann, O. Burylko, and R. Borisyuk. An interactive channel model of the basal ganglia: bifurcation analysis under healthy and Parkinsonian conditions. *The Journal of Mathematical Neuroscience*, 3(1):14, 2013. 16, 73

[96] U. Meyer, J. Shao, S. Chakrabarty, S.F. Brandt, H. Luksch, and R. Wessel. Distributed delays stabilize neural feedback systems. *Biological Cybernetics*, 99(1):79–87, 2008. 2, 9

[97] J. Miake, E. Marbán, and H.B. Nuss. Gene therapy: Biological pacemaker created by gene transfer. *Nature*, 419:132–133, 2002. 2, 14

[98] R. E Mirollo and S.H. Strogatz. Amplitude death in an array of limit-cycle oscillators. *J. Stat. Phys.*, 60(1-2):245–262, 1990. 14, 60

[99] C. Mitra, G. Ambika, and S. Banerjee. Dynamical behaviors in time-delay systems with delayed feedback and digitized coupling. *Chaos, Solitons & Fractals*, 69:188–200, 2014. 13, 96

[100] J.E. Mittler, B. Sulzer, A.U. Neumann, and A.S. Perelson. Influence of delayed viral production on viral dynamics in hiv-1 infected patients. *Math. Biosci.*, 152:143–163, 1998. 8

[101] L.H.A. Monteiro, M.A. Bussab, and J.G. Chaui Berlinck. Analytical results on a Wilson-Cowan neuronal network modified model. *Journal of Theoretical Biology*, 219(1):83–91, 2002. 16

[102] K. Morino, G. Tanaka, and K. Aihara. Robustness of multilayer oscillator networks. *Phys. Rev. E*, 83(5):056208, 2011. 14

[103] K. Morino, G. Tanaka, and K. Aihara. Efficient recovery of dynamic behavior in coupled oscillator networks. *Phys. Rev. E*, 88(3):032909, 2013. 14

[104] H. Nakanishi, H. Kita, and S.T. Kitai. Intracellular study of rat substantia nigra pars reticulata neurons in an in vitro slice preparation: electrical membrane properties and response characteristics to subthalamic stimulation. *Brain Research*, 437(1):45–55, 1987. 74

[105] A.J. Nevado-Holgado, N. Mallet, P.J. Magill, and R. Bogacz. Effective connectivity of the subthalamic nucleus–globus pallidus network during Parkinsonian oscillations. *The Journal of Physiology*, 592(7):1429–1455, 2014. 16

[106] A.J. Nevado-Holgado, J.R. Terry, and R. Bogacz. Conditions for the generation of beta oscillations in the subthalamic nucleus–globus pallidus network. *The Journal of Neuroscience*, 30(37):12340–12352, 2010. 16, 72, 73, 74, 86

[107] L. Nunney. Short time delays in population models: a role in enhancing stability. *Ecology*, 66:1849–1858, 1985. 7

[108] M.N. Ogŭztöreli. Activity analysis of neural networks. *Biological Cybernetics*, 34(3):159–169, 1979. 11

[109] I. Omelchenko, Y. Maistrenko, P. Hövel, and E. Schöll. Loss of coherence in dynamical networks: spatial chaos and chimera states. *Phys. Rev. Lett.*, 106(23):234102, 2011. 2

[110] A. Panchuk, M. Dahlem, and E. Schöll. Regular spiking in asymmetrically delay-coupled fitzhugh-nagumo systems. *arXiv preprint arXiv:0911.2071*, 2009. 74

[111] A. Panchuk, D. P. Rosin, P. Hövel, and E. Schöll. Synchronization of coupled neural oscillators with heterogeneous delays. *International Journal of Bifurcation and Chaos*, 23(12):1330039, 2013. 6, 74

[112] J. Parkinson. An essay on the shaking palsy. *J Neuropsychiatry Clin Neurosci*, 14:223–236, 2002. 15

[113] W. Pasillas-Lépine. Delay-induced oscillations in Wilson and Cowan's model: an analysis of the subthalamo-pallidal feedback loop in healthy and Parkinsonian subjects. *Biological Cybernetics*, 107(3):289–308, 2013. 16, 17

[114] A. Pavlides, S. J. Hogan, and R. Bogacz. Improved conditions for the generation of beta oscillations in the subthalamic nucleus–globus pallidus network. *European Journal of Neuroscience*, 36(2):2229–2239, 2012. 16

[115] J.T. Paz, J.-M. Deniau, and S. Charpier. Rhythmic bursting in the cortico-subthalamo-pallidal network during spontaneous genetically determined spike and wave discharges. *The Journal of Neuroscience*, 25(8):2092–2101, 2005. 74

[116] D. Pazó and E. Montbrió. Universal behavior in populations composed of excitable and self-oscillatory elements. *Phys. Rev. E*, 73(5):055202(R), 2006. 14

[117] Y. Peng and Y. Song. Stability switches and hopf bifurcations in a pair of identical tri-neuron network loops. *Physics Letters A*, 373(20):1744–1749, 2009. 12

[118] J. Plaza, A. Plaza, R. Perez, and P. Martinez. On the use of small training sets for neural network-based characterization of mixed pixels in remotely sensed hyperspectral images. *Pattern Recognition*, 42(11):3032–3045, 2009. 1

[119] B. Rahman, K.B. Blyuss, and Y.N. Kyrychko. Dynamics of neural systems with discrete and distributed time delays. *SIAM J. Appl. Dyn. Syst.*, 14:2069–2095, 2015. 19, 71

[120] D.V.R. Reddy, A. Sen, and G.L. Johnston. Time delay induced death in coupled limit cycle oscillators. *Phys. Rev. Lett.*, 80(23):5109–5112, 1998. 14

[121] D.V.R. Reddy, A. Sen, and G.L. Johnston. Time delay effects on coupled limit cycle oscillators at hopf bifurcation. *Physica D*, 129(1):15–34, 1999. 14

[122] D.V.R. Reddy, A. Sen, and G.L. Johnston. Experimental evidence of time-delay-induced death in coupled limit-cycle oscillators. *Phys. Rev. Lett.*, 85(16):3381–3384, 2000. 14

[123] M. Rohden, A. Sorge, M. Timme, and D. Witthaut. Self-organized synchronization in decentralized power grids. *Phys. Rev. Lett.*, 109:064101, 2012. 2

[124] S. Ruan. Absolute stability, conditional stability and bifurcation in Kolmogorov-type predator-prey systems with discrete delays. *Quarterly of Applied Mathematics*, 59(1):159–174, 2001. 78

[125] S. Ruan. Delay differential equations in single species dynamics. In *Delay Differential Equations and Applications*, pages 477–517. Springer, 2006. 8

[126] S. Ruan and R.S. Filfil. Dynamics of a two-neuron system with discrete and distributed delays. *Physica D: Nonlinear Phenomena*, 191(3):323–342, 2004. 11, 16

[127] S. Ruan and J. Wei. Periodic solutions of planar systems with two delays. *Proceedings of the Royal Society of Edinburgh: Section A Mathematics*, 129(05):1017–1032, 1999. 16

[128] E.J. Sanz-Arigita, M.M. Schoonheim, J.S. Damoiseaux, S.A. Rombouts, E. Maris, F. Barkhof, P. Scheltens, and C.J. Stam. Loss of 'small-world' networks in Alzheimer's disease: graph analysis of FMRI resting-state functional connectivity. *PloS ONE*, 5(11):e13788, 2010. 15

[129] T. Sasai, K. Morino, G. Tanaka, J.A. Almendral, and K. Aihara. Robustness of oscillatory behavior in correlated networks. *PLoS ONE*, 10:e0123722, 2015. 71

[130] E. Schöll, S. H.L. Klapp, and P. Hövel. Control of self-organizing nonlinear systems. *Understanding complex systems (*, 2016. 14

[131] E. Schöll and H. G. Schuster. *Handbook of chaos control*. John Wiley & Sons, 2008. 5

[132] W. Schultz and R. Romo. Neuronal activity in the monkey striatum during the initiation of movements. *Experimental Brain Research*, 71(2):431–436, 1988. 74

[133] L.P. Shayer and S.A. Campbell. Stability, bifurcation, and multistability in a system of two coupled neurons with multiple time delays. *SIAM Journal on Applied Mathematics*, 61(2):673–700, 2000. 96

[134] M. Shiino and M. Frankowicz. Synchronization of infinitely many coupled limit-cycle type oscillators. *Phys. Lett. A*, 136(3):103–108, 1989. 60

[135] P.K. Simpson. Artificial neural systemfoundation, paradigm, application and implementations, 1990. 4

[136] R. Sipahi, F.M. Atay, and S.-I. Niculescu. Stability of traffic flow behaviour with distributed delays modeling the memory effects of the drivers. *SIAM J. Appl. Math.*, 68:738–759, 2007. 7

[137] H. Smith. *An introduction to delay differential equations with applications to the life sciences*, volume 57. Springer Science & Business Media, 2010. 8

[138] Y. Smith, T. Wichmann, S.A. Factor, and M.R. DeLong. Parkinson's disease therapeutics: new developments and challenges since the introduction of levodopa. *Neuropsychopharmacology*, 37(1):213–246, 2011. 15

[139] P.G. Sokolove. Computer simulation of after-inhibition in crayfish slowly adapting stretch receptor neuron. *Biophysical Journal*, 12(11):1429, 1972. 11

[140] Y. Song, Y. Han, and Y. Peng. Stability and hopf bifurcation in an unidirectional ring of n neurons with distributed delays. *Neurocomputing*, 121:442–452, 2013. 11

[141] Y. Song, V.A. Makarov, and M.G. Velarde. Stability switches, oscillatory multistability, and spatio-temporal patterns of nonlinear oscillations in recurrently delay coupled neural networks. *Biological Cybernetics*, 101(2):147–167, 2009. 12, 21, 22

[142] Y. Song and Y. Peng. Stability and bifurcation analysis on a logistic model with discrete and distributed delays. *Applied Mathematics and Computation*, 181(2):1745–1757, 2006. 78

[143] Y. Song, T. Zhang, and M.O. Tadé. Stability switches, hopf bifurcations, and spatio-temporal patterns in a delayed neural model with bidirectional coupling. *Journal of Nonlinear Science*, 19(6):597–632, 2009. 12, 20, 21, 24, 33

[144] M.C. Soriano, J. García-Ojalvo, C.R. Mirasso, and I. Fischer. Complex photonics: Dynamics and applications of delay-coupled semiconductors lasers. *Reviews of Modern Physics*, 85(1):421, 2013. 5

[145] G. Stépán. *Retarded dynamical systems: stability and characteristic functions*. Longman Scientific & Technical, 1989. 2

[146] G. Stépán. Delay-differential equation models for machine tool chatter. *Dynamics and Chaos in Manufacturing Processes*, 471152935:165–192, 1998. 8

[147] S.H. Strogatz. Exploring complex networks. *Nature*, 410(6825):268–276, 2001. 1

[148] J.-Q. Sun and Q. Ding. *Advances in analysis and control of time-delayed dynamical systems*. World Scientific, 2013. 4

[149] K. Supekar, V. Menon, D. Rubin, M. Musen, and M.D. Greicius. Network analysis of intrinsic functional brain connectivity in alzheimer's disease. *PLoS Computational Biology*, 4(6):e1000100, 2008. 15

[150] G. Tanaka, K. Morino, and K. Aihara. Phase transitions in complex networks of active and inactive oscillators. *Proc. PHYSCON11, Leon*, 2011. 14

[151] G. Tanaka, K. Morino, H. Daido, and K. Aihara. Dynamical robustness of coupled heterogeneous oscillators. *Phys. Rev. E*, 89(5):059206, 2014. 71

[152] G. Tanaka, Y. Okada, and K. Aihara. Phase transitions in mixed populations composed of two types of self-oscillatory elements with different periods. *Phys. Rev. E*, 82(3):035202(R), 2010. 14

[153] B. Thakur, D. Sharma, and A. Sen. Time-delay effects on the aging transition in a population of coupled oscillators. *Phys. Rev. E*, 90(4):042904, 2014. 14, 60, 62

[154] A. Thiel, H. Schwegler, and C.W. Eurich. Complex dynamics is abolished in delayed recurrent systems with distributed feedback times. *Complexity*, 8(4):102–108, 2003. 9

[155] J. Wei and S. Ruan. Stability and bifurcation in a neural network model with two delays. *Physica D: Nonlinear Phenomena*, 130(3):255–272, 1999. 20

[156] K. Wiesenfeld, P. Colet, and S.H. Strogatz. Synchronization transitions in a disordered josephson series array. *Phys. Rev. Lett.*, 76:404–407, Jan 1996. 2

[157] C.R.S. Williams, F. Sorrentino, T.E. Murphy, and R. Roy. Synchronization states and multistability in a ring of periodic oscillators: Experimentally variable coupling delays. *Chaos: An Interdisciplinary Journal of Nonlinear Science*, 23(4):043117, 2013. 96

[158] H.R. Wilson and J.D. Cowan. Excitatory and inhibitory interactions in localized populations of model neurons. *Biophysical Journal*, 12(1):1, 1972. 15, 22, 72

[159] J. Wu. *Introduction to neural dynamics and signal transmission delay*, volume 6. Walter de Gruyter, 2001. 1, 3, 4

[160] S. Xin-Fang and W. Wen-Yuan. Target inactivation and recovery in two-layer networks. *Chinese Phys. Lett.*, 32(11):110502, 2015. 14

[161] X. Xu. Complicated dynamics of a ring neural network with time delays. *Journal of Physics A: Mathematical and Theoretical*, 41(3):035102, 2008. 13, 121

[162] Y. Yamaguchi and H. Shimizu. Theory of self-synchronization in the presence of native frequency distribution and external noises. *Physica D*, 11(1):212–226, 1984. 60

[163] N. Yao, R. S.-K. Chang, C. Cheung, S. Pang, K.K. Lau, J. Suckling, J.B. Rowe, K. Yu, H. K.-F. Mak, and S.-E. Chua. The default mode network is disrupted in

Parkinson's disease with visual hallucinations. *Human Brain Mapping*, 35(11):5658–5666, 2014. 15

[164] S. Yuan and X. Li. Stability and bifurcation analysis of an annular delayed neural network with self-connection. *Neurocomputing*, 73(16):2905–2912, 2010. 96

[165] Y. Yuan and J. Bélair. Stability and hopf bifurcation analysis for functional differential equation with distributed delay. *SIAM Journal on Applied Dynamical Systems*, 10(2):551–581, 2011. 10

[166] Y. Yuan and S.A. Campbell. Stability and synchronization of a ring of identical cells with delayed coupling. *Journal of Dynamics and Differential Equations*, 16(3):709–744, 2004. 13, 121

[167] A. Zakharova, I. Schneider, Y.N. Kyrychko, K.B. Blyuss, A. Koseska, B. Fiedler, and E. Schöll. Time delay control of symmetry-breaking primary and secondary oscillation death. *EPL*, 104(5):50004, 2013. 5, 14

[168] Z. Zeng, D.S. Huang, and Z. Wang. Pattern memory analysis based on stability theory of cellular neural networks. *Applied Mathematical Modelling*, 32(1):112–121, 2008. 1

[169] F. Zenke, G. Hennequin, and W. Gerstner. Synaptic plasticity in neural networks needs homeostasis with a fast rate detector. *PLoS Computational Biology*, 9(11):e1003330, 2013. 22

[170] D. Zhang, X. Liu, J. Chen, and B. Liu. Distinguishing patients with Parkinson's disease subtypes from normal controls based on functional network regional efficiencies. *PloS ONE*, 9(12):e115131, 2014. 15

[171] H. Zhao. Global asymptotic stability of hopfield neural network involving distributed delays. *Neural Networks*, 17(1):47–53, 2004. 6

[172] H. Zhu and L. Huang. Stability and bifurcation in a tri-neuron network model with discrete and distributed delays. *Applied Mathematics and Computation*, 188(2):1742–1756, 2007. 11

[173] W. Zou, D.V. Senthilkumar, Y. Tang, Y. Wu, J. Lu, and J. Kurths. Amplitude death in nonlinear oscillators with mixed time-delayed coupling. *Phys. Rev. E*, 88(3):032916, 2013. 60, 71